

Novel anti-infective delivery systems for the treatment of pulmonary bacterial infections

Dissertation
zur Erlangung des Grades
des Doktors der Naturwissenschaften
der Naturwissenschaftlich-Technischen Fakultät
der Universität des Saarlandes

von
Duy-Khiet Ho

Saarbrücken
2018

Tag des Kolloquiums: 16th Jan. 2019
Dekan: Prof. Dr. Guido Kickelbick
Berichterstatter: Prof. Dr. Claus-Michael Lehr
Prof. Dr. Gerhard Wenz
Prof. Dr. Dr. Lorenz Meinel

Vorsitz: Prof. Dr. Rolf W. Hartmann
Akad. Mitarbeiter: Dr. Silke Wenzel

Die vorliegende Arbeit wurde von Oktober 2015 bis Juli 2018 unter der Leitung von Herrn Prof. Dr. Claus-Michael Lehr und Frau Dr. Brigitta Loretz am Institut für Pharmazeutische Technologie der Universität des Saarlandes und am Helmholtz-Institut für Pharmazeutische Forschung Saarland angefertigt.

TABLE OF CONTENTS

I. SUMMARY.....	VI
II. ZUSAMMENFASSUNG	VII
III. ABBREVIATION	VIII
1. INTRODUCTION.....	9
1.1. ANTIBIOTICS UTILITIES IN COMBATING INFECTION AND BENEFITS OF LOCAL DELIVERY.....	9
1.2. CHALLENGES IN PULMONARY INFECTION TREATMENT AND IN FINDING SOLUTIONS ...	12
1.3. DRUG DELIVERY SYSTEMS AIM FOR PULMONARY INFECTIONS TREATMENT	19
1.3.1. <i>Advantages of drug delivery systems in pulmonary infections treatment</i>	19
1.3.2. <i>Requirements in preparation of drug delivery systems.....</i>	22
1.3.3. <i>Recent development of anti-infective delivery systems for pulmonary infections treatment.</i>	24
1.3.4. <i>Interaction between drug delivery systems and pulmonary biological barriers... </i>	30
2. RESEARCH STRATEGIES, WORKING HYPOTHESIS AND AIMS OF THE THESIS.....	33
3. MAIN FINDINGS	36
4. CONCLUSIONS AND OUTLOOK.....	42
5. REFERENCES.....	44
6. SCIENTIFIC OUTPUT.....	57
6.1. PAPER 1: “STARCH-CHITOSAN POLYPLEXES: A VERSATILE CARRIER SYSTEM FOR ANTI-INFECTIVES AND GENE DELIVERY”	58
6.2. PAPER 2: “POLYSACCHARIDE SUBMICROCARRIER FOR IMPROVED PULMONARY DELIVERY OF POORLY SOLUBLE ANTI-INFECTIVE CIPROFLOXACIN: PREPARATION, CHARACTERIZATION, AND INFLUENCE OF SIZE ON CELLULAR UPTAKE”	80

6.3. PAPER 3: “FARNESYLATED GLYCOL CHITOSAN AS A PLATFORM FOR DRUG DELIVERY: SYNTHESIS, CHARACTERIZATION, AND INVESTIGATION OF MUCUS–PARTICLE INTERACTIONS”	97
6.4. PAPER 4: “SQUALENYL HYDROGEN SULFATE NANOPARTICLES FOR SIMULTANEOUS DELIVERY OF TOBRAMYCIN AND ALKYLQUINOLONE QUORUM SENSING INHIBITOR TO COMBAT <i>P. AERUGINOSA</i> BIOFILM INFECTIONS”	111
6.5. PATENT APPLICATION: “EXCIPIENT-FREE NANO-ASSEMBLIES OF AMINOGLYCOSIDE ANTIBIOTIC AND FARNESYL QUORUM SENSING INHIBITORS FOR COMBATTING BACTERIAL BIOFILM INFECTIONS”	123
6.5.1. <i>Proof of European Patent Application</i>	124
6.5.2. <i>Proof of International Patent Application</i>	125
6.5.3. <i>Summary of the invention</i>	127
7. LIST OF PATENTS, PUBLICATIONS, ORAL AND POSTER PRESENTATIONS	140
8. ACKNOWLEDGEMENTS	145
CURRICULUM VITAE	147

I. SUMMARY

Drug delivery systems (DDS) have the capacity to overcome biological barriers limiting the bioavailability of inhaled anti-infectives. This is important to eradicate bacterial infections and to prevent the development of bacterial resistance. Despite substantial efforts in the field, the current state-of-the-art often fails to achieve those goals, and we still observe an increase in bacterial resistance. In the context of drug delivery of pulmonary anti-infectives, this work proposes three novel strategies (i) polyplexes based on natural polysaccharides (starch, chitosan and cyclodextrin), (ii) self-assembly of amphiphilic excipients (farnesylated chitosan, squalenyl hydrogen sulfate), (iii) innovative excipient-free nano-assemblies of aminoglycoside antibiotics and farnesyl quorum sensing inhibitors. The latter invention allows an exceptional 100% co-loading capacity of established antibiotics and innovative pathoblockers without the need of any additional excipients. The biofilm eradicating efficacy of such DDS increased 16-fold compared to free actives. Finally, the interaction between the DDS and some important pulmonary biological barriers, such as biofilm, mucus, and macrophages, was also investigated. The knowledge gained in this thesis advances the research in pulmonary anti-infectives delivery beyond the state-of-the-art.

II. ZUSAMMENFASSUNG

Drug Delivery Systeme (DDS) haben die Fähigkeit, biologische Barrieren zu überwinden, welche die Bioverfügbarkeit inhalierter Antiinfektiva begrenzen. Dies ist wichtig, um bakterielle Infektionen zu beseitigen und die Entwicklung bakterieller Resistenz zu verhindern. Trotz erheblicher Anstrengungen auf diesem Gebiet werden diese Ziele vom derzeitigen Stand der Technik oft nicht erreicht, und wir beobachten immer noch eine Zunahme der bakteriellen Resistenz. Im Rahmen der pulmonalen Wirkstofffreisetzung von Antiinfektiva werden in dieser Arbeit drei neue Strategien vorgeschlagen: (i) Polyplexe auf der Basis natürlicher Polysaccharide (Stärke, Chitosan und Cyclodextrin), (ii) Selbstorganisations-Partikel aus amphiphilen Hilfsstoffen (farnesyliertes Chitosan, Squalenylhydrogensulfat), und (iii) innovative Hilfsstoff-freie Nano-Assemblies aus Aminoglycosid-Antibiotika und Farnesyl-Quorum-Sensing-Inhibitoren (QSI). Die letztgenannte Erfindung ermöglicht eine bemerkenswerte 100 %-ige Beladung, da sowohl das Antibiotikum als auch der Pathoblocker QSI Wirkstoffe darstellen und keine Hilfsstoffe mehr benötigt werden. Ein solches DDS verbessert die Biofilm-Elimination 16-fach im Vergleich zur Behandlung mit freien Wirkstoffen. Abschließend wurde die Interaktion zwischen den DDSs und einigen wichtigen biologischen Lungenbarrieren, wie Biofilm, Schleim und Makrophagen, untersucht, was die Forschung im Bereich der Verabreichung von pulmonalen Antiinfektiva weiter über den Stand der Technik hinaus vorantreibt.

III. ABBREVIATION

MIC	Minimum inhibitory concentration
PA	<i>Pseudomonas aeruginosa</i>
QSI	Quorum sensing inhibitor
APIs	Active pharmaceutical ingredients
NPs	Nanoparticles
DDS	Drug delivery systems
LC	Loading capacity
EE	Encapsulation efficacy
MBEC	Minimum biofilm eradicating concentration
PLGA	Poly lactic-co-glycolic acid
PVA	Polyvinylalcohol
Sq	Squelenenyl Hydrogen Sulfate
SqNPs	Squelenenyl Hydrogen Sulfate nanoparticles
QSI	Quorum sensing inhibitor
Pqs	<i>Pseudomonas</i> quinolone signal
PPGAS	Proteose peptone glucose ammonium salt medium
Tob	Tobramycin
FDA	US Food and Drug Administration
Cryo-TEM	Cryo-Transmission Electron Microscopy
CLSM	Confocal Laser Scanning Microscopy

1. INTRODUCTION

1.1. Antibiotics utilities in combatting infection and benefits of local delivery

Bacteria are present all around us. Most of them, e.g. bacteria in the intestines, are harmless and actually helpful; while others can cause infections, once they enter and colonize the host. Bacterial infectious diseases in humans, caused by dangerous pathogens, e.g. *Staphylococcus* (1,2), *Enterococcus* (3), *Pseudomonas aeruginosa* (PA) (4,5), etc., account for a significant proportion of global mortality (6–9). In most cases, infected patients are treated with powerful antibiotics that are generally safe in fighting infectious diseases. Antibiotics are most preferably administered orally and/or intravenously (10,11). For the treatment of chronic infection, in particular, administration pathways with the high doses of antibiotics are frequently employed. Despite good therapeutic efficacy against infection, systemic delivery of antibiotics has some disadvantages:

- (i) Adverse drug effects as well as cumulative and acute toxicity might occur with repeated use of antibiotics at high doses (12,13). The effects are unexpected reactions of living systems to antibiotics, e.g. repeatedly administering high doses of tobramycin could cause acute/chronic toxicity, a reduction in glomerular filtration (14–16).
- (ii) Taking and/or accumulating antibiotics unnecessarily in body sites without infection could lead to the development of antibiotic resistance, which further causes the impotency of antibiotics against bacteria (17).
- (iii) Most importantly, the poor bioavailability of antibiotics in the infected region, which leads to sub- minimum inhibitory concentration (MIC), would cause fast resistance development (17,18).

While adverse drug effects could be avoided by careful prescription of antibiotics (17,19), antimicrobial resistance has become one of the most pressing health threats. Infections from resistant bacteria are now too common, and some pathogens have even become resistant to multiple classes of antibiotics (7,17,20). Table 1 summarizes the timeline of the discovery, introduction and observed resistance for antibiotic classes used to treat infections. Few new drug classes have been discovered and approved for clinical

use since the discovery of penicillin, a member of the β -lactams class. In most cases, antimicrobial resistance has been observed shortly after the discovery of antibiotics, in some cases even before the year of introduction (21–23). This problem might be primarily caused by incorrect and uncontrolled utilizations of these antibiotics.

Table 1. Timeline of the discovery, introduction and resistance observed of antibiotics (17,22,23)

Antibiotic class	Year of discovery	Year of introduction	Year of resistance observed
β -Lactams	1928	1938	1945
Sulfadruugs	1932	1936	1942
Aminoglycosides	1943	1946	1946
Tetracyclines	1944	1952	1950
Chloramphenicols	1946	1948	1955
Macrolides	1948	1951	1955
Fidaxomicin	1948	2011	1977
Glycopeptides	1953	1958	1960
Oxazilidinones	1955	2000	2001
Rifamycins	1957	1958	1962
Quinolones	1961	1968	1968
Streptogramins	1963	1998	1964
Lipopetides	1986	2003	1987
Diarylquinolines	1997	2012	2006

Amongst the bacterial resistance problems, gram-negative pathogens are particularly vexatious. The most severe gram-negative infections and common pathogens are *Enterobacteriaceae*, *Pseudomonas aeruginosa* (PA), and *Acinetobacter*, as these strains are becoming resistant to nearly all anti-infective drugs that would be considered for treatment (7). The same holds true, at least to some extent, for some of the gram-positive pathogens, e.g. *Staphylococcus* and *Enterococcus* (6). The challenges in combatting gram-negative pathogens are: (i) they are, in particular, highly efficient at

keeping out drugs using their naturally sophisticated cell-wall structure. On the one hand, the outer membrane is a barrier for amphiphilic compounds which are usually necessary for water-solubility and penetrating the cytoplasmic membrane (24,25). The multidrug-resistant pumps, in addition, extrude any compounds that cross the outer membrane and chemically recognize unrelated molecules based mainly on polarity, preferring amphiphilic molecules (26,27). On the other hand, the penetration of hydrophilic actives is restricted by the inner membrane (25,28). (ii) Moreover, bacterial mutations which change the targeted hits of antibiotics cause inactivation of antimicrobial agents (29) and the possible production of antibiotic-degrading and/or antibiotic-inactivating enzymes which could also account for resistance development (20,30). Consequently, these naturally biological properties result in tight barriers that help gram-negative bacteria becoming resistant.

As indicated in Figure 1, the site of action of currently approved antibiotics is either located at the bacterial cell envelope or somewhere in the bacterial cytoplasm (9,22,31). It is hence important that the antimicrobial molecules reach their target at high concentration to possibly overcome the low drug susceptibility. As a result, topical delivery of antibiotic, such as e.g. in case of inhalation aerosols for the treatment of pulmonary infections, may be postulated to have two major advantages: First, higher drug concentrations at the infected body site will lead to more effective bacterial killing and decrease the risk of resistance development. Secondly, a reduced exposure at non-infected body sites will reduce the risk of adverse drug effects, in particular compared to systemic drug delivery (32–34).

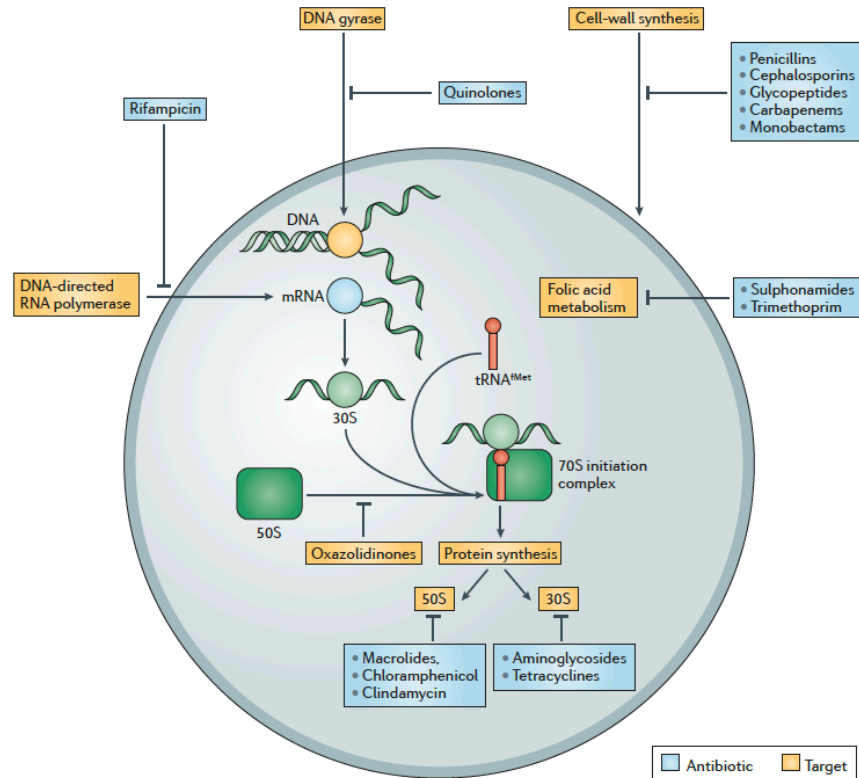


Figure 1. Targets of antibiotics: The three most successful antibiotics hit targets including (i) the ribosome (which consists of 50S and 30S subunits), (ii) cell wall synthesis, (iii) and DNA gyrase or DNA topoisomerase. Reprinted with permission from Reference (22)

1.2. Challenges in pulmonary infection treatment and in finding solutions

Considering pulmonary infection, in particular, *Pseudomonas aeruginosa* – the opportunistic bacterial pathogen, is one of the leading causes of nosocomial infections worldwide (35). This pathogen is ranked the second most prevalent among the gram-negative pathogens reported to the National Nosocomial Infection Surveillance System (17,36). Besides causing acute infections, PA is also accountable for debilitating chronic lung infection in immunocompromised patients, and is the most commonly isolated pathogen in cystic fibrosis sufferers, and is considered the leading cause for morbidity and mortality in such patients (37,38). Inhaled therapy has been reported as the most effective treatment for those mentioned respiratory bacterial infections due to the locally increasing relevance of drug bioavailability (34,37). As a result, inhalation of antibiotics has been reported to reduce the frequency of exacerbations, decrease significantly airway bacterial density, recover pulmonary function, and most importantly improve quality of life for

patients with pulmonary infection (39). However, the current inhaled antibiotics are not showing the maximum therapeutic efficacy to eradicate bacterial infection entirely, as they still face some limitations and challenges:

- (i) Enhancing drug bioavailability in the lungs by inhalation, however, still requires sufficient water solubility (40). This is especially true if we consider that the total volume of the pulmonary lining fluid is rather small (approx. 150ml) and distributed as a rather thin liquid film, (not more than 30 μm) over the rather large epithelial surface area (140 – 160 m^2) (41–43). At the same time, the relative low potency of inhaled anti-infectives requires the delivery of rather high doses (up to several 100mg) in comparison to e.g. bronchodilators or corticosteroids for the inhalation therapy of asthma or COPD. For this reason, the water solubility of inhaled anti-infectives is essential and highlights the need to design strategies to enhance water solubility significantly. This objective is the subject of ongoing discussions in the context of a pulmonary biopharmaceutics classification systems (PBCS) (40).
- (ii) While increasing drug solubility in the pulmonary lining fluid is a problem on its own for poorly water-soluble antibiotics, it is also essential to maintain the concentration of drug in this compartment above the MICs as long as possible (44). This again, however, is restrained by systemic absorption across the air-blood barrier, in addition to the efficient clearance mechanisms of the lungs, e.g. mucociliary (45) and macrophage clearance (46). Furthermore, the repeated use of high doses of antibiotics without controlled release and nonspecific targeting at the lung site would also induce toxicity to healthy lung cells (47,48).
- (iii) In the past years, clinical studies have revealed that the current inhaled antibiotic formulations could only be fully proficient in termination of the spread of the pathogen and reduction in the demolition of the airway tissues (49). As a gram-negative pathogen, PA is naturally resistant to many antibiotics due to the reasons mentioned above. Moreover, pulmonary PA infections are complicated by the formation of PA biofilms. The latter are multiple-cellular surface-attached and spatially oriented bacterial communities (described in Figure 2), composed

of bacterial cells in high metabolic outer regions and low metabolic/persister central regions which are crucially accountable for the development of PA resistance (50–52). As discussed in Figure 1, the antibiotics exert their mechanism of actions most efficiently on metabolically active bacterial cells (22); as a result, the persister bacterial cells in the dormant regions of biofilms foster the survival of biofilm and the recurrent infection. Furthermore, the structure of extracellular matrix in a biofilm, which is mainly composed of alginate, extracellular polymers, lipids and DNA, displays a significant barrier to the penetration of antimicrobial agents (53–55). For instance, the effectiveness of aminoglycosides, in particular tobramycin – a positively charged antibiotic, which is widely used as a first-line therapy in the cystic fibrosis infections – is provenly decreased by the strong interaction between the drugs molecules and the biofilm materials, causing slow and incomplete penetration of the drug into the biofilm matrix (55,56). Besides, the low pH in the surrounding infected environment and in the biofilm would promote the drug molecules, e.g. ciprofloxacin, to interact with alginate by charge interaction, which further causes the remarkable reduction in drug concentration at the action site (57). Consequently, the antibiotic concentrations will be hardly above the MIC, promoting mirco-environmental pressure and further fostering the biofilm formation, as well as generating drug-resistant bacterial sub-populations.

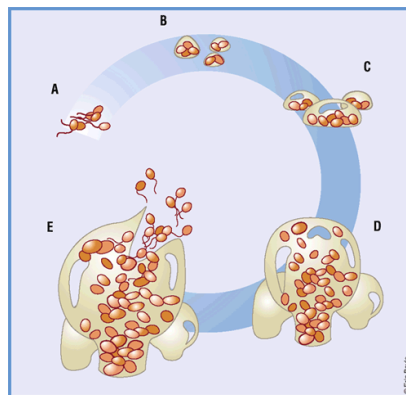


Figure 2. Biofilm development (A) Planktonic bacteria attach reversibly to surface (B) irreversible adhesion to the surface, and effect of quorum sensing begins (C) Maturation

phase: micro colony formation (D) extracellular matrix synthesis and biofilm maturation to reach maximum thickness (E) Dispersion/Migration of planktonic bacteria from biofilm matrix. Reprinted with permission from Reference (50).

In the pulmonary air space, the epithelia are covered with a layer of mucus which has hydrogel-like structure mainly composed of water, mucins (glycoproteins), DNA, proteins, lipids, and cell debris (58). This mucosa represents the first landing spot and the primary site of entry for pathogens to interact with and colonize the host tissues (59). Despite its barrier functions, mucus only insufficiently protects the exposed epithelia from external threats like pathogen colonization (59,60). Neutrophils, macrophages, dendritic cells, natural killer cells, e.g. T and B lymphocytes, glycoproteins, effector peptides and proteins, e.g. defensins, complement, C-reactive protein, as well as pro-inflammatory chemokines and cytokines, which are of the innate and adaptive immune systems, are usually contained in mucosal epithelia to serve as host immune response to infections (59). Once the pathogen, however, surpasses these naturally defending systems, the mucosa is in part hypothesized as a possibly superior environment for bacterial infection and resistance development (61). Notably, the thick and sticky mucus build-up in the lungs makes cystic fibrosis sufferers more apposite to the fast development of bacterial infections that could last for a long time. Although it is recognized in the clinic, the understanding of mucosal biofilm structure and behaviors of bacteria persist in mucosal biofilms are not fully revealed. Nevertheless, it has been recognized that mucus-embedded biofilms persist for decades and cannot be wholly eradicated (62). One might simply hypothesize that the naturally negatively charged matrix of mucus in addition to the extracellular matrix of biofilm would form a physically stronger barrier which might highly prohibit the penetration of antibiotics to the site of action (56,62,63). As a result of such embedment, the mucosal biofilm is an even harder-to-treat infection that conventional inhaled therapy could not completely eradicate.

- (iv) Despite a variety of available potent antibiotics, the attraction of clinical benefits as well as the aggressive therapeutic development and drug discovery, there is only a limited number of antibiotics that are approved as inhaled therapy for the treatment of pulmonary infections (34,44,64). Considering PA infections associated in cystic fibrosis patients which are considered as a severe disease, there are just four inhaled antibiotics which are approved for clinical use in Europe, including colistin (and its prodrug), tobramycin, levofloxacin, and aztreonam (their structures are depicted in Figure 3) (64,65). Moreover, there is just a finite number of drugs undergoing clinical trials for treatment pulmonary infections in general. This slows down the progress in developing novel anti-infectives (22), although the fact that clinical studies need tremendous efforts, supports and time, is accepted. As a consequence, it remains challenging to combat with infection considering the limited portfolio of alternative antibiotics once pathogens become resistant to one drug (64).

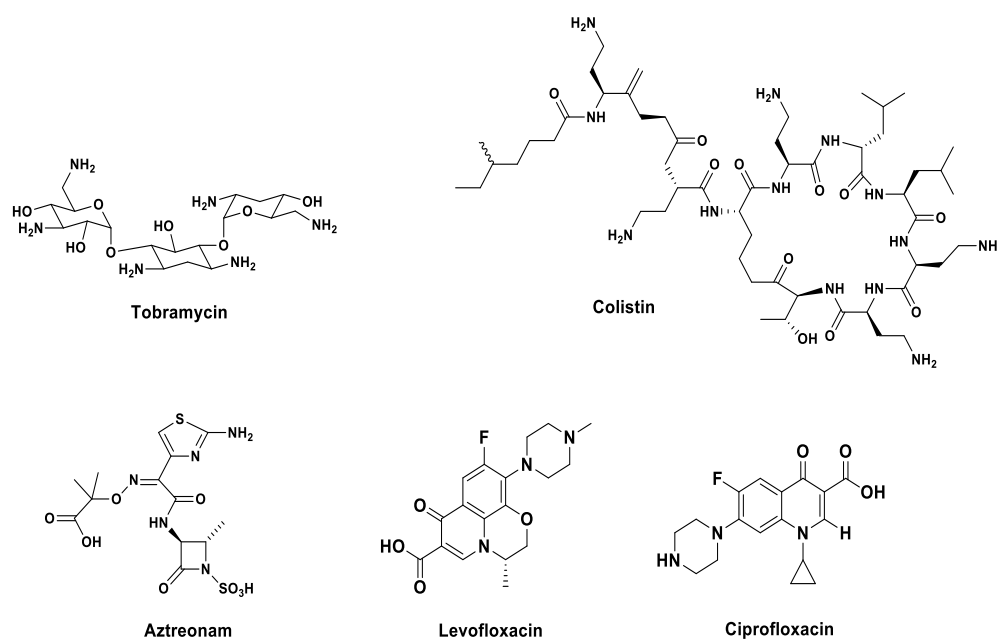


Figure 3. Structure of approved inhaled antibiotics for treatment of pulmonary infection in cystic fibrosis patients in Europe: colistin, tobramycin, levofloxacin, aztreonam. Ciprofloxacin has been being studied in clinical trials.

Having considered the recognized challenges and knowledge gaps in combatting antimicrobial resistance pathogens, scientists have proposed and been working on different approaches to discover effective strategies to overcome or at least slow down the resistance development, which in overall means to improve the life quality of the patients. There are significant efforts in finding new antimicrobials and strategies for therapeutic improvement of the approved antibiotics which are summarized in Figure 4.

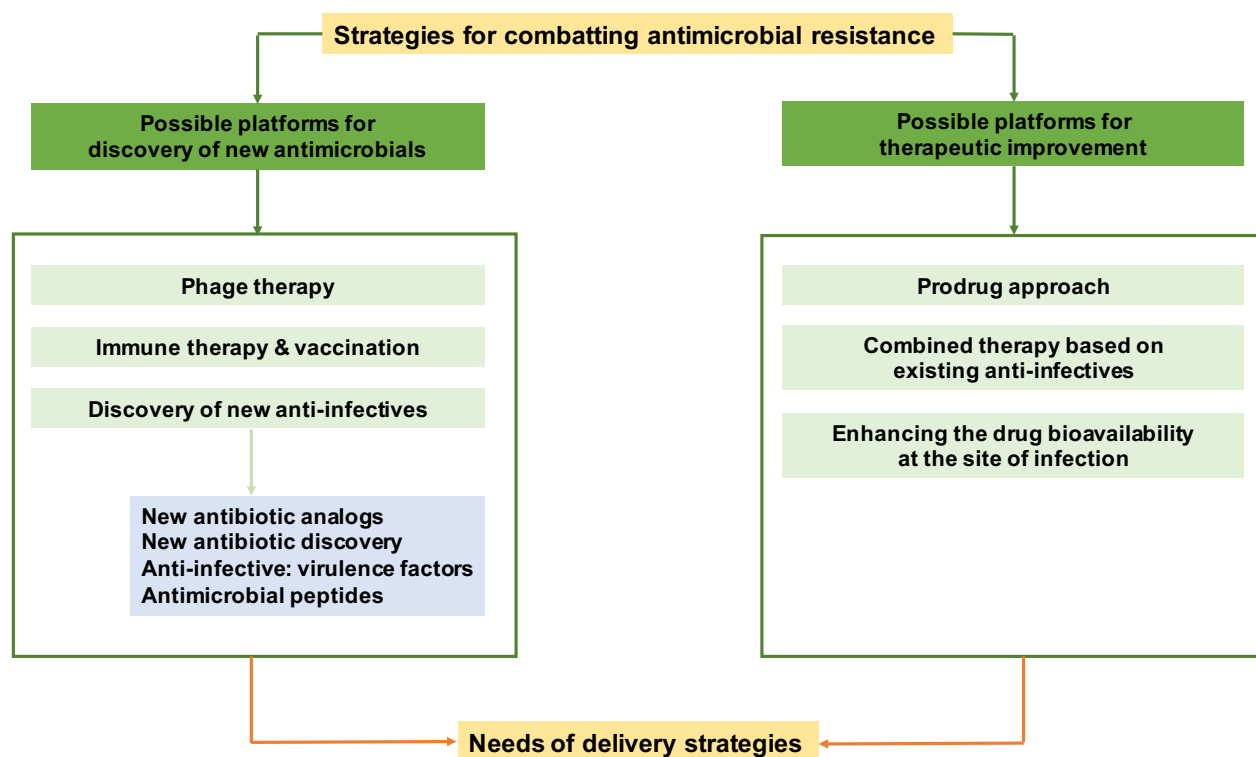


Figure 4. Flow chart indicates different strategies for combatting antimicrobial resistance, and the needs of delivery strategies.

On the one hand, the new antimicrobials have been discovered by using a variety of advanced approaches, including phage therapy, immune therapy, and vaccination, as well as discovery and synthesis of new anti-infectives based on newly discovered and existing platforms. In general, these pathways mainly aim to obtain more potent agents which could have better drug bioavailability at the site of action by better penetration through the bacterial cell wall and the surrounding environmental barriers, e.g. biofilm, cellular membrane (22,66–69). These discovered actives also aim to have species-

specific targets that would be selective and sensitive to specific bacteria, and be safe to the healthy tissues, in agreement with the pioneering concept postulated by Erlich in 1906 who had referred to targeted drugs as 'magic bullets'. Nevertheless, as stressed by R. Duncan (1997), the development of targeted drugs is inevitably lengthy process, and breakthroughs are more frequently a dream rather than reality' (70). One of the important reasons is that there is a limited number of exploited targets, out of nearly 200 conserved, vital proteins in bacteria, has been discovered and considered effective targeting for antibiotics (22), described in Figure 1.

Despite the intensive focus on the discovery of new antimicrobials, the therapeutic value of such agents still has to be demonstrated clinically (22). And it is true that there is a very finite prospect of successfully discovering and bringing an antimicrobial from leading agent identified in preclinical studies (22). In most of cases, the antimicrobials have been designed to eradicate infection by interfering with bacterial growth, which intrinsically will put stress on bacteria and therefore might quickly lead to resistance development (71). Consequently, the approach would again have to deal with the existing challenges recognized from approved antibiotics. Taking a different view, the concept of pathoblocker such as e.g. quorum sensing inhibitors (QSI) may be considered as a promising strategy to overcome the growing and challenging resistance problem. The QSI would not interfere with bacteria growth and therefore avoid the stress caused by antibiotics that leads to resistance. Instead they just would prevent the biofilm formation by inhibiting the bacterial communications via quorum sensing and signal transduction systems which are suggested to mediate drug resistance (72). Upon being treated with QSI, the biofilm structure would not grow strongly. The bacteria would thus be prevented to form persister cells, and be more sensitive to antibiotics. The approach has shown some promising results in previous studies, especially when combining with approved antibiotics the efficacy against bacterial biofilm has been increased significantly (73,74). Still, however, most of the discovered QSI compounds have poor water-solubility which limits the bioavailability and thus therapeutic efficacy of these molecules, and also impedes their administration, also by way of inhalation (75).

On the other hand, being attracted by the obvious clinical benefits of the available approved antibiotics, scientists have been trying to improve the therapeutic efficacy of those compounds to overcome the bacterial resistance. Based on the approved agents, prodrugs which would only act in the targeted site have been synthesized (22,76). This approach has been expected to prevent the toxicity caused by the antibiotic itself, like e.g. for colistin and some of its prodrugs (77,78). The reduction in resistance development has, however not been convincingly proved. Alternatively, combining antibiotics which would hit different targets is hypothesized to overcome the significant antibiotic tolerance that individual antibiotic therapy often fails, is another strategy to eradicate a broad spectrum (79–82). Moreover, to enhance the drug concentration directly at the action site, breaking the biological barriers such as mucus by using mucolytic N-acetylcysteine has been also considered and successfully applied (83,84). These approaches require the concurrent administration and action of such compounds. However, these aims remain challenging to be achieved due to the differences in physicochemical properties and pharmaceutical characteristics of the active pharmaceutical ingredients (80).

Taking together the discussions above, there are a variety of approaches, progress and remaining limitations in the discovery and development of strategies against antibiotic resistant bacterial infection. Either focusing on the discovery of new antimicrobials or improving the therapeutic effects of the available, approved compounds, one crucial factor to move forward in combating bacterial resistance is enhancing the bioavailability of the drugs at the infection site. Thus, there is a need for efficient delivery strategies which could accomplish the correctly sustained distribution of antimicrobials in the infected regions at a high concentration.

1.3. Drug delivery systems aim for pulmonary infections treatment

1.3.1. Advantages of drug delivery systems in pulmonary infections treatment

As discussed above, the pulmonary delivery of antibiotics has shown increasing relevance for the treatment of respiratory bacterial infection compared to the conventional administrations of antibiotics, including oral and intravenous administrations. The method also offers less risk of systemic serious adverse effects and an improvement of the antibiotics bioavailability and bio-distribution in the targeted lung sites. The hypothesis

seems to be promising, but the pulmonary delivery of drugs is in general challenging due to the mentioned reasons. To address those problems, appropriate formulations of drugs with pharmaceutical excipients, which are later considered as drug delivery systems (DDS), are hence required.

The drug formulating strategies are usually defined depending on the physiochemical properties of drug molecules and their intended application. In general, the delivery systems would first address the limitations in therapeutic efficacy observed in many currently used and discovered active pharmaceutical ingredients (APIs) which are due to (i) the poor water-solubility, (ii) problem in delivering the molecules to biological environment (e.g., reduced in vivo half-life/stability), and (iii) the potential to induce high toxicity (85,86). In the field of drug delivery, nanotechnology has particularly attracted remarkable attention, which means to engineer drug-loaded nanostructures and nanomaterials with a size range between 10 and 1000 nm for the improvement of APIs performance (87). As a consequence, this “tiny-technology” would increase the water-solubility of poorly water-soluble drugs, and also protect unstable molecules from degradation in the presence of enzymes, as well as minimize the possible adverse effects by encapsulating the drugs into small vehicles (88). Considering pulmonary administration, the utility of nanotechnology for antibiotics delivery would not only increase the drug solubility of poorly water-soluble drugs in the thin pulmonary lining fluid, but also prevent the fast drug-clearance. The latter is of particular impact for hydrophilic drugs due to the systemic absorption across the air-blood barrier, and moreover the efficient clearance mechanisms of the lungs, including mucociliary clearance and alveolar macrophages (89). Thus, the drug bioavailability at the site of infection is improved. The binding properties of drug molecules to the pharmaceutical excipients and thus release from the nanocarriers would be tuned by linkages between drug molecule-materials, chemically designing the structure of the excipients, and method of preparing the drug-loaded carriers. In addition to the achievement of temporal and spatial site-specific delivery, nanomedicine hence allows the administration of a sustainably sufficient dose in a controlled release manner (90–92). Especially for the delivery of antibiotics, their concentration would be maintained above the MIC values for longer time (44). The design and engineering of excipients used in nanomedicine would further offer better affinity

towards the bacterial cell envelope. More importantly, despite the controversy and lack of clinical evidence, nanomedicine is believed to improve drug transport across biological barriers, e.g. biofilm and/or mucus, to deliver drugs more directly to the persister bacteria, which would possibly improve their antibacterial activity, and reduce the potential of bacterial resistance and recurrent infections (93,94). Lastly, nanomedicines could be designed to efficiently deliver established or emerging drug molecules, or even a combination of different functional actives in a targeted manner, which is so-called multifunctional carrier systems (an example of the carrier structure is shown in Figure 5). This flexibility of nanotechnology in drug delivery offers additional possibilities to combat bacterial resistance, and in particular pulmonary bacterial infections. The advantages of using DDS is summarized in Figure 5.

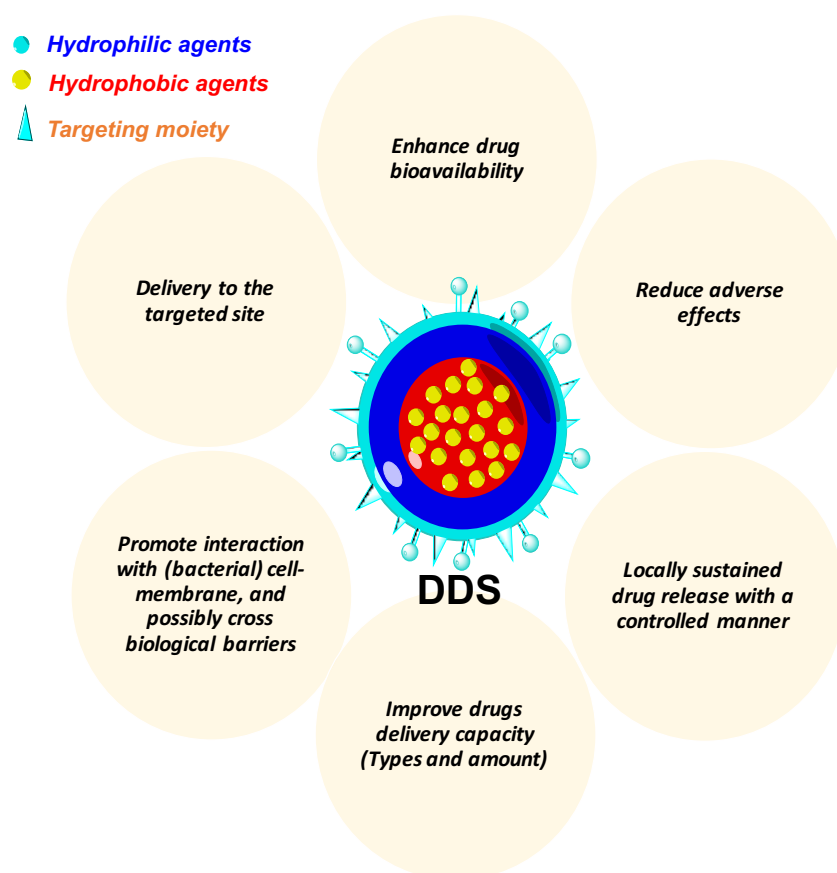


Figure 5. Advantages of drug delivery systems.

1.3.2. Requirements in preparation of drug delivery systems

The approach of using DDS is to improve the therapeutic efficacy of drugs which would further aim to transfer the technology closer to clinical use. Thus, it is important to firstly develop strategies that have capacity to improve drug bioavailability, which means that the carrier systems can encapsulate drug at high loading capacity (w/w ratio, the calculation is shown in equation (i)) and good encapsulation efficacy (the calculation is shown in equation (ii)). Furthermore, the carrier systems should also allow the simultaneous delivery of diverse active cargoes which would provide complementary therapeutic effects (95,96). The flexibility for further modification of the systems should also be enabled to potentially enhance the interaction and affinity with the targeted sites of infections (88,97). Those kinds of functionalization are also good approaches to even more reduce the risk of adverse effects. Most importantly, the materials that are used for the preparation of such carriers should be nontoxic and biodegradable which are cleared after it fulfilled the function in vivo (83,98–102). As have been discussing, there are many challenges in pulmonary delivery of drugs, and using DDS would help to solve those pronounced problems. As a consequence, the more sophisticated systems should be developed to fulfill all requirements that would finally help improve the therapeutic effects of drugs. Although nanotechnology is in general one such avenue – a scientifically diverse discipline that encompasses engineering, materials science, physics, chemistry, and the biological sciences, its use in the field of drug delivery has been remarkably developing, which has proposed plenty of strategies for preparing DDS (103,104). Remarkably, the focus in this field has been shifted from making just simple drug-loaded carriers to engineer the carriers with new desired properties to better control the delivery profile and overcome biological barriers, have specific targeting action and even for imaging, thus rendering them attractive for treating applications. However, the number of nanomedicines that are marketed is indeed finite, as those sophisticated systems often fail to move closer to preclinical studies due to the complexity of the producing procedure. In addition to that, the reproducibility of multi-functionalization of the carrier system, which would offer a better therapeutic efficacy, is hard to achieve at large scale production. And it is no doubt that the price for such advanced development could not be competitive compared to the established therapy (105,106). Figure 6 depicted the general

requirements in the development of DDS. To have good DDS, there should be a compromise between the pharmaceutical and engineering requirements in the selection of materials. Thus, the search for the pharmaceutical excipients used in DDS which qualify all requirements still remained challenging. Especially, it is even harder in the development of anti-infectives delivery systems, as the high dose of such drugs are frequently required (106). Therefore, it is necessary to have the facile strategies that use conventional materials for developing high antibiotic loading capacity carrier systems, and that still allows the further modification for the advanced therapeutic improvement.

The advantages of DDS would profoundly improve the therapeutic effect once the drug loading capacity of such carriers is achieved at a high level. Having in mind that the active cargos should be delivered not materials, the optimization of drug loading capacity is critical to consider in the process of developing DDS.

The drug loading capacity (LC%) and encapsulation efficacy (EE%) are calculated as the equations below:

$$EE\% = \frac{\text{Weight of encapsulated drug in NPs}}{\text{Initial weight of used drug}} \times 100 \quad (i)$$

$$LC\% = \frac{\text{Weight of drug in NPs}}{\text{Weight of NPs}} \times 100 \quad (ii)$$

“Weight of NPs” was calculated as (Weight of NPs = Weight of polymeric materials + Weight of encapsulated drug in NPs).

On the one hand, the EE% indicates the efficiency of the drug loading procedure, which is important in planning the amount of drug used in loading procedure so that the amount of un-loaded and thus wasted drug would be minimized. On the other hand, the LC% demonstrates the actual drug amount in comparison to the actual total weight of the whole DDS, which is needed in calculating the dose when using the drug-loaded DDS in treatment. Notably, the LC% is crucial in pulmonary delivery, since only a finite dose can be applied to the lung, e.g. by inhalation of dry powder. While EE% is rather easy to maximize by optimizing the initial in-put drug amount, the achievement of LC% at high value remains challenging resulting in less chance to move on in preclinical studies. Thus, LC% is one of the first factors that need to be improved to obtain a good DDS.

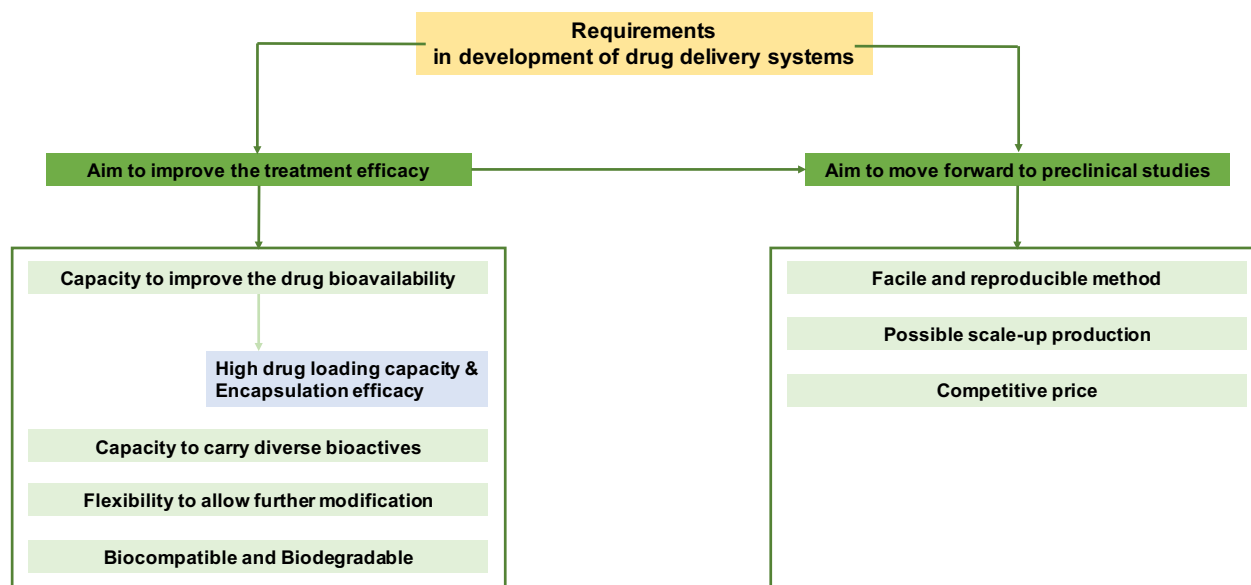


Figure 6. General requirements in development of drug delivery systems.

1.3.3. Recent development of anti-infective delivery systems for pulmonary infections treatment

Recognizing the advantages of local delivery, inhaled antibiotic therapy has been used to treat chronic respiratory infection since the 1940s (107). The earliest formulation was not explicitly designed for inhalation, so it caused significant bronchial irritation. A major advancement of such development took place in 1997, when the FDA first approved a designed formulation for inhalation, which was tobramycin for use in PA infected patients with cystic fibrosis (108,109). The approach has shown significant clinical benefits. Subsequently, dry powder formulations, which are kinds of DDS, were developed to enhance the delivery of antibiotics to the lungs sites (110). This strategy allowed to notably decrease the dose of antibiotic per application (111). This development has been considered as a very promising approach to have a safer profile when using antibiotics and also avoid the fast resistance development. And the interest in the use of such formulation has been not only for infections associated with cystic fibrosis, but also for other lower respiratory tract infections (112,113).

In this thesis, only respiratory PA associated infection and strategies for the treatment of such diseases will be focused on. The most common dry powder inhalation

antibiotics considered for PA infection are tobramycin (110) and colistin (113). The dry powder form of ciprofloxacin has also been investigated in a phase III randomized study and appeared to be favorable for the treatment of pulmonary PA infections (114). However, in many severe and resistant infected cases, e.g. infections associated with cystic fibrosis patients, the efficacy of the dry powder, in particular tobramycin dry powder, is still limited by the ability to achieve sufficient concentration levels at the site of infection (115). It is noted that the drug loading capacity of the dry powder antibiotic, in particular in the case of tobramycin, is really high at ~50% (w/w ratio) (116,117). Hence, this consequence can be attributed by rapid clearance of the drug as well as the poor mucus and biofilm penetration and inactivation of the drug through binding interactions in these environments. Those problems could be explained by the typical particles size of dry powder antibiotics produced mostly by spray-dry technology which is frequently in micron range (1-10 μm) and not uniform (116). Therefore, novel strategies for improving antibiotic delivery could enhance the activity of those vital antibiotics. In addition to developing the delivery systems for those available, potent antibiotics, there are chances to combine into the delivery systems novel anti-infectives by taking advantages of recent drug delivery techniques to even better enhance the therapeutic effects of the established antibiotics.

As discussed above, although nanotechnology has been aggressively pursued in drug delivery, simple approaches for drug delivery should still be advanced with the aim to achieve higher and faster rate of translation into clinical use. There is an uncountable number of studies aiming to prepare the vital antibiotics loaded carrier systems. The popular carrier systems used are (i) liposome (118,119); (ii) microemulsions and nanoemulsions (118); (iii) solid lipid NPs (23,120); (iv) polymeric particles, including particles made from synthetic polymers, e.g. silica particles, poly lactic-co-glycolic acid (PLGA) particles, as well as made from natural polymers, e.g. chitosan derivatives, alginate (89,121–123). Metallic NPs, e.g. silver, gold, titanium dioxide NPs, are known to have antimicrobial properties, and also widely developed and applied to prevent the bacterial colonization and eradicate biofilm infection (117). Considering the long-term administration, especially for inhaled therapy, these non-biodegradable materials are, however not preferred. Table 2 summarizes representatives of antibiotic-loaded liposomal and particulate systems that are developed for inhaled therapy to treat PA associated

infections. There is a vast number of publications concerning the preparation of antibiotic-loaded carrier systems, in which the EE% was reported carefully. LC%, one of the essential factors deciding the success of a DDS, was, however not explicitly reported. Thus, there are just some representatives shown in Table 2 with LC% presented as the maximum obtained values in the corresponding publications.

Table 2. Summary of representative delivery systems of inhaled antibiotics aimed for PA infections treatment. Drug, production method, major excipients and loading capacity (LC%) are highlighted. LC% is presented as the maximum value reported in the corresponding publications.

Summary of representative liposomal delivery systems of inhaled antibiotics aimed for PA infections treatment				
Drug	Production method	Major excipients	LC%	Ref.
Amikacin (Arikace®)	N/A ^(a)	N/A	~60%	(124)
Tobramycin	Membrane extrusion	1,2-Distearoyl-sn-glycero-3-phosphocholine, cholesterol	~60%	(125)
Ciprofloxacin (Lipoquin® and Pulmaquin®)	Membrane extrusion	Polysorbate 20, 0.4% (w/v), hydrogenated soy phosphatidylcholine, cholesterol	16-33%	(126)(127)
Colistin	Sonication/ Membrane extrusion	1,2-dipalmitoyl-sn-glycero-3-phosphocholine, cholesterol, 1-palmitoyl-2-oleoyl-sn-glycero-3-phosphocholine	12-55%	(128)
Summary of representative polymeric delivery systems of inhaled antibiotics aimed for PA infections treatment				
Drug	Production method	Major excipients	LC%	Ref.

Levofloxacin	Lipid-coated nanoparticles via an emulsification-solvent-evaporation method followed by spray drying	PLGA, phosphatidylcholine, leucine	PVA, L-	<1.1%	(129)
Tobramycin	Nanoparticle suspension by the emulsion/solvent diffusion method followed by spray drying	PLGA, alginate, lactose	PVA, chitosan,	<2%	(130)
Tobramycin	Polyplexes	Alginate, chitosan		<9%	(115)
Gentamicin	Emulsion/solvent diffusion	PLGA, PVA		<2%	(131)
Ciprofloxacin	Polyplexes	Chitosan, tripolyphosphate of sodium salt		<5%	(132)

^(a)N/A: not available

It is undoubted that liposomal carrier systems which could be prepared by conventional techniques actually capable of loading the high percentage of antibiotic, at maximum nearly to 60%. Such loading capacity is promising to improve the antibiotic bioavailability in the targeted sides which as a result benefits the therapeutic effect against infections. In addition to the better bioavailability, reported data pronounces that the adverse effects caused by antimicrobials in the lungs cells significantly reduced when using the drug loaded liposomes compared to free drugs inhaled as a solution. However, the antibiotic loaded liposomal formulation could only improve the therapeutic

effect slightly considering the decrease in MIC values. The retention time in the infected regions was not remarkably improved, which could be explained by the fast release of antibiotics from the liposomal formulation. In most cases, the cumulative antibiotics reached 100% in a biologically relevant medium in a short time ranged from 10 minutes to 2 h (133,134). This burst effect is often seen in most of the drug-loaded liposome due to the non-specific binding of drug molecules and liposomal excipients. A further modification, e.g. surface coating and/or crosslinking, would possibly prevent such problem. The approach in turn sometimes affects the stability of the system and actually complicates the mean of this conventional method (135,136). The same holds true for the antibiotic-loaded systems produced from microemulsions and nanoemulsions as well as solid lipid NPs technologies, but the LC% in these cases are not as high as ones obtained from liposomal formulations.

Polymeric NPs appear to be promising candidates to better prevent the burst effect as the binding between drug and excipients either covalently or noncovalently could be flexibly tuned by changes of polymer properties and particles preparation methods. The approach does show better controlled release profile of encapsulated drugs. Furthermore, polymeric carrier system would allow further modification with more desired properties of delivery systems, thus rendering them attractive for nanomedicines. Nevertheless, the LC% is a considerable limitation when using these DDS, which is in most cases lower than 5% (133). Consequently, the DDS based on this technique has still mostly remained in research.

Furthermore, the particle size is also a design parameter which can affect therapeutic effect of DDS. The importance of LC% is recognized, so optimizing such value might also increase the size of the carrier systems. Thus, while true nanomaterials are considered smaller than 100nm in size, the so-called submicron range (i.e., 100 – 900nm) is defined as size range for nanomedicine, which appears to provide the better opportunities to carry higher amount of drug (87). For such reason, the maximum recorded drug LC% in liposome and polymeric particulates usually have the sizes larger than 500nm, which is actually not favorable for crossing biological barriers, but at the same time becomes the target for the natural clearance mechanism (87,137). Thus, the

site-specific delivery of therapeutics will remain a distant reality unless drug carrier systems cross through the biological barriers, which is, in the case of extracellular infections, biofilm. Such biological barrier significantly contributes to the fails of those DDS.

Most importantly, those single antibiotic loaded carrier systems could in general not decrease the dose of antibiotic used in the treatment of infection, in some cases the dosage should even be increased. Thus, the recent status of antibiotic delivery would just decrease bacterial susceptibility, but it is still challenging to overcome the bacterial resistance development. Despite the pronounced limitations, the developed carrier systems have shown promising results in decreasing the viability of bacteria in biofilm, and such efficacy is better than the treatment with free antibiotics. Thus, there is the need to develop the better antimicrobial delivery systems for combatting with bacterial infections.

Taking advantages of DDS, the advanced development in nanotechnology, and the discovery of novel anti-infectives, some researches have been focusing on advancing the carrier system and/or developing strategies for efficiently co-delivery of diverse active agents, which consequently achieve the enhancement in complementary therapeutic effects. Among many research, there are some that could be highlighted including: (i) polymyxin B containing polyion complex nanoparticles in which polymyxin B was complexed with different molecular weight poly(styrene sulphonate), shown 10,000 times improvement in inhibitory effect against PA (138); (ii) the combination of tobramycin and mucolytic agent, dornase alfa (DNase) were achieved in a chitosan-alginate polyplexed system, such simultaneous delivery of the two active compounds improved the therapeutic effect of tobramycin in the contact with cystic fibrosis sputum (115); (iii) Bismuth-ethanedithiol, a biofilm reducer, and aminoglycoside tobramycin were co-loaded in a liposome system which shown a decrease of CFU counts in vivo in comparison to ones treated with free drug (125); (iii) Incorporation of farnesol, a natural quorum sensing inhibitor, and ciprofloxacin in a liposomal formulation exhibited a very interesting outcome. The minimum biofilm eradicating concentration (MBEC) value obtained by using the co-delivery system was reported at 0.128 $\mu\text{g}/\text{mL}$ of ciprofloxacin

which is actually same as the reported MIC value of ciprofloxacin for planktonic bacteria at 0.125 µg/mL (73). The results of these studies were promising and shown the possibility to reduce the use of antibiotic when applying them in a combination with other complementary agents, which is important to further prevent antimicrobial resistance. However, more relevant in vivo data which proves the complete infection eradication has been not reported yet. Furthermore, despite having a promising concept to combat with bacterial biofilm, those formulation characteristics, including the particulate characteristics (importantly the size and charge surface) and drug release profile, were actually not best optimized. Thus, such specific research area in developing nanotherapeutics has been recently attracting more attention in combatting resistant bacterial biofilm, which will be focused on this thesis.

1.3.4. Interaction between drug delivery systems and pulmonary biological barriers

Having discussed that the successful accumulation of either drug molecules or nanotherapeutics specifically at the diseased sites, thus restricting effective responses in disease processes is prevented by biological barriers. Particularly considering respiratory bacterial biofilm infection, the means of biological barriers that limit the drug transport are bacterial cell membrane, biofilm, mucus, mucosal biofilm, and the pulmonary immune regulators (139). The crucial biological barriers to inhaled DDS are depicted in Figure 7. As the ultimate aim is to treat biofilm infection and overcome the antimicrobial resistance, the antibiotic drug molecules should travel through all aforementioned barriers and be accumulated either in the bacterial membrane or in bacterial cytoplasm. However, the free drug molecules usually fail to fully accomplish the aim, the DDS is thus needed. Although considerable research efforts have focused on incorporating multiple surface functionalities and moieties within the overall NP design and preparation, many of these strategies fail to successfully address these barriers successfully. A reinterpreting of conventional drug delivery systems is thus needed to successfully negotiate these impediments to a single carrier system. By successively understanding and addressing each of these biological barriers, appropriate design features of drug delivery systems could be rationally incorporated that will create a successful generation of particulate-based drug delivery systems.

In drug delivery system features design, particulate size, surface properties and morphology and particles shape of are frequently tuned to aim for better penetration through the biological barriers (93). Ideally, the particles would successfully penetrate through such obstacles would have the characteristics, including (i) small size, the smaller the better for the transport. The destiny of the particulate system is to carry drug which as a consequence could not be too small, so the appropriate size range is in most of the cases considered below 200nm; (ii) anti-fouling surface which is covered with polyethylene glycol (PEG) or zwitterion materials; (iii) smooth surface morphology. With these requirements, spherical PEGylated NPs with size range below 200nm are known to have a high rate in transportation through biological barriers including mucus and biofilm. Moreover, the small size range and neutral charge surface would also be responded slowly by the immune systems, the systems would hence have a prolonged in vivo residence time (93). However, having PEGylated or zwitterionic surface would simultaneously lose or decrease the potential of drug loading on the surface. In addition to that, the small size range would limit the drug loading capacity in the core side of the particles. Hence, the design of biological barriers penetrating NPs should find a compromise with the loading capacity of such systems.

Considering more carefully, the mucosal epithelia, e.g. airway epithelia, are covered with a retentive viscoelastic mucus layer, a three-dimensional macromolecular network with the ability to entrap and remove NPs in a size-dependent manner and mucociliary clearance (58,140). Additionally, such mucus layer together with biofilm/mucosal biofilm could also interact and adsorb the particles as well as molecules via electrostatic interactions (58). Instead of fighting and overcoming these natural characteristics of mucus and biofilm/mucosal biofilm, those have been exploited as a method to prolong the residence time of DDS, in particular for positively charge NPs, e.g. chitosan based NPs as DDS in mucosal surface (141,142). The natural clearance is, in turn, inevitable when applying foreign particulate materials in vivo. The clearance rate is another important factor which decides in vivo residence time of the DDS. For those DDS used the as inhaled therapy, the key regulators of pulmonary immunity, e.g. lung macrophages and dendritic cells, should be carefully taken into consideration (137,143). Therefore, the dependence of macrophage uptake efficiency on particle size

and surface properties should be investigated and predicted in vivo. Thus, the future use of the drug-loaded carrier systems would be accurately recommended.

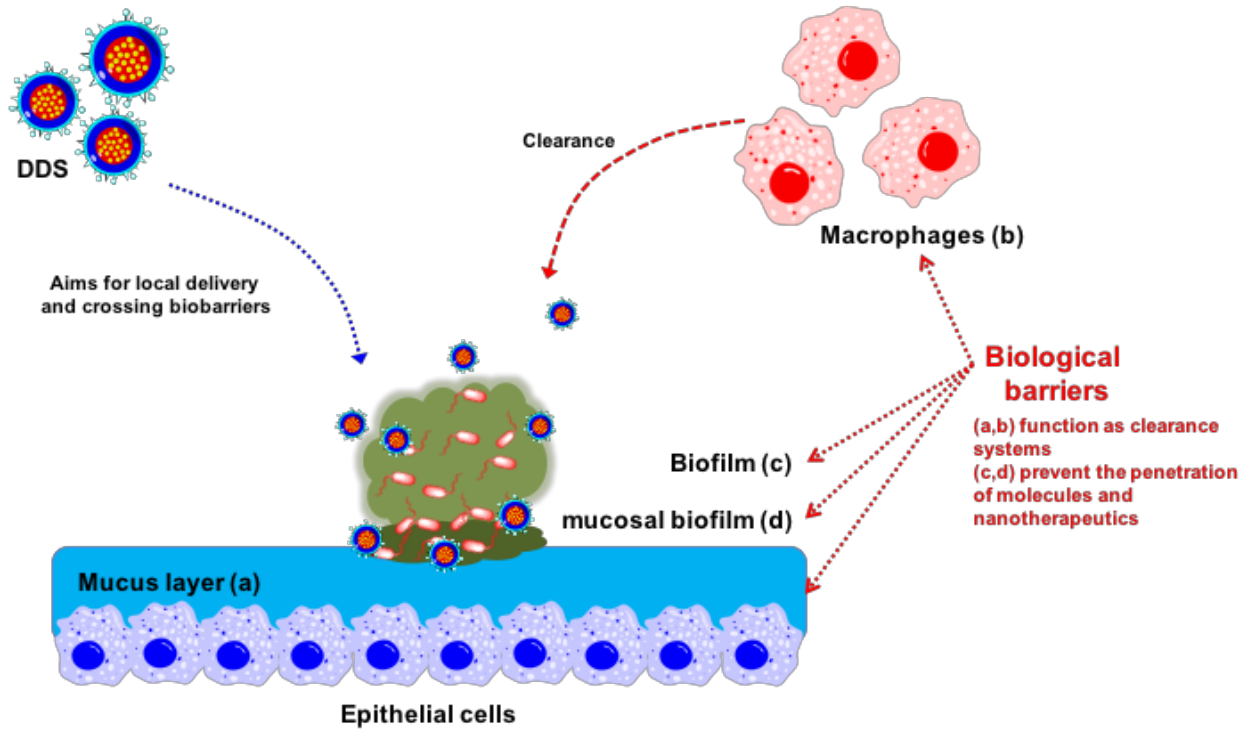


Figure 7. Biological barriers to inhaled anti-infective-loaded drug delivery systems.

2. RESEARCH STRATEGIES, WORKING HYPOTHESIS AND AIMS OF THE THESIS

The overarching purpose of this thesis is to develop the existing strategies further and to discover novel platforms for anti-infective DDS aiming for the treatment of pulmonary bacterial infections. These DDS are devoted to the delivery of clinically relevant antibiotics for inhalation, including tobramycin, colistin and ciprofloxacin, as well as exploited the simultaneous co-delivery of diverse anti-infectives. It is hypothesized that such DDS would address the significant problems in utilization of the aforementioned drugs, overcome biological barriers and improve drug bioavailability at the infection site. Moreover, the DDS would also allow the simultaneous delivery of antibiotic and quorum sensing inhibitor as a complementary therapy against bacterial biofilm infection. Hence, the antimicrobial efficacy of the antibiotics could be enhanced, eventually allowing to reduce the dosage of the used antibiotics and avoiding the development of bacterial resistance.

To achieve those goals, this thesis aimed to design and synthesize the DDS which hold an optimized balance between the ability to overcome biological barriers and the drug loading capacity. This thesis also aimed to propose facile strategies for the synthesis and preparation of such DDS, which are suitable for large scale production and more relevant for the future potential clinical studies. Additionally, materials structural design and synthesis (e.g. degree of oxidation in starch, length of hydrophobic moiety and degree of hydrophobic substitution in amphiphilic chitosan derivative, the amphiphilicity of squalenyl derivatives) and conventional chemistry were carefully employed in tuning the DDS characteristics, maximizing the drug loading capacity, and controlling the drug release profile.

In the first part of the thesis, the simple polysaccharides-based polyplexes technology was reinterpreted which aimed to produce versatile DDS holding high drug loading capacity. In the subsequent studies, the novel farnesylated chitosan derivative, and amphiphilic squalenyl derivatives were designed and synthesized, with which I aimed

to prepare DDS based on self-assembling technology. Such DDS were hypothesized having core-shell structure, which was aimed to host a diversity of actives without sacrificing the colloidal stability and characteristics. The drug loading capacity of such DDS would be improved compared to that could be achieved by using the polyplexes technique. This hypothesis was proposed to potentially reduce the use of the excipients in DDS, while the drug bioavailability would be maximized in the targeted site. Hence, the novel self-assembled systems would be nominated as the versatile platforms for drug delivery. Notably, I aimed to go beyond the current state-of-the-art to design and synthesize the nano-assemblies of aminoglycoside antibiotics and farnesyl quorum sensing inhibitors as a dual-functional DDS that would completely avoid the use of any additional excipients. Such innovative DDS would thus reach 100% drug loading capacity, while its characteristics, in particular the size, are optimized to overcome the biological barriers.

Finally, this thesis further investigated the interaction between DDS and biological barriers, such as macrophages, mucus, and biofilm to be able to evaluate the advantages as well as the limitations of proposed strategies for anti-infective delivery.

In this context, the major steps to achieve the aims are followed:

- (i) Structural design, synthesis and characterization of novel pharmaceutical excipients: the biocompatible and biodegradable materials based on carbohydrate polymers (starch, cyclodextrin, and chitosan derivatives), and natural lipids (terpenyl derivatives: squalenyl derivatives, and farnesyl derivatives) were employed in this work. The structure of the synthetic/modified excipients was designed to produce stable and uniform DDS, and to maximize the future loading of anti-infectives.
- (ii) Optimizing the preparation of delivery systems based on different techniques
 - Facile polyplex technology
 - Self-assembling technology
 - ✓ Amphiphilic polymer-based nano-assemblies
 - ✓ Amphiphilic lipid derivatives-based nano-assemblies

✓ Innovative excipient-free nano-assemblies

(iii) Optimizing the loading of clinically relevant antibiotics (tobramycin, colistin, ciprofloxacin), and a novel anti-infective QSI, as well as the co-loading of an antibiotic and a QSI as a complementary therapeutic formulation.

(iv) Characterization and in-vitro safety studies of the novel DDS.

(v) Investigation of the interaction between DDS and some important pulmonary biological barriers, such as macrophages, mucus/mucin and biofilm.

(vi) Investigation of the efficacy of drug-loaded and drugs co-loaded delivery systems against bacterial biofilm infection.

3. MAIN FINDINGS

In this thesis, the main findings section presents the significant results from three peer reviewed publications, a manuscript still in preparation for submission, and an international patent application. A summary about all the research discussed in this thesis will be in the following text, while detailed information of each publication and the summary of the invention will be presented in the scientific output, section 6.

The first two publications present researches which aim to develop versatile drug delivery systems for pulmonary anti-infectives delivery based on biodegradable polysaccharides (starch, β -cyclodextrin (β -CD) and chitosan) using a facile method. The systems could encapsulate a variety of clinically relevant anti-infectives including highly water-soluble aminoglycosides, antimicrobial peptide, or poorly water-soluble quinolone. The materials used in these researches are biodegradable and biocompatible for nanomedicine applications, they are moreover suitable for large scale production as its environmentally friendly properties, and adaption to facile production procedures. However, the carrier systems produced from such natural polymers still confront some limitations including (i) in the controls of NPs characteristics and their physicochemical stability; and (ii) the reproducibility. These two issues are usually accounted for the heterogeneous properties of natural polymers, especially the molecular weight which is somehow not consistent in different batches; (iii) the lack of advanced multiple functionalization of the NPs due to the poor selectivity for further physical and chemical modification on particles surface (144). In these two chapters, the preparation of the anionic starch and anionic β -cyclodextrin was revisited to have better control in molecular weight and degree of oxidation of resulting products. The products were then used for the complexation with chitosan derivatives to assemble NPs. The NPs characteristics (size and ζ -potential) could be easily tuned to benefit the future application as drug delivery systems. Notably, the NPs size was ranged from 150 – 900nm. The system based on starch-chitosan polyplexes exhibited good drug loading capacity for hydrophilic tobramycin and colistin. The highest loading capacity of colistin in such simple system was nearly 23%. The β -cyclodextrin-chitosan polyplexes significantly improved water-solubility and shown controlled release profile of ciprofloxacin with the drug loading

capacity ~10%. The NPs systems proposed in these two chapter are stable in biologically relevant medium and non-toxic (up to 1 mg/mL concentration) on human cell lines. The encapsulation of antibiotic into the complexation of these polysaccharides did not compromise the intrinsic antimicrobial efficacy of either compound. In the subsequent study, the dependence of NPs size on macrophage binding and uptake was investigated for the β -cyclodextrin-chitosan particles having sizes ranged from 400 – 900nm. The overall research scheme carried in these chapters is depicted in Figure 8, and the detailed information of each research is presented in section 6.1 and 6.2, respectively.

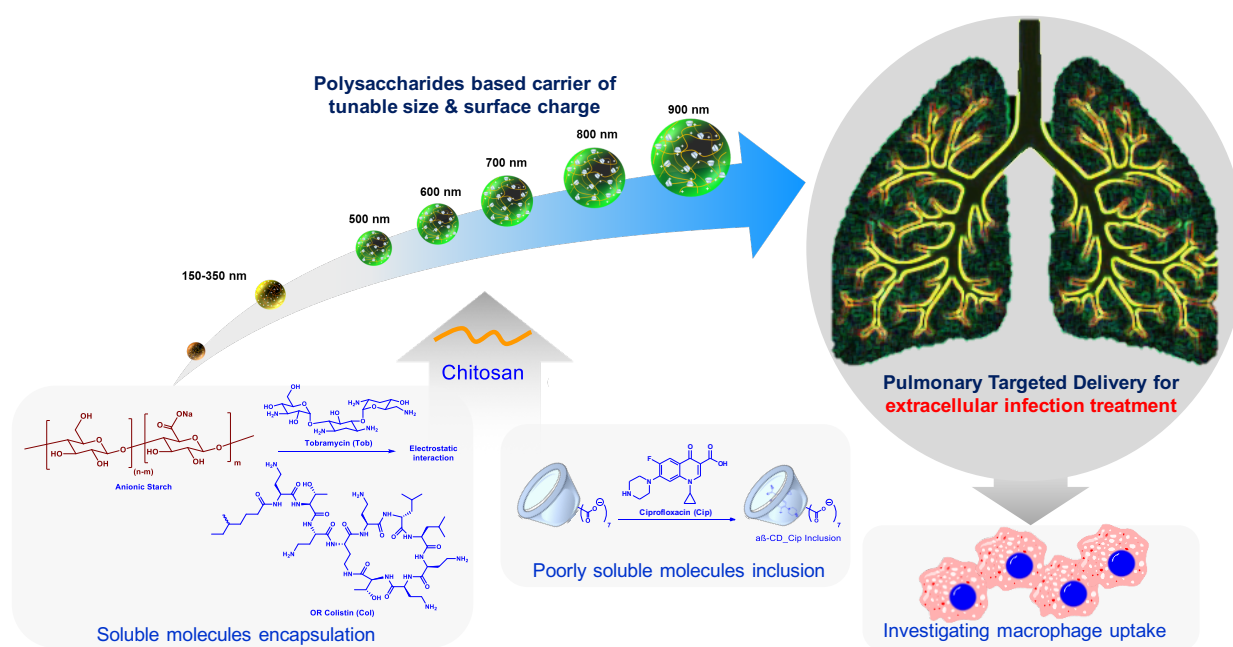


Figure 8. Overall research scheme discussed in section 6.1 and 6.2.

In the next publication, the preparation of self-assembled nanocarriers based on a novel synthetic amphiphilic chitosan derivative, farnesylated glycol chitosan, is proposed. Having discussed that the majority of currently available, developed and discovered antimicrobial agents suffer from poor drug bioavailability due to their (i) poorly water-solubility; (ii) short in vivo half-life in biological environment; and the potential adverse effects (86,145,146). Moreover, the co-delivery of diverse bioactive compounds is essential to enhance the therapeutic effects, in particular against bacterial infection (80). In chapter 6.3, in addition to the promising biocompatibility and biodegradability of the

used excipients, the core-shell structure of the assembled NPs is moreover expected to be capable of carrying both hydrophilic and hydrophobic molecules which is the major limitation in loading capacity of the delivery systems composed by polysaccharides polyplexes. I proposed in this chapter a facile and high isolated yield method with one-step synthetic reaction to prepare the farnesylated glycol chitosan. The uniform and stable NPs would be self-assembled in aqueous media at the relatively low degree of farnesylation (~11%), and was tuned in the size range of 200 – 500nm. The NPs drug loading capacity was investigated with different model compounds. And we convincingly proved the co-loading of both hydrophobic Nile red and hydrophilic fluorescent albumin protein in such NPs by CLSM, with reasonable drug loading capacity. Furthermore, the NPs exhibited excellent physicochemical stability in a wide range of biological relevant pH environment. Finally, the potential use of such nanoassemblies as mucosal drug delivery systems was investigated by studying the interaction between mucus-particle. An overall research scheme carried in this chapter is briefly summarized in Figure 9, and the detailed information of this chapter is presented in section 6.3.

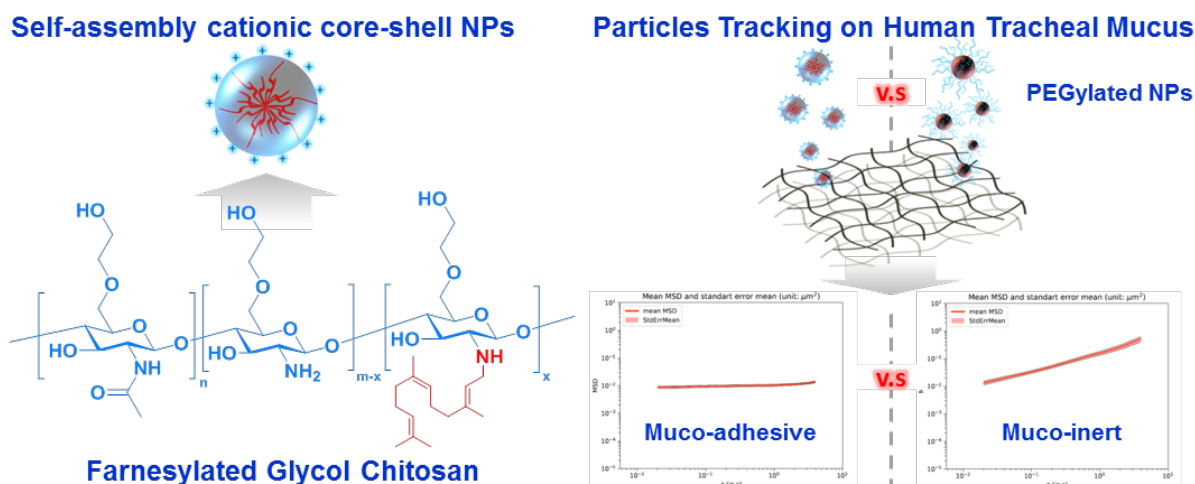


Figure 9. Overall research scheme discussed in section 6.3. Reprinted with permission from Reference (142)

The subsequent chapter is presented in section 6.4, Squalenyl Hydrogen Sulfate NPs (SqNPs) for simultaneous delivery of tobramycin and alkylquinolone quorum sensing inhibitor to combat PA biofilm infections. This chapter pays more attention to the limitation of anti-infective penetration through bacterial biofilm, and bacterial communication via

quorum sensing systems which are suggested contributing to the fast resistance of PA biofilm infections. Furthermore, the influence of mucus/mucin on pyocyanin production level from PA was studied. Because such a layer is always present in the airway adding more challenge to the treatment of such infectious diseases (80). While drug-loaded nanocarrier is a promising strategy enhancing local drug delivery by crossing bio-barriers, a complementary to antibiotics, quorum sensing inhibitors (QSI), has been discovered capable to interfere with the biofilm formation (74,80). The dual-delivery of antibiotic and QSI is hypothesized to improve biofilm eradicating efficacy (73). Taking advantage of the self-assembling property of the newly synthesized anionic amphiphilic lipid, Squalenyl Hydrogen Sulfate (Sq), this chapter describes a dual-delivery nanocarrier with high loading capacity for both a lipophilic QSI (~10%) and the hydrophilic antibiotic tobramycin (~33%). The co-loaded system is expected to show actions on different stages of PA infection. Especially, the influence of mucus and mucin on the production of pyocyanin level from PA, as well as the function of QSI both in free form and loaded-SqNPs were also carefully investigated and reported. The novel platform in this study shows a significant therapeutic effect on eradicating PA biofilm infection. The tobramycin concentration used for a complete biofilm eradication is around 12.5 µg/mL when using dual-loaded carrier systems, while more than 200 µg/mL tobramycin alone is needed to show the same efficacy. Furthermore, the transport of the carrier system through biofilm was studied by live CLSM to clearly prove the improvement of therapeutic effect against PA biofilm infection. Figure 10 summarizes the hypothesis and research strategies in section 6.4.

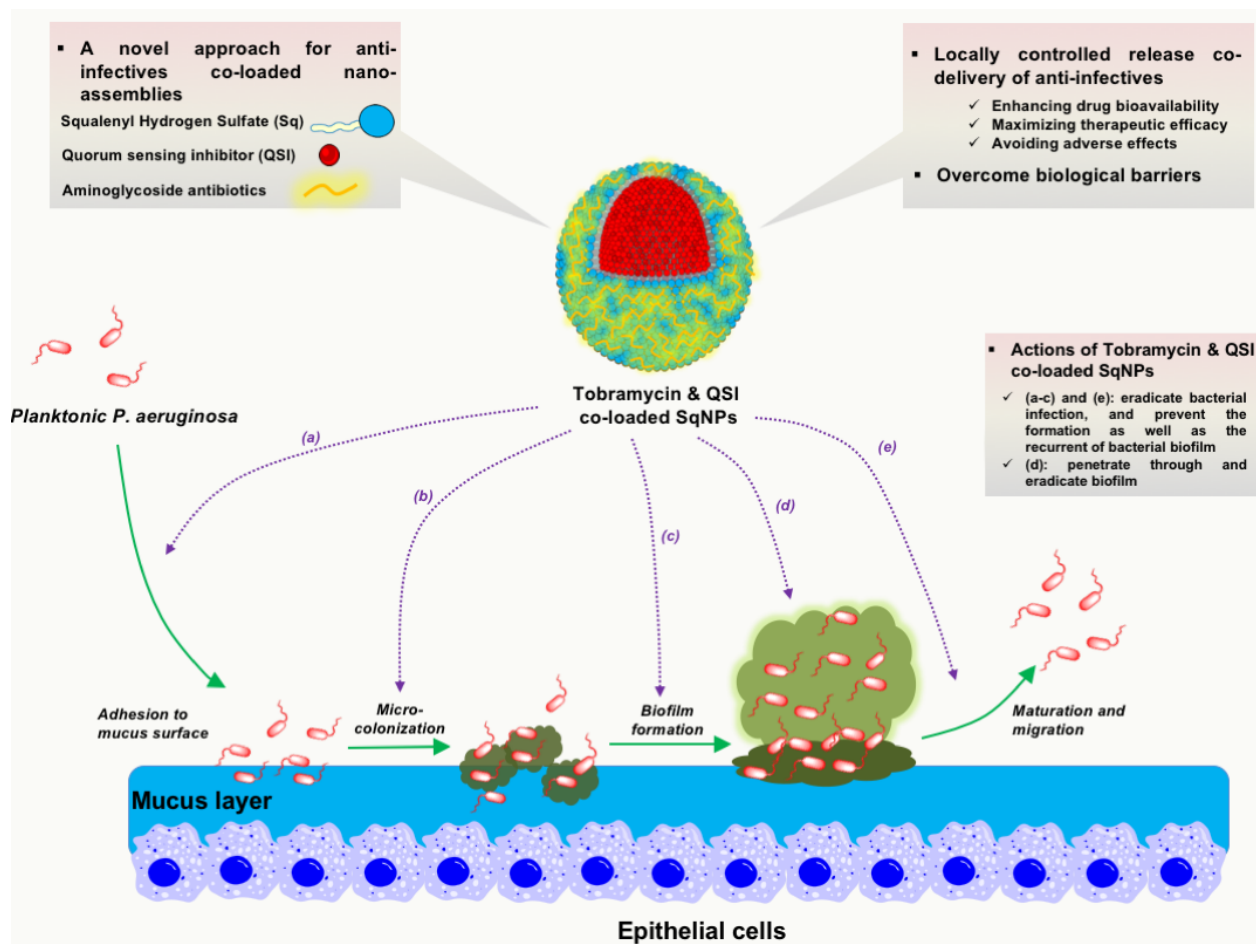


Figure 10. Overall research scheme discussed in section 6.4.

Finally, the last chapter, summarized in section 6.5, presents an innovative excipient-free nano-assemblies of aminoglycoside antibiotic and farnesyl quorum sensing inhibitors for combatting bacterial biofilm infections. The present invention relates to conjugates of aminoglycosides and terpenoids, in particular, sesquiterpenoids. Furthermore, the present invention relates to nano-assemblies formed by the inventive conjugates and to a method for producing the conjugates and/or the nano-assemblies. The present invention also relates to the inventive conjugates and nano-assemblies for use in therapy, in particular for use in the treatment of infectious diseases. Particularly preferred embodiments of the present invention relate to farnesylated aminoglycosides and nano-assemblies thereof, in which farnesol and its derivatives do not only function as a carrier for the aminoglycosides but do themselves have pharmaceutical activity upon cleavage of the conjugate, in particular quorum sensing inhibitory activity. Such nano-assemblies of tobramycin and farnesyl quorum sensing inhibitor significantly enhance the

Pseudomonas aeruginosa biofilm eradicating efficacy 16-folds compared to the treatment of free tobramycin.

4. CONCLUSIONS AND OUTLOOK

This thesis proposes different innovative strategies and platforms for the improved delivery of anti-infectives, especially for the treatment of pulmonary infections. The described delivery systems are biocompatible and biodegradable, and are manufactured using facile operations. They are stable in biologically relevant media and their physiochemical properties can be designed to fit the intended use. Materials structure design and conventional chemistry were successfully employed to explore and maximize the drug loading capacity and the potential of co-loading diverse agents in all studies with the aim to combat bacterial infection and to prevent the development of bacterial resistance. The efficacy against bacterial infection at different stages was evaluated in different biologically relevant environments (e.g. presence/absence of mucus or biofilm). Moreover, studying the interaction of these carrier systems with biological barriers, such as biofilm, mucus, and macrophages, allows to design and to prepare the drug delivery systems to overcome these barriers as needed for future therapeutic applications.

In the first two chapters, section 6.1 and 6.2, the results clearly demonstrate that by overcoming the shortages of natural polymers properties, stable NPs could be formed by anionic polysaccharides based on starch or β -cyclodextrin polyplexes with chitosan derivatives using a facile method. The technique allows to flexibly tune size and surface characteristics, and the encapsulation of various types of anti-infectives without compromising their anti-microbial function. In addition, the size dependence of macrophage uptake recommended the use of the sub-micro carriers for the treatment of extracellular infections. Moreover, the research in these chapters also show the potential of flexible surface modification of those carriers with hydrophilic enzymes or nucleases (e.g. deoxyribonuclease I) to enhance drug penetration through biofilm or mucus. This approach has good prospects for developing inhalation nanomedicines against pulmonary infections.

In the next chapter, section 6.3, the natural polymer chitosan was chemically modified by coupling to a hydrophobic farnesyl moieties resulting in a novel amphiphilic polymer. The latter shown an interesting self-assembling to core-shell particles, capable to overcome the limitation of natural polysaccharides carrier systems in various ways: (i)

allowing the encapsulation of the hydrophobic compounds, (ii) enabling the simultaneous delivery of a second active with different structure and physiochemical properties, (iii) and allowing the further surface modification to render the system more flexible to various applications. In this chapter, the interaction of the particles with mucus as a biological barrier was explored in more detail, and the novel system appeared as a versatile DDS for various mucosal routes of application.

The last two chapters describe two novel carrier systems, capable to simultaneously deliver antibiotics and QSI molecules as high efficiency and loading capacity. The first system was formed by the simultaneous self-assembly of squalenyl hydrogen sulfate, aminoglycoside antibiotics, and QSI molecules. The second system is the excipient-free nano-assembly of an aminoglycoside (tobramycin) and farnesyl QSI. In study the efficacy against PA infection, it was surprisingly found that the presence of mucin/mucus increased the production of the virulence factor pyocyanin. Both DDS systems shown impressive effects against biofilm forming PA bacteria, indicating a remarkable improvement in bioavailability of both active compounds at the site of infection and in particular inside the biofilm, which was also supported by CLSM images. Based on these promising results *in vitro*, *in vivo* studies on infection relevant models are currently ongoing.

Altogether, this thesis describes some novel strategies for anti-infective delivery systems, their advantages and limitations, and the understanding gained from investigating the interaction of such systems with various biological barriers. The author is convinced that these data will provide valuable information for the comprehensive investigation and development of novel therapeutic modalities to better combat bacterial infections in the future.

5. REFERENCES

1. Skinner D, Keefer CS. Significance of bacteremia caused by staphylococcus aureus: A study of one hundred and twenty-two cases and a review of the literature concerned with experimental infection in animals. *Arch Intern Med.* 1941;68(5):851–75.
2. Lowy FD. Staphylococcus aureus infections. *N Engl J Med.* 1998;339:520–32.
3. Maki DG, Agger WA. Enterococcal bacteremia: Clinical features, the risk of endocarditis, and management. *Med (United States).* 1988;67(4):248–69.
4. Bodey GP, Bolivar R, Fainstein V, Jadeja L. Infections caused by *Pseudomonas aeruginosa*. *Rev Infect Dis.* 1983;5(2):279–313.
5. Bartlett JG. Nosocomial bloodstream infections in US hospitals: Analysis of 24,179 cases from a prospective nationwide surveillance study. *Infect Dis Clin Pract.* 2004;5(5):837–45.
6. Woodford N, Livermore DM. Infections caused by Gram-positive bacteria: a review of the global challenge. *J Infect.* 2009;59(1):4–16.
7. Falagas ME, Bliziotis IA. Pandrug-resistant Gram-negative bacteria: the dawn of the post-antibiotic era? *Int J Antimicrob Agents.* 2007;29(6):630–6.
8. Peleg AY, Hooper DC. Hospital-acquired infections due to gram-negative bacteria. *N Engl J Med.* 2010;362:1804–13.
9. Brown D. Antibiotic resistance breakers: Can repurposed drugs fill the antibiotic discovery void? *Nat Rev Drug Discov.* 2015;14:821–32.
10. Sevinç F, Prins JM, Koopmans RP, Langendijk PN, Bossuyt PM, Dankert J, et al. Early switch from intravenous to oral antibiotics: guidelines and implementation in a large teaching hospital. *J Antimicrob Chemother.* 1999;43(4):601–6.
11. MacGregor RR, Graziani AL. Oral administration of antibiotics: A rational alternative to the parenteral route. *Clin Infect Dis.* 1997;24(3):457–67.
12. Cunha BA. Antibiotic side effects. *Med Clin North Am.* 2001;85(1):149–85.
13. Carl P, Nord E. Effect of Antimicrobial Agents on Human Microflora. *Lancet Infect Dis.* 2001;1(2):159–62.
14. Alothman GA, Alsaadi MM, Ho BL, Ho SL, Dupuis A, Corey M, et al. Evaluation of bronchial constriction in children with cystic fibrosis after inhaling two different

- preparations of tobramycin. *Chest*. 2002;122(3):930–4.
15. Prayle A, Watson A, Fortnum H, Smyth A. Side effects of aminoglycosides on the kidney, ear and balance in cystic fibrosis. *Thorax*. 2010;65(7).
 16. Mondorf AW, Breier J, Hendus J, Scherberich JE, Mackenrodt G, Shah PM, et al. Effect of aminoglycosides on proximal tubular membranes of the human kidney. *Eur J Clin Pharmacol*. 1978;13(2):133–42.
 17. CDC. Antibiotic resistance threats in the United States, 2013. *Current*. 2013.
 18. Wistrand-Yuen E, Knopp M, Hjort K, Koskiniemi S, Berg OG, Andersson DI. Evolution of high-level resistance during low-level antibiotic exposure. *Nat Commun*. 2018;9.
 19. Loke YK, Price D, Herxheimer A. Systematic reviews of adverse effects: Framework for a structured approach. *BMC Med Res Methodol*. 2007;7(32).
 20. Levy SB, Bonnie M. Antibacterial resistance worldwide: Causes, challenges and responses. *Nat Med*. 2004;10:122–9.
 21. Ventola CL. The antibiotic resistance crisis: part 1: causes and threats. *P T A peer-reviewed J Formul Manag*. 2015;40(4):277–83.
 22. Lewis K. Platforms for antibiotic discovery. *Nat Rev Drug Discov*. 2013;12(5):371–87.
 23. Huh AJ, Kwon YJ. “Nanoantibiotics”: A new paradigm for treating infectious diseases using nanomaterials in the antibiotics resistant era. *J Control Release*. 2011;156:128–45.
 24. Nikaido H. Outer membrane barrier as a mechanism of antimicrobial resistance. *Antimicrob Agents Chemother*. 1989;33(11):1831–6.
 25. Leive L. THE BARRIER FUNCTION OF THE GRAM-NEGATIVE ENVELOPE. *Ann N Y Acad Sci*. 1974;235(1):109–29.
 26. Ma D, Cook DN, Hearst JE, Nikaido H. Efflux pumps and drug resistance in gram-negative bacteria. *Trends Microbiol*. 1994;2(12):489–93.
 27. Poole K. Efflux-mediated multiresistance in Gram-negative bacteria. *Clin Microbiol Infect*. 2004;10:12–26.
 28. Pagès JM, James CE, Winterhalter M. The porin and the permeating antibiotic: A selective diffusion barrier in Gram-negative bacteria. *Nat Rev Microbiol*.

- 2008;6:893–903.
29. Hancock REW. Resistance Mechanisms in *Pseudomonas aeruginosa* and Other Nonfermentative Gram-Negative Bacteria. *Clin Infect Dis*. 1998;27(1):93–9.
 30. Tenover FC. Mechanisms of Antimicrobial Resistance in Bacteria. *Am J Med*. 2006;34(5):3–10.
 31. Blair JMA, Webber MA, Baylay AJ, Ogbolu DO, Piddock LJV. Molecular mechanisms of antibiotic resistance. *Nat Rev Microbiol*. 2011;13:42–51.
 32. Geller DE, Pitlick WH, Nardella PA, Tracewell WG, Ramsey BW. Pharmacokinetics and bioavailability of aerosolized tobramycin in cystic fibrosis. *Chest*. 2002;122(1):219–26.
 33. Flume PA, VanDevanter DR. Clinical applications of pulmonary delivery of antibiotics. *Adv Drug Deliv Rev*. 2015;85:1–6.
 34. Wenzler E, Fraidenburg DR, Scardina T, Danziger LH. Inhaled antibiotics for gram-negative respiratory infections. *Clin Microbiol Rev*. 2016;29(3):581–632.
 35. Yusuf E, Van Herendael B, Verbrugghe W, Ieven M, Goovaerts E, Bergs K, et al. Emergence of antimicrobial resistance to *Pseudomonas aeruginosa* in the intensive care unit: association with the duration of antibiotic exposure and mode of administration. *Ann Intensive Care*. 2017;7(72).
 36. Richards MJ, Edwards JR, Culver DH, Gaynes RP. Nosocomial Infections in Combined Medical-Surgical Intensive Care Units in the United States. *Infect Control Hosp Epidemiol*. 2000;21(8):510–5.
 37. Langton Hower SC, Smyth AR. Antibiotic strategies for eradicating *Pseudomonas aeruginosa* in people with cystic fibrosis. *Cochrane Database Syst Rev*. 2017;(11).
 38. Emerson J, Rosenfeld M, McNamara S, Ramsey B, Gibson RL. *Pseudomonas aeruginosa* and other predictors of mortality and morbidity in young children with cystic fibrosis. *Pediatr Pulmonol*. 2002;34(2):91–100.
 39. Cohen-Cymerknoh M, Shoseyov D, Kerem E. Managing cystic fibrosis: Strategies that increase life expectancy and improve quality of life. *Am J Respir Crit Care Med*. 2011;183(11):1463–71.
 40. Hastedt JE, Bäckman P, Clark AR, Doub W, Hickey A, Hochhaus G, et al. Scope and relevance of a pulmonary biopharmaceutical classification system

- AAPS/FDA/USP Workshop March 16-17th, 2015 in Baltimore, MD. AAPS Open. 2016;2(1).
41. Wauthoz N, Amighi K. Pulmonary Drug Delivery, Chapter 5. Formulation Strategies for Pulmonary Delivery of Poorly Soluble Drugs. John Wiley & Sons, Ltd: Chichester, UK,. 2015.
 42. Borok Z, Verkman a S. Lung edema clearance: 20 years of progress: invited review: role of aquaporin water channels in fluid transport in lung and airways. *J Appl Physiol.* 2002;93:299–2206.
 43. Fröhlich E, Mercuri A, Wu S, Salar-Behzadi S. Measurements of deposition, lung surface area and lung fluid for simulation of inhaled compounds. *Front Pharmacol.* 2016;7(181).
 44. Zhou QT, Leung SSY, Tang P, Parumasivam T, Loh ZH, Chan HK. Inhaled formulations and pulmonary drug delivery systems for respiratory infections. *Adv Drug Deliv Rev.* 2015;85:83–99.
 45. Pérez B F, Méndez G A, Lagos R A, Vargas M SL. Mucociliary clearance system in lung defense. *Rev médica Chile.* 2014;142(5):606–15.
 46. Hardy CL, LeMasurier JS, Mohamud R, Yao J, Xiang SD, Rolland JM, et al. Differential Uptake of Nanoparticles and Microparticles by Pulmonary APC Subsets Induces Discrete Immunological Imprints. *J Immunol.* 2013;193:5278–90.
 47. d'Angelo I, Conte C, La Rotonda MI, Miro A, Quaglia F, Ungaro F. Improving the efficacy of inhaled drugs in cystic fibrosis: Challenges and emerging drug delivery strategies. *Adv Drug Deliv Rev.* 2014;75:92–111.
 48. Hoffmann IM, Rubin BK, Iskandar SS, Schechter MS, Nagaraj SK, Bitzan MM. Acute renal failure in cystic fibrosis: Association with inhaled tobramycin therapy. *Pediatr Pulmonol.* 2002;34(5):375–7.
 49. Tolker-Nielsen T. Pseudomonas aeruginosa biofilm infections: From molecular biofilm biology to new treatment possibilities. *APMIS.* 2014;138:1–51.
 50. Schachter B. Slimy business--the biotechnology of biofilms. *Nat Biotechnol.* 2003;21:361–5.
 51. Costerton JW, Stewart PS, Greenberg EP. Bacterial biofilms: a common cause of persistent infections. *Science.* 1999;284(5418):1318–22.

52. Mah T-F, Pitts B, Pellock B, Walker GC, Stewart PS, O'Toole GA. A genetic basis for *Pseudomonas aeruginosa* biofilm antibiotic resistance. *Nature*. 2003;426:306–310.
53. Branda SS, Vik Å, Friedman L, Kolter R. Biofilms: The matrix revisited. *Trends Microbiol*. 2005;13(1):20–6.
54. Mah TFC, O'Toole GA. Mechanisms of biofilm resistance to antimicrobial agents. *Trends Microbiol*. 2001;9(1):34–9.
55. Tseng BS, Zhang W, Harrison JJ, Quach TP, Song JL, Penterman J, et al. The extracellular matrix protects *Pseudomonas aeruginosa* biofilms by limiting the penetration of tobramycin. *Environ Microbiol*. 2013;15(10):2865–78.
56. Mu L, Murgia X, Siebenbu L, Schwarzkopf K, Sewald K, Ha S, et al. Human airway mucus alters susceptibility of *Pseudomonas aeruginosa* biofilms to tobramycin, but not colistin. *J Antimicrob Chemother*. 2018;1–8.
57. Suci PA, Mittelman MW, Yu FP, Geesey GG. Investigation of ciprofloxacin penetration into *Pseudomonas aeruginosa* biofilms. *Antimicrob Agents Chemother*. 1994;3(9):2125–33.
58. Murgia X, Loretz B, Hartwig O, Hittinger M, Lehr C-M. The role of mucus on drug transport and its potential to affect therapeutic outcomes. *Adv Drug Deliv Rev*. 2018;124:82–97.
59. Anderson MJ, Parks PJ, Peterson ML. A mucosal model to study microbial biofilm development and anti-biofilm therapeutics. *J Microbiol Methods*. 2013;92(2):201–208.
60. Knowles MR, Boucher RC. Mucus clearance as a primary innate defense mechanism for mammalian airways. *J Clin Invest*. 2002;109(5):571–7.
61. Evans CM, Koo JS. Airway mucus: The good, the bad, the sticky. *Pharmacol Ther*. 2009;121(3):332–48.
62. Hassett DJ, Cuppoletti J, Trapnell B, Lyman S V, Rowe JJ, Yoon S, et al. Anaerobic metabolism and quorum sensing by *Pseudomonas aeruginosa* biofilms in chronically infected cystic fibrosis airways: rethinking antibiotic treatment strategies and drug targets. *Adv Drug Deliv Rev*. 2002;54(11):1425–43.
63. Bjarnsholt T, Jensen PØ, Fiandaca MJ, Pedersen J, Hansen CR, Andersen CB, et

- al. *Pseudomonas aeruginosa* biofilms in the respiratory tract of cystic fibrosis patients. *Pediatr Pulmonol*. 2009;44(6):547–58.
64. Velkov T, Abdul Rahim N, Zhou QT, Chan HK, Li J. Inhaled anti-infective chemotherapy for respiratory tract infections: Successes, challenges and the road ahead. *Adv Drug Deliv Rev*. 2015;85:65–82.
65. Elborn JS, Vataire AL, Fukushima A, Aballea S, Khemiri A, Moore C, et al. Comparison of Inhaled Antibiotics for the Treatment of Chronic *Pseudomonas aeruginosa* Lung Infection in Patients With Cystic Fibrosis: Systematic Literature Review and Network Meta-analysis. *Clin Ther*. 2016;38(10):2204–26.
66. Brown ED, Wright GD. Antibacterial drug discovery in the resistance era. *Nature*. 2016;529:336–343.
67. Braff D, Shis D, Collins JJ. Synthetic biology platform technologies for antimicrobial applications. *Adv Drug Deliv Rev*. 2016;105(A):35–43.
68. Roemer T, Boone C. Systems-level antimicrobial drug and drug synergy discovery. *Nat Chem Biol*. 2013;9:222–231.
69. Liu J, Dehbi M, Moeck G, Arhin F, Banda P, Bergeron D, et al. Antimicrobial drug discovery through bacteriophage genomics. *Nat Biotechnol*. 2004;22:185–191.
70. Pinto-Alphandary H, Andremont A, Couvreur P. Targeted delivery of antibiotics using liposomes and nanoparticles: Research and applications. *Int J Antimicrob Agents*. 2000;13(3):155–68.
71. Drenkard E. Antimicrobial resistance of *Pseudomonas aeruginosa* biofilms. *Microbes Infect*. 2003;5(13):1213–9.
72. Rasmussen TB, Givskov M. Quorum-sensing inhibitors as anti-pathogenic drugs. *Int J Med Microbiol*. 2006;296(2–3):149–61.
73. Bandara HMHN, Herpin MJ, Kolacny D, Harb A, Romanovicz D, Smyth HDC. Incorporation of Farnesol Significantly Increases the Efficacy of Liposomal Ciprofloxacin against *Pseudomonas aeruginosa* Biofilms in Vitro. *Mol Pharm*. 2016;13(8):2760–70.
74. Brackman G, Cos P, Maes L, Nelis HJ, Coenye T. Quorum sensing inhibitors increase the susceptibility of bacterial biofilms to antibiotics in vitro and in vivo. *Antimicrob Agents Chemother*. 2011;55(6):2655–2661.

75. Nafee N, Husari A, Maurer CK, Lu C, De Rossi C, Steinbach A, et al. Antibiotic-free nanotherapeutics: Ultra-small, mucus-penetrating solid lipid nanoparticles enhance the pulmonary delivery and anti-virulence efficacy of novel quorum sensing inhibitors. *J Control Release*. 2014;192:131–40.
76. Miramoth NS, Di Meo C, Zouhiri F, Saïd-Hassane F, Valetti S, Gorges R, et al. Self-assembled squalenoylated penicillin bioconjugates: An original approach for the treatment of intracellular infections. *ACS Nano*. 2012;6(5):3820–3831.
77. Bergen PJ, Li J, Rayner CR, Nation RL. Colistin methanesulfonate is an inactive prodrug of colistin against *Pseudomonas aeruginosa*. *Antimicrob Agents Chemother*. 2006;50(6):1953–1958.
78. Wallace SJ, Li J, Nation RL, Prankerd RJ, Velkov T, Boyd BJ. Self-assembly behavior of colistin and its prodrug colistin methanesulfonate: Implications for solution stability and solubilization. *J Phys Chem B*. 2010;114(14):4836–4840.
79. Pokrovskaya V, Baasov T. Dual-acting hybrid antibiotics: a promising strategy to combat bacterial resistance. *Expert Opin Drug Discov*. 2010;5(9):883–902.
80. Cottarel G, Wierzbowski J. Combination drugs, an emerging option for antibacterial therapy. *Trends Biotechnol*. 2007;25(12):547–55.
81. Takahashi K, Kanno H. Synergistic activities of combinations of β -lactams, fosfomicin, and tobramycin against *Pseudomonas aeruginosa*. *Antimicrob Agents Chemother*. 1984;26(5):789–91.
82. MacLeod DL, Velayudhan J, Kenney TF, Therrien JH, Sutherland JL, Barker LM, et al. Fosfomicin enhances the active transport of tobramycin in *Pseudomonas aeruginosa*. *Antimicrob Agents Chemother*. 2012;56(3):1529–1538.
83. Høiby N. New antimicrobials in the management of cystic fibrosis. *Int Congr Symp Ser - R Soc Med*. 2003;49(2):235–238.
84. Kelly GS. Clinical applications of N-acetylcysteine. *Altern Med Rev*. 1998;3(2):114–27.
85. Stella VJ, Nti-Addae KW. Prodrug strategies to overcome poor water solubility. Vol. 59, *Advanced Drug Delivery Reviews*. 2007. p. 677–94.
86. Savjani KT, Gajjar AK, Savjani JK. Drug Solubility: Importance and Enhancement Techniques. *ISRN Pharm [Internet]*. 2012;2012:1–10. Available from:

<http://www.hindawi.com/journals/isrn/2012/195727/>

87. De Jong WH, Borm PJ a. Drug delivery and nanoparticles: applications and hazards. *Int J Nanomedicine*. 2008;3(2):133–49.
88. Zhang L, Pornpattananangkul D, Hu C-M, Huang C-M. Development of Nanoparticles for Antimicrobial Drug Delivery. *Curr Med Chem*. 2010;17:585–94.
89. Ho DK, Costa A, De Rossi C, De Souza Carvalho-Wodarz C, Loretz B, Lehr CM. Polysaccharide Submicrocarrier for Improved Pulmonary Delivery of Poorly Soluble Anti-infective Ciprofloxacin: Preparation, Characterization, and Influence of Size on Cellular Uptake. *Mol Pharm*. 2018;15(3):1081–96.
90. Markman JL, Rekechenetskiy A, Holler E, Ljubimova JY. Nanomedicine therapeutic approaches to overcome cancer drug resistance. Vol. 65, *Advanced Drug Delivery Reviews*. 2013. p. 1866–79.
91. Zhu X, Radovic-Moreno AF, Wu J, Langer R, Shi J. Nanomedicine in the management of microbial infection - Overview and perspectives. *Nano Today*. 2014;9(4):479–98.
92. Abed N, Couvreur P. Nanocarriers for antibiotics: A promising solution to treat intracellular bacterial infections. Vol. 43, *International Journal of Antimicrobial Agents*. 2014. p. 485–96.
93. Champion JA, Katare YK, Mitragotri S. Particle shape: A new design parameter for micro- and nanoscale drug delivery carriers. *J Control Release*. 2007;121(1–2):3–9.
94. Gao W, Thamphiwatana S, Angsantikul P, Zhang L. Nanoparticle approaches against bacterial infections. *Wiley Interdiscip Rev Nanomedicine Nanobiotechnology*. 2014;6(6):532–47.
95. Langer R. Drug delivery and targeting. *Nature*. 1998;392.
96. Allen TM, Cullis PR. Drug Delivery Systems: Entering the Mainstream. *Science* (80-). 2004;303(5665):1818–22.
97. Zhang L, Gu FX, Chan JM, Wang AZ, Langer RS, Farokhzad OC. Nanoparticles in medicine: Therapeutic applications and developments. *Clin Pharmacol Ther*. 2008;83(5):761–9.
98. Hamidi M, Azadi A, Rafiei P. Hydrogel nanoparticles in drug delivery. *Adv Drug Deliv*

- Rev. 2008;60(15):1638–49.
99. Anderson JM, Shive MS. Biodegradation and biocompatibility of PLA and PLGA microspheres. *Adv Drug Deliv Rev.* 2012;28(1):5–24.
 100. Kumari A, Yadav SK, Yadav SC. Biodegradable polymeric nanoparticles based drug delivery systems. *Colloids Surfaces B Biointerfaces.* 2010;75(1):1–18.
 101. Müller R. Solid lipid nanoparticles (SLN) for controlled drug delivery: a review of the state of the art. *Eur J Pharm Biopharm.* 2000;50(1):161–77.
 102. Wissing SA, Kayser O, Müller RH. Solid lipid nanoparticles for parenteral drug delivery. *Adv Drug Deliv Rev.* 2004;56(9):1257–72.
 103. Farokhzad OC, Langer R. Impact of nanotechnology on drug delivery. *ACS Nano.* 2009;3(1):16–20.
 104. Shi J, Votruba AR, Farokhzad OC, Langer R. Nanotechnology in drug delivery and tissue engineering: From discovery to applications. *Nano Lett.* 2010;10(9):3223–30.
 105. Sanhai WR, Sakamoto JH, Canady R, Ferrari M. Seven challenges for nanomedicine. *Nat Nanotechnol.* 2008;3:241–4.
 106. Wagner V, Dullaart A, Bock AK, Zweck A. The emerging nanomedicine landscape. *Nat Biotechnol.* 2006;24:1211–1217.
 107. Macfarlane JT, Worboys M. The changing management of acute bronchitis in Britain, 1940-1970: The impact of antibiotics. *Med Hist.* 2008;52(1):47–72.
 108. Ramsey BW, Pepe MS, Quan JM, Otto KL, Montgomery AB, Williams-Warren J, et al. Intermittent Administration of Inhaled Tobramycin in Patients with Cystic Fibrosis. *N Engl J Med.* 1999;340:23–30.
 109. Pai VB, Nahata MC. Efficacy and safety of aerosolized tobramycin in cystic fibrosis. *Pediatr Pulmonol.* 2001;32(4):314–27.
 110. Newhouse MT, Hirst PH, Duddu SP, Walter YH, Tarara TE, Clark AR, et al. Inhalation of a dry powder tobramycin pulmosphere formulation in healthy volunteers. *Chest.* 2003;124(1):360–6.
 111. Konstan MW, Flume PA, Kappler M, Chiron R, Higgins M, Brockhaus F, et al. Safety, efficacy and convenience of tobramycin inhalation powder in cystic fibrosis patients: The EAGER trial. *J Cyst Fibros.* 2011;10(1):54–61.
 112. Drobnic ME, Suñé P, Montoro JB, Ferrer A, Orriols R. Inhaled tobramycin in non-

- cystic fibrosis patients with bronchiectasis and chronic bronchial infection with *Pseudomonas aeruginosa*. *Ann Pharmacother*. 2005;93(7):476–80.
113. Le Brun PPH, De Boer AH, Mannes GPM, De Frature DMI, Brimicombe RW, Touw DJ, et al. Dry powder inhalation of antibiotics in cystic fibrosis therapy: Part 2. Inhalation of a novel colistin dry powder formulation: A feasibility study in healthy volunteers and patients. *Eur J Pharm Biopharm*. 2002;54(1):25–32.
114. Aksamit T, Bandel TJ, Criollo M, De Soyza A, Elborn JS, Operschall E, et al. The RESPIRE trials: Two phase III, randomized, multicentre, placebo-controlled trials of Ciprofloxacin Dry Powder for Inhalation (Ciprofloxacin DPI) in non-cystic fibrosis bronchiectasis. *Contemp Clin Trials*. 2017;58(78–85).
115. Deacon J, Abdelghany SM, Quinn DJ, Schmid D, Megaw J, Donnelly RF, et al. Antimicrobial efficacy of tobramycin polymeric nanoparticles for *Pseudomonas aeruginosa* infections in cystic fibrosis: Formulation, characterisation and functionalisation with dornase alfa (DNase). *J Control Release*. 2015;198:55–61.
116. Geller DE, Weers J, Heuerding S. Development of an Inhaled Dry-Powder Formulation of Tobramycin Using PulmoSphere™ Technology. *J Aerosol Med Pulm Drug Deliv*. 2011;24(4):175–82.
117. Weers J, Tarara T. The PulmoSphere™ platform for pulmonary drug delivery. *Ther Deliv*. 2014;5(3):277–295.
118. Dos Santos Ramos MA, Da Silva PB, Spósito L, De Toledo LG, Bonifácio B vidal, Rodero CF, et al. Nanotechnology-based drug delivery systems for control of microbial biofilms: A review. *Int J Nanomedicine*. 2018;13:1179–213.
119. Drulis-Kawa Z, Dorotkiewicz-Jach A. Liposomes as delivery systems for antibiotics. *Int J Pharm*. 2010;387(1–2):187–98.
120. Moreno-Sastre M, Pastor M, Esquisabel A, Sans E, Viñas M, Fleischer A, et al. Pulmonary delivery of tobramycin-loaded nanostructured lipid carriers for *Pseudomonas aeruginosa* infections associated with cystic fibrosis. *Int J Pharm*. 2016;498(1–2):263–73.
121. Elsabahy M, Wooley KL. Design of polymeric nanoparticles for biomedical delivery applications. *Chem Soc Rev*. 2012;41:2545–61.
122. Duceppe N, Tabrizian M. Advances in using chitosan-based nanoparticles for in

- vitro and in vivo drug and gene delivery. *Expert Opin Drug Deliv.* 2010;7(10):1191–207.
123. Yasar H, Ho DK, De Rossi C, Herrmann J, Gordon S, Loretz B, et al. Starch-chitosan polyplexes: A versatile carrier system for anti-infectives and gene delivery. *Polymers (Basel).* 2018;10(3):252.
 124. Li Z, Zhang Y, Wurtz W, Lee JK, Malinin VS, Durwas-Krishnan S, et al. Characterization of Nebulized Liposomal Amikacin (ArikaceTM) as a Function of Droplet Size. *J Aerosol Med Pulm Drug Deliv.* 2008;21(3):245–53.
 125. Alhariri M, Omri A. Efficacy of liposomal bismuth-ethanedithiol-loaded tobramycin after intratracheal administration in rats with pulmonary *Pseudomonas aeruginosa* infection. *Antimicrob Agents Chemother.* 2013;57(1):569–78.
 126. Cipolla D, Wu H, Eastman S, Redelmeier T, Gonda I, Chan HK. Development and characterization of an in vitro release assay for liposomal ciprofloxacin for inhalation. *J Pharm Sci.* 2014;103(1):314–27.
 127. Cipolla D, Blanchard J, Gonda I. Development of liposomal ciprofloxacin to treat lung infections. *Pharmaceutics.* 2016.
 128. Alipour M, Halwani M, Omri A, Suntres ZE. Antimicrobial effectiveness of liposomal polymyxin B against resistant Gram-negative bacterial strains. *Int J Pharm.* 2008;355(1–2):293–8.
 129. Cheow WS, Chang MW, Hadinoto K. Antibacterial efficacy of inhalable levofloxacin-loaded polymeric nanoparticles against *E. coli* biofilm cells: The effect of antibiotic release profile. *Pharm Res.* 2010;27(8):1597–1609.
 130. Ungaro F, D'Angelo I, Coletta C, D'Emmanuele Di Villa Bianca R, Sorrentino R, Perfetto B, et al. Dry powders based on PLGA nanoparticles for pulmonary delivery of antibiotics: Modulation of encapsulation efficiency, release rate and lung deposition pattern by hydrophilic polymers. *J Control Release.* 2012;157:149–59.
 131. Abdelghany SM, Quinn DJ, Ingram RJ, Gilmore BF, Donnelly RF, Taggart CC, et al. Gentamicin-loaded nanoparticles show improved antimicrobial effects towards *Pseudomonas aeruginosa* infection. *Int J Nanomedicine.* 2012;7:4053–4063.
 132. Singh K, Mishra A, Singh A. Synthesis Characterization and In Vitro Release Study of Ciprofloxacin-Loaded Chitosan Nanoparticle. *Bionanoscience.* 2018;8(1):229–

- 36.
133. Couvreur P. Nanoparticles in drug delivery: Past, present and future. *Adv Drug Deliv Rev.* 2013;65(1):21–3.
134. D C, J F. Emerging Opportunities for Inhaled Antibiotic Therapy. *J Antimicrob Agents.* 2015;01(01):1–5.
135. Ta T, Porter TM. Thermosensitive liposomes for localized delivery and triggered release of chemotherapy. *J Control Release.* 2013;169(1–2):112–25.
136. Drummond DC, Noble CO, Hayes ME, Park JW, Kirpotin DB. Pharmacokinetics and in vivo drug release rates in liposomal nanocarrier development. *J Pharm Sci.* 2008;97(11):4696–740.
137. Lee W-H, Loo C-Y, Traini D, Young PM. Nano- and micro-based inhaled drug delivery systems for targeting alveolar macrophages. *Expert Opin Drug Deliv.* 2015;12:1009–1026.
138. Insua I, Zizmare L, Peacock AFA, Krachler AM, Fernandez-Trillo F. Polymyxin B containing polyion complex (PIC) nanoparticles: Improving the antimicrobial activity by tailoring the degree of polymerisation of the inert component. *Sci Rep.* 2017;7(9396).
139. Suk JS, Lai SK, Boylan NJ, Dawson MR, Boyle MP, Hanes J. Rapid transport of muco-inert nanoparticles in cystic fibrosis sputum treated with N-acetyl cysteine. *Nanomedicine.* 2011;6(2):365–375.
140. Murgia X, Pawelzyk P, Schaefer UF, Wagner C, Willenbacher N, Lehr C-M. Size-limited penetration of nanoparticles into porcine respiratory mucus after aerosol deposition. *Biomacromolecules.* 2016;17(4):1536–42.
141. Bernkop-Schnürch A, Dünnhaupt S. Chitosan-based drug delivery systems. Vol. 81, *European Journal of Pharmaceutics and Biopharmaceutics.* 2012. p. 463–9.
142. Ho DK, Frisch S, Biehl A, Terriac E, De Rossi C, Schwarzkopf K, et al. Farnesylated Glycol Chitosan as a Platform for Drug Delivery: Synthesis, Characterization and Investigation of Mucus-Particle Interactions. *Biomacromolecules.* 2018;19(8):3499–501.
143. Rodrigues S, Grenha A. Activation of macrophages: Establishing a role for polysaccharides in drug delivery strategies envisaging antibacterial therapy. *Curr*

- Pharm Des. 2015;21:4869– 4887.
144. Liu Z, Jiao Y, Wang Y, Zhou C, Zhang Z. Polysaccharides-based nanoparticles as drug delivery systems. Vol. 60, *Advanced Drug Delivery Reviews*. 2008. p. 1650–62.
 145. Almeida AJ, Souto E. Solid lipid nanoparticles as a drug delivery system for peptides and proteins. Vol. 59, *Advanced Drug Delivery Reviews*. 2007. p. 478–90.
 146. Stegemann S, Leveiller F, Franchi D, de Jong H, Lindén H. When poor solubility becomes an issue: From early stage to proof of concept. *European Journal of Pharmaceutical Sciences*. 2007.

6. SCIENTIFIC OUTPUT

6.1. PAPER 1: “Starch-Chitosan Polyplexes: A Versatile Carrier System for Anti-Infectives and Gene Delivery”

This chapter is the following publication:

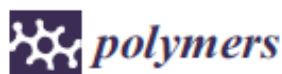
Starch-Chitosan Polyplexes: A Versatile Carrier System for Anti-Infectives and Gene Delivery

Hanzey Yasar*, **Duy-Khiet Ho***, Chiara De Rossi, Jennifer Herrmann, Sarah Gordon, Brigitta Loretz and Claus-Michael Lehr; *Polymers*. 2018, 10, 252.

** These authors contributed equally to this work.*

DOI: 10.3390 / polym10030252

Reprinted from *Polymers*, Open Access MDPI



Article

Starch-Chitosan Polyplexes: A Versatile Carrier System for Anti-Infectives and Gene Delivery

Hanzey Yasar ^{1,2,†}, Duy-Khiet Ho ^{1,2,†}, Chiara De Rossi ¹, Jennifer Herrmann ¹, Sarah Gordon ¹ , Brigitta Loretz ^{1,*} and Claus-Michael Lehr ^{1,2} 

¹ Helmholtz Institute for Pharmaceutical Research Saarland (HIPS), Helmholtz Center for Infection Research (HZI), Saarland University, D-66123 Saarbrücken, Germany; Hanzey.Yasar@helmholtz-hzi.de (H.Y.); DuyKhiet.Ho@helmholtz-hzi.de (D.-K.H.); Chiara.DeRossi@helmholtz-hzi.de (C.D.R.); jennifer.herrmann@helmholtz-hzi.de (J.H.); S.C.Gordon@ljmu.ac.uk (S.G.); Claus-Michael.Lehr@helmholtz-hzi.de (C.-M.L.)

² Department of Pharmacy, Saarland University, D-66123 Saarbrücken, Germany

* Correspondence: Brigitta.Loretz@helmholtz-hzi.de; Tel.: +49-681-98806-1030

† These authors contributed equally to this work.

Received: 8 December 2017; Accepted: 27 February 2018; Published: 1 March 2018

Abstract: Despite the enormous potential of nanomedicine, the search for materials from renewable resources that balance bio-medical requirements and engineering aspects is still challenging. This study proposes an easy method to make nanoparticles composed of oxidized starch and chitosan, both isolated from natural biopolymers. The careful adjustment of C/N ratio, polymer concentration and molecular weight allowed for tuning of particle characteristics. The system's carrier capability was assessed both for anti-infectives and for nucleic acid. Higher starch content polyplexes were found to be suitable for high encapsulation efficiency of cationic anti-infectives and preserving their bactericidal function. A cationic carrier was obtained by coating the anionic polyplex with chitosan. Coating allowed for a minimal amount of cationic polymer to be employed and facilitated plasmid DNA loading both within the particle core and on the surface. Transfection studies showed encouraging result, approximately 5% of A549 cells with reporter gene expression. In summary, starch-chitosan complexes are suitable carriers with promising perspectives for pharmaceutical use.

Keywords: polymeric nanoparticles; renewable polysaccharides; anionic starch; cationic anti-infectives; transfection

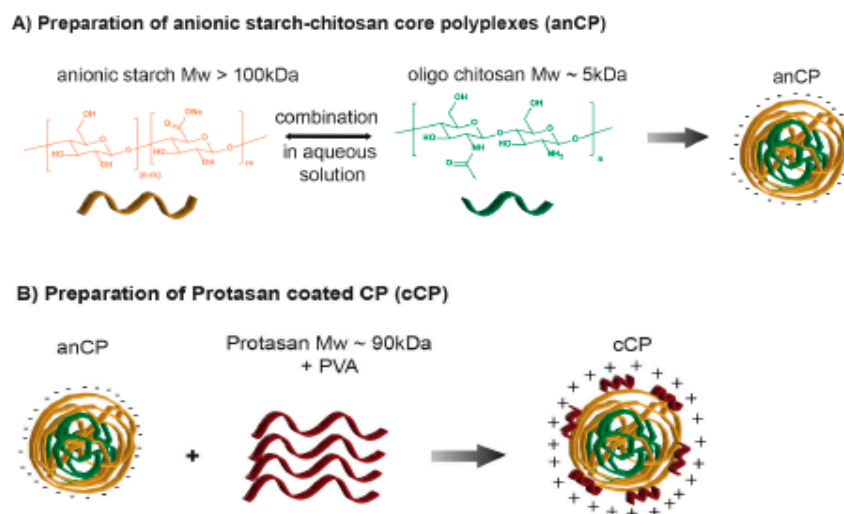
1. Introduction

Nanoparticulate carrier systems represent a well established platform for vaccination and treatment of severe diseases, such as infection and cancer, by protecting active agents, preventing burst release kinetics, providing the potential to enhance crossing of biological barriers and improving local drug delivery [1–4]. However, the selection of materials or excipients for nanomedical applications remains challenging due to strict requirements of the field. Such materials should be biocompatible and biodegradable, safe and at the same time provide good drug loading capacity as well as a potential to carry diverse bioactive agents [3]. Moreover, for large scale production, the used materials should be environmentally friendly, and able to be manufactured by facile processes. In recent years, a variety of polymeric materials derived from natural biopolymers have been synthesized and investigated to formulate vehicles to deliver bioactive molecules. These molecules have been embedded inside the polymeric matrix or adsorbed onto the colloidal surface [5] by either physical interaction (e.g., electrostatic complexation) or chemical modification. Nevertheless, the number of biodegradable and biocompatible polymers which are further compatible with water (as a solvent suitable for pharmaceutical use) and can form nanoparticles with a high and versatile active agent

encapsulation capacity are still limited. Hence, the production of excipients for nanomedicine with a balance between pharmaceutical requirements and engineering aspects as well as a tunable potential for drug delivery has gained considerable attention. In particular, natural and modified polysaccharides such as chitosan, alginate, starch and dextrin, and their synthetic derivatives, have been considered as efficient candidates for drug carrier systems [1,6,7]. However, achieving a consistent and robust production of polysaccharide nanoparticles is challenging due to the heterogeneous physicochemical properties of natural and synthetic polymers. In addition, depending on the actives to be delivered and the route of administration, different protocols are needed [8] to prepare polysaccharide-based polymeric nanoparticles [9,10]. Thus, the chosen polymers need to be appropriately tailored, chemically modified and optimized to qualify for targeted applications [1].

Among natural polysaccharides, starch and chitosan have many promising properties. Starch is a biocompatible and biodegradable polysaccharide, which is degraded by α -amylase, and available at relatively low cost. It has been widely used in tablets and capsules, e.g., as a binder or diluent [11]. Slightly modified derivatives of starch with fractional molecular weights have previously been studied as a platform to formulate homogenous carrier systems for gene delivery [12]. Other researchers have also studied starch-based particulate systems for drug delivery [13–15]. Chitosan is similarly biodegradable and biocompatible, and has been investigated and widely used in pharmaceutical research for drug [16,17], protein [18] and nucleic acid delivery, and for vaccination purposes [19–21]. It has also been used as a biomedical material for artificial skin and wound healing bandages [22] as a biodegradable polysaccharide [23]. Moreover, chitosan has good biocompatibility as tested in humans [24]. Yamada et al. [12] has reported the preparation of anionic starch derivatives by mild chemical modification, and the separation of different molecular weights by a fractional cut-off protocol, which was later aimed for transfection study. The research showed promising perspectives of starch derivatives as drug carrier system. However, the charge mediated complexation of fractional starch derivatives was not fully explored in that study; the carrier capacity of such system thus remains to be investigated.

In light of these advantages, the aim of this work was to produce versatile and flexible nanocarriers using both starch and chitosan, with a facile and organic solvent-free preparation method combining the advantages of these two polymers into a carrier system. The investigated systems were composed of starch derivatives of molecular weight (M_w) >100 kDa or with M_w range of 30–100 kDa, and oligochitosan M_w 5 kDa or Protasan M_w 90 kDa as chitosan derivatives. A wide range of molecular weights was used to achieve complex stability. We also explored the design space of the system to obtain particles with high colloidal stability as well as tunable surface charge and size. Thus, the varied production parameters of starch-chitosan polyplexes (Scheme 1A) were: (i) molar ratio of carboxylate and amine functional groups (C/N ratio) of starch and chitosan, respectively; (ii) polymer concentration; and (iii) counter polymer type. The loading capacity and versatility of these simple carriers was then investigated using tobramycin and colistin as clinically relevant models of small molecule and peptide anti-infectives respectively [25,26], as well as nucleic acids (plasmid DNA). Furthermore, to improve encapsulation capacity, we coated the starch-chitosan polyplexes with an additional chitosan (Protasan) layer (Scheme 1B), and explored the loading capacity of the resulting nanoparticles. Coating the polyplexes enabled drug loading on the surface of particles, which led to a better encapsulation particularly in the case of the utilized nucleic acids. This approach also creates the further potential for formulating a multifunctional delivery system. The novel approach of starch-chitosan-based complex-coacervation suggested in this study is a straightforward and promising technique to prepare versatile carrier systems with potential in nanomedicine applications. Therefore, we undertook preliminary studies of design, synthesis, and formulation of such carrier systems, and explored their flexibility and capacity for encapsulating selected model macromolecular drugs.



Scheme 1. Illustration of drug-free (plain) starch-chitosan polyplex-preparation.

2. Experimental Section

2.1. Materials

As raw material, partially hydrolyzed potato starch (M_w of 1300 kDa), which was a kind gift from AVEBE (Veendam, The Netherlands), was used. Selective oxidation of the primary alcohol on starch was performed to increase water solubility and obtain an anionic charge. The oxidation procedure and molecular weight fractionation of three M_w samples (5, 30–100, and >100 kDa) was conducted in accordance with the protocol of Yamada et al. [12]. The obtained starch derivatives had an oxidation degree of 45%. The M_w fraction >100 kDa is used unless stated otherwise and is termed “anionic starch” in all further descriptions.

Chitosan oligosaccharide lactate (oligochitosan; M_w 5 kDa), polyvinyl alcohol (PVA; Mowiol[®] 4-88), sodium hydroxide, trifluoroacetic acid (TFA), acetonitrile and acetic acid were purchased from Sigma-Aldrich (Darmstadt, Germany). Tobramycin sulfate salt and colistin sulfate salt were used as received also from Sigma-Aldrich. Ultrapure chitosan chloride salt (Protasan UP CL113; M_w ~90 kDa, deacetylation degree 75–90%) was obtained from FMC Biopolymer AS NovaMatrix (Sandvika, Norway). Purified water was produced by a Milli-Q water purification system from Merck Millipore (Darmstadt, Germany). O-Phthalaldehyde (OPA), 2-mercaptoethanol, phosphotungstic acid (PTA) and boric acid were used as purchased from Sigma-Aldrich.

Agarose SERVA for DNA Electrophoresis of research grade was bought from Serva (Heidelberg, Germany). Ethidium bromide solution (10 mg/mL), heparin sodium salt from porcine intestinal mucosa, 3-(4,5-dimethylthiazol-2-yl)-2,5-diphenyltetrazolium bromide (MTT reagent), Triton[™] X-100, dimethyl sulfoxide (DMSO) and Dulbecco's phosphate buffered saline solution (PBS) were obtained from Sigma-Aldrich. Gibco Hanks' balanced salt solution (HBSS) buffer was purchased from Thermo Fisher Scientific (Darmstadt, Germany). A549 cells (human lung carcinoma cell line, No. ACC 107) were obtained from DSMZ GmbH (Braunschweig, Germany). Cell culture medium (RPMI 1640) was purchased from PAA laboratories GmbH (Pasching, Austria) and supplemented with 10% fetal calf serum (FCS, Sigma-Aldrich). Plasmid DNA (pDNA) encoding for the fluorescent protein AmCyan was bought from Clontech Laboratories, Inc. (pAmCyan 1-N1, Mountain View, CA, USA). The plasmid

was propagated in *Escherichia coli* DH5 α and isolated with Qiagen EndoFree Plasmid Mega Kit (Qiagen, Hilden, Germany) to obtain pDNA of cell culture quality. jetPRIME[®] transfection reagent was purchased from Polyplus-transfection (Illkirch, France). Rhodamine *Ricinus communis* agglutinin I (RGA I) was obtained from Vector Laboratories. 4',6-diamidino-2-phenylindole (DAPI) was purchased from Life Technologies (Darmstadt, Germany).

2.2. Preparation, Optimization and Characterization of Starch–Chitosan Core Polyplexes

2.2.1. Preparation and Optimization of Starch–Chitosan Core Polyplexes (CP)

Starch-chitosan core polyplexes (CP) were prepared by self-assembly of anionic starch derivatives and chitosan derivatives in aqueous medium. CP characteristics, including their: (i) surface properties; (ii) size; and (iii) physicochemical stability were varied by: (i) the molecular weight of utilized anionic starch and chitosan derivatives; (ii) polymer concentration; and (iii) molar ratio of carboxylate (COONa) to amine (NH₂) groups (C/N ratio) in oxidized starch and chitosan, respectively. The polyplex formulation procedure is described in Scheme 1A. Briefly, a solution of anionic starch was prepared in Milli-Q water at a defined concentration, while the utilized chitosan derivative was solubilized in 0.02 M acetic acid, followed by pH adjustment to 5.5. The assembly into CP of oxidized starch and its counter cation occurred by the addition of an appropriate amount of starch polymer solution into the pre-warmed solution of chitosan derivative, followed by 2 min of vortexing and 1 h incubation at room temperature. To prepare anionic core polyplexes (anCP), anionic starch (M_w of >100 kDa) and oligochitosan (M_w of 5 kDa) were employed at various C/N ratios, ranging from 50:1 to 10:1 and further to 1:1, designed to optimize the formulation and stability of the polyplexes. Cationic core polyplexes (cationic CP) were prepared by co-assembly of negative starch (M_w of 30–100 kDa) and Protasan (M_w of 90 kDa) having a higher amount of positively charged amine groups. The optimal C/N ratio was identified by investigating the ratios of 1:30, 1:10 and 1:1. All samples with a solvent pH-value of 5.5 were characterized by dynamic light scattering (DLS), using a Zetasizer Nano from Malvern Instruments (UK) to obtain hydrodynamic size, polydispersity index (PDI), and using laser Doppler velocimetry to obtain ζ -potential. All samples were prepared at least in three different batches.

2.2.2. Preparation and Optimization of Protasan Coated CP (cCP)

Another approach taken to further improve the loading capacity of starch-chitosan carriers was to prepare coated polyplexes with a further layer of Protasan on anCP. The optimized coating method is described briefly as following: anCP were prepared as described and then coated with an additional layer of positively charged Protasan, by an association of amine functional groups of the chitosan and the anionic surface of the anCP (Scheme 1B). The coating solution was prepared by dissolving 3 mg of Protasan in 1 mL PVA 2% (*w/v*) solution, which was then diluted with Milli-Q water to a 1.5 mg/5 mL concentration for coating. A 500 μ L volume (6.6 mg/mL) of anCP was added dropwise to the prepared Protasan solution, which was continuously stirred for 30 min at 150 rpm. This was followed by incubation at room temperature for 3 h prior to characterization. The resulting Protasan-coated anCP (cCP, $c = 0.87$ mg/mL) were kept for further studies. Samples were prepared in at least three different batches. All particle samples were characterized for their hydrodynamic size, PDI and ζ -potential. This method was also applied to investigate the physicochemical stability of anCP and cationic CP under storage conditions of 4 °C for 27 days.

2.2.3. pH-Stability of Drug-Free CP and cCP

The colloidal stability of anCP and cCP at different pH values was investigated by incubating particle suspensions at pH values of 3.5, 4.0, 4.5, 5.5, 6.0, 7.5 and 8.0, all within the physiologically-relevant range. Samples were analyzed to obtain hydrodynamic size, PDI, and ζ -potential, after predetermined incubation times (30 min, 1 h, 3 h and 24 h). The pH-value was adjusted following polyplex preparation at pH 5.5 (as described above) by using either 0.02 M acetic acid solution or 1 M NaOH solution.

All experiments were conducted in triplicates with $n = 3$, and results expressed as mean \pm standard deviation (SD).

2.2.4. Morphology

The morphology of all produced polyplexes was visualized by transmission electron microscopy (TEM, JEM 2011, JEOL, St Andrews, UK). Before the TEM visualization, 8.7 $\mu\text{g}/10 \mu\text{L}$ of polyplexes were added on a copper grid (carbon films on 400 mesh copper grids, Plano GmbH, Wetzlar, Germany) and incubated for 10 min to allow an adhesion of polyplexes to the surface. The excess was removed, and polyplexes were further stained with 0.5% (*w/v*) PTA to improve the contrast of TEM images.

2.2.5. Cytotoxicity Study: MTT Assay

A549 cells were seeded in a 96 well plate at a density of 1×10^5 cells per well, in 200 μL of RPMI cell culture medium supplemented with 10% FCS. Cells were grown for 4 days prior to the conduction of the assay to allow for approximately 95% cell confluency. On Day 4, CP and cCP samples were diluted with a suitable amount of RPMI medium (without FCS) to achieve test concentrations of 5, 10, 40, 70, 100, 200 and 500 $\mu\text{g}/\text{mL}$. Cells were then washed twice with 200 μL HBSS buffer (pH 7.4), and polyplex samples were added to cells in triplicate. Cells incubated with only RPMI medium were used as a negative control (determined to result in 100% cell viability) and cells treated with 1% Triton™ X-100 in RPMI medium were used as positive control (designated as 0% cell viability). All samples were incubated with cells for 4 h, on a horizontal shaker with careful shaking at 150 rpm at 37 °C and 5% CO₂. Subsequently, the supernatant was removed, and cells were washed once with HBSS. Then, 200 μL of the MTT-reagent (5 mg/mL) in HBSS was applied to each well and further incubated for 4 h with gentle shaking. The supernatant was then removed and DMSO was immediately added to achieve cell lysis. Cells were incubated in DMSO for 15 min under careful shaking and protected from light. The absorbance of each well at 550 nm was then measured with a plate reader (Infinite® 200 Pro, TECAN, Männedorf, Switzerland). The percentage of viable cells was calculated in comparison to negative and positive controls as described by Nafee et al. [27].

2.3. Cationic Anti-Infective Loaded anCP

2.3.1. Preparation and Optimization of Cationic Anti-Infective Loaded anCP

Isothermal Titration Calorimetry

Two relevant anti-infectives were used to test the loading capacity of anCP. Tobramycin was used as an example of a cationic small molecule antibiotic having a molecular weight of 467.5 Da, and colistin (polymyxin E) was used as an example of a peptide antibiotic with a molecular weight of 1267.5 Da (Scheme 2A).

Interaction between anionic starch and the cationic anti-infectives tobramycin and colistin was investigated by isothermal titration calorimetry (ITC) using a NanoITC 2G (TA Instruments, New Castle, DE, USA). The purpose of such measurement was to optimize excipient to cargo ratio in drug loaded carrier production. Briefly, all drug and anionic starch solutions were prepared in milli-Q water. A 25 mM solution of tobramycin or colistin was prepared in a 250 μL syringe and used to saturate 1.5 mL of anionic starch at a concentration of 0.1 mM filled in the sample cell. Following an initial delay of 300 s, 250 μL of drug solution was repeatedly injected into the sample cell with a spacing of 500 s between injections, and at a reference power of 10 $\mu\text{Cal}/\text{s}$. The final thermogram and thermodynamic parameters were produced by subtracting the heat of dilution of either tobramycin or colistin (25 mM in 1.5 mL milli-Q water), followed by fitting using the One Set of Sites model in the data analysis software NanoAnalyze. The free energy of binding (ΔG) was calculated using the equation $\Delta G = \Delta H - T\Delta S$, where ΔH is the enthalpy change, T is temperature (Kelvin), and ΔS is the change in entropy. All measurements were performed at 25 °C.

Preparation and Optimization of Cationic Anti-Infective Loaded anCP

Both tobramycin and colistin were loaded using the same procedure, during formation of anCP, employing various C/N ratios, as follows: (i) 1 mg tobramycin or 3 mg colistin was incubated with an appropriate amount of anionic starch solution for 2 h; and (ii) pre-warmed chitosan solution at pH 5.5 was added, and coacervation was achieved by vortex mixing (2 min).

The anti-infective loaded anCP suspension was then centrifuged at $13,000\times g$ and $4\text{ }^{\circ}\text{C}$ for 20 min at least twice and allowed to equilibrate at $4\text{ }^{\circ}\text{C}$ overnight before conducting further experiments. In all experiments the supernatant produced by centrifugation was collected for drug loading quantification.

Loading Quantification

The degree of anti-infective loading in anCP was determined using an indirect quantification method (drug amount inside anCP = initial drug amount – drug amount in the supernatant). Colistin was quantified by high-performance liquid chromatography (HPLC), while tobramycin was quantified based on a protocol for detection of aminoglycosides [28], as detailed below.

HPLC Analysis

The HPLC analysis was performed on a Dionex UltiMate 3000 system (Thermo-Fischer Scientific, Dreieich, Germany) equipped with LPG-3400 SD pump, WPS-3000 autosampler, DAD3000 detector, and TCC-3000 column oven. Chromeleon software (Chromeleon 6.80 SP2 build 9.68, Thermo Scientific Dionex, Dreieich, Germany) was used for data analysis. A column set of LiChrospher[®] 100 RP-18 ($5\text{ }\mu\text{m}$) LiChroCART[®] 125-4, consisting of a $125\text{ mm} \times 4\text{ mm}$ LiChrospher 100/RP-18 column (Merck-Hitachi, Darmstadt, Germany) with a LiChrospher 100/RP-18 guard column ($5\text{ }\mu\text{m}$) (Merck-Hitachi, Darmstadt, Germany) at $30\text{ }^{\circ}\text{C}$ was used as stationary phase for all substances. A gradient method was used starting with 20% A, increasing to 50% A within 2 min, and holding for 1.5 min (A = acetonitrile, B = 0.1% TFA solution in water). Before injection, the samples were filtered through a cellulose acetate $0.2\text{ }\mu\text{m}$ membrane. The flow rate was 1.0 mL/min , and the injection volume was $50\text{ }\mu\text{L}$. A calibration curve was constructed using eight different concentrations of colistin in water, ranging from 0.2 mg/mL to 0.005 mg/mL ($r^2 = 0.9955$). All 8 standards were measured 5 times, and a percent relative standard deviation (% RSD) of less than 3.9% was calculated. The run time was 6 min, and a retention time of 3.6 min and 3.9 min was observed for colistin A and colistin B, respectively. As colistin is a mixture of two main fractions, colistin A and colistin B, both were quantified to determine colistin loading. The detection wavelength was 210 nm for colistin A and 214 nm for colistin B.

Aminoglycoside Detection Protocol

The product fluorescence of tobramycin reacted with a fluorescent reagent was measured at 344/450 nm (Ex/Em) using a Tecan microplate reader following a published method [28]. To prepare the reagent solution, a 0.2 g amount of OPA reagent was dissolved in a mixture of 1 mL methanol, 19 mL boric acid 0.4 M at pH 10.4, and 0.4 mL of 14.3 M 2-mercaptoethanol. A 2 mL of the resulting mixture was then diluted with 16 mL methanol before use. A calibration curve was constructed using five different concentrations of tobramycin in water ($0.04\text{--}0.005\text{ mg/mL}$, $r^2 = 0.9976$).

In both cases, the encapsulation efficiency (EE) and the drug loading rate (LR) were calculated according to the following equations:

$$\begin{aligned} \text{EE} &= \frac{\text{Weight of encapsulated drug in nanoparticles}}{\text{Initial amount of drug in the system}} \times 100 \\ \text{LR} &= \frac{\text{Weight of drug in nanoparticles}}{\text{Weight of nanoparticles}} \times 100 \end{aligned} \quad (1)$$

where "weight of nanoparticles" was calculated as weight of polymeric material + weight of encapsulated drug in nanoparticles.

Each sample was assayed at least in triplicate, and results are reported as the mean \pm SD.

Drug Release Study

Tobramycin or colistin release profiles from tobramycin loaded anCP or colistin loaded anCP was performed in PBS (pH 7.4) at 37 °C. Briefly, either tobramycin loaded anCP or colistin loaded anCP was diluted in PBS to have final tobramycin or colistin concentration at 10% (*w/w*) and loaded into dialysis membrane (MWCO 1 kDa, Spectrum Labs, Rancho Dominguez, CA, USA) in the case of tobramycin, or dialysis membrane (MWCO 3.5–5 kDa, Spectrum Labs, USA) in the case of colistin. After that, the whole system was put into 20 mL PBS and placed on a shaker at 400 rpm at 37 °C. The concentration of released drug was analyzed by collecting samples from the supernatant during the period from 1 h to 24 h. The amount of colistin and tobramycin were determined by HPLC and aminoglycoside detection protocol, respectively. The volume was kept constant by refilling with an identical volume of PBS. The cumulative released drug (%) was calculated (mean \pm SD of $n = 3$). Three independent experiments were conducted in triplicates, and results expressed as the mean \pm standard deviation (SD).

2.3.2. Minimum Inhibitory Concentration (MIC) Assay

The antimicrobial properties of anCP, anti-infective loaded anCP, and free drugs were performed by standard microbroth dilution assays with *Escherichia coli* (DH5 α) and *Pseudomonas aeruginosa* (PA14) in 96 well plates. A suspension of *E. coli* or *P. aeruginosa* prepared from mid log cultures in Mueller-Hinton broth or Lysogeny Broth medium (at 25 °C) was first diluted to OD₆₀₀ (absorption at 600 nm) 0.01, which corresponds to approximately 5×10^6 CFU/mL (CFU, colony-forming units). Polyplex samples (anCP, drug-loaded anCP), free drug solution and PBS as control were then added to bacteria-containing wells by serial dilution over a range of 0.03–64 μ g/mL. After incubation for 16 h at 37 °C, inhibitory concentration (IC) IC₅₀ values were determined by sigmoidal curve fitting of absorption values (600 nm) that were measured on a Tecan microplate reader. The experiments were conducted in duplicate.

2.4. Preparation of pDNA Loaded cCP

Plasmid DNA pAmCyan was incorporated into the polyplexes to evaluate the potential of the carrier system with respect to nucleic acid actives. A ratio of amine groups (chitosan) to phosphate groups (pDNA) of 20/1 was chosen and is referred to as N/P ratio. The preparation was performed in three steps: first, an appropriate amount of pAmCyan was added to a solution of anionic starch and mixed thoroughly. A 1 mL volume of this pAmCyan-starch solution was added to 1 mL of oligochitosan solution (650 μ g/mL) and mixed immediately by vortex for 15 s. A further incubation for 1 h at room temperature was then carried out, leading to the formation of pAmCyan-loaded anCP. In the second step, the pAmCyan loaded anCP were coated by Protasan as described in Section 2.2, to form pAmCyan-loaded cCP. In the third step, a further layer of pAmCyan was applied to pAmCyan-loaded cCP (1:30 *w/w*) resulting in pAmCyan double loaded cCP (Scheme 2B). The pDNA encapsulation efficiency of each step was analyzed by pelleting the samples down and measuring the absorbance of unbound pDNA (at 260/280 nm with NanoDrop Spectrophotometer) remaining in the supernatant after centrifugation for 30 min at 24,400 \times *g*. Thus, the amount of bound pDNA was examined indirectly. The products of each step were characterized to obtain hydrodynamic size, PDI, and ζ -potential, and their morphology was observed by TEM.

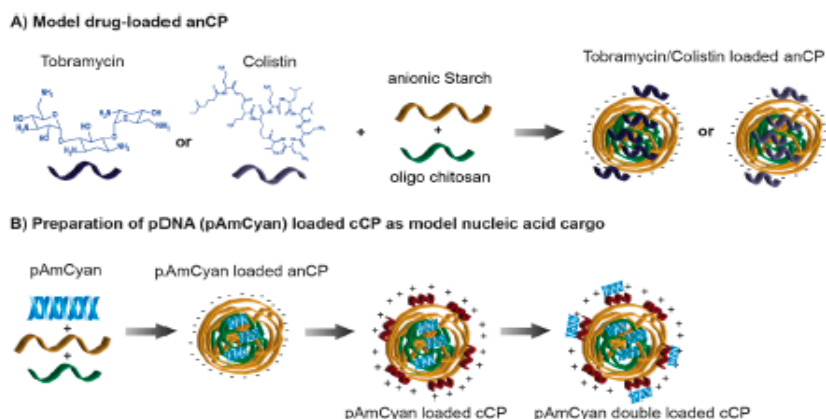
2.4.1. Determination the Complexation of pAmCyan in Starch-Chitosan Polyplexes

Complexation and stability of pAmCyan in starch-chitosan polyplexes was evaluated by a gel retardation assay using agarose gel electrophoresis. Further, to facilitate DNA fragmentation, the endonuclease BamHI was used, which linearizes the plasmid, and heparin addition to cause the release of pDNA from the complex. Polyplexes containing 500 ng of pDNA per sample from each step of the formulation process were first digested with 0.5 μ L BamHI for 2 h at 37 °C with

shaking. Afterward, 3 μL (30 mg/mL) heparin was added to solutions of digested polyplexes, incubated for 15 min at room temperature and then mixed with 2 μL of orange DNA loading dye (6 \times ; Thermo Fisher Scientific, Waltham, MA, USA). These mixtures were then loaded into 0.75% (*w/v*) agarose gel containing 5 μL of ethidium bromide and run for 60 min at 50 V in 0.5 \times TBE-buffer. The visualization of the bands was performed with a UV illuminator, Fusion FX7 imaging system from Peqlab (Erlangen, Germany).

2.4.2. In Vitro Transfection Studies in A549 Cells

To test the efficiency of the pAmCyan loaded polyplexes, in vitro transfection studies were performed in A549 cells. Briefly, A549 cells were seeded in 24-well plates, at a density of 25×10^4 cells per well in 500 μL of RPMI cell culture medium with 10% FCS. Cells were grown for 2 days to reach a cell confluency of 60–70%. Polyplexes of the pAmCyan double loaded carrier system (see Section 2.4) containing 1 μg of pAmCyan (polyplex concentration $\sim 60 \mu\text{g}/\text{mL}$) were prepared with a ratio of 1:30, 1:50 and 1:100 between pDNA:polyplexes in 500 μL of HBSS buffer. Then, cells were washed twice with HBSS buffer and incubated with the polyplexes for 6 h. After 6 h of incubation, polyplexes were removed and replaced with RPMI containing 10% FCS. Cells were further grown for 2, 3 and 4 days to identify the time point of maximum reporter gene expression. For comparison, the commercially available transfection reagent jetPRIME[®] was used as positive control. Cells treated with pAmCyan-free cCP and cell culture medium alone were used as negative controls. For confocal laser scanning microscope (CLSM; Leica TCS SP 8, Leica, Wetzlar, Germany) visualization, cell membranes were stained using RGA I (15 $\mu\text{g}/\text{mL}$), and cell nuclei were stained with DAPI (0.1 $\mu\text{g}/\text{mL}$). Samples were then fixed with 3% paraformaldehyde and stored at 4 $^{\circ}\text{C}$ until analysis. All images were acquired using a 25 \times water immersion objective at 1024 \times 1024 resolution and further processed with LAS X software (LAS X 1.8.013370, Leica Microsystems, Leica, Germany). The percentage efficiency of transfected cells was quantified using flow cytometry (BD LSRFortessa[™] Cell Analyzer, Biosciences, Heidelberg, Germany). Fifty thousand cells per sample were counted by the cytometer and data were analyzed using FlowJo software (FlowJo 7.6.5, FlowJo LLC, Ashland, OR, USA). Three independent experiments were performed in triplicates, and results expressed as the mean \pm standard deviation (SD).



Scheme 2. Illustration of starch-chitosan polyplex-preparation for drug-loaded polyplexes.

3. Results and Discussion

3.1. Preparation and Characterization of Drug-Free Starch-Chitosan Polyplexes

This study represents an extension in comparison to the particle preparation approach of Barthold et al. [29], in which the large poly dispersity index modified starch was employed for colloidal formation. Furthermore, the chemical modification in that reported study, which was used to produce cationic starch derivative, resulted in unfavorably additional synthesis step. Although the particle preparation was well established, the lack of cationic strength due to an obviously low converting yield of cationic starch synthesis limited the carrier capacity for anionic net charge actives of such system. Thus, we used fractionally modified starch derivatives to have better control of colloidal stability, and different molecular weight chitosan derivatives as strong counter excipient for the polyplexes produce. Both excipients are polysaccharides and therefore have favorable characteristics with respect to biological safety, biocompatibility and biodegradability. The simple production of polyplexes using these excipients has the perspective to be readily up-scaled. In the first series of preparations, we studied the plain polymeric complexes by combining both excipients in aqueous solution, with the electrostatic interaction between opposite charges of the individual polymers resulting in polyplex self-assembly. During the optimization of this process, various combinations of types of polymers, C/N ratio, and initial polymer solution concentration were investigated to find a stable and narrow size distribution of the produced colloidal structures (details of the optimization can be found in the Supplementary Materials, Tables S1 and S2). The best of several stable polyplex formulations was produced using a C/N ratio of 10:1, utilizing anionic starch and oligochitosan. Starch-chitosan polyplexes were obtained with an anionic surface charge evidenced by a ζ -potential of around -30 mV. The size of polyplexes could be varied from 150 nm to 350 nm by changing of polymer concentration, with a narrow PDI (<0.3) in all cases. The impact of polymer concentration on polyplex size was expected and already described for comparable systems [30,31]. Spherical polyplex morphology was visualized using TEM (Figure 1A).

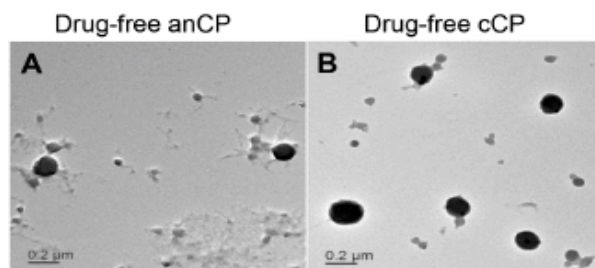


Figure 1. Transmission electron microscope (TEM) images of drug-free starch-chitosan polyplexes stained by 0.5% phosphotungstic acid solution: (A) drug-free anCP; and (B) drug-free cCP.

Reversing the C/N ratio to 1:10, and using starch (M_w 30–100 kDa) and Protasan (M_w ~90 kDa) resulted in a switch of the surface charge from anionic to cationic (further termed as cationic CP), with a ζ -potential of around $+40$ mV. The size of particles varied from 214.3 nm to approximately 400 nm depending on the polymer concentration and C/N ratio (Supplementary Materials, Tables S1 and S2). As both anCP and cationic CP systems formed as a result of attractive forces of polymer functional groups, further aggregation of systems over time may potentially occur; the physical stability of the polyplexes was therefore studied over a time course with storage at 4 °C. The colloidal characteristics of both, anCP and cationic CP, remained stable for 27 days with a PDI of ~ 0.18 and a ζ -potential of -30 mV and $+35$ mV for anCP and cationic CP, respectively (Supplementary Materials,

Figure S1). Consequently, the utilized preparation process represents a straightforward approach for the formulation of versatile nanoparticles.

The possibility to control the surface charge of a nanocarrier is advantageous for both improving the interaction with the drug to be encapsulated as well as in a later stage the interaction with the target cell [32]. Therefore, the ability to tune surface charge by changing the C/N ratio and molecular weight of starch and chitosan derivatives is a distinct advantage of this novel type of carrier. The ability to load drug molecules of differing structure size and charge, such as e.g., low- M_w anti-infectives as well as high- M_w plasmid DNA, into these carriers was then investigated. Furthermore, a simple coating process was employed to minimize the use of cationic polymer, while still allowing for positive surface charge tuning of particles. The anCP were coated with an additional layer of Protasan (M_w of 90 kDa) resulting in cationic coated polyplexes, cCP. The organic solvent-free procedure was performed in aqueous solution in the presence of PVA as a stabilizer, and led to stable cationic particles with a ζ -potential of +27.1 mV, and a spherical morphology (Figure 1B). The hydrodynamic size and PDI decreased in comparison to anCP (Table 1, Supplementary Materials Table S3) due to the improved electrostatic interaction between the excipients. Furthermore, the anionic, cationic and coated polyplexes overall indicated ζ -potential values of around ± 30 mV at which the value ensures improved colloidal stability [33–35], giving the polyplexes the possibility to survive and overcome various biological barriers and reach a specific site of interest.

Table 1. Summary of characteristics of representative drug-free (plain) polyplexes. All measurements were conducted in triplicates. $n = 3$, mean \pm SD.

Polyplexes	Size (nm)	PDI	ζ -potential (mV)
Drug-free anCP	287.9 \pm 5.0	0.22 \pm 0.01	−29.7 \pm 0.4
Drug-free cCP	205.4 \pm 3.9	0.14 \pm 0.02	27.1 \pm 1.0

3.1.1. Colloidal Stability of Drug-Free anCP and cCP

To explore the potential to administer anCP and cCP by various routes, the physicochemical stability of these systems was investigated at pH values ranging from 3.5 to 8.0, as relevant for various drug administration pathways. The stability of the polyplexes in different conditions of pH was investigated following 30 min, 1 h, 3 h and 24 h of incubation. As the assembly of the polysaccharide nanoparticulate systems was based on electrostatic interaction, stability of such systems mainly depends on its surface properties which are, in turn, influenced by surrounding environmental factors, e.g., ionic strength and pH values [35,36]. anCP showed stable characteristics regarding size, PDI and ζ -potential, even at the lowest investigated pH value of 3.5 after 3 h incubation (Supplementary Materials, Figure S2). In agreement with the results of Yamada et al. [12], the relatively high M_w (>100 kDa) of the anionic starch clearly aids in stabilization of the particles.

However, the possible dissociation of carboxylate groups on particle surfaces may have eventually led to colloidal aggregation [36] at pH 3.5 and hence destabilized the polyplexes, as indicated by stability data after 24 h of incubation. By contrast the anCP remained stable at all other, higher, pH values after a 24 h incubation (Figure 2), which could be explained by an enhanced repulsive force among anionic particles due to increasing deprotonation of surface carboxylate groups at high pH values. The stability test performed on cCP revealed a stable particle size and PDI at all pH values after 24 h, however a reduction in cCP ζ -potential was seen from pH 3.5 to 8.0 (Figure 2). This behavior is explained by protonation of chitosan molecules, which, being a weak polyelectrolyte with a pK_a of approximately 6.5, has a changing protonation degree depending on the pH of the surrounding solution [37]. An increase in pH value up to 8.0 resulted in a diminishing protonation degree of the chitosan polymer [37,38], thereby resulting in a decrease ζ -potential. Nevertheless, a continued stability of cCP at all tested pH values, especially at pH 7.5 and 8, which are higher than the chitosan pK_a value, could be conferred by the presence of PVA, as a stabilizer that interrupts colloid interaction and aggregation. The stability of both anCP and cCP over a broad range of pH values clearly indicated

flexibility in the potential application of such a tunable carrier system, for drug delivery via various routes of administration. The system could be considered for use in pulmonary delivery, where the local pH is nearly neutral; for gastrointestinal and vaginal delivery, where a low pH environment is encountered [39–41]; and in other applications.

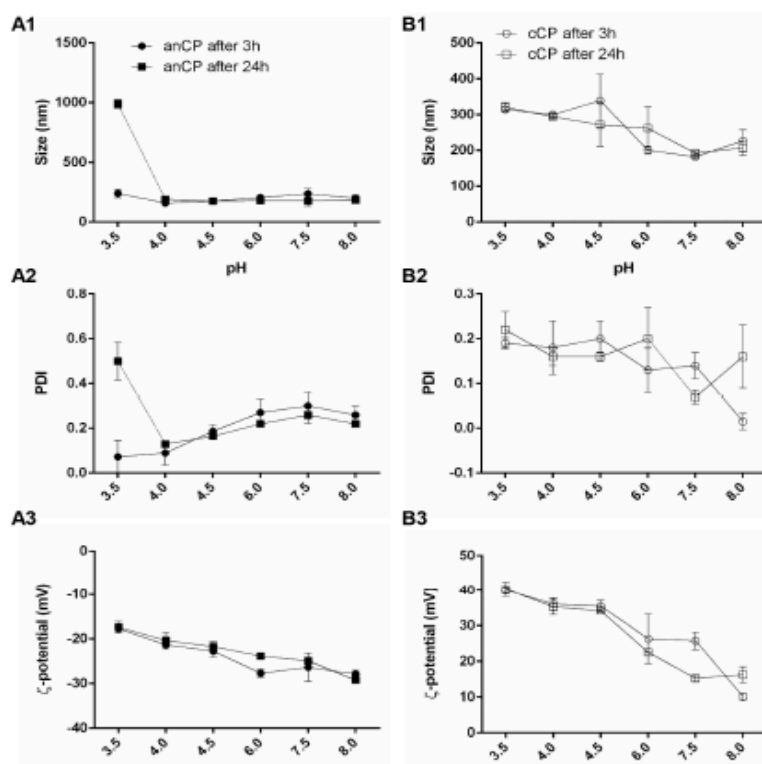


Figure 2. Characteristics of anionic core polyplexes (anCP, **A1**, **A2** and **A3**) and Protasnan-coated core polyplexes (cCP, **B1**, **B2** and **B3**) after 3 h and 24 h incubation in pH conditions ranging from 3.5 to 8.0. The pH-values changed accordingly starting from an initial pH-value of the samples of 5.5. $n = 3$, mean \pm SD.

3.1.2. Cytotoxicity Assessment

A549 cells were used in our study as a model cell line to test the potential of our carrier system. Figure 3 shows the viability of A549 cells exposed to anCP and cCP with concentrations up to 500 $\mu\text{g}/\text{mL}$, with the light grey area marking the concentration used for later MIC assays and the dark grey showing the concentration employed in subsequent transfection studies. The anCP demonstrated almost no cytotoxicity over the tested concentration range, with an observed cell viability of nearly 100% at all concentrations. However, in contrast, cell viability decreased markedly following treatment with increasing concentrations of cCP. This may be due to their cationic surface charge [42], which, on the other hand, could potentially facilitate a higher cellular uptake of cCP [43], as is particularly relevant for pDNA delivery applications. Ultimately, the cationic surface charge of such pDNA polyplex must be carefully tuned towards an acceptable compromise between transfection efficacy and biocompatibility.

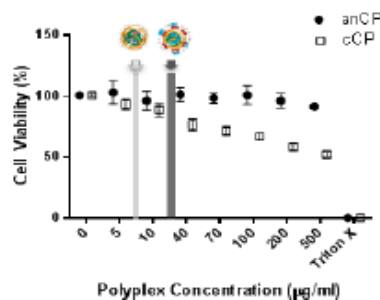


Figure 3. Cell viability assayed by MTT after 4 h incubation (mean \pm SD, $n = 9$ from three independent experiments).

3.2. Loading of anCP with Low-Mw Anti-Infectives

3.2.1. Optimization of the Preparation Process and Drug-Loading

To explore the potential of anCP as a carrier for diverse drug cargos, the aminoglycoside tobramycin ($M_w = 467.5$ Da), and the oligopeptide colistin ($M_w = 1267.5$ Da) were chosen as low molecular weight cargos. Tobramycin and colistin are active against Gram negative bacteria, and are two of the four drugs specifically approved in Europe for application as inhaled therapies for chronic bronchopulmonary *P. aeruginosa* infection in cystic fibrosis patients [25,26,44]. Fast elimination and poor permeability however often limit the delivery of hydrophilic anti-infectives, such as tobramycin and colistin, requiring frequent and high dosing with the risk of adverse drug effects and the development of bacterial resistance. Approaches to encapsulate these essential anti-infectives within drug carrier systems to avoid such delivery problems and preserve their activity have therefore been described [30,45]. Tobramycin and colistin both have net positive charges at a neutral pH value due to the presence of amine functional groups in their structures. Thus, it was hypothesized that their properties would be conducive to incorporation into anionic starch-based particles. Consequently, the interaction of further applied chitosan molecules and anionic starch would be affected, which would eventually lead to unstable colloids and aggregation of the resulting system. Therefore, before coacervation, the potential binding of anti-infective molecules to oxidized starch polymer (M_w of >100 kDa), was investigated by isothermal titration calorimetry (ITC), which revealed the thermodynamics of the binding and helped to estimate the optimal drug amount for loading in anCP. Tobramycin and colistin respectively were injected as aqueous solutions to saturate an anionic starch solution, as shown in Figure 4. Values in the inset tables were calculated by the software NanoAnalyze, yielding the same Gibbs free energy (ΔG) for the interaction of around -17.12 kJ/mol for both tobramycin and colistin respectively with the anionic starch polymer. Moreover, based on the thermograms from the ITC analysis, the amount of tobramycin or colistin needed to completely saturate the anionic starch polymer is known. To completely saturate the fixed amount of anionic starch (e.g., 5 mg), there is a need of 1 mg tobramycin, while the needed amount of colistin is 3 mg. The interaction between drug molecule-anionic starch, as well as the number of amine groups on each drug molecule are similar; their molecular weight, however, are nearly three times different. Thus, the amount of the used colistin was three times higher than that of tobramycin. With the aforementioned optimization, the amounts of drugs were selected and for further investigation of drug-loaded anCP.

Having illustrated a clear interaction of tobramycin and colistin with anionic starch, preparation of drug-loaded anCP using chitosan as a counter polymer was investigated. Anionic starch and the selected anti-infective were first incubated, followed by the addition of an appropriate amount of pre-warmed chitosan solution, leading to the formation of polyplexes by self-assembly of these polyelectrolytes. A comparable particle preparing procedure was described by Deacon et al. for

tobramycin and alginate [30]. The C/N ratio and the initial concentrations of the three components (anionic starch, chitosan, and tobramycin or colistin) were varied, and the characteristics of the resulting polyplexes were investigated in order to achieve an optimal formulation. The results of this optimization work are highlighted in Table 2, with additional data shown in the Supplementary Materials (Tables S4 and S5).

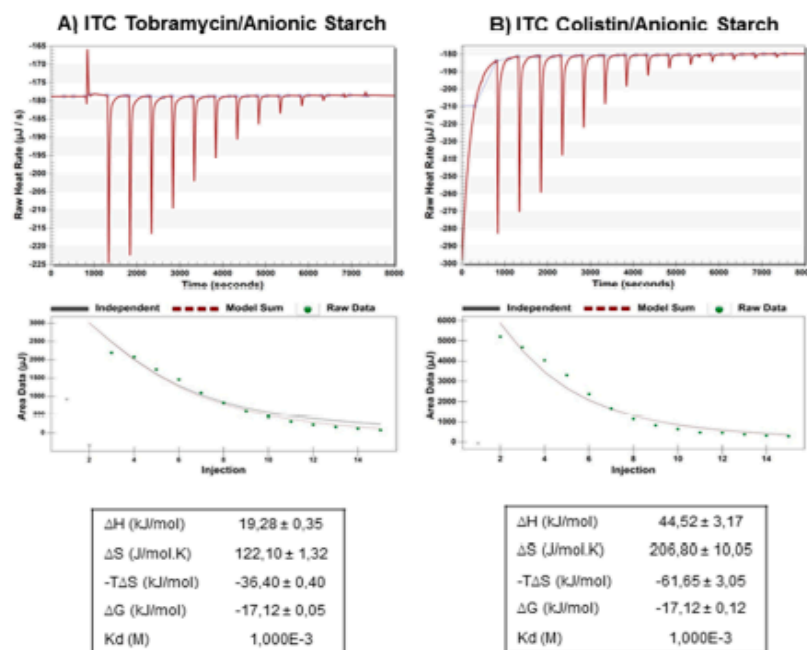


Figure 4. Isothermal titration calorimetry (ITC): (A) titration of tobramycin (25 mM) into anionic starch derivative (M_w of >100 kDa) (0.1 mM); and (B) titration of colistin (25 mM) into anionic starch derivative (M_w of >100 kDa) (0.1 mM).

The loading capacity of tobramycin and colistin in anCP was then evaluated. Encapsulation of these molecules into anCP was based on the association of anionic ions of oxidized starch and cationic ions of drug molecules. Hence, by using a fixed amount of drug molecules, and varying the C/N ratio (by varying the amount of added chitosan derivative) as well as the initial concentration of polymer solution, stable drug-loaded colloids could be produced. As shown in Table S4, tobramycin-loaded anCP ranging in size from 165.8 ± 0.8 nm to 375.9 ± 1.8 nm with a homogenous distribution ($PDI < 0.3$) were formed. The ζ -potential of tobramycin-loaded anCP generally increased from nearly -30 mV to average -17 mV, which suggested the presence of cationic drug molecules not only within the polyplex matrix, but also on the surface of polyplexes. An increasing C/N ratio also resulted in a tendency for decreasing particle size from 375.9 ± 1.8 nm to 175.2 ± 2.8 nm. This decrease in size could be due to a condensing effect when using a higher amount of starch, which introduced an excess of available anionic ions for interaction with chitosan, even after incubation with tobramycin. As a result, the colloidal characteristics of tobramycin-loaded nanoparticles were not significantly different to those of unloaded systems. To obtain colistin-loaded anCP, an amount of colistin three times higher in comparison to tobramycin was employed for pre-incubation with anionic starch, due to the molecular

weight difference between the two drugs. Colistin-loaded anCP were prepared again using varying polymer concentrations. As the final concentration decreased, while C/N ratio was maintained at 40/1, the particle size decreased from 324.4 ± 3.6 nm to 266.3 ± 6.5 nm (Table S5). The colistin loaded systems were also stable and homogenous with PDI values lower than 0.3. The results, therefore, clearly show that a reduction in polyplex size resulted from a decrease in employed polymer concentration; this is also in accordance with observations in previous studies [31]. Overall, there was an increase in the ζ -potential of drug loaded carriers as compared to unloaded, which is evidence for the presence of positive net charge anti-infective molecules on carrier surfaces. The size of colistin-loaded anCP was generally larger than the corresponding tobramycin-loaded anCP, which could be explained by the possible formation of colistin micelles during incubation with starch solution. This is made possible by the amphiphilic molecular structure of colistin, which possesses a lipophilic fatty acyl tail and a hydrophilic head group [46]. Consequently, the addition of chitosan supported the colloidal stability of the polyplex system. The morphology of anti-infective loaded anCP was spherical as investigated by TEM (Figure 5A,B). The encapsulation efficiency (EE) and loading rate (LR) of colistin- and tobramycin-loaded anCP are highlighted in Table 2 and Tables S6 and S7. The EE and LR values were indirectly calculated by collecting supernatants after two washing steps. As determined using HPLC, colistin encapsulated within anCP showed maximum values of $96.57 \pm 0.19\%$ and $22.70 \pm 0.33\%$ for EE and LR, respectively. Incorporation of tobramycin, determined by product fluorescence at 344/450 nm, also showed an EE higher than 98% in all cases, but comparatively lower LR values ($2.9 \pm 0.0\%$ maximum). The high EE of both model drugs (>90% in all cases) was a result of pre-determination of the interaction between drug molecules and anionic starch, which allowed estimating the amount of used drug in encapsulation and thereby maximization of the encapsulation efficiency. The LR of tobramycin-loaded anCP showed a rational loading capacity for polymeric nanoparticles with a size of approximately 200 nm, while the LR of colistin-loaded anCP was surprisingly high. This might be due to the aforementioned micelle formation of colistin molecules, stabilized by the starch polymer solution. Hence, colistin could be localized in the core of nanoparticles, covered by starch polymer molecules, and could also be loaded on the surface of the system due to charge interaction. The results clearly demonstrate the capacity of the anCP carrier system to be loaded with either type of low- M_w anti-infectives.

Table 2. Summary of characteristics of drug-loaded anCP, %EE = encapsulation efficiency and %LR = loading rate. All measurements were conducted in triplicates. $n = 3$, mean \pm SD.

Polyplexes	Size (nm)	PDI	ζ -potential (mV)	%EE	%LR
Tobramycin loaded anCP	175.2 ± 2.8	0.18 ± 0.00	-16.8 ± 1.0	98.7 ± 0.1	2.9 ± 0.0
Colistin loaded anCP	266.3 ± 6.5	0.27 ± 0.01	-14.6 ± 0.5	96.6 ± 0.2	17.2 ± 0.1
pAmCyan loaded anCP	271.8 ± 2.4	0.25 ± 0.01	-29.8 ± 0.6	76.6 ± 0.6	0.3 ± 0.002
pAmCyan loaded cCP	214.0 ± 3.5	0.17 ± 0.01	28.0 ± 0.6	67.7 ± 14.1	0.2 ± 0.036
pAmCyan double loaded cCP	204.6 ± 3.5	0.16 ± 0.02	25.5 ± 0.6	93.9 ± 4.5	3.3 ± 0.150

Furthermore, the cumulative release profile of both tobramycin and colistin from drug-loaded anCP were studied in PBS at 37°C , the results are shown in Figure S3. Clearly, the controlled release of anti-infective in PBS could be observed in both cases, with over 40% and 20% of drug released over the period 16–24 h for tobramycin and colistin, respectively. The initial burst after 4–6 h incubation was recorded as on average nearly 30% for tobramycin and 20% for colistin. The percentage of initial anti-infective released from the anCP would represent the amount of drug molecule loaded on the particles surface. Interestingly, the release of colistin at all time points are relatively lower than that of tobramycin, which would again be explained by the aforementioned micelle formation of colistin molecules that are stabilized and maybe then embedded inside the polymeric polyplex. The release results would help predict the drug carriers behavior in further in vitro experiments. To evaluate the release of the anti-infectives from drug-loaded anCP, and have better insight into the controlled

release in vitro or in vivo, in which other components exist, e.g., bacteria, would require more complex biologically simulated tests that were beyond the scope of the present study.

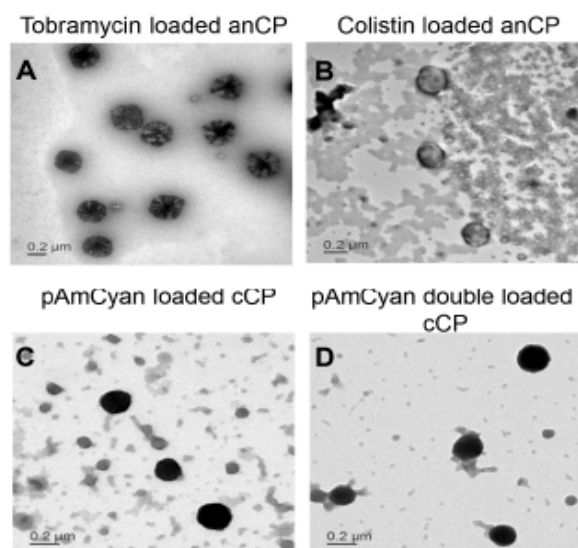


Figure 5. Transmission electron microscope (TEM) images of drug-loaded starch-chitosan polyplexes stained by 0.5% phosphotungstic acid solution: (A) tobramycin loaded anCP; (B) colistin loaded anCP; (C) pAmCyan loaded cCP; and (D) pAmCyan double loaded cCP.

3.2.2. Efficacy of Anti-Infective Loaded anCP

While anCP have the capacity to load different types of anti-infectives including small molecule and peptide drugs, it is important that the particle excipients do not interfere with action of active agents which might confound the further evaluation of drug delivery systems. Hence, the anti-microbial activity of blank anCP and anti-infective loaded anCP were studied against *E. coli* and *P. aeruginosa* in comparison to the use of free drugs. As shown in Table 3, the antibacterial activity of drug-loaded anCP was relatively similar to that of the corresponding free drug. MIC values obtained show that blank anCP were not active against *E. coli* and *P. aeruginosa* at the highest tested concentrations, which means the formation of polyplexes with anCP did not compromise the intrinsic anti-microbial efficiency of either antibiotic. To demonstrate a superior safety and efficiency profile of such nanocarriers in comparison to the free drug would require some more complex biological test systems that were beyond the scope of the present study.

Table 3. MIC assay results against *E. coli* and *P. aeruginosa*.

Samples	IC90 against <i>E. coli</i> (μg/mL)	IC90 against <i>P. aeruginosa</i> (μg/mL)
Tobramycin	0.2–0.3	1.56
Tobramycin loaded anCP	0.2–0.3 *	1.56 *
Colistin	0.4–0.5	3.125
Colistin loaded anCP	0.5 *	3.125–6.25 *
anCP	>64	>64
PBS buffer	no inhibition	no inhibition

* Drug content in anCP.

3.3. Loading of anCP with High-Mw pDNA

A model plasmid DNA encoding a fluorescent dye (pAmCyan) was further incorporated into the carrier system in a three-step procedure (core formation, Protasan coating and pDNA complexation), to demonstrate the ability of the polyplexes to deliver a broad spectrum of cargos. The three-step procedure also lead to an increase of nucleic acid encapsulation within the polyplexes, protecting nucleic acids from enzymatic degradation. Produced pAmCyan loaded polyplexes were again found to have a spherical structure (Figure 5C,D). The physiochemical characteristics of all intermediate and final polyplexes in this stepwise production can be found in Table 2. Each subsequent step in the preparation procedure results in a denser complexation, with the pAmCyan double loaded cCP showing the smallest size and most narrow size distribution (lowest PDI value). Furthermore, the ζ -potential was observed to switch from negative to positive after coating with Protasan, with a further slight decrease after complexation with negatively charged pAmCyan. The additional complexation with pAmCyan resulted in a 15% higher encapsulation efficiency in comparison to the intermediate step 2 (Table 2). Additionally, agarose gel electrophoresis (Figure 6, left) elucidates that no pDNA could run through the gel, which indicates that pDNA is strongly complexed within the polyplexes. Only further treatment with BamHI and heparin causes pDNA release as seen through the bands (Figure 6, right). Furthermore, pDNA loaded anCP and pDNA associated on the surface of polyplexes (pDNA double loaded cCP) allow an easier intercalation of EtBr and faster release with heparin, whereas pDNA loaded cCP is densely packed impeding pDNA release as no free pDNA bands can be observed in the gel.

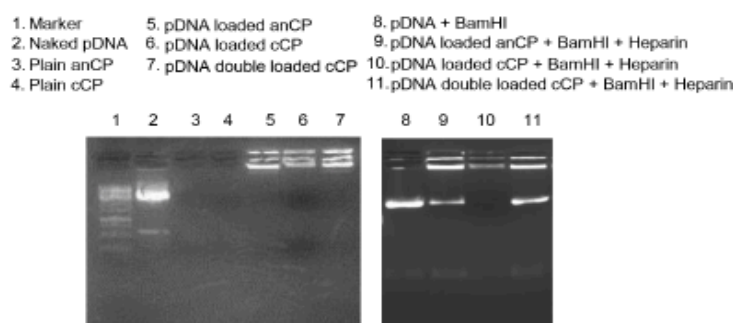


Figure 6. Gel retardation assay using agarose gel electrophoresis of plain and pDNA (pAmCyan) incorporated polyplexes for all three preparation steps in comparison with naked pDNA (undigested pDNA) and digested pDNA (pDNA + BamHI).

Potential of Polyplexes for pDNA Delivery

Using nanoparticles as a non-viral delivery system for gene therapy represents a significant challenge, as nanocarriers need to cross several biological barriers while preserving the functionality of carried pDNA. pDNA condensed inside the nanocarriers must survive the acidic conditions inside the lysosomes and escape the lysosomal compartment in order to cross the nuclear membrane [43]. Current knowledge of polymeric transfection systems suggests that a good pH-buffering capacity (a process known as the “proton sponge effect”) [47] is an important factor in the achievement of endosomal escape. Here, the potential of starch–chitosan polyplexes for nucleic acid delivery was explored by *in vitro* transfection studies using A549 cells. Three different ratios between pDNA:polyplexes have been studied to investigate the best transfection rate. While 1:50 and 1:100 show no significant transfection (data not shown), 1:30 mediated successful transfection, with the highest reporter gene expression observed after 48 h with 5% of transfected cells. In comparison, jetPRIME[®] as positive

control had a higher transfection efficiency (45%) after 48 h, which rapidly decreased to 30% after 72 h and to 25% after 96 h (Figure 7). The comparatively lower transfection efficiency of the polyplexes may be due to a high stability of condensed pDNA, leading to an incomplete release of pDNA inside the cytoplasmic compartment [48,49]. Further improvement of the transfection efficiency would presumably be achievable by addition of endosomal escape moieties [50,51], or with chitosan derivatives (e.g., trimethylation or amino acid conjugation) [52,53]. However, such efficacy improvements often impact the biocompatibility. Thus, optimization between safety and efficacy should be performed for a selected nucleotide type, target application, and delivery route, since carrier stability, cellular uptake, and functional efficacy are highly dependent on all these factors.

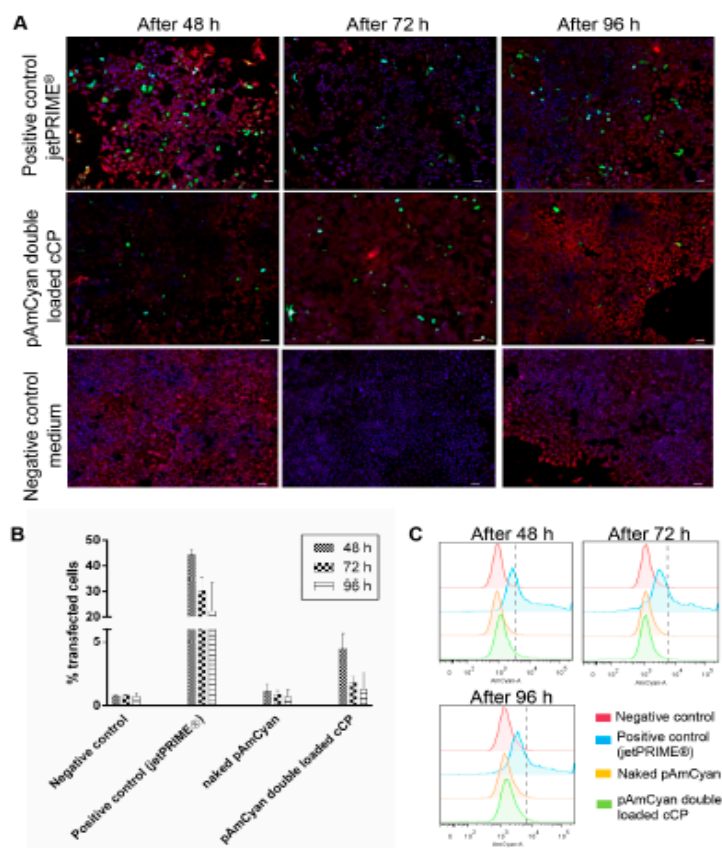


Figure 7. (A) Representative confocal images of A549 cells transfected with pAmCyan double loaded pAmCyan by using jetPRIME® as positive control and only cell culture medium as negative control. Transfection was analyzed with CLSM after 48 h, 72 h, and 96 h. Green fluorescence reveals cells successfully transfected with the polyplexes while their morphology remains consistent with non-transfected cells (red: cell membrane; blue: cell nucleus; scale bar 50 μ m). (B) The transfection efficiency was further quantified using flow cytometry, which indicated the highest amount of transfection after 48 h for pAmCyan double loaded cCP. (C) Representative graphs obtained with flow cytometer.

4. Conclusions

In this work, we produced a flexible, straightforward and organic solvent-free procedure for the manufacture of nanocarrier systems based on the natural, biodegradable and biocompatible polysaccharides starch and chitosan. Starch and chitosan derivatives of different M_w ranges were combined by adjusting the molar ratio of carboxyl and amine functional groups, polymer concentration and counter polymer type to obtain a delivery system with tunable properties including surface charge and size. Core polyplexes (CP) were built by complex coacervation of anionic starch ($M_w \sim 100$ kDa) with positively charged chitosan derivatives ($M_w \sim 5$ kDa) in aqueous solution. The polyplexes with the best colloidal properties were obtained at a molar ratio of carboxyl and amine groups of 10:1. The negatively charged core polyplexes remained stable on storage for over 27 days. We further focused on optimizing anionic CPs by coating them with an additional layer of chitosan (Protasan, $M_w \sim 90$ kDa). Cell viability testing of anCPs and cCPs indicated a low level of cytotoxicity acceptable for use in biological systems, and colloidal stability at different tested pH values. The developed anCP system further showed good carrier properties, allowing for high encapsulation efficiency (>90%) of cationic peptide (colistin) and small molecule (tobramycin) anti-infectives without compromising antimicrobial activity. Moreover, the cationic polyplexes, cCP, allowed for double encapsulation of plasmid DNA (pAmCyan) for intracellular delivery as confirmed by gel retardation assay, and facilitating in-vitro transfection in A549 cells.

Starch-chitosan polyplexes show high flexibility for designing multifunctional carriers, in which for example the core polyplexes can encapsulate anti-infectives, while the outer coating layer could be used to incorporate other components like enzymes or nucleases (e.g., deoxyribonuclease I) to enhance drug penetration through biofilms or mucus [30]. For gene therapy purposes the inner polyplex can be used to carry and protect plasmid DNA, while the surface could be decorated with a second polynucleotide.

Supplementary Materials: The following are available online at <http://www.mdpi.com/2073-4360/10/3/252/s1>, Figure S1: Physicochemical stability of starch-chitosan CP, in which anCP was produced with C/N ratio 10/1, and catCP was produced with C/N ratio 1/10, upon storage (4 °C). The particles were diluted into Milli-Q water at each time point for the measurement of size, PDI and ζ -potential. $N = 3, n = 3$, mean \pm SD; Figure S2: Physicochemical stability of starch-chitosan anCP and cCP at different pH values ranging from 3.5 to 8.0, after 30 min and 1 h incubation. The initial pH-value of the samples was 5.5. $N = 3, n = 3$, mean \pm SD; Figure S3: Cumulative release of tobramycin from tobramycin loaded anCP, and colistin from colistin loaded anCP performed in PBS at 37 °C. $N = 3, n = 3$, mean \pm SD; Table S1: Summary of starch-chitosan CP characteristics obtained by varying polymer types, polymer concentration, and C/N molar ratio. $N > 3, n = 3$, mean \pm SD; Table S2: Summary of starch-chitosan CP characterization with optimal C/N ratio varied by change of polymer concentration. $N > 3, n = 3$, mean \pm SD; Table S3: Summary of anionic CP (anCP) and Protasan coated anCP (cCP) characteristics, in which anCP was produced with parameters, namely C/N ratio 10/1, and polymer concentration at 6.5 mg/mL. $N > 3, n = 3$, mean \pm SD; Table S4: Summary of tobramycin-loaded anCP characteristics achieved by variation of C/N ratio and polymer concentration. $N > 3, n = 3$, mean \pm SD; Table S5: Summary of colistin-loaded anCP characteristics resulting from variation of polymer concentration. $N > 3, n = 3$, mean \pm SD; Table S6: Summary of drug loading quantification of tobramycin-loaded anCP. $N > 3, n = 3$, mean \pm SD; Table S7: Summary of drug loading quantification of colistin-loaded anCP. $N > 3, n = 3$, mean \pm SD.

Acknowledgments: The authors thank Xabier Murgia Esteve, Florian Gräf, and Arianna Castoldi for fruitful discussions; Petra König and Jana Westhues for support and handling of cell cultures; and Viktoria Schmitt for bacteria culture. This project has received funding from the European Union Framework Programme for Research and Innovation Horizon 2020 (2014–2020) under the Marie Skłodowska-Curie Grant Agreement No. 642028.

Author Contributions: Harzey Yasar and Duy-Khiet Ho contributed equally in this study in which they initiated the research idea, conceived and designed all experiments. Harzey Yasar and Duy-Khiet Ho synthesized and prepared molecular weight fractionalized anionic starch, and optimized particles preparing process of starch and chitosan (including negative, positive and coated surface particles), as well as investigated stability of all particles at storage condition and different pH environments. Harzey Yasar further studied cytotoxicity (by MTT assay) and plasmid (pAmCyan) loading capacity (by a gel retardation assay) of the particles, and performed transfection study on A549 cell line by CLSM and quantification method using flow cytometry. Duy-Khiet Ho further studied and optimized cationic anti-infectives (tobramycin and colistin) loading capacity (by isothermal titration calorimetry) of the particles, and performed the minimum inhibitory concentration (MIC) assay on *E. coli* and *P. aeruginosa*. Harzey Yasar and Duy-Khiet Ho analyzed all the data and wrote the manuscript with an equal manner. Chiara De Rossi visualized the developed particles by using TEM, performed HPLC, and contributed

her expertise in imaging and analyzing the transfection study by using CLSM. Jennifer Herrmann contributed her expertise in bacteria study and analyzed the data. Sarah Gordon, Brigitta Loretz and Claus-Michael Lehr supervised Hanzey Yasar and Duy-Khiet Ho, initiated the project and have been responsible for the overall scientific approach. All authors contributed with their scientific input to the written manuscript.

Conflicts of Interest: The authors declare no competing financial interest.

Abbreviations

CP	core polyplexes
anCP	anionic core polyplexes
cationic CP (or catCP)	cationic core polyplexes
cCP	coated polyplexes

References

- Kang, B.; Opatz, T.; Landfester, K.; Wurm, F.R. Carbohydrate nanocarriers in biomedical applications: Functionalization and construction. *Chem. Soc. Rev.* **2015**, *44*, 8301–8325. [[CrossRef](#)] [[PubMed](#)]
- Bachmann, M.F.; Jennings, G.T. Vaccine delivery: A matter of size, geometry, kinetics and molecular patterns. *Nat. Rev. Immunol.* **2010**, *10*, 787–796. [[CrossRef](#)] [[PubMed](#)]
- Abed, N.; Couvreur, P. Nanocarriers for antibiotics: A promising solution to treat intracellular bacterial infections. *Int. J. Antimicrob. Agents* **2014**, *43*, 485–496. [[CrossRef](#)] [[PubMed](#)]
- D'Angelo, L.; Conte, C.; Miro, A.; Quaglia, E.; Ungaro, F. Pulmonary drug delivery: A role for polymeric nanoparticles? *Curr. Top. Med. Chem.* **2015**, *15*, 386–400. [[CrossRef](#)] [[PubMed](#)]
- Mahapatro, A.; Singh, D.K. Biodegradable nanoparticles are excellent vehicle for site directed in-vivo delivery of drugs and vaccines. *J. Nanobiotechnol.* **2011**, *9*, 55. [[CrossRef](#)] [[PubMed](#)]
- Baldwin, A.D.; Kiick, K.L. Polysaccharide-modified synthetic polymeric biomaterials. *Biopolymers* **2010**, *94*, 128–140. [[CrossRef](#)] [[PubMed](#)]
- Wikström, J.; Elomaa, M.; Syväjärvi, H.; Kuokkanen, J.; Yliperttula, M.; Honkakoski, P.; Urtti, A. Alginate-based microencapsulation of retinal pigment epithelial cell line for cell therapy. *Biomaterials* **2008**, *29*, 869–876. [[CrossRef](#)] [[PubMed](#)]
- Hans, M.L.; Lowman, A.M. Biodegradable nanoparticles for drug delivery and targeting. *Curr. Opin. Solid State Mater. Sci.* **2002**, *6*, 319–327. [[CrossRef](#)]
- Azzam, T.; Eliyahu, H.; Shapira, L.; Linial, M.; Barenholz, Y.; Domb, A.J. Polysaccharide? Oligoamine Based Conjugates for Gene Delivery. *J. Med. Chem.* **2002**, *45*, 1817–1824. [[CrossRef](#)] [[PubMed](#)]
- Sim, H.J.; Thambi, T.; Lee, D.S. Heparin-based temperature-sensitive injectable hydrogels for protein delivery. *J. Mater. Chem. B* **2015**, *3*, 8892–8901. [[CrossRef](#)]
- Builders, P.E.; Arbewoh, M.I. Pharmaceutical applications of native starch in conventional drug delivery. *Starch Stärke* **2016**, *68*, 864–873. [[CrossRef](#)]
- Yamada, H.; Loretz, B.; Lehr, C.-M. Design of starch-graft-PEI polymers: An effective and biodegradable gene delivery platform. *Biomacromolecules* **2014**, *15*, 1753–1761. [[CrossRef](#)] [[PubMed](#)]
- Mahmoudi Najafi, S.H.; Baghaie, M.; Ashori, A. Preparation and characterization of acetylated starch nanoparticles as drug carrier: Ciprofloxacin as a model. *Int. J. Biol. Macromol.* **2016**, *87*, 48–54. [[CrossRef](#)] [[PubMed](#)]
- Balmayor, E.R.; Baran, E.T.; Azevedo, H.S.; Reis, R.L. Injectable biodegradable starch/chitosan delivery system for the sustained release of gentamicin to treat bone infections. *Carbohydr. Polym.* **2012**, *87*, 32–39. [[CrossRef](#)]
- Santander-Ortega, M.J.; Stauner, T.; Loretz, B.; Ortega-Vinuesa, J.L.; Bastos-González, D.; Wenz, G.; Schaefer, U.F.; Lehr, C.M. Nanoparticles made from novel starch derivatives for transdermal drug delivery. *J. Control. Release* **2010**, *141*, 85–92. [[CrossRef](#)] [[PubMed](#)]
- Bernkop-Schnurch, A.; Dunnhaupt, S. Chitosan-based drug delivery systems. *Eur. J. Pharm. Biopharm.* **2012**, *81*, 463–469. [[CrossRef](#)] [[PubMed](#)]
- Grenha, A.; Gomes, M.E.; Rodrigues, M.; Santo, V.E.; Mano, J.E.; Neves, N.M.; Reis, R.L. Development of new chitosan/carrageenan nanoparticles for drug delivery applications. *J. Biomed. Mater. Res. Part A* **2010**, *92*, 1265–1272. [[CrossRef](#)] [[PubMed](#)]

18. Gan, Q.; Wang, T. Chitosan nanoparticle as protein delivery carrier—Systematic examination of fabrication conditions for efficient loading and release. *Colloids Surf. B Biointerfaces* **2007**, *59*, 24–34. [[CrossRef](#)] [[PubMed](#)]
19. Wen, Z.-S.; Xu, Y.-L.; Zou, X.-T.; Xu, Z.-R. Chitosan nanoparticles act as an adjuvant to promote both Th1 and Th2 immune responses induced by ovalbumin in mice. *Mar. Drugs* **2011**, *9*, 1038–1055. [[CrossRef](#)] [[PubMed](#)]
20. De Campos, A.M.; Sánchez, A.; Alonso, M.J. Chitosan nanoparticles: A new vehicle for the improvement of the delivery of drugs to the ocular surface. Application to cyclosporin A. *Int. J. Pharm.* **2001**, *224*, 159–168. [[CrossRef](#)]
21. Van der Lubben, I.M.; Verhoef, J.C.; van Aelst, A.C.; Borchard, G.; Junginger, H.E. Chitosan microparticles for oral vaccination: Preparation, characterization and preliminary in vivo uptake studies in murine Peyer's patches. *Biomaterials* **2001**, *22*, 687–694. [[CrossRef](#)]
22. Dodane, V.; Viliivalam, V.D. Pharmaceutical applications of chitosan. *Pharm. Sci. Technol. Today* **1998**, *1*, 246–253. [[CrossRef](#)]
23. Onishi, H.; Machida, Y. Biodegradation and distribution of water-soluble chitosan in mice. *Biomaterials* **1999**, *20*, 175–182. [[CrossRef](#)]
24. Aspden, T.J.; Mason, J.D.; Jones, N.S.; Lowe, J.; Skaugrud, O.; Illum, L. Chitosan as a nasal delivery system: The effect of chitosan solutions on in vitro and in vivo mucociliary transport rates in human turbinates and volunteers. *J. Pharm. Sci.* **1997**, *86*, 509–513. [[CrossRef](#)] [[PubMed](#)]
25. Elborn, J.S.; Vataire, A.-L.; Fukushima, A.; Aballea, S.; Khemiri, A.; Moore, C.; Medic, G.; Hemels, M.E.H. Comparison of Inhaled Antibiotics for the Treatment of Chronic *Pseudomonas aeruginosa* Lung Infection in Patients with Cystic Fibrosis: Systematic Literature Review and Network Meta-analysis. *Clin. Ther.* **2016**, *38*, 2204–2226. [[CrossRef](#)] [[PubMed](#)]
26. Elborn, S.; Vataire, A.-L.; Fukushima, A.; Aballea, S.; Khemiri, A.; Moore, C.; Medic, G.; Hemels, M. Efficacy and safety of inhaled antibiotics for chronic pseudomonas infection in cystic fibrosis: Network meta-analysis. *Eur. Respir. J.* **2016**, *48*, PA4863. [[CrossRef](#)]
27. Nafee, N.; Schneider, M.; Schaefer, U.F.; Lehr, C.-M. Relevance of the colloidal stability of chitosan/PLGA nanoparticles on their cytotoxicity profile. *Int. J. Pharm.* **2009**, *381*, 130–139. [[CrossRef](#)] [[PubMed](#)]
28. Benson, J.R.; Hare, P.E. O-phthalaldehyde: Fluorogenic detection of primary amines in the picomole range. Comparison with fluorecamine and ninhydrin. *Proc. Natl. Acad. Sci. USA* **1975**, *72*, 619–622. [[CrossRef](#)] [[PubMed](#)]
29. Barthold, S.; Kletting, S.; Taffner, J.; de Souza Carvalho-Wodarz, C.; Lepeltier, E.; Loretz, B.; Lehr, C.-M. Preparation of nanosized coacervates of positive and negative starch derivatives intended for pulmonary delivery of proteins. *J. Mater. Chem. B* **2016**, *4*, 2377–2386. [[CrossRef](#)]
30. Deacon, J.; Abdelghany, S.M.; Quinn, D.J.; Schmid, D.; Megaw, J.; Donnelly, R.F.; Jones, D.S.; Kissenpennig, A.; Elborn, J.S.; Gilmore, B.F.; et al. Antimicrobial efficacy of tobramycin polymeric nanoparticles for *Pseudomonas aeruginosa* infections in cystic fibrosis: Formulation, characterisation and functionalisation with dornase alfa (DNase). *J. Control. Release* **2015**, *198*, 55–61. [[CrossRef](#)] [[PubMed](#)]
31. Dul, M.; Paluch, K.J.; Kelly, H.; Healy, A.M.; Sasse, A.; Tajber, L. Self-assembled carrageenan/protamine polyelectrolyte nanoplexes—Investigation of critical parameters governing their formation and characteristics. *Carbohydr. Polym.* **2015**, *123*, 339–349. [[CrossRef](#)] [[PubMed](#)]
32. Radovic-Moreno, A.F.; Lu, T.K.; Puscasu, V.A.; Yoon, C.J.; Langer, R.; Farokhzad, O.C. Surface charge-switching polymeric nanoparticles for bacterial cell wall-targeted delivery of antibiotics. *ACS Nano* **2012**, *6*, 4279–4287. [[CrossRef](#)] [[PubMed](#)]
33. Mandzy, N.; Grulke, E.; Druffel, T. Breakage of TiO₂ agglomerates in electrostatically stabilized aqueous dispersions. *Powder Technol.* **2005**, *160*, 121–126. [[CrossRef](#)]
34. Jonassen, H.; Kjoniksen, A.-L.; Hiorth, M. Stability of chitosan nanoparticles cross-linked with tripolyphosphate. *Biomacromolecules* **2012**, *13*, 3747–3756. [[CrossRef](#)] [[PubMed](#)]
35. Honary, S.; Zahir, F. Effect of Zeta Potential on the Properties of Nano-Drug Delivery Systems—A Review (Part 2). *Trop. J. Pharm. Res.* **2013**, *12*, 265–273. [[CrossRef](#)]
36. Yoo, M.K.; Sung, Y.K.; Chong, S.C.; Young, M.L. Effect of polymer complex formation on the cloud-point of poly(*N*-isopropyl acrylamide) (PNIPAAm) in the poly(NIPAAm-co-acrylic acid): Polyelectrolyte complex between poly(acrylic acid) and poly(allylamine). *Polymer* **1997**, *38*, 2759–2765. [[CrossRef](#)]
37. Fan, W.; Yan, W.; Xu, Z.; Ni, H. Formation mechanism of monodisperse, low molecular weight chitosan nanoparticles by ionic gelation technique. *Colloids Surf. B Biointerfaces* **2012**, *90*, 21–27. [[CrossRef](#)] [[PubMed](#)]

38. Shu, X.; Zhu, K. The influence of multivalent phosphate structure on the properties of ionically cross-linked chitosan films for controlled drug release. *Eur. J. Pharm. Biopharm.* **2002**, *54*, 235–243. [[CrossRef](#)]
39. Ensign, L.M.; Cone, R.; Hanes, J. Nanoparticle-based drug delivery to the vagina: A review. *J. Control. Release* **2014**, *190*, 500–514. [[CrossRef](#)] [[PubMed](#)]
40. Evans, D.E.; Pye, G.; Bramley, R.; Clark, A.G.; Dyson, T.J.; Hardcastle, J.D. Measurement of gastrointestinal pH profiles in normal ambulant human subjects. *Gut* **1988**, *29*, 1035–1041. [[CrossRef](#)] [[PubMed](#)]
41. Melis, G.B.; Ibba, M.T.; Steri, B.; Kotsonis, P.; Matta, V.; Paoletti, A.M. Ruolo del pH come modulatore dell'equilibrio fisiopatologico vaginale. *Min. Ginecol.* **2000**, *52*, 111–121.
42. Fischer, D.; Li, Y.; Ahlemeyer, B.; Krieglstein, J.; Kissel, T. In vitro cytotoxicity testing of polycations: Influence of polymer structure on cell viability and hemolysis. *Biomaterials* **2003**, *24*, 1121–1131. [[CrossRef](#)]
43. Frohlich, E. The role of surface charge in cellular uptake and cytotoxicity of medical nanoparticles. *Int. J. Nanomed.* **2012**, *7*, 5577–5591. [[CrossRef](#)] [[PubMed](#)]
44. Maiz, L.; Giron, R.M.; Oliveira, C.; Quintana, E.; Lamas, A.; Pastor, D.; Canton, R.; Mensa, J. Inhaled antibiotics for the treatment of chronic bronchopulmonary *Pseudomonas aeruginosa* infection in cystic fibrosis: Systematic review of randomised controlled trials. *Expert Opin. Pharmacother.* **2013**, *14*, 1135–1149. [[CrossRef](#)] [[PubMed](#)]
45. Bargoni, A.; Cavalli, R.; Zara, G.P.; Fundaro, A.; Caputo, O.; Gasco, M.R. Transmucosal transport of tobramycin incorporated in solid lipid nanoparticles (SLN) after duodenal administration to rats. Part II—Tissue distribution. *Pharmacol. Res.* **2001**, *43*, 497–502. [[CrossRef](#)] [[PubMed](#)]
46. Wallace, S.J.; Li, J.; Nation, R.L.; Prankerd, R.J.; Velkov, T.; Boyd, B.J. Self-assembly behavior of colistin and its prodrug colistin methanesulfonate: Implications for solution stability and solubilization. *J. Phys. Chem. B* **2010**, *114*, 4836–4840. [[CrossRef](#)] [[PubMed](#)]
47. Akinc, A.; Thomas, M.; Klivanov, A.M.; Langer, R. Exploring polyethylenimine-mediated DNA transfection and the proton sponge hypothesis. *J. Gene Med.* **2005**, *7*, 657–663. [[CrossRef](#)] [[PubMed](#)]
48. Truong, N.P.; Jia, Z.; Burgess, M.; Payne, L.; McMillan, N.A.J.; Monteiro, M.J. Self-catalyzed degradable cationic polymer for release of DNA. *Biomacromolecules* **2011**, *12*, 3540–3548. [[CrossRef](#)] [[PubMed](#)]
49. Hartono, S.B.; Phuoc, N.T.; Yu, M.; Jia, Z.; Monteiro, M.J.; Qiao, S.; Yu, C. Functionalized large pore mesoporous silica nanoparticles for gene delivery featuring controlled release and co-delivery. *J. Mater. Chem. B* **2014**, *2*, 718–726. [[CrossRef](#)]
50. Truong, N.P.; Gu, W.; Prasad, L.; Jia, Z.; Crawford, R.; Xiao, Y.; Monteiro, M.J. An influenza virus-inspired polymer system for the timed release of siRNA. *Nat. Commun.* **2013**, *4*, 1902. [[CrossRef](#)] [[PubMed](#)]
51. Sanz, V.; Coley, H.M.; Silva, S.R.P.; McFadden, J. Protamine and Chloroquine Enhance Gene Delivery and Expression Mediated by RNA-Wrapped Single Walled Carbon Nanotubes. *J. Nanosci. Nanotechnol.* **2012**, *12*, 1739–1747. [[CrossRef](#)] [[PubMed](#)]
52. Kean, T.; Roth, S.; Thanou, M. Trimethylated chitosans as non-viral gene delivery vectors: Cytotoxicity and transfection efficiency. *J. Control. Release* **2005**, *103*, 643–653. [[CrossRef](#)] [[PubMed](#)]
53. Zheng, H.; Tang, C.; Yin, C. Exploring advantages/disadvantages and improvements in overcoming gene delivery barriers of amino acid modified trimethylated chitosan. *Pharm. Res.* **2015**, *32*, 2038–2050. [[CrossRef](#)] [[PubMed](#)]



© 2018 by the authors. Licensee MDPI, Basel, Switzerland. This article is an open access article distributed under the terms and conditions of the Creative Commons Attribution (CC BY) license (<http://creativecommons.org/licenses/by/4.0/>).

6.2. PAPER 2: “Polysaccharide Submicrocarrier for Improved Pulmonary Delivery of Poorly Soluble Anti-infective Ciprofloxacin: Preparation, Characterization, and Influence of Size on Cellular Uptake”

This chapter is the following publication:

Polysaccharide Submicrocarrier for Improved Pulmonary Delivery of Poorly Soluble Anti-infective Ciprofloxacin: Preparation, Characterization, and Influence of Size on Cellular Uptake

Duy-Khiet Ho, Ana Costa, Chiara De Rossi, Cristiane de Souza Carvalho-Wodarz, Brigitta Loretz, and Claus-Michael Lehr; *Mol. Pharmaceutics*. 2018, 15, 1081-1096

DOI: 10.1021/acs.molpharmaceut.7b00967

Reprinted from *Molecular Pharmaceutics*, Polysaccharide Submicrocarrier for Improved Pulmonary Delivery of Poorly Soluble Anti-infective Ciprofloxacin: Preparation, Characterization, and Influence of Size on Cellular Uptake; Duy-Khiet Ho, Ana Costa, Chiara De Rossi, Cristiane de Souza Carvalho-Wodarz, Brigitta Loretz, and Claus-Michael Lehr; 2018, 15, 1081-1096 Copyright (2018) American Chemical Society, published by Copyright Clearance Center, Inc., with permission from American Chemical Society.

Polysaccharide Submicrocarrier for Improved Pulmonary Delivery of Poorly Soluble Anti-infective Ciprofloxacin: Preparation, Characterization, and Influence of Size on Cellular Uptake

Duy-Khiet Ho,^{†,¶} Ana Costa,^{‡,§,⊥} Chiara De Rossi,[†] Cristiane de Souza Carvalho-Wodarz,[†] Brigitta Loretz,^{*,†,⊕} and Claus-Michael Lehr^{†,¶}

[†]Helmholtz Institute for Pharmaceutical Research Saarland (HIPS), Helmholtz Center for Infection Research (HZI), Saarland University, D-66123 Saarbrücken, Germany

[‡]13S, Instituto de Investigação e Inovação em Saúde Universidade do Porto, 4200-135 Porto, Portugal

[§]Instituto Nacional de Engenharia Biomédica (INEB), Universidade do Porto, 4200-135 Porto, Portugal

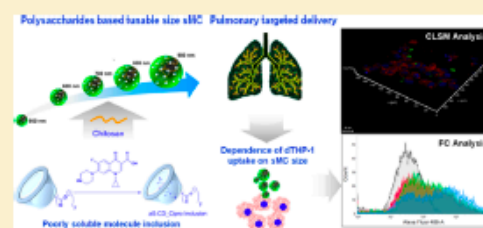
[⊥]Instituto Ciências Biomédicas Abel Salazar (ICBAS), Universidade do Porto, 4050-313 Porto, Portugal

[¶]Department of Pharmacy, Saarland University, D-66123 Saarbrücken, Germany

Supporting Information

ABSTRACT: The majority of the currently used and developed anti-infectives are poorly water-soluble molecules. The poor solubility might lead to limited bioavailability and pharmacological action of the drug. Novel pharmaceutical materials have thus been designed to solve those problems and improve drug delivery. In this study, we propose a facile method to produce submicrocarriers (sMCs) by electrostatic gelation of anionic β -cyclodextrin ($\alpha\beta$ -CD) and chitosan. The average hydrodynamic size ranged from 400 to 900 nm by carefully adjusting polymer concentrations and N/C ratio. The distinct host–guest reaction of cyclodextrin derivative is considered as a good approach to enhance solubility, and prevent drug recrystallization, and thus was used to develop sMC to improve the controlled release profile of a poorly soluble and clinically relevant anti-infective ciprofloxacin. The optimal molar ratio of ciprofloxacin to $\alpha\beta$ -CD was found to be 1:1, which helped maximize encapsulation efficiency (~90%) and loading capacity (~9%) of ciprofloxacin loaded sMCs. Furthermore, to recommend the future application of the developed sMCs, the dependence of cell uptake on sMCs size (500, 700, and 900 nm) was investigated *in vitro* on dTHP-1 by both flow cytometry and confocal microscopy. The results demonstrate that, regardless of their size, an only comparatively small fraction of the sMCs were taken up by the macrophage-like cells, while most of the carriers were merely adsorbed to the cell surface after 2 h incubation. After continuing the incubation to reach 24 h, the majority of the sMCs were found intracellularly. However, the sMCs had been designed to release sufficient amount of drug within 24 h, and the subsequent phagocytosis of the carrier may be considered as an efficient pathway for its safe degradation and elimination. In summary, the developed sMC is a suitable system with promising perspectives recommended for pulmonary extracellular infection therapeutics.

KEYWORDS: *ciprofloxacin, polysaccharide, macrophage uptake, cyclodextrin, chitosan, drug delivery, pulmonary delivery*



1. INTRODUCTION

Drug bioavailability is often limited by poor water solubility.^{1–6} This not only holds true for systemic bioavailability after oral administration, but also for drug delivery to the lungs, which is of increasing relevance for the treatment of respiratory bacterial infections.^{3,5–8} While the total epithelial surface area of the lungs is quite large (approximately 140–160 m²), the amount of liquid covering the air space of the lungs as a rather thin lining (not more than 30 μ m) is not more than approximately 40 mL.^{5,6,9,10} The problem of poor drug solubility has already been recognized in the contexts of a so-called inhalation biopharmaceutical classification system (iBCS), and is, in particular, relevant for anti-infective, which must be typically

administered in rather high doses of 100 mg and more.¹¹ While increasing drug solubility in the pulmonary lining fluid is one part of the problem, it is also important to keep the concentrations of anti-infective in this compartment above the minimally inhibitory concentration as long as possible.¹² This again, however, is impeded by the rather efficient clearance mechanisms of the lungs, which besides systemic absorption across the air–blood barrier also includes mucociliary

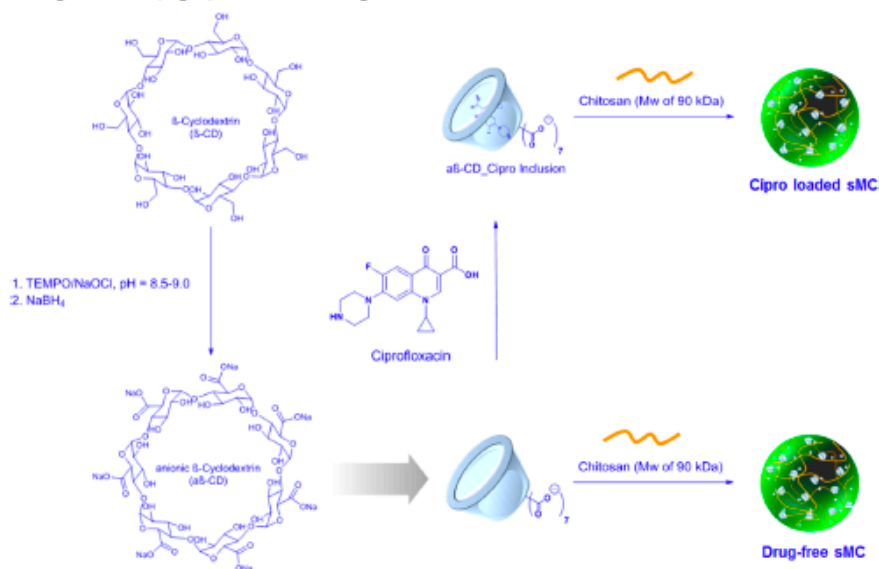
Received: November 3, 2017

Revised: February 8, 2018

Accepted: February 9, 2018

Published: February 9, 2018

Scheme 1. General Description of Experimental Design: Anionic β -Cyclodextrin ($\alpha\beta$ -CD) Synthesis, Drug-Free Submicrocarrier (sMC), and Ciprofloxacin (Cipro) Loaded sMC Preparation



clearance.¹³ For particulate matter, for example, drug carrier systems, clearance by alveolar macrophages is of additional importance.¹⁴ For these reasons, novel pharmaceutical materials are needed, which allow on the one hand to significantly enhance the solubility of poorly water-soluble drugs, and on the other hand to prepare carrier systems capable to control drug release over a longer period of time, and at the same time capable to escape from premature mucociliary or macrophage clearance.¹⁵ While true nanoparticles (<100 nm) might be too small for such purposes, the so-called submicron range (i.e., 100–900 nm) appears to provide the best opportunities.¹⁶ In the end, it must not be ignored that for efficient deposition in the respiratory tract, such carriers need to be formulated as pharmaceutical aerosols with adequate aerodynamic properties, that is, typically an aerodynamic diameter between 1 and 5 μm .¹⁷ Nevertheless, as a plethora of novel technologies to convert nanoparticles into respirable aerosol powders,¹⁸ as well as novel dry powder inhalation (DPI) devices, have been described in the recent years,^{19–24} we have decided to focus on the two aforementioned biopharmaceutical problems. First, we investigated pharmaceutical excipients that can not only significantly improve the water solubility of poorly soluble antibiotics, but also allow the fabrication of submicron sized carriers, capable to provide good loading capacity (~10%) and encapsulation efficacy (>90%) as well as controlled release of the active over a period of 24 h. Second, such material should be nontoxic and biodegradable to be safely eliminated from the body once its task has been accomplished. Cyclodextrins (CDs) are interesting amphiphilic molecules, which have a unique structure consisting of a lipophilic cavity and hydrophilic moieties.^{25,26} Such particular structure helps enhance the solubility of poorly soluble or even insoluble low molecular weight (Mw) molecules by forming host–guest complex inclusion.^{27,28} The inclusion complex is also considered as a

good approach to prevent the polymorphism and crystallization for some particular drug molecules.^{29,30} Hence, CD derivatives have already been widely used in many pharmaceutical applications to improve solubility and thus bioavailability.^{31–33}

However, application of the drug-CD inclusion still suffers from the problem of rapid release and burst effect. Hence, formulation of CDs into nano- and microsize carriers has been studied to further improve drug delivery by CD inclusion complexes for various route of administration including pulmonary delivery.^{34,35} For the latter study, we have chosen ciprofloxacin, which is the drug of choice for the treatment of pulmonary infections by *Pseudomonas aeruginosa*,^{36,37} but for which, as a consequence of the aforementioned problems, pulmonary delivery is still challenged, and a marketed formulation is still not available.

Chitosan, in turn, has many good promising properties for medical applications. It has been studied and applied in drug delivery research, including small drug molecules, proteins, or nucleic acids delivery, as a biodegradable polysaccharide.^{38–40} Furthermore, the safety of chitosan appears to be favorable as the result from several trials.^{41–43} A moderate cationic net charge of the polymer and formulation thereof might lead to a favorable bioadhesive interaction with mucosal surfaces.^{44–47}

In this study, we propose a novel submicrocarrier (sMC) composed of β -cyclodextrin and chitosan. To form a colloidal charge mediated complex with chitosan, some anionic β -cyclodextrin ($\alpha\beta$ -CD) derivative was prepared by complete oxidation of primary alcohol groups (the preparation strategy is described in Scheme 1). Stable submicrocarriers (sMCs) could be easily obtained by simply assembling the two polymers in aqueous solution. This simple but flexible particle preparation method allowed generating particles with average hydrodynamic size in the range from 400 to 900 nm. The process was optimized and varied by changes of (i) initial polymer

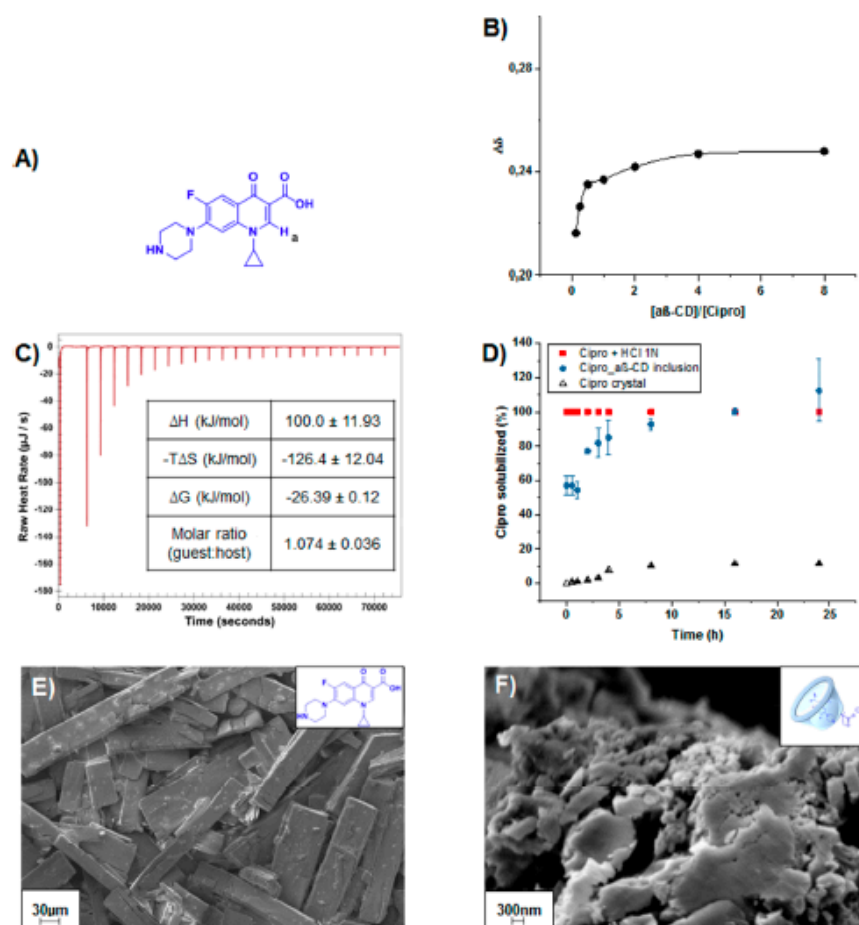


Figure 1. (A) Chemical structure of Cipro; (B) molar ratio of $\alpha\text{-CD}$ to Cipro versus $\Delta\delta$ plot; (C) isothermal titration calorimetry (ITC): titration of $\alpha\text{-CD}$ into Cipro; (D) comparison of solubility of Cipro_ $\alpha\text{-CD}$ inclusion to Cipro solubilized in addition of HCl 1N, and to Cipro crystal, at 10% concentration (w/w) in PBS, at 37 °C; (E) SEM image of Cipro crystal obtained from Cipro 0.1% (w/w) solution, scale bar 30 μm ; (F) SEM image of Cipro_ $\alpha\text{-CD}$ powder obtained from lyophilization of inclusion complex after keeping solution at 4 °C for overnight, scale bar 300 nm.

concentration and (ii) molar ratio of amine and carboxylate groups (N/C ratio) in chitosan and $\alpha\text{-CD}$, respectively. Poorly water-soluble drug loading capacity of the sMCs was investigated with a medical relevant anti-infective, ciprofloxacin (Cipro). Drug-loaded sMCs having similar colloidal characteristics as drug-free sMCs could be obtained by performing the same process with Cipro_ $\alpha\text{-CD}$ inclusion complex.

In subsequent studies, we could demonstrate that these sMCs could significantly enhance the solubility of ciprofloxacin in a physiologically relevant liquid, and improve its controlled release profile, as well as show good biocompatibility with human cell lines (macrophage-like cell differentiated THP-1 (dTHP-1) and lung epithelial cell NCI-H411). Furthermore, the size-dependence of cellular binding and uptake for sMC was investigated by flow cytometry (FC) and confocal microscopy (CLSM) using the macrophage-like cell line dTHP-1 as a model.

2. MATERIALS AND METHODS

2.1. Materials. Ultrapure chitosan chloride salt (Mw of ~90 kDa; Protasan UP CL113 with a deacetylation degree of 75–90%) was obtained from FMC Biopolymer AS Novamatix (Norway). β -Cyclodextrin (β -CD) (CAVAMAXW7) was obtained from Wacker Chemie AG (Germany). Ciprofloxacin, 4-chloro-7-nitrobenzofurazan (NBD-Cl), 2,2,6,6-tetramethyl-1-piperidinyloxy (TEMPO), sodium hypochlorite solution (12% (w/w)) (NaOCl), D_2O , acetic acid, ethanol, sodium hydroxide, sodium borohydride (NaBH_4), and phosphotungstic acid (PTA) were purchased from Sigma-Aldrich and used as received. Purified water is produced by Milli-Q water purification system (Merk Millipore, Billerica, MA). RPMI 1640 with L-glutamine 0.05% (v/v) and Trypsin EDTA (1X) were purchased from Gibco, Life Technologies (Invitrogen Corporation, USA). Penicillin–streptomycin (Pen/Strep)

(10 000 U/mL) and 4,6-diamidino-2-phenylindole (DAPI) were also purchased from Invitrogen Corporation. SAGM Small Airway Epithelial Cell Growth Medium was purchased from Lonza (Switzerland). Fetal bovine serum (FBS), Dulbecco's phosphate buffered saline (PBS), Thiazolyl Blue Tetrazolium Blue (MTT), phorbol 12-myristate 13-acetate (PMA), dimethyl sulfoxide (DMSO), and Triton X-100 were purchased from Sigma-Aldrich (USA). Rhodamine-labeled *Ricinus communis* Agglutinin I (RCA I) was purchased from Vector Laboratories Inc. (USA). Paraformaldehyde (PFA) 16% solution was obtained from Electron Microscopy Science (USA). Fluorescence Mounting Medium was purchased from Dako (Denmark).

2.2. Material Synthesis. **2.2.1. Anionic β -Cyclodextrin ($\alpha\beta$ -CD) Synthesis.** We aimed to obtain a complete oxidation of β -CD's primary face. $\alpha\beta$ -CD was prepared by selective oxidation of primary alcohol groups of β -CD in presence of TEMPO and NaOCl shown in Scheme 1.^{48–50} The synthesis procedure was modified and optimized from Frascini et al.⁵¹ Briefly, dried β -CD was dissolved in Milli-Q water at 50 °C, at 0.1% (w/w) concentration. The solution was then cooled to room temperature (RT), and TEMPO (using 0.65% of primary alcohol group's molar) was added. Four times molar of NaOCl (compared to primary alcohol group's) in its (12% (w/w)) solution was added slowly to the solution in 2 h, which allowed the carboxylation process to happen. During the addition of NaOCl, pH of the mixture was adjusted to the range of 8.5–9.0 by 1 M sodium hydroxide solution. After that, NaBH₄ was added slowly, and the mixture was stirred at RT overnight and purified by membrane dialysis (molecular weight cutoff (MWCO) 100–500 Da, Spectrum Laboratories, USA). Purified water was used for dialysis. The product was dried by lyophilization (Alpha 2–4, Martin Christ GmbH, Osterode, Germany) and characterized by ¹H NMR (Bruker Fourier 300) and FTIR (Spectrum 400 FT-IR/FT-NIR spectrometer (PerkinElmer)).

2.2.2. Green Fluorescent Labeled Chitosan Synthesis. Chitosan was solubilized in purified water at 0.05% (w/w) concentration, 1 day before reaction. Ethanol was then added to the chitosan solution until the ratio of ethanol to water reached 1.2:1 (v/v). After that, 30 equiv molar of the fluorescent reagent NBD-Cl was added, and the reaction was carried out for 24 h, at RT (shown in Scheme S1). The product was purified by membrane dialysis (MWCO 30 000 Da, Spectrum Laboratories, USA) against an excess of purified water. The product was dried by lyophilization (Alpha 2–4, Martin Christ GmbH, Osterode, Germany).

2.2.3. Optimization of Anionic β -Cyclodextrin-Ciprofloxacin ($\alpha\beta$ -CD-Cipro) Inclusion. The $\alpha\beta$ -CD-Cipro inclusion was studied by proton nuclear magnetic resonance (¹H NMR, Bruker Fourier 300), isothermal titration calorimetry (ITC), Fourier-transform infrared spectroscopy (FTIR, Spectrum 400 FT-IR/FT-NIR spectrometer (PerkinElmer)), and scanning electron microscopy (SEM).

¹H NMR and ITC were used to identify the optimal molar ratio of $\alpha\beta$ -CD to Cipro in the complex inclusion. To study the inclusion by ¹H NMR, the appropriate amount of Cipro was dissolved in D₂O for recording its ¹H NMR used as a control. $\alpha\beta$ -CD and Cipro were prepared as the powder in the same flask with the correct molar ratio of $\alpha\beta$ -CD to Cipro ranged 1:8, 1:4, 1:2, 1:1, 2:1, 4:1, and 8:1, respectively. The powder mixture was then dissolved in 0.5 mL of D₂O. The mixture was stirred at 50 °C for 2 h and then kept at RT overnight. The ¹H NMR

spectra of all resulting solutions were analyzed. The shifting of the proton at 'a' position on Cipro's structure (Figure 1A) was obtained to identify the optimal molar ratio of $\alpha\beta$ -CD and Cipro in the inclusion.

The inclusion complex of $\alpha\beta$ -CD and Cipro was also investigated by isothermal titration calorimetry (ITC) using a NanoITC 2G (TA Instruments). The measurement was used to optimize $\alpha\beta$ -CD to Cipro molar ratio in the inclusion thereof maximizing drug loading in Cipro loaded sMC production. Briefly, a 7.5 mM solution of $\alpha\beta$ -CD was prepared in a 250 μ L syringe and used to saturate 1.5 mL of Cipro solution at a concentration of 0.6 mM filled in the sample cell. Following an initial delay of 1000 s, 250 μ L of the $\alpha\beta$ -CD solution was repeatedly injected into the sample cell with a spacing of 3000 s between injections and at a reference power of 10 μ Cal/s. The final thermogram and thermodynamic parameters were produced by subtracting the heat of dilution of $\alpha\beta$ -CD (7.5 mM in 1.5 mL Milli-Q water), followed by fitting using the One Set of Sites model in the data analysis software NanoAnalyze. The free energy of binding (ΔG) was calculated using the equation $\Delta G = \Delta H - T\Delta S$, where ΔH is the enthalpy change, T is temperature (Kelvin), and ΔS is the change in entropy. All measurements were performed at 25 °C.

For further drug loaded sMC formulation, the inclusion complex was prepared with the optimal molar ratio of $\alpha\beta$ -CD and Cipro, which was obtained from ¹H NMR and ITC analysis. Briefly, the two compounds were accurately weighed in a flask, then dissolved in purified water to a final concentration of 0.5% (w/w). The mixture was stirred at 50 °C for 2 h, and then at RT overnight to form the inclusion complex (Scheme 1). The inclusion formation was further checked by keeping the resulting solution at 4 °C for 24 h to observe the crystallization phenomenon in comparison to the control, a Cipro 0.1% (w/w) solution which crystallized at these conditions. The $\alpha\beta$ -CD-Cipro complex was collected from the solution by lyophilization (Alpha 2–4, Martin Christ GmbH, Osterode, Germany). The obtained product was visualized by SEM (details in section 2.5.4) and confirmed by FTIR.

2.2.4. Comparison of Solubility. The solubility of the $\alpha\beta$ -CD-Cipro inclusion in PBS, at 10% concentration (w/w) and 37 °C, was compared to Cipro solubilized in addition of HCl 1N, and Cipro crystal obtained from Cipro solution kept at 4 °C (as mentioned). The solubility degree of Cipro after predetermined time points was normalized and presented in percentage of solubilized Cipro in PBS solution. Three independent experiments were conducted in triplicates and results expressed as the mean \pm standard deviation (SD).

2.3. β -Cyclodextrin-Chitosan Based Submicrocarrier (sMC) Preparation. **2.3.1. Drug-Free sMC Preparation.** The sMC was prepared by electrostatic gelation of the anionic macromolecule, $\alpha\beta$ -CD, and cationic polymer, chitosan (Mw of ~90 kDa), in purified water (Scheme 1). Characteristics, especially hydrodynamic diameter, of the resulting sMCs were carefully varied by changes of initial solution of $\alpha\beta$ -CD and chitosan, and the molar ratio of amine to carboxylate functional groups (N/C ratio). Briefly, the solutions of $\alpha\beta$ -CD and chitosan were prepared at a defined concentration (detailed information shown in Table S1). Chitosan solution was adjusted to pH value 5.5 and prewarmed at 40 °C for 30 min before assembling with the appropriate amount of $\alpha\beta$ -CD solution. The mixture was vortexed for 2 min and allowed to stand at RT for 3 h to allow equilibration of stable colloids

before further characterization and experiments. The characteristics of sMCs were obtained from more than three independently different batches.

Fluorescent sMCs were prepared by the same method as drug-free sMC but with 10% (w/w) NBD-Cl-labeled chitosan/total chitosan.

2.3.2. Stability of sMCs in Cell Culture Medium. The colloidal stability of different sMC size (500 nm, 700 nm, 900 nm) in cell culture medium was investigated by incubating particle suspensions in serum-free RPMI medium, at 37 °C. Samples were analyzed by DLS (for hydrodynamic size, PDI, and ζ -potential) after predetermined incubation times (2 and 24 h). Three independent experiments were conducted in triplicates and results expressed as the mean \pm standard deviation (SD).

2.4. Drug-Loaded sMCs. **2.4.1. Preparation and Optimization of Ciprofloxacin-Loaded sMCs.** **2.4.1.1. Preparation of Drug-Loaded sMCs (Cipro-Loaded sMCs).** The drug-loaded sMCs were prepared using the same protocol as drug-free sMCs (mentioned in section 2.3) procedure in which a β -CD was replaced by a β -CD_Cipro inclusion (Scheme 1). The drug-loaded sMC preparation using chitosan as a countering polymer was optimized, whereby the anionically charged inclusion was dissolved in MilliQ water at the same concentration as a β -CD, followed by the addition of appropriate amount of prewarmed chitosan solution for the assembly. The mixture was then vortexed for 2 min and allowed to equilibrate before further experiments and analysis as described in section 2.3.1. Characteristics of resulting sMCs were also varied by initial polymer concentration and N/C ratio (detailed information is shown in Table S2). All Cipro loaded sMC samples were prepared in minimum three independently different batches.

2.4.1.2. Drug Loading Quantification. The Cipro loading was determined indirectly by measurement of the free drug in the supernatant (amount inside = initial amount – amount in the supernatant). Drug quantification was done by fluorescent intensity analysis of Cipro at 330/430 nm (E_e/E_m).²⁹ A Calibration curve was performed with nine different defined concentrations ranged from 0 to 10 μ g/mL of Cipro in water ($r^2 = 0.9939$). All standards were measured five times, and all measurements were done at RT (Figure S1 shows the calibration curve).

The encapsulation efficiency (EE%) and the drug loading capacity (LC%) were calculated according to the following equations:

$$EE\% = \frac{\text{Weight of encapsulated drug in nanoparticles}}{\text{Initial weight of used drug}} \times 100$$

$$LC\% = \frac{\text{Weight of drug in nanoparticles}}{\text{Weight of nanoparticles}} \times 100$$

Whereas "Weight of nanoparticles" was calculated as (Weight of nanoparticles = Weight of polymeric materials + Weight of encapsulated drug in nanoparticles).

Three independent experiments were conducted in triplicates and results expressed as the mean \pm standard deviation (SD).

2.4.2. Drug Release Study. Ciprofloxacin release profiles from the a β -CD_Cipro inclusion complex and Cipro loaded sMCs 900 nm were performed in PBS (pH 7.4) at 37 °C. Briefly, either a β -CD_Cipro inclusion or Cipro-loaded sMCs was diluted in PBS to have final Cipro concentration at 10%

(w/w) and loaded into dialysis membrane (MWCO 100–500 Da, Spectrum Laboratories, USA). After that, the whole system was put into 20 mL of PBS and placed on a shaker at 400 rpm at 37 °C. The concentration of released drug was analyzed by collecting samples from the supernatant during the period from 30 min to 24 h. The volume was kept constant by refilling with an identical volume of PBS. The cumulative released drug (%) was calculated (mean \pm SD of $n = 3$). Three independent experiments were conducted in triplicates, and results expressed as the mean \pm standard deviation (SD).

2.5. Characterization Methods. **2.5.1. sMC Characterization.** The sMC characteristics, including average hydrodynamic diameter, polydispersity index (PDI), and ζ -potential, were measured using a Zetasizer Nano (Malvern Instruments, Malvern, UK) at 25 °C.

2.5.2. Transmission Electron Microscopy (TEM). The morphology of sMC colloid was investigated by transmission electron microscopy (TEM, JEM 2011, JEOL). Samples for TEM were prepared by adding appropriate amount of sMC suspension on a copper grid (carbon films on 400 mesh copper grids, Plano GmbH, Germany). The grid was blotted after 10 min incubation, and samples were stained with 0.5% (w/w) of PTA solution to enhance the contrast for TEM visualization.

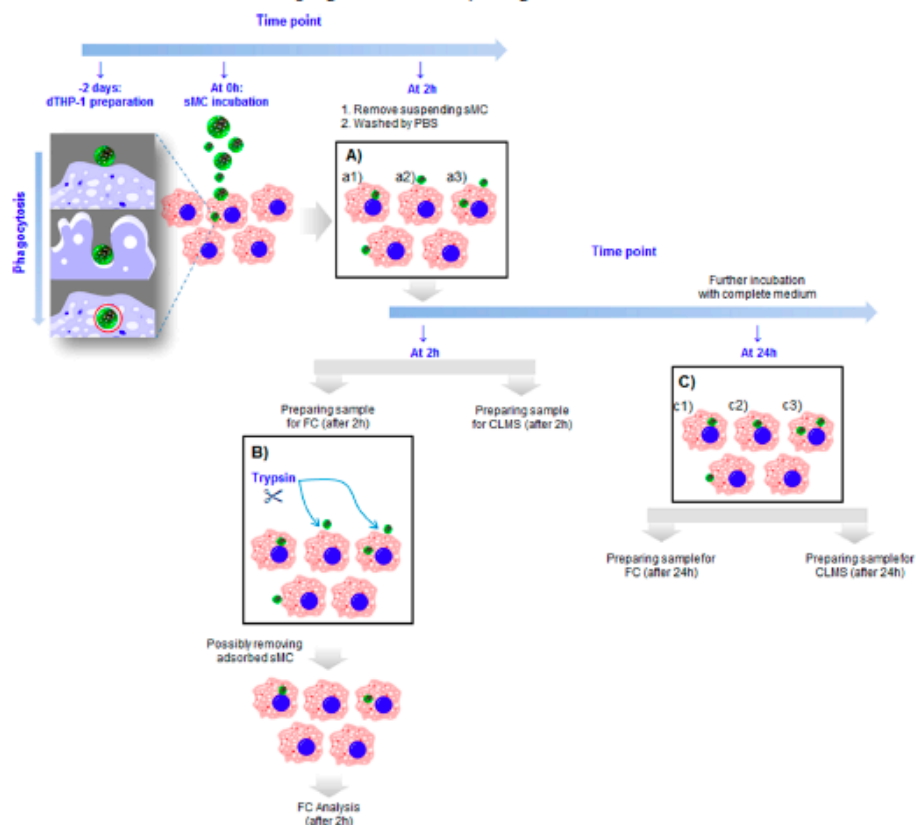
2.5.3. Fluorescent Microscopy. Green fluorescent sMC 900 nm was visualized by fluorescent microscopy (Nikon Ti-U, Netherlands) before *in vitro* experiments. The fluorescent-labeled sMC suspension was diluted in complete cell culture medium (10% FBS in RPMI medium) to 50 μ g/mL concentration for observation.

2.5.4. Scanning Electron Microscopy (SEM). The physical characteristics of a β -CD_Cipro were also observed by SEM. An appropriate amount of a β -CD_Cipro inclusion complex powder was deposited on carbon discs (12 mm) mounted on pin stubs (12 mm). As a reference, dried crystal of Cipro resulting from Cipro 0.1% (w/w) solution was also observed. Images were obtained on a scanning electron microscope (Evo HD 15, Zeiss Göttingen, Germany) at 5 kV acceleration voltage and were representative of the sample visualized.

2.6. Minimum Inhibitory Concentration (MIC) Assay. The antimicrobial properties of sMCs, free Cipro, a β -CD_Cipro inclusion, and Cipro-loaded sMCs were investigated by standard microbroth dilution assays with *Escherichia coli* (DH5 α) and *Pseudomonas aeruginosa* (PA14) in 96-well plates. A suspension of *E. coli* or *P. aeruginosa* prepared from mid log cultures in Mueller-Hinton broth or Lysogeny Broth medium was first diluted to OD600 (absorption at 600 nm) 0.01, which corresponds to approximately 5×10^6 CFU/mL (CFU, colony-forming units). Test samples were sMCs (drug-free sMC, Cipro-loaded sMCs), the a β -CD_Cipro inclusion, and free Cipro solution. PBS served as control. Bacteria-containing wells were then treated with the respective samples and serially diluted over a range of 0.0003–64 μ g/mL. After incubation for 16 h at 37 °C, inhibitory concentration (IC) IC90 values were determined by sigmoidal curve fitting of absorption values (600 nm) that were measured on a Tecan microplate reader. The IC90 values are defined as the Cipro concentrations at which the growth of bacteria is inhibited by 90%. Three independent experiments were conducted in triplicate.

Standard cell culture propagation and maintenance is reported in the Supporting Information.

2.7. Cell Viability: MTT Assay. Cell viability after sMC incubation was assessed by MTT assay. On a 96-well plate, THP-1, NCI-H441, or human alveolar epithelial lentivirus

Scheme 2. Interaction of sMC and Macrophages: *In Vitro* Study Design^a

^asMCs are expected to be either adsorbed or phagocytosed by macrophages. The macrophage-like cell line dTHP-1 was chosen as a model. After 2 h incubation and washing with PBS, (A) there may be cells with sMCs internalized (in a1), cells with sMCs adsorbed (in a2), and cell with both sMCs internalized and adsorbed (in a3). (B) After 2 h of incubation, a part of the samples were treated with Trypsin to remove merely adsorbed sMCs as reported by Gudewicz et al.⁷⁶ and Kage et al.⁷⁷ (C) Other samples were just washed with PBS and further incubated for another 22 h. To quantify the amount of internalized sMCs and adsorbed sMCs, respectively, the cells were analyzed by FC and CLSM.

immortalized (hAELVi) cells were seeded at a density of 1.25×10^5 , 4×10^4 , or 1×10^4 cells per well, respectively. THP-1 cells were differentiated into macrophages in the 96-well plate, as described in the Supporting Information.

Both THP-1 and NCI-H411 cells were grown for 2 days, while hAELVi cells were grown for 4–5 days before the conduction of the assay to allow for approximately 80% cell confluency. The cells were further incubated with different concentrations of drug-free sMCs (size of 500, 700, and 900 nm) for 24 h, at 37 °C, 5% CO₂. After the incubation time, cells were washed once with PBS, and MTT reagent (concentration of 0.5 mg/mL diluted in HBSS) was incubated for 4 h in the dark. The supernatant was further removed from the well, and the formed formazan crystals were dissolved in DMSO. Finally, the absorbance was measured at 550 nm by an Infinite M200Pro plate reader (Tecan, Germany). Cells incubated with only RPMI medium were used as a negative control (corresponding to 100% cell viability) and cells treated with 1% Triton X-100 in RPMI medium were used as positive

control (designated as 0% cell viability). The percentage of viable cells was calculated in comparison to negative and positive controls as described by Nafee et al.⁵² Three independent experiments were conducted in at least triplicate.

2.8. *In Vitro* Uptake Study on dTHP-1 Cells. Uptake study on dTHP-1 cells was performed using fluorescent labeled sMCs of three different average sizes, 500, 700, and 900 nm and analyzed by the flow cytometer (FC). Furthermore, confocal laser scanning microscopy (CLMS) was used to study cell uptake of the largest targeted average size, sMC 900 nm.

The general design of *in vitro* uptake study is described in Scheme 2. For both experiments, THP-1 cells were seeded either without sterile coverslip (for FC analysis) or on sterile coverslip (for imaging by CLMS) in a 24-well plate (5×10^5 cells/well) with RPMI 1640 medium containing 10 ng/mL of PMA during 48 h to allow cell differentiation into macrophage-like cells. Cells were then washed once with PBS, at 37 °C. Fluorescent sMCs, concentration of 50 µg/mL, were incubated for 2 h in serum-free RPMI 1640 medium. After 2 h incubation,

cells were washed two times with PBS to remove the suspended sMCs. The cells were then ready for further steps: either for (i) sample preparation for FC or CLSM to determine cell uptake after 2 h incubation or (ii) further incubation with complete cell culture medium to reach 24 h, at 37 °C, 5% of CO₂; the cells were then prepared for FC analysis or CLSM to determine cell uptake after 24 h incubation. Particle uptake at each time point was determined by FC or CLSM, and sample preparation for each technique is described below.

2.8.1. Uptake Analyzed by Flow Cytometer (FC). After sMC incubation period as mentioned above, the medium was removed, and the cells were washed two times with PBS. Following, cells were detached by applying trypsin enzyme for 10 min at 37 °C. After centrifugation at 1000 × g for 5 min, at 4 °C, the cell pellet was resuspended in 300 µL of cell culture medium (2% FBS in PBS), and immediately analyzed with a BD FACSCalibur (Becton-Dickinson, Heidelberg, Germany). The percentage of sMCs associated cells was determined by defining a positive fluorescent region on the basis of control cells (without particles), which were NBD-Cl-negative. For that, the mean value was obtained and used for gating. Then 10 000 cells were analyzed for each sample. An argon laser with a wavelength of 488 nm was used for excitation, and emission was recorded through a 515–545 nm filter. Results were calculated and diagrams prepared with FlowJo software (version 7.2.5, Tree Star, Stanford, CA, USA). Three independent experiments were conducted in triplicates, and results expressed as the mean ± standard deviation (SD).

2.8.2. Uptake Analyzed by Confocal Laser Scanning Microscopy (CLSM). For all samples, live cells were stained with Rhodamine labeled *Riñus communis* Agglutinin I 2 µg/mL for 20 min, at 37 °C. After that, the samples were washed with PBS and fixed with paraformaldehyde 3% for 30 min, at room temperature. All samples were counterstained with DAPI (100 ng/mL), for 15 min, washed with PBS, and mounted in DAKO mounting medium.

Samples were imaged by CLSM Zeiss LSM710, Axio Observer (Oberkochen, Germany) or Leica TCS SP8, Leica Microsystems (Wetzlar, Germany). Images were acquired with a 63× water immersion objective with a resolution at 1660 × 1660, a bit depth of 8, and zoom of 1.0; z-stack images were collected with a frame mode and a thickness of 1 µm per each focal plane. In each experiment, the green autofluorescence of the differentiated THP-1 cells was compensated by adjusting the green intensity gain related to the respective untreated control. Confocal images were analyzed using Zen 2 2011 software (Carl Zeiss Microscopy GmbH, Oberkochen, Germany). Cross-section images were acquired on a Leica TCS SP8 using a 63× water objective, zoom of 1.23, a resolution of 1024 × 512, and a scan speed of 400 Hz.

The number of cells that presented adsorbed or internalized sMCs was determined by analysis of Z-stacks images, and the results were expressed in percentage according to the number of counted cells.

2.9. Statistical Analysis. All values are given as mean ± standard error of the mean (SE), from at least three independent experiments. Statistical analysis was performed through GraphPad Prism Software version 7.03 (GraphPad Software Inc., La Jolla, USA) or OriginPro 2017 Software (OriginLab Corp., Massachusetts, USA). Significance was determined by one-way ANOVA or two-way ANOVA as indicated in the respective figure captions.

3. RESULTS AND DISCUSSION

3.1. Excipient Synthesis and Characterization.

3.1.1. Anionic β-Cyclodextrin (αβ-CD) Synthesis. β-Cyclodextrin (β-CD) was mildly modified by selective oxidation of primary alcohol groups to prepare anionic β-cyclodextrin (αβ-CD). As characterized in Figure S2, the ¹H NMR spectrum of αβ-CD in comparison to that of β-CD in D₂O shows the absence of proton at 4.993 ppm, which proves that the primary alcohol groups of β-CD have been fully oxidized to form carboxylate groups. Furthermore, FTIR spectra in Figure S3 also confirmed the primary face oxidation of β-CD. There is a frequency recorded at 1688.6 cm⁻¹, which corresponds to the carboxylate groups. Hence, the αβ-CD was ready to be used in sMC preparation.

3.1.2. Anionic β-Cyclodextrin_Ciprofloxacin Inclusion. Ciprofloxacin (Cipro) is an important anti-infective that is widely used to treat a variety of infectious diseases including both Gram-negative and Gram-positive pathogens.⁵³ The drug, however, has short *in vivo* oral elimination half-life, which might require frequent dosing.^{54,55} Hence, applying Cipro by inhalation has been investigated in a phase III randomized study and appeared to be favorable for the treatment of respiratory infections.^{37,56,57} Despite its high activity against bacteria, the poor solubility and quick recrystallization are particularly unfavorable pharmaceutical characteristics for its applications, especially in inhalation.⁵⁸ Therefore, in this study, Cipro was chosen as a clinically relevant anti-infective to explore drug loading capacity of the submicrocarrier (sMC) system.

Applying cyclodextrins (CDs) to enhance solubility and prevent crystallization is known as an effective approach for many pharmaceutical applications.^{26,59,60} Moreover, many modified cyclodextrin derivatives, including anionic cyclodextrin, cationic cyclodextrin, and polymer-based cyclodextrin, have been studied and found to have good potential for improving drug delivery.^{25,27,32} Nevertheless, the inclusion of CD and drug molecules has always been recharacterized after chemical modification of CD derivatives. Hence, although β-CD derivative and Cipro inclusion complex were already reported in literature,^{29,30} which suggested the molar ratio 1:1 of β-CD to Cipro in the inclusion, we carefully characterized the host-guest complex of αβ-CD (host) and Cipro (guest). The investigation was to optimize the molar ratio of each compound for the inclusion and further maximize drug encapsulation efficiency in drug-loaded sMCs.

3.1.2.1. ¹H NMR Study. The ¹H NMR was used to investigate the possible influence of the inclusion formation on proton 'a' of Cipro (described in Figure 1A) due to the diminishment of rotational freedom once Cipro molecule is localized in an αβ-CD cavity. The proton 'a' of Cipro experienced a downfield shifting upon increasing concentration of αβ-CD in inclusion forming procedure (described in Figure 1B). When the molar ratio of αβ-CD to Cipro went higher than 1:1, the Δδ became plateaued apparently indicating the formation of 1:1 molar ratio complex.

3.1.2.2. Isothermal Titration Calorimetry Analysis. The αβ-CD_Cipro complex was also investigated by isothermal titration calorimetry (ITC), which revealed the thermodynamic of the host-guest reaction and helped to estimate optimized drugs amount which can be included with αβ-CD. The αβ-CD solution was injected to saturate Cipro solution, and the final thermogram is shown in Figure 1C. The values in the inset

tables were calculated by software NanoAnalyze indicating the free energy (ΔG) of the interaction to be -27.62 ± 0.12 (kJ/mol) for binding, which proves the favorable host-guest interaction between Cipro and $\alpha\beta$ -CD. Moreover, the ratio of Cipro (guest) to $\alpha\beta$ -CD (host) was also determined at 1.074 ± 0.036 proving 1:1 molar ratio in inclusion complex formation of $\alpha\beta$ -CD and Cipro.

3.1.2.3. Fourier Transform Infrared Spectroscopy (FTIR). In agreement with Jiao et al.⁶¹ and Sambasevam et al.,⁶² the existence of both guest (Cipro) and host ($\alpha\beta$ -CD) molecules in their inclusion complex is also convincingly proven by using FTIR. Figure S5 shows the FTIR spectra for the (a) ciprofloxacin, (b) anionic β -cyclodextrin, and (c) $\alpha\beta$ -CD_Cipro inclusion. The spectrum of the inclusion complex generally looks similar to $\alpha\beta$ -CD's, but there are some major differences in stretching vibration. In the FTIR spectrum of Cipro, there is one prominent characteristic peak found between 3200 and 2900 cm^{-1} (Figure S5a), which is assigned to an OH stretching vibration. Another band found at 2850–2750 cm^{-1} mainly represents C–H stretching vibration of aromatic-enes. As the inclusion complex formed, Cipro molecule was localized in cavity of $\alpha\beta$ -CD, so those bands of OH, alkenes, and aromatic C–H stretching vibration became less significant and overlapped as one broad peak between 3700 and 2700 cm^{-1} (Figure S5c). The peak at 1650 to 1600 cm^{-1} of Cipro's FTIR spectrum that was assigned to quinolone experienced a small shift in the spectrum of $\alpha\beta$ -CD_Cipro inclusion from 1614 to 1625 cm^{-1} , while the carboxylate stretching of $\alpha\beta$ -CD at 1688.6 cm^{-1} was then overlapped with the one from Cipro. Furthermore, a strong absorption peak between 1050 and 1000 cm^{-1} assigned to the C–F bond of Cipro also became overlapped in the spectrum of $\alpha\beta$ -CD_Cipro inclusion but still recognizable and assigned. In summary, the inclusion complex of $\alpha\beta$ -CD and Cipro was successfully prepared and confirmed by FTIR.

3.1.2.4. SEM Images. Cipro is known as a poorly soluble drug and molecule which is prone to fast crystal formation. Consequently, application of Cipro as in solution, or via a different route from the oral administration could be problematic. β -CD is not only applied to enhance the solubility of the hydrophobic compound, but also to prevent the crystallization or polymorphism of drug molecules.⁵⁹ Hence, after inclusion formation, we also compared the crystallinity of $\alpha\beta$ -CD_Cipro 0.5% (w/w) concentration to Cipro 0.1% (w/w) concentration solution, which were kept at 4 °C overnight. As can be seen in Figure 1E, well-structured and large crystals were formed and observed by SEM from Cipro solution even at low magnification (scale bar 30 μm). In contrast, if the inclusion solution was prepared at five-times higher Cipro concentration, crystallinity of the solution was not visualized by SEM even at high magnification (scale bar 300 nm, Figure 1F). The different magnifications of SEM images from both samples are shown in Figure S6. This result proves an additional advantage of $\alpha\beta$ -CD_Cipro inclusion, which is the prevention of Cipro crystallization.

3.1.2.5. Comparison of Solubility. The inclusion of $\alpha\beta$ -CD and Cipro significantly increased solubility of Cipro in PBS, at 10% (w/w), 37 °C, after 3–4 h incubation, which resulted similar to the solubility of Cipro in addition of HCl 1N served as control (results showed in Figure 1D). Furthermore, the inclusion was much faster and completely solubilized in PBS over the studied period compared to the crystal form of Cipro, which was obtained from the previously mentioned experiment. Hence, the inclusion is expected to have better bioavailability;

the better solubility, however, would lead to fast elimination and burst effect. Consequently, a novel carrier approach is needed for the controlled release of the $\alpha\beta$ -CD_Cipro inclusion.

3.2. Preparation, Optimization, and Stability of Submicrocarrier.

3.2.1. Drug-Free Submicrocarrier (sMC).

The size range of nanomedicine is generally considered smaller than 1 μm .¹⁸ In this study, we proposed a facile approach for establishing a submicrocarrier (sMC) system by an ionotropic assembly of $\alpha\beta$ -CD and cationic chitosan (Mw of ~ 90 kDa). $\alpha\beta$ -CD provides electrostatically networking interaction with chitosan polymer, but it cannot help to stabilize the colloidal formation due to its low molecular weight (Mw of 1386 Da) small cyclic molecules.³² Hence, the stability of the sMC colloid would be mainly dependent on chitosan derivative's physicochemical properties. Therefore, a chitosan derivative with a high molecular weight and low degree of acetylation was selected for colloidal formation. The sMC size was carefully tuned in the range from 400 to 900 nm, with the size difference between samples of approximately 100 nm, by changes of initial concentration of polymer solution, and the molar ratio of amine and carboxylate functional groups (N/C ratio) on chitosan and $\alpha\beta$ -CD, respectively. The summary of sMC characteristics is shown in Figure 2 (diagram depicting results of DLS measurement) and Table S1 (impact of N/C ratio and polymer concentration). By using the ratio of the initial concentration of chitosan solution to the $\alpha\beta$ -CD solution at 1.0/1.0 and 2.0/1.0, the sMC size was increased from 400 to 800 nm with the decrease of N/C ratio, which could be explained by a denser assembly of chitosan and $\alpha\beta$ -CD when increasing the amount of amine groups. When using the same N/C ratio at a higher concentration of initial chitosan solution, the resulting sMC was approximately 100 nm larger. The sMC with an average diameter of 900 nm was obtained by using a high initial concentration of $\alpha\beta$ -CD. Uniform sMC size with a narrow polydispersity index (PDI < 0.3) was recorded in all samples. The presence of cationic chitosan polymer in the assembly caused all sMC samples to have positively charged surfaces. The ζ -potential values were recorded decreasing responding to the raising of carboxylate ratio used in sMC formation. This tendency could be explained by the higher binding degree of $\alpha\beta$ -CD with chitosan on particle's surface due to charge interaction and hydrogen bonding between them. Furthermore, morphology of sMC representatives was spherical, as confirmed by TEM images (Figure 3B–D). As all sMC samples share similar characteristics, the sMC with average diameter 500, 700, and 900 nm were selected to be presented.

3.2.2. Green Fluorescent Labeled sMC Preparation. Green fluorescent labeled sMCs were prepared using the same protocol as drug-free sMCs, in which 10% fluorescent labeled chitosan out of total applied chitosan was added. The green fluorescent labeled chitosan was synthesized by covalently conjugating NBD-Cl to primary amine groups (Scheme S1). The FTIR spectra (Figure S4) were not suitable to confirm successful labeling of chitosan, which is assumed to result from the low amount of conjugated NBD-Cl. However, NBD-Cl is known to have strong fluorescent intensity upon conjugating with a primary amine, as NBD-amines are excited by visible light (464 nm) with the emission maximum of approximately 512 nm.^{63,64} As a result, the green fluorescent labeled sMCs could be observed by fluorescent microscopy (Figure 3A) and confocal laser scanning microscopy (CLSM), which proved a

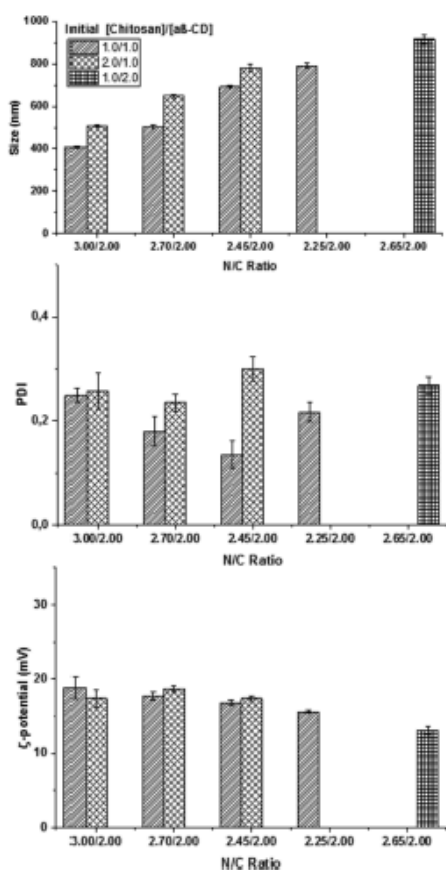


Figure 2. Colloidal properties of sMC batches, depending on initial concentration (mg/mL) of chitosan and $\alpha\beta$ -CD, respectively, and N/C ratio, based on the average content of amine groups in chitosan according to manufacturer's information and content of carboxylate groups in $\alpha\beta$ -CD (N/C ratio).

successful synthesis of green fluorescent labeled chitosan derivative. Representative fluorescent labeled sMCs with 500, 700, and 900 nm average diameters were chosen for further *in vitro* study.

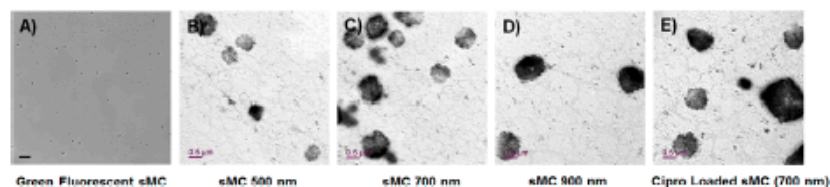


Figure 3. Fluorescent microscopy image (A) sMC 900 nm (dispersed in serum-free cell culture medium RPMI at 50 μ g/mL, 37 $^{\circ}$ C, for 24 h) confirming successful fluorescent and colloidal stability of sMCs in such medium, scale bar 5 μ m; (B–E) TEM images of: (B) sMC 500 nm, (C) sMC 700 nm, (D) sMC 900 nm, and (E) Cipro loaded sMC (700 nm).

3.2.3. Stability of sMCs in Cell Culture Medium. Cell culture medium (RPMI) was used to dilute the sMC suspension during *in vitro* experiments. Hence, characteristics of sMCs diluted in RPMI were recorded after 2 and 24 h incubation for not confounding dependence of uptake efficiency on particle size. The results of average size, PDI, and ζ -potential of sMC suspended in RPMI are given in Figure S11. The sMCs, regardless of size range, have stable average diameter, and acceptable PDI value (<0.3). Carefully considering the average size, there is a slight decrease after 2 h incubation. That could be explained by the change of pH environment from 5.5 (sMC preparation pH) to around 7 (pH value of RPMI). In this condition, amine groups on chitosan became partly dissociated causing a shrinking of the hydrodynamic particle size.⁶⁵ The same process is also the reason for a substantial decrease of ζ -potential from around +17 mV to nearly neutral values. Further checking after 24 h incubation, the particle size slightly raised about 30–60 nm. Chitosan is known as a cationic polymer, with a pK_a of approximately 6.5, which allows interaction with negative net charged agents,⁴³ and there are different kinds of ions, sugars, and vitamins in RPMI medium, which could adsorb on the surface of sMCs resulting in the size increase. However, the association of such molecules on the surface was not severe enough to destabilize the sMC system. As the particles were produced by the assembly of $\alpha\beta$ -CD and chitosan, $\alpha\beta$ -CD molecules are present on the sMC surface (described in Scheme S2). Consequently, the colloidal surface is coated with the secondary face of $\alpha\beta$ -CD, which possibly helps to prevent an interaction between ingredients in the medium and particles.⁶⁶ Furthermore, 900 nm sMCs suspended in RPMI were also visualized by fluorescent microscopy, which shows the nonaggregated colloidal system (Figure 3A). Conclusively, the prepared sMCs are stable to be used for studying dependence of dTHP-1 uptake on particle size.

3.3. Drug-Loaded Submicrocarrier. **3.3.1. Ciprofloxacin-Loaded sMCs: Preparation, Optimization, and Characterization.** The obtained characterizations of Cipro loaded sMCs were similar to those of drug-free sMCs using the same conditions for sMC preparation (showed in Figure 4A (size), Table S2 (impact of preparation parameters), and Figure S7 (PDI and zeta-potential)). This could be explained by similarity of physicochemical properties of $\alpha\beta$ -CD independent from the Cipro inclusion. All samples achieved high encapsulation efficiencies (EE) in the range of 70–90%. Both EE and LC increased when the targeted size was raised, which suggests that higher applied ratio of $\alpha\beta$ -CD helped to increase the amount of Cipro in the sMC system (details are shown in Figure 4B, Table S3). Furthermore, it is clear that Cipro LC of the sMCs

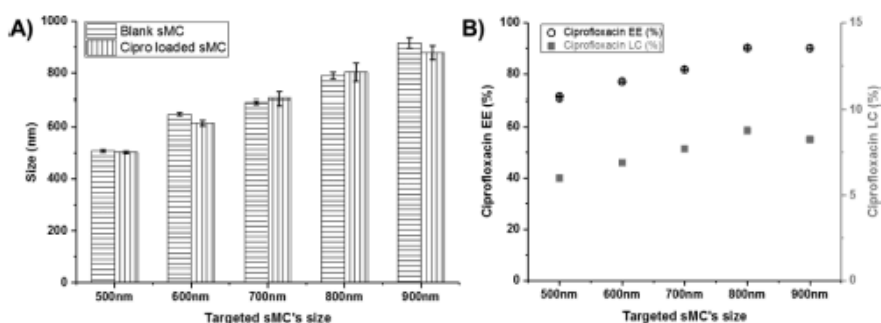


Figure 4. (A) Hydrodynamic diameter (determined by DLS) of Cipro loaded sMCs in comparison to blank sMCs, (B) ciprofloxacin encapsulation efficiency (EE) (%) (right y-axis) and loading capacity (LC) (%) (left y-axis) for different sMC sizes.

mainly depends on the applied amount of chitosan, as Cipro is complexed with $\alpha\beta$ -CD. As a result, to further improve the drug LC of the here developed system, other particles preparation techniques, for example, spray drying, would be possible options to optimize the used amount of chitosan at which the characteristics and stability of the system would be controlled and maintained.

3.3.2. Release Study. We conducted the release study in PBS at 37 °C to investigate the release profile of Cipro from the inclusion and the particles at predetermined time points. Although the formation of the $\alpha\beta$ -CD_Cipro inclusion complex is favorable as examined in section 3.1.2, ciprofloxacin was released from the inclusion complex at the studied conditions, as shown in Figure 5. It is suggested that Cipro has better

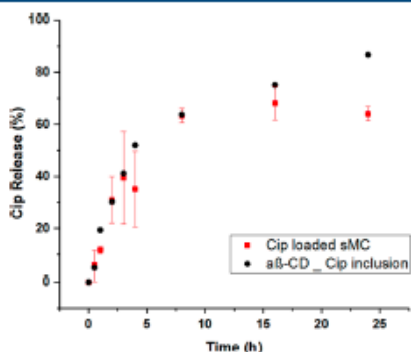


Figure 5. Cumulative release of Cipro from $\alpha\beta$ -CD_Cipro inclusion complex, and after assembly to Cipro loaded sMC 900 nm performed in PBS at 37 °C.

solubility in water at 37 °C,⁶⁷ which consequently enhances the mobility of Cipro molecule and initiate the release of Cipro from the complex. An experimental setup with a dialysis membrane was used. The membrane was permeable for the Cipro but not the complex or sMC sample. The released Cipro found in the permeation kept increasing during the study period. Cipro loaded sMCs, in turn, shown burst release of Cipro during the first 4 h, particularly between 2 to 4h, with release percentage of Cipro reaching an average value of approximately 40%. The initial release could be mainly from the

inclusions that bind on sMC surface. Large standard deviations of Cipro released percentage was recorded between 2 to 4 h. That could be explained by the presence of another excipient, chitosan, in the system which interfered with $\alpha\beta$ -CD by charged interaction thereof influencing the host-guest reaction of $\alpha\beta$ -CD and Cipro. As a result, a high amount of released Cipro was experienced. Cipro released percentage from drug loaded sMCs became stable at around 60% after 4 h until the end of release study. The result suggests that embedded inclusions would be released from chitosan matrix after 4 h explaining the plateaued release profile of Cipro loaded sMCs. The release results help to relatively predict the behavior of drug carrier in further *in vitro* experiments. To predict the release of Cipro from the inclusion complex and Cipro loaded sMCs, and have better comparison between the two released profiles in the alveolar space would require more complex biologically simulated tests which, however, were beyond the scope of the present study.

3.4. Minimum Inhibiting Concentration (MIC) Assay. The sMCs can load poorly soluble drug, particularly in this study, ciprofloxacin. Although the release of Cipro is demonstrated in section 3.3.2, it is also important to prove that the excipients for formulation do not interfere with drug function which possibly confounds the further evaluation of carrier system. Hence, the antimicrobial activity of drug-free sMCs, $\alpha\beta$ -CD_Cipro inclusion, and Cipro-loaded sMCs was studied against *E. coli* and *P. aeruginosa* in comparison to the use of the free drug. As shown in Table 1, the bactericidal activities of $\alpha\beta$ -CD_Cipro inclusion and Cipro-loaded sMCs were similar to that of the corresponding free drug. On the contrary, the IC₉₀ values obtained for drug-free sMCs did not show activity against either *E. coli* or *P. aeruginosa* at the highest tested concentrations. In conclusion, neither inclusion into $\alpha\beta$ -

Table 1. Results of MIC Assay against *E. Coli* and *P. aeruginosa*

samples	IC ₉₀ against <i>E. coli</i> ($\mu\text{g/mL}$)	IC ₉₀ against <i>P. aeruginosa</i> ($\mu\text{g/mL}$)
ciprofloxacin	0.004–0.01	1.6–3.2
$\alpha\beta$ -CD_Cipro inclusion	0.004–0.01 ^a	1.6–3.2 ^a
Cipro-loaded sMC	0.004–0.01 ^a	1.6–3.2 ^a
drug-free sMC	>64	>64
PBS buffer	no inhibition	no inhibition

^aDrug content.

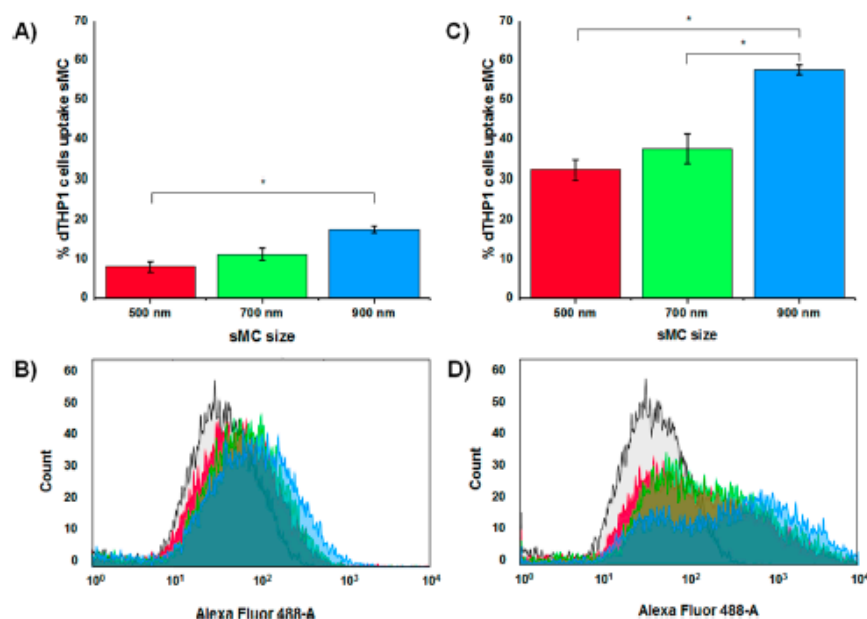


Figure 6. Summarized results from flow cytometry study: (A, B) percentage of dTHP-1 cells uptake for different size of sMCs (500, 700, and 900 nm) at 2 h postincubation. After 2 h incubation, sMC suspension was removed, and the cells were washed with PBS and further incubated with complete cell culture media; (C, D) percentage of dTHP-1 cells uptake for different size of sMCs (500, 700, and 900 nm) at 24 h postincubation. Statistically significant differences were determined with one-way ANOVA, through OriginPro 2017 Software (OriginLab Corp., Massachusetts, USA). Differences were considered significant at a level of $p < 0.005$ (*).

CD nor encapsulation into sMCs interferes with the antimicrobial function of Cipro.

3.5. Cell Viability: MTT Assay. As we aim to prepare the sMCs for pulmonary delivery of anti-infective, the biocompatibility of the drug-free carrier system was investigated on human relevant cell lines. At the alveolar space, aerosolized particles can be phagocytosed not only by alveolar macrophages, as a professional phagocyte, but also by dendritic cells or alveolar epithelium. Therefore, we assessed the sMC toxicity in three representative human cell lines: the macrophage-like cells (dTHP-1), the lung epithelial cells (NCI-H441), and human alveolar epithelial lentivirus immortalized cell line (hAELVi). We determined the biocompatibility of sMCs via cell viability, assessed by mitochondrial activity, after 24 h incubation (results are shown in Figure S8 (dTHP-1), Figure S9 (NCI-H441), and Figure S10 (hAELVi)). The sMC concentration range was chosen to reach with the highest test concentration a 5–10-times the observed IC₉₀ values of ciprofloxacin in the MIC assay. Regardless of the sMC size, dTHP-1 cell viability was not reduced after incubation with sMC concentration lower than 50 $\mu\text{g}/\text{mL}$. Nevertheless, at higher concentrations (between 50 and 100 $\mu\text{g}/\text{mL}$), sMC 500 nm induced apparent toxicity, which resulted in 50% cell death. This reduction of viability may be due to the smaller size of this system that originate a higher surface of exposition when in contact with the cell membrane, leading to a reduction of cell viability.⁶⁸ The epithelial cell types, in turn, were tested with the biggest particle system sMC 900 nm, which did not show any reduction in viability after 24 h of incubation in the tested concentration up to 200 $\mu\text{g}/\text{mL}$. The result that phagocytosing

cells like dTHP-1 are more sensitive to particles than epithelial cells was expected.

3.6. Uptake Study on dTHP-1 Cells. In this study, the sMCs with size range higher than 400 nm were prepared to aim for pulmonary delivery. Hence, *in vitro* uptake studies on macrophages were performed to assess the ability of this system to be phagocytosed by macrophages, which will also define the potential of the sMCs for either treatment of intracellular or extracellular bacterial infections. Having the size range from 400–900 nm, the applied sMCs will potentially be a target of macrophages, which are essential to clear particulates via phagocytosis.^{14,69,70} Rate of phagocytic uptake of particles is known to be dependent on surface properties and size.^{71–73} In our study, the particle size was prepared with approximately 100 nm difference (as described in section 3.2.1), so the fluorescent sMCs with different sizes, including 500, 700, and 900 nm, were chosen and expected to show the dependence in uptake study. The initial incubation period of 2 h was selected because the inherent clearance mechanisms at alveolar space presented at *in vivo*-like situation suggest this period.^{74,75} The later time point was chosen at 24 h to analyze the uptake of particles that might remain on macrophages for a period longer than 2 h. The uptake of different sMC sizes on dTHP-1 was determined by flow cytometer (FC) (for sMCs 500, 700, and 900 nm) and CSLM (for sMC 900 nm). The *in vitro* uptake study design is showed in Scheme 2.

Figure 6A and B summarize the FC results of the population of cells that uptake green labeled sMCs after 2 h incubation. The study indicated a low uptake (<20%) in dTHP-1 cells for all size ranges of sMCs. The highest percentage of cells with

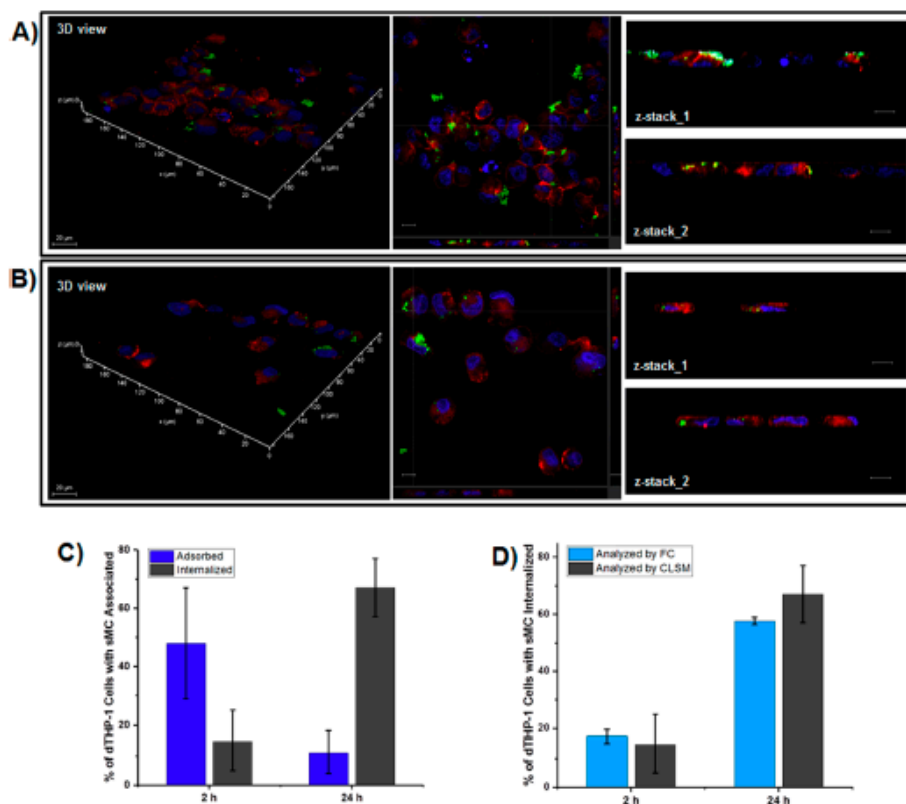


Figure 7. CLSM study of sMC (900 nm) interaction with dTHP-1 cells (nuclei stained in blue, cell membrane in red, and sMCs labeled in green): (A) after incubation for 2 h; (B) after washing the cells to remove surface adsorbed sMCs and continuing incubation for totally 24 h. Cross-sections are shown on the right of each image, the scale bar presents 10 μm . (C) Quantitative image analysis of CLSM data to compare the percentage of sMC 900 nm adsorbed and internalized, at two time points (mean % \pm SD, after counting at least 100 cells from 3 independent experiments). (D) Comparison of data for internalized sMC 900 nm as analyzed by CLMS and FC (data from Figure 6).

sMCs uptake was recorded at $17.45 \pm 2.15\%$ for sMCs 900 nm, following by $11.05 \pm 3.77\%$ and $7.88 \pm 3.44\%$ for sMCs 700 nm, and sMCs 500 nm, respectively. The particles were unexpectedly not uptaken much by macrophages like cells. It might be because of particle stability and the reduction of the surface charge, which possibly reduces interaction of the sMCs and cell membrane to initiate the phagocytosis process. Hence, the number of internalized particles was not high. The difference in cell uptake percentage was not significant but still mainly dependent on sMC size. The sMCs with the largest size, 900 nm, could probably result in faster sedimentation under *in vitro* experiment condition causing a fast adherence of particles to cells membrane. Taken together the higher local concentration, and the larger contact area, it could be explained that the 900 nm sMCs were adsorbed on higher percentage of cells and later uptaken. On the other hand, the smaller size ranges need longer time to adhere to cells membrane from particle suspension, so the cell population positive for sMC uptake of the smaller particles was lower.

Nevertheless, when a washing step was applied at 2 h postincubation to remove suspended sMCs, and the dTHP-1

cells were further incubated with complete cell culture medium until reaching 24 h, a different pattern regarding internalized sMCs was observed. Figure 6C and D show FC results analyzed after 24 h incubation, which indicate a higher percentage of dTHP-1 cell uptake, in all different sized sMC samples. Hence, it was hypothesized that after 2 h incubation, larger amounts of sMCs had already adhered on cells surface after the washing step, but not been uptaken yet (as shown in Scheme 2A). It is possible that the adsorbed sMCs were removed from cells surface during the cell detaching procedure by applying trypsin, and the washing step before FC analysis (as shown in Scheme 2B), which was also reported by Gudewicz et al.⁷⁶ and Kage et al.⁷⁷ Consequently, the percentages of cells associated sMCs analyzed after 2 h by FC were recorded at low numbers.

However, by further incubation until 24 h after removing sMC suspension, we expected to monitor the internalization of sMCs that were already attached to the cell surface (as shown in Scheme 2C). Considering the same size of sMCs, the cell population that was stained as an indication of sMC uptake at 24 h postincubation was approximately 30–40% higher than that after 2 h experiments. This observation suggests that there

were higher percentages of cells with adsorbed sMC on the surface after 2 h incubation compared to ones with sMCs internalized. That means the cells need more time to uptake sMCs. Additionally, the analysis at 24 h postincubation also revealed that the sMC size that was most efficiently phagocytosed with $57.55 \pm 1.25\%$ was 900 nm. The cell uptake, expressed as the percentage of positive cells, was $37.48 \pm 3.74\%$ and $32.28 \pm 2.41\%$, for sMC 500 nm and sMC 700 nm, respectively. The differences in cell uptake between the particles of 500 and 700 nm size were not statistically significant. As the sMC system has stable characteristics as discussed in section 3.2.3, and all samples contain the same excipients and do not show large variation in their surface charge, the results clearly support for our discussion that the uptake efficiency of dTHP-1 was mainly dependent on particle size. The larger sMCs would sediment faster to the cells membrane, which consequently initiated the phagocytosis and resulted in higher number of cells having particles internalized.

To confirm the results obtained by flow cytometry (FC), CLSM was performed as an alternative method to differentiate the adsorbed sMCs from the internalized sMCs. Through the acquisition of several images by CLSM, the percentage of cells that presented either internalized or adsorbed sMCs was determined. It is noted that the CLSM analysis was only performed on dTHP-1 incubated with sMC 900 nm, which gave the highest percentages of uptake at both time points when analyzed by FC.

Through CLSM images, it was verified that after 2 h, sMC 900 nm was mainly adsorbed on cell surfaces, while after 24 h, the particles were internalized by the macrophages, as shown in the cross-section of images (Figure 7A,B). This information was correlated with the percentage of cells with sMC 900 nm associated (Figure 7C): after 2 h of incubation, the percentage of cells with sMC 900 nm adsorbed was $48 \pm 19\%$, while only $15 \pm 10\%$ of cells presented internalized sMCs. However, a longer period of cell incubation up to 24 h showed that the percentage of cells with adsorbed sMCs significant decreased to $11 \pm 7\%$, while the number of cells with internalized sMCs increased to $67 \pm 10\%$. Interestingly, the percentage of cells with internalized 900 nm sMCs obtained by CLSM was relatively similar to that of the corresponding FC analysis (shown in Figure 7D). Hence, the two methodologies are comparable and reliable in our study.

Having obtained and evaluated the results from *in vitro* uptake study by both FC analysis and CLSM, the developed sMC system had been concluded to have low uptake by macrophage-like cells, particularly for sMC size equal or smaller than 700 nm. Taken together, the relatively large size range of the sMCs (400–900 nm), the strict pores size of mucus⁷⁸ and the intrinsic mucoadhesive property of chitosan,^{39,44–46,79} the developed sMC system is expected to have strong interaction with airway mucus upon aerosol delivery, providing platform for sustained drug delivery. Furthermore, as shown in Figure S12, the percentages of lung epithelial cells, hAELVi, uptake sMC 900 nm, are $7.93 \pm 2.68\%$ and $19.95 \pm 4.78\%$ after 2 and 24 h, respectively, which are significantly lower compared to the percentages of dTHP-1 uptake sMC 900 nm at the same time points. Consequently, we recommend the use of Cipro-loaded sMCs for extracellular infection, for example, *Pseudomonas aeruginosa* infection in cystic fibrosis patients.

4. CONCLUSION

Our study proposes an easy method to prepare a submicrocarrier system based on ionotropic gelation of anionic β -cyclodextrin and chitosan. The sMC characteristics were tuned by careful adjustment of initial polymer concentration and N/C ratio. Notably, the average size of resulting sMCs could be varied in a range from 400 to 900 nm. The larger particles showed good biocompatibility as assessed by a cell viability assay (MTT) on macrophage-like cells (dTHP-1) and lung epithelial cells (NCI-H411). Epithelial cells showed >90% viability after 24 h incubation at a concentration of 100 $\mu\text{g}/\text{mL}$ sMC. Furthermore, poorly soluble drug loading capacity of α -CD was investigated and optimized with a relevant anti-infective, ciprofloxacin, by a host–guest complex reaction. The outcome of inclusion analysis suggested the molar ratio 1:1 of α -CD and Cipro. Consequently, it helped not only to significantly enhance the solubility of Cipro, but also to maximize drug encapsulation efficiency (90%) and loading capacity (~9%) of drug loaded sMCs. The uptake experiments conducted on dTHP-1 showed the dependence of uptake efficiency on sMC size, which was confirmed by both FC and CLSM analysis. The larger sMCs were uptaken by a higher population of dTHP-1 cells. However, regardless of the particle size, the percentage of cells having particles internalized was lower than 20% after 2 h incubation. At the same time, a higher amount of sMCs, which merely adsorbed on the cell membranes, was revealed by FC and CLSM. After further incubation to reach 24 h, they were internalized into the cell resulting in high percentage of cells uptaking sMCs. Interesting enough, however, as the release study of Cipro-loaded sMCs showed that the sufficient amount of drug could be delivered before 24 h, the subsequent phagocytosis of the carrier may be considered as an important pathway for its safe degradation and elimination. The combination of mucoadhesive properties from chitosan, good biocompatibility of β -CD and chitosan, and low rate of internalization by macrophages suggests the developed sMC system as a promising drug delivery system namely for the treatment of respiratory extracellular infection, for example, *Pseudomonas aeruginosa* or *Staphylococcus aureus*.

■ ASSOCIATED CONTENT

Supporting Information

The Supporting Information is available free of charge on the ACS Publications website at DOI: 10.1021/acs.molpharmaceut.7b00967.

Cell culture procedure; synthesis of green-fluorescent chitosan; summarized results of sMC preparation; summarized results of Cipro loaded sMC preparation; calibration curve of ciprofloxacin concentrations; ¹H NMR spectra of β -CD and α -CD; FTIR spectra of β -CD and α -CD; FTIR spectra of 4-chloro-7-nitrobenzofurazan, chitosan, and green fluorescent labeled chitosan; FTIR spectra of ciprofloxacin, anionic β -cyclodextrin, and inclusion complex of α -CD_Cipro; different magnifications of SEM images of Cipro crystal, and α -CD_Cipro amorphous powder; summarized results of Cipro loaded sMC characteristics; summarized results of EE and LC from Cipro loaded sMC; MTT assay performed on dTHP-1 cells; MTT assay performed on NCI-H441 cells; MTT assay performed on hAELVi cells; summarized results of stability test of sMC analyzed

by Zetasizer Nano; suggested sMC surface structure; summarized results from FC study (PDF)

AUTHOR INFORMATION

Corresponding Author

*E-mail: Brigitta.Loretz@helmholtz-hzi.de.

ORCID

Brigitta Loretz: 0000-0003-0057-5181

Author Contributions

The manuscript was written through contributions of all authors. All authors have given approval to the final version of the manuscript.

Notes

The authors declare no competing financial interest.

ACKNOWLEDGMENTS

The authors thank Dr. Xabier Murgia Esteve and Arianna Castoldi for fruitful discussion and Petra König, Patrick Carius, and Jana Westhues for support and handling in cell cultures. A.C. gratefully acknowledges Fundação para a Ciência e a Tecnologia (FCT), Portugal for financial support (Grant No. SFRH/BD/95227/2013). This project received funding from the European Union's Framework Programme for Research and Innovation Horizon 2020 (2014–2020) under the Marie Skłodowska-Curie Grant Agreement No. 642028.

ABBREVIATIONS

sMC, submicrocarrier; Cipro, ciprofloxacin; CD, cyclodextrin; β -CD, β -cyclodextrin; a β -CD, anionic β -cyclodextrin; CLSM, confocal laser scanning microscopy; FC, flow cytometer

REFERENCES

- Savjani, K. T.; Gajjar, A. K.; Savjani, J. K. Drug solubility: importance and enhancement techniques. *ISRN Pharm.* 2012, 2012, 195727.
- Stella, V. J.; Nti-Addae, K. W. Prodrug strategies to overcome poor water solubility. *Adv. Drug Delivery Rev.* 2007, 59, 677–694.
- Chen, L.; Okuda, T.; Lu, X.-Y.; Chan, H.-K. Amorphous powders for inhalation drug delivery. *Adv. Drug Delivery Rev.* 2016, 100, 102–115.
- Stegemann, S.; Leveiller, F.; Franchi, D.; de Jong, H.; Lindén, H. When poor solubility becomes an issue: from early stage to proof of concept. *Eur. J. Pharm. Sci.* 2007, 31, 249–261.
- Dugas, H. L.; Williams, R. O., III. Nanotechnology for Pulmonary and Nasal Drug Delivery. *Nanotechnology and Drug Delivery, Volume Two: Nano-Engineering Strategies and Nanomedicines against Severe Diseases* 2016, 102.
- Wauthoz, N.; Anighi, K. *Pulmonary Drug Delivery, Chapter 5. Formulation Strategies for Pulmonary Delivery of Poorly Soluble Drugs*; John Wiley & Sons, Ltd: Chichester, UK, 2015.
- Tolman, J. A.; Williams, R. O. Advances in the pulmonary delivery of poorly water-soluble drugs: influence of solubilization on pharmacokinetic properties. *Drug Dev. Ind. Pharm.* 2010, 36, 1–30.
- Gao, L.; Zhang, D.; Chen, M. Drug nanocrystals for the formulation of poorly soluble drugs and its application as a potential drug delivery system. *J. Nanopart. Res.* 2008, 10, 845–862.
- Borok, Z.; Verkman, A. S. Lung edema clearance: 20 years of progress: invited review: role of aquaporin water channels in fluid transport in lung and airways. *J. Appl. Physiol.* 2002, 93, 2199–2206.
- Fröhlich, E.; Mercuri, A.; Wu, S.; Salar-Behzadi, S. Measurements of Deposition, Lung Surface Area and Lung Fluid for Simulation of Inhaled Compounds. *Front. Pharmacol.* 2016, 7, 181.
- Hastedt, J. E.; Bäckman, P.; Clark, A. R.; Doub, W.; Hickey, A.; Hochhaus, G.; Kuehl, P. J.; Lehr, C.-M.; Mauser, P.; McConville, J.; et al. Scope and relevance of a pulmonary biopharmaceutical classification system AAPS/FDA/USP Workshop March 16–17th, 2015 in Baltimore, MD. *AAPS Open* 2016, 2, 147.
- Zhou, Q. T.; Leung, S. S. Y.; Tang, P.; Parumasivam, T.; Loh, Z. H.; Chan, H.-K. Inhaled formulations and pulmonary drug delivery systems for respiratory infections. *Adv. Drug Delivery Rev.* 2015, 85, 83–99.
- Mortensen, J.; Lange, P.; Nyboe, J.; Groth, S. Lung mucociliary clearance. *Eur. J. Nucl. Med.* 1994, 21, 953–961.
- Hardy, C. L.; Lemaurier, J. S.; Mohamud, R.; Yao, J.; Xiang, S. D.; Rolland, J. M.; O'Hehir, R. E.; Plebanski, M. Differential uptake of nanoparticles and microparticles by pulmonary APC subsets induces discrete immunological imprints. *J. Immunol.* 2013, 191, 5278–5290.
- Lim, Y. H.; Tiemann, K. M.; Hunstad, D. A.; Eltabahy, M.; Wooley, K. L. Polymeric nanoparticles in development for treatment of pulmonary infectious diseases. *Wiley interdisciplinary reviews. Nanomedicine and nanotechnology* 2016, 8, 842–871.
- De Jong, W. H.; Borm, P. J. Drug delivery and nanoparticles: Applications and hazards. *Int. J. Nanomed.* 2008, 3, 133–149.
- Qiao, H.; Liu, W.; Gu, H.; Wang, D.; Wang, Y. The Transport and Deposition of Nanoparticles in Respiratory System by Inhalation. *J. Nanomater.* 2015, 2015, 1–8.
- Sham, J. O.-H.; Zhang, Y.; Finlay, W. H.; Roa, W. H.; Löbenberg, R. Formulation and characterization of spray-dried powders containing nanoparticles for aerosol delivery to the lung. *Int. J. Pharm.* 2004, 269, 457–467.
- Cheer, S. M.; Waugh, J.; Noble, S. Inhaled tobramycin (TOBI): a review of its use in the management of *Pseudomonas aeruginosa* infections in patients with cystic fibrosis. *Drugs* 2003, 63, 2501–2520.
- Cipolla, D.; Blanchard, J.; Gonda, I. Development of Liposomal Ciprofloxacin to Treat Lung Infections. *Pharmaceutics* 2016, 8, 6.
- Parkins, M. D.; Elborn, J. S. Tobramycin Inhalation Powder: a novel drug delivery system for treating chronic *Pseudomonas aeruginosa* infection in cystic fibrosis. *Expert Rev. Respir. Med.* 2011, 5, 609–622.
- Vendrell, M.; Muñoz, G.; Gracia, J. de. Evidence of inhaled tobramycin in non-cystic fibrosis bronchiectasis. *Open Respir. Med. J.* 2015, 9, 30–36.
- Konstan, M. W.; Flume, P. A.; Kappler, M.; Chiron, R.; Higgins, M.; Brodchhaus, F.; Zhang, J.; Angyalosi, G.; He, E.; Geller, D. E. Safety, efficacy and convenience of tobramycin inhalation powder in cystic fibrosis patients: The EAGER trial. *J. Cystic Fibrosis* 2011, 10, 54–61.
- Konstan, M. W.; Geller, D. E.; Minić, P.; Brodchhaus, F.; Zhang, J.; Angyalosi, G. Tobramycin inhalation powder for *P. aeruginosa* infection in cystic fibrosis: the EVOLVE trial. *Pediatric pulmonology* 2011, 46, 230–238.
- Loftsson, T.; Brewster, M. E. Pharmaceutical applications of cyclodextrins. 1. Drug solubilization and stabilization. *J. Pharm. Sci.* 1996, 85, 1017–1025.
- Boulmedar, L.; Bochet, A.; Lesieur, S.; Fattal, E. Evaluation of buccal methyl-beta-cyclodextrin toxicity on human oral epithelial cell culture model. *J. Pharm. Sci.* 2005, 94, 1300–1309.
- Rasheed, A. Cyclodextrins as Drug Carrier Molecule: A Review. *Sci. Pharm.* 2008, 76, 567–598.
- Zhang, J.; Ma, P. X. Cyclodextrin-based supramolecular systems for drug delivery: recent progress and future perspective. *Adv. Drug Delivery Rev.* 2013, 65, 1215–1233.
- Jianbin, C.; Liang, C.; Hao, X.; Dongpin, M. Preparation and study on the solid inclusion complex of ciprofloxacin with β -cyclodextrin. *Spectrochim. Acta, Part A* 2002, 58, 2809–2815.
- Chao, J.; Meng, D.; Li, J.; Xu, H.; Huang, S. Preparation and study on the novel solid inclusion complex of ciprofloxacin with HP- β -cyclodextrin. *Spectrochim. Acta, Part A* 2004, 60, 729–734.
- Kumar, S. S. D.; Surianarayanan, M.; Vijayaraghavan, R.; Mandal, A. B.; MacFarlane, D. R. Curcumin loaded poly(2-hydroxyethyl methacrylate) nanoparticles from gelled ionic liquid-in vitro cytotoxicity and anti-cancer activity in SKOV-3 cells. *Eur. J. Pharm. Sci.* 2014, 51, 34–44.

- (32) Nafee, N.; Hirose, M.; Loretz, B.; Wenz, G.; Lehr, C.-M. Cyclodextrin-based star polymers as a versatile platform for nano-chemotherapeutics: Enhanced entrapment and uptake of idarubicin. *Colloids Surf. B* 2015, 129, 30–38.
- (33) Teuchert, C.; Michel, C.; Hausen, F.; Park, D.-Y.; Beckham, H. W.; Wenz, G. Cylindrical Polymer Brushes by Atom Transfer Radical Polymerization from Cyclodextrin-PEG Polyrotaxanes: Synthesis and Mechanical Stability. *Macromolecules* 2013, 46, 2–7.
- (34) Singh, B.; Dhiman, A.; Rajneesh; Kumar, A. Slow release of ciprofloxacin from β -cyclodextrin containing drug delivery system through network formation and supramolecular interactions. *Int. J. Biol. Macromol.* 2016, 92, 390–400.
- (35) Yuan, Z.; Ye, Y.; Gao, F.; Yuan, H.; Lan, M.; Lou, K.; Wang, W. Chitosan-graft- β -cyclodextrin nanoparticles as a carrier for controlled drug release. *Int. J. Pharm.* 2013, 446, 191–198.
- (36) Elborn, J. S. Ciprofloxacin dry powder inhaler in cystic fibrosis. *BMJ open respiratory research* 2016, 3, e000125.
- (37) Wilson, R.; Welte, T.; Polverino, E.; de Souza, A.; Greville, H.; O'Donnell, A.; Alder, J.; Reimnitz, P.; Hampel, B. Ciprofloxacin dry powder for inhalation in non-cystic fibrosis bronchiectasis: a phase II randomised study. *Eur. Respir. J.* 2013, 41, 1107–1115.
- (38) Menon, J. U.; Ravikumar, P.; Pise, A.; Gyawali, D.; Hsia, C. C. W.; Nguyen, K. T. Polymeric nanoparticles for pulmonary protein and DNA delivery. *Acta Biomater.* 2014, 10, 2643–2652.
- (39) Garcia-Fuentes, M.; Alonso, M. J. Chitosan-based drug nanocarriers: where do we stand? *J. Controlled Release* 2012, 161, 496–504.
- (40) Cordeiro, A. S.; Alonso, M. J.; De La Fuente, M. Nano-engineering of vaccines using natural polysaccharides. *Biotechnol. Adv.* 2015, 33, 1279–1293.
- (41) Aspden, T. J.; Mason, J. D.; Jones, N. S.; Lowe, J.; Skaugrud, O.; Illum, L. Chitosan as a nasal delivery system: the effect of chitosan solutions on in vitro and in vivo mucociliary transport rates in human turbinates and volunteers. *J. Pharm. Sci.* 1997, 86, 509–513.
- (42) Bernkop-Schnürch, A.; Dünnhaupt, S. Chitosan-based drug delivery systems. *Eur. J. Pharm. Biopharm.* 2012, 81, 463–469.
- (43) Dodane, V.; Vålvalam, V. D. Pharmaceutical applications of chitosan. *Pharm. Sci. Technol. Today* 1998, 1, 246–253.
- (44) Murgia, X.; Yasar, H.; Carvalho-Wodarz, C.; Loretz, B.; Gordon, S.; Schwanzkopf, K.; Schaefer, U.; Lehr, C.-M. Modelling the bronchial barrier in pulmonary drug delivery: A human bronchial epithelial cell line supplemented with human tracheal mucus. *Eur. J. Pharm. Biopharm.* 2017, 118, 79.
- (45) Grabovac, V.; Guggi, D.; Bernkop-Schnürch, A. Comparison of the mucoadhesive properties of various polymers. *Adv. Drug Delivery Rev.* 2005, 57, 1713–1723.
- (46) Sogias, I. A.; Williams, A. C.; Khutoryanskiy, V. V. Why is chitosan mucoadhesive? *Biomacromolecules* 2008, 9, 1837–1842.
- (47) Iyer, R.; Hsia, C. C. W.; Nguyen, K. T. Nano-Therapeutics for the Lung: State-of-the-Art and Future Perspectives. *Curr. Pharm. Des.* 2015, 21, 5233–5244.
- (48) Kanber, E.; Yamada, H.; Loretz, B.; Lepeltier, E.; Lehr, C.-M. Design of Polyamine-Grafted Starches for Nucleotide Analogue Delivery: In Vitro Evaluation of the Anticancer Activity. *Bioconjugate Chem.* 2016, 27, 2431.
- (49) Cohen, J. L.; Schubert, S.; Wich, P. R.; Cui, L.; Cohen, J. A.; Mynar, J. L.; Fréchet, J. M. J. Acid-degradable cationic dextran particles for the delivery of siRNA therapeutics. *Bioconjugate Chem.* 2011, 22, 1056–1065.
- (50) Yamada, H.; Loretz, B.; Lehr, C.-M. Design of starch-graft-PEI polymers: an effective and biodegradable gene delivery platform. *Biomacromolecules* 2014, 15, 1753–1761.
- (51) Fraschini, C.; Vignon, M. R. Selective oxidation of primary alcohol groups of β -cyclodextrin mediated by 2,2,6,6-tetramethylpiperidine-1-oxyl radical (TEMPO). *Carbohydr. Res.* 2000, 328, 585–589.
- (52) Nafee, N.; Schneider, M.; Schaefer, U. F.; Lehr, C.-M. Relevance of the colloidal stability of chitosan/PLGA nanoparticles on their cytotoxicity profile. *Int. J. Pharm.* 2009, 381, 130–139.
- (53) Hoogkamp-Korstanje, J. In-vitro activities of ciprofloxacin, levofloxacin, lomefloxacin, ofloxacin, pefloxacin, sparfloxacin and trovafloxacin against gram-positive and gram-negative pathogens from respiratory tract infections. *J. Antimicrob. Chemother.* 1997, 40, 427–431.
- (54) Lubasch, A.; Keller, L.; Bomer, K.; Koeppel, P.; Lode, H. Comparative Pharmacokinetics of Ciprofloxacin, Gatifloxacin, Grepafloxacin, Levofloxacin, Trovafloxacin, and Moxifloxacin after Single Oral Administration in Healthy Volunteers. *Antimicrob. Agents Chemother.* 2000, 44, 2600–2603.
- (55) Mukker, J. K.; Singh, R. S. P.; Derendorf, H. Pharmacokinetic and pharmacodynamic implications in inhalable antimicrobial therapy. *Adv. Drug Delivery Rev.* 2015, 85, 57–64.
- (56) Cartledge, M. K.; Hill, A. T. Inhaled or nebulised ciprofloxacin for the maintenance treatment of bronchiectasis. *Expert Opin. Invest. Drugs* 2017, 26, 1091–1097.
- (57) Aksamat, T.; Bandel, T.-J.; Criollo, M.; De Souza, A.; Elborn, J. S.; Operschall, E.; Polverino, E.; Roth, K.; Winthrop, K. L.; Wilson, R. The RESPIRE trials: Two phase III, randomized, multicentre, placebo-controlled trials of Ciprofloxacin Dry Powder for Inhalation (Ciprofloxacin DPI) in non-cystic fibrosis bronchiectasis. *Contemp. Clin. Trials* 2017, 58, 78–85.
- (58) Chadha, R.; Singh, P.; Khullar, S.; Mandal, S. K. Ciprofloxacin Hippurate Salt: Crystallization Tactics, Structural Aspects, and Biopharmaceutical Performance. *Cryst. Growth Des.* 2016, 16, 4960–4967.
- (59) Tiwari, G.; Tiwari, R.; Rai, A. K. Cyclodextrins in delivery systems: Applications. *J. Pharm. BioAllied Sci.* 2010, 2, 72–79.
- (60) Amaro, M. L.; Tajber, L.; Corrigan, O. L.; Healy, A. M. Co-spray dried carbohydrate microparticles: crystallisation delay/inhibition and improved aerosolization characteristics through the incorporation of hydroxypropyl- β -cyclodextrin with amorphous raffinose or trehalose. *Pharm. Res.* 2015, 32, 180–195.
- (61) Jiao, H.; Goh, S. H.; Valiyaveetil, S. Inclusion Complexes of Poly(neopentyl glycol sebacate) with Cyclodextrins. *Macromolecules* 2001, 34, 8138–8142.
- (62) Sambasevam, K. P.; Mohamad, S.; Sarifi, N. M.; Ismail, N. A. Synthesis and Characterization of the Inclusion Complex of β -cyclodextrin and Azomethine. *Int. J. Mol. Sci.* 2013, 14, 3671–3682.
- (63) Forbes, D. C.; Peppas, N. A. Polymeric nanocarriers for siRNA delivery to murine macrophages. *Macromol Biosci* 2014, 14, 1096–1105.
- (64) Knipe, J. M.; Strong, L. E.; Peppas, N. A. Enzyme- and pH-Responsive Microencapsulated Nanogels for Oral Delivery of siRNA to Induce TNF- α Knockdown in the Intestine. *Biomacromolecules* 2016, 17, 788–797.
- (65) Fan, W.; Yan, W.; Xu, Z.; Ni, H. Formation mechanism of monodisperse, low molecular weight chitosan nanoparticles by ionic gelation technique. *Colloids Surf. B* 2012, 90, 21–27.
- (66) Agostoni, V.; Horcajada, P.; Noiray, M.; Malanga, M.; Aykaç, A.; Jicsinszky, L.; Vargas-Berenguel, A.; Semiramo, N.; Daoud-Mahammed, S.; Nicolas, V.; et al. A “green” strategy to construct non-covalent, stable and bioactive coatings on porous MOF nanoparticles. *Sci. Rep.* 2015, 5, 7925.
- (67) Caço, A. L.; Varanda, F.; Pratas de Melo, Maria, J.; Dias, A. M. A.; Dohm, R.; Marrucho, I. M. Solubility of Antibiotics in Different Solvents. Part II. Non-Hydrochloride Forms of Tetracycline and Ciprofloxacin. *Ind. Eng. Chem. Res.* 2008, 47, 8083–8089.
- (68) Elsasser, A.; Howard, C. V. Toxicology of nanoparticles. *Adv. Drug Delivery Rev.* 2012, 64, 129–137.
- (69) Lee, W.-H.; Loo, C.-Y.; Traini, D.; Young, P. M. Nano- and micro-based inhaled drug delivery systems for targeting alveolar macrophages. *Expert Opin. Drug Delivery* 2015, 12, 1009–1026.
- (70) Rodrigues, S.; Grenha, A. Activation of Macrophages: Establishing a Role for Polysaccharides in Drug Delivery Strategies Envisaging Antibacterial Therapy. *Curr. Pharm. Des.* 2015, 21, 4869–4887.

- (71) Zauner, W.; Farrow, N. A.; Haines, A. M. In vitro uptake of polystyrene microspheres: Effect of particle size, cell line and cell density. *J. Controlled Release* **2001**, *71*, 39–51.
- (72) Champion, J. A.; Walker, A.; Mitragotri, S. Role of particle size in phagocytosis of polymeric microspheres. *Pharm. Res.* **2008**, *25*, 1815–1821.
- (73) Makino, K.; Yamamoto, N.; Higuchi, K.; Harada, N.; Ohshima, H.; Terada, H. Phagocytic uptake of polystyrene microspheres by alveolar macrophages: Effects of the size and surface properties of the microspheres. *Colloids Surf., B* **2003**, *27*, 33–39.
- (74) Ruge, C. A.; Schaefer, U. F.; Herrmann, J.; Kirch, J.; Cañadas, O.; Echaide, M.; Pérez-Gil, J.; Casals, C.; Müller, R.; Lehr, C.-M. The interplay of lung surfactant proteins and lipids assimilates the macrophage clearance of nanoparticles. *PLoS One* **2012**, *7*, e40775.
- (75) Chono, S.; Tanino, T.; Seki, T.; Morimoto, K. Influence of particle size on drug delivery to rat alveolar macrophages following pulmonary administration of ciprofloxacin incorporated into liposomes. *J. Drug Targeting* **2006**, *14*, 557–566.
- (76) Gudewicz, P. W.; Molnar, J.; Lai, M. Z.; Beezhold, D. W.; Siefing, G. E.; Credo, R. B.; Lorand, L. Fibronectin-mediated uptake of gelatin-coated latex particles by peritoneal macrophages. *J. Cell Biol* **1980**, *87*, 427–433.
- (77) Kage, A.; Shoolian, E.; Rokos, K.; Özel, M.; Nuck, R.; Reutter, W.; Köttgen, E.; Pauli, G. Epithelial Uptake and Transport of Cell-Free Human Immunodeficiency Virus Type 1 and gp120-Coated Micro-particles. *J. Virol* **1998**, *72*, 4231–4236.
- (78) Murgia, X.; Pawelczyk, P.; Schaefer, U. F.; Wagner, C.; Willenbacher, N.; Lehr, C.-M. Size-Limited Penetration of Nanoparticles into Porcine Respiratory Mucus after Aerosol Deposition. *Biomacromolecules* **2016**, *17*, 1536–1542.
- (79) Mura, S.; Hillaireau, H.; Nicolas, J.; Kerdine-Römer, S.; Le Droumaguet, B.; Deloménie, C.; Nicolas, V.; Pallardy, M.; Tsapis, N.; Fattal, E. Biodegradable nanoparticles meet the bronchial airway barrier: how surface properties affect their interaction with mucus and epithelial cells. *Biomacromolecules* **2011**, *12*, 4136–4143.

6.3. PAPER 3: “Farnesylated Glycol Chitosan as a Platform for Drug Delivery: Synthesis, Characterization, and Investigation of Mucus–Particle Interactions”

This chapter is the following publication:

Farnesylated Glycol Chitosan as a Platform for Drug Delivery: Synthesis, Characterization, and Investigation of Mucus–Particle Interactions

Duy-Khiet Ho, Sarah Frisch, Alexander Biehl, Emmanuel Terriac, Chiara De Rossi, Konrad Schwarzkopf, Franziska Lautenschläger, Brigitta Loretz, Xabier Murgia, and Claus-Michael Lehr; *Biomacromolecules*. 2018, 19, 3489-3501.

DOI: 10.1021/acs.biomac.8b00795

Reprinted from *Biomacromolecules*, Farnesylated Glycol Chitosan as a Platform for Drug Delivery: Synthesis, Characterization, and Investigation of Mucus–Particle Interactions; Duy-Khiet Ho, Sarah Frisch, Alexander Biehl, Emmanuel Terriac, Chiara De Rossi, Konrad Schwarzkopf, Franziska Lautenschläger, Brigitta Loretz, Xabier Murgia, and Claus-Michael Lehr; 2018 Copyright (2018) American Chemical Society, published by Copyright Clearance Center, Inc., with permission from American Chemical Society.



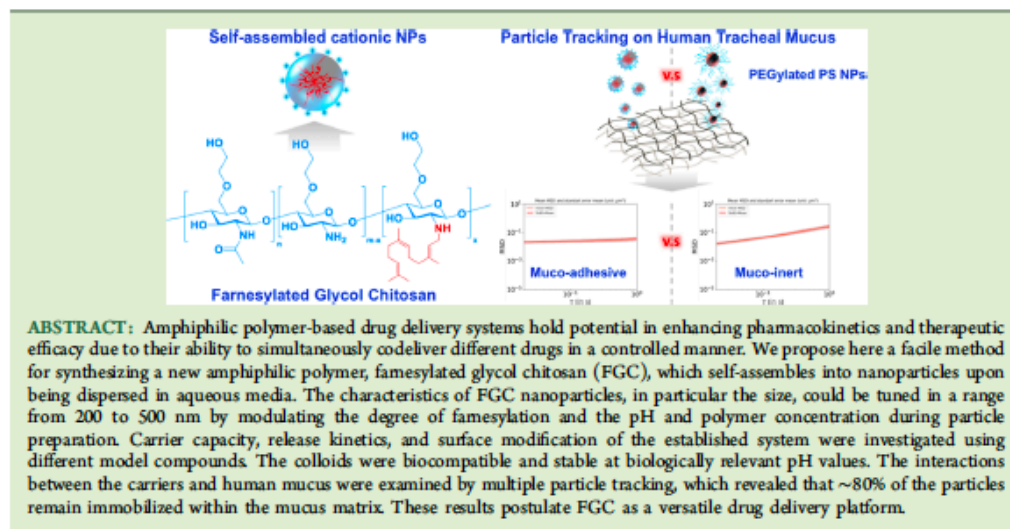
Farnesylated Glycol Chitosan as a Platform for Drug Delivery: Synthesis, Characterization, and Investigation of Mucus–Particle Interactions

Duy-Khiet Ho,^{†,‡} Sarah Frisch,[†] Alexander Biehl,[†] Emmanuel Terriac,[§] Chiara De Rossi,[†] Konrad Schwarzkopf,^{||} Franziska Lautenschläger,[§] Brigitta Loretz,[†] Xabier Murgia,^{*,†,||,⊖} and Claus-Michael Lehr^{†,‡}

[†]Helmholtz Institute for Pharmaceutical Research Saarland (HIPS), Helmholtz Center for Infection Research (HZI), [‡]Department of Pharmacy, [§]INM–Leibniz Institute for New Materials, and ^{||}Korea Institute of Science and Technology, KIST Europe, Saarland University, D-66123 Saarbrücken, Germany

^{||}Department of Anesthesia and Intensive Care, Klinikum Saarbrücken, 66119 Saarbrücken, Germany

Supporting Information



1. INTRODUCTION

Despite the utility of currently used and discovered drugs, many of these active pharmaceutical ingredients (APIs) exhibit limitations in therapeutic efficacy due to (i) their poor water-solubility, (ii) problems in delivering them to biological systems (e.g., reduced in vivo half-life/stability), and (iii) their potential to induce high toxicity.^{1–4} Appropriate formulations of drugs with pharmaceutical excipients, which are then considered drug delivery systems, are thus required to address these problems. Depending on the physicochemical properties of drug molecules and their intended application, the drug formulating strategy could be defined. Nanotechnology in particular has attracted significant attention in the field of drug delivery. Nanomedicine enables engineering drug-loaded nanostructures and nanomaterials with a size range between 10 and 1000 nm for improved API performance.⁵ Furthermore,

nanomedicine is a priori capable of achieving temporal and spatial site-specific delivery with a sufficient dose in a controlled release manner.^{6–9} Expert voices in nanomedicine have recently heightened the demand for developing drug delivery platforms with more than one functionality.^{10–13} In this regard, core–shell structured carrier systems allow integrating components with different physicochemical characteristics by employing both its lipophilic core as a preservative for poorly water-soluble drugs and the hydrophilic shell for loading water-soluble yet unstable compounds. Additionally, such systems could be further tailored and functionalized in the exterior shells, which would endow the

Received: May 18, 2018

Revised: July 5, 2018

Published: July 10, 2018

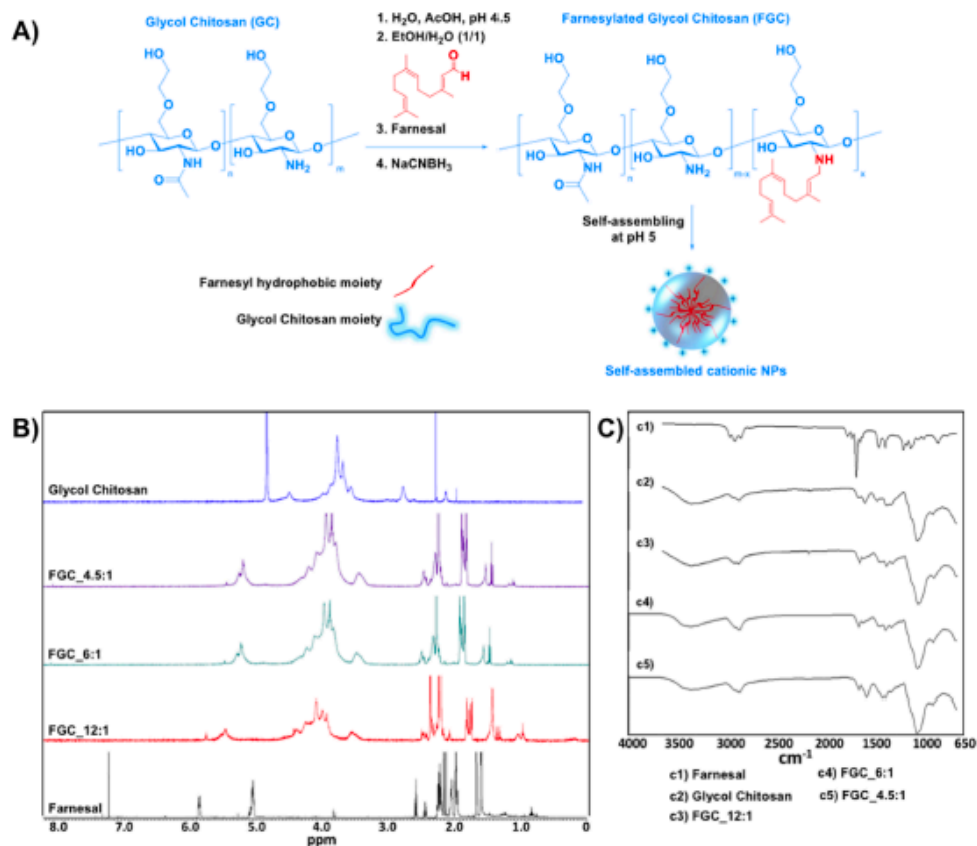


Figure 1. (A) General synthetic scheme of FGC and illustration of self-assembly of FGC nanoparticles. (B) NMR and (C) FTIR spectra of FGC obtained from different feeding glucosamine/farnesal (G/F) molar ratios: FGC_4.5:1, FGC_6:1, and FGC_12:1 compared to the spectra of glycol chitosan and farnesal.

drug delivery systems with new desired properties, e.g., engineered antifouling or mucoadhesive surface, thus rendering them attractive for applications in nanomedicine.^{13–17}

Core–shell structured nanoparticles (NPs) could be prepared by different approaches.^{18,19} The preparation of conventional core–shell structured carriers, such as liposomes, lipid-based NPs, and block polymer-based micelle/partides, has been widely described.^{20,21} Alternatively, the more sophisticated amphiphilic polymeric core–shell NPs may show some advantages over the aforementioned systems including a relatively facile fabrication, particle tuning, simultaneous codelivery of APIs, as well as controlled release.^{22,23}

Over the last few years, the state of art of amphiphilic polymer-based core–shell structured drug delivery systems has gradually shifted from synthesis, morphology control, and property measurements to the investigation of their biocompatibility, biodegradability, functionalization, and biomedical applications.^{24,25} Although the synthesis and preparation of advanced amphiphilic polymer-based core–shell nanocarriers have been achieved, the lack of available biocompatible and

biodegradable materials that would further allow large-scale and high purity development of such drug delivery systems remains an unresolved issue.

Chitosan and its derivatives, the biodegradable polysaccharides, have been widely studied, engineered, and applied in drug delivery research via different strategies reaching clinical applications.^{26–31} The cationic net charge of chitosan polymers and formulations thereof leads to a favorable bioadhesive interaction of the carriers.^{32,33} This is particularly relevant for drug delivery systems targeting mucosal tissues, e.g., the gastrointestinal tract and the pulmonary airways, which are major routes for drug absorption.³² Mucosal epithelia are covered with a tenacious viscoelastic mucus layer, a three-dimensional macromolecular network with the ability to entrap NPs in a size-dependent manner³⁴ and to adsorb positively charged macromolecules via electrostatic interactions.³⁵ In turn, the natural characteristics of mucus have been exploited as a method to prolong the residence time of chitosan-based drug delivery systems in mucosal tissues.²⁷

The self-assembly of hydrophobically modified chitosan derivatives into core–shell structured carriers holds great

potential for versatile drug delivery systems.^{29,36} Glycol chitosan, a highly water-soluble chitosan derivative, has been extensively employed in the preparation of various multifunctional core-shell-structured drug carriers.^{29,37–39} Amphiphilic chitosan derivatives have been synthesized by chemical modification of chitosan derivatives with steroid acid derivatives,^{40–42} fatty acids,²⁹ or hydrophobic polymers,^{43,44} which could further readily self-assemble into NPs. The characteristics of these self-assemblies mainly depend on the degree of hydrophobic substitution, pH and/or ionic strength, and molecular weight of the polymer. Nevertheless, the choice of the appropriate hydrophobic moiety will further decide the extent of the hydrophobic interaction, which in turn will play an essential role in colloid formation and stability. Long-term storage, stability at different pH values, as well as tunability of NP formation (e.g., of particle size) are affected by the hydrophobic interactions as a driving force in the colloid assembly.^{42,45} Taking advantage of the spectacular self-assembling properties of linear terpenyl derivatives, especially squalenyl derivatives,^{46,47} Lepeltier et al. have recently described the synthesis of squalenylated chitosan, which could self-assemble into a stable and uniform particulate system with just ~2.5% squalenyl substitution. Nevertheless, this system showed clear limitations such as poor solubility in common solvents and the inability to tune down the particle size below 600 nm.⁴⁸

To address the limitations raised in that research, we propose a facile synthesis of a new amphiphilic glycol chitosan derivative, famesylated glycol chitosan (FGC), by chemically conjugating the amine functional groups of the polymer with famesal, a derivative of the natural hydrophobic oil Farnesol. The synthesis of the new materials based on two derivatives of natural compounds is expected to have good biocompatibility. Moreover, the conjugation of the more hydrophilic glycol chitosan with famesal, which is half in terms of molecule size compared to the squalenyl derivative proposed by Lepeltier et al., should allow a solubility improvement while having strong enough hydrophobic interactions for the self-assembly. The self-assembling properties of farnesyl moieties would render spontaneous formation of cationic NPs in an aqueous medium. The colloidal characteristics, including hydrodynamic diameter, polydispersity index (PDI), and ζ -potential, could be tuned by (i) different degrees of famesylation (DoF), which were varied by changing feeding glucosamine/famesal (G/F) molar ratio and (ii) particle-forming environmental factors including pH and concentration. We also explored the carrier capacity and release kinetics of several model compounds. Further surface modification of the NPs can be achieved, which was exemplified by the conjugation of NPs and the fluorescence dye 4-chloro-7-nitrobenzofurazan (NBD-Cl) in an aqueous medium. In subsequent studies, we could further demonstrate that the FGC NPs are stable in different physiologically relevant pH environments as well as biocompatible with the A549 cell line. Moreover, nanoparticle-mucus interactions of differently sized FGC NPs were investigated by applying multiple particle tracking analysis upon mixing FGC NPs with native human mucus.

2. MATERIALS AND METHODS

Materials. Glycol chitosan (GC) (degree of polymerization > 400, $M_w = 2.5 \times 10^5$ Da, deacetylation degree of ~90% as calculated in Figure S1) (CAS Number: 123938-86-3) and famesal (mixture of isomers) were obtained from Sigma-Aldrich and used as received.

Acetic acid- d_4 , D_2O , acetic acid, ethanol, chloroform, hydrochloric acid (HCl), sodium hydroxide (NaOH), sodium cyanoborohydride ($NaCNBH_3$), phosphotungstic acid (PTA), Nile red, 4-chloro-7-nitrobenzofurazan (NBD-Cl), 4-(4,6-dimethoxy-1,3,5-triazin-2-yl)-4-methylmorpholinium chloride (DMTMM), methoxypolyethylene glycol amine (5 kDa), albumin-fluorescein isothiocyanate conjugate (fluorescent albumin), fetal bovine serum (FBS), Dulbecco's phosphate-buffered saline (PBS), Hanks' balanced salt solution (HBSS), thiazolyl blue tetrazolium blue (MTT), dimethyl sulfoxide (DMSO), and Triton X-100 were purchased from Sigma-Aldrich. CholEsteryl 4,4-difluoro-5,7-dimethyl-4-bora-3a,4a-diaza-s-indacene-3-dodecanoate (CholEsteryl BODIPY FL C12, later in this manuscript referred to as CholEsteryl BODIPY) was purchased from Thermo Fisher Scientific. Purified water was produced by Milli-Q water purification system (Merk Millipore, Billerica, MA).

Synthesis and Characterization of Farnesylated Glycol Chitosan Nanoparticles. *Synthesis of Farnesylated Glycol Chitosan (FGC).* The general synthetic scheme of FGC is described in Figure 1A. Briefly, glycol chitosan (GC) was entirely solubilized in a solution of acetic acid (0.02 M) at a concentration of 4 mg/mL before starting the reaction. Then, ethanol was added to the solution to reach the ratio 1:1 (v/v), and the pH was adjusted to the range of 4–5 by adding 1 M HCl or 1 M NaOH. The famesylation of chitosan was done by reductive amination reaction between amine functional groups of GC and the aldehyde functional group of famesal. The degree of famesylation (DoF) was varied by changes of G/F feeding molar ratio, which was 12:1, 6:1, and 4.5:1, respectively. To obtain well-distributed conjugation of famesyl moieties to GC backbone, the corresponding amount of famesal was presolubilized in 1 mL of ethanol and added dropwise to the prepared GC solution. The resulting mixture was stirred vigorously for 2 h before an excess amount of $NaCNBH_3$ (5 equiv molar of famesal) was added to the solution. The reaction was then kept for 24 h at room temperature, and resulting FGC was completely soluble in the reacting solution. Before isolating FGC, an appropriate amount of 1 M HCl solution was dropped into the solution to quench the excess amount of $NaCNBH_3$. Afterward, water was added to the solution to reach a 1:3 ratio (v/v) of ethanol:water. Chloroform was then used to extract unreacted famesal. Following, the aqueous phase was collected, and ethanol was removed by rotary evaporator. As a result, FGC was precipitated in the aqueous phase and collected by centrifugation at 24,400g for 30 min at room temperature. The product was then dried by lyophilization (Alpha 2-4, Martin Christ GmbH, Osterode, Germany) and characterized by proton nuclear magnetic resonance (1H NMR) using acetic acid- d_4 as solubilizing solvent (Bruker Fourier 300) and Fourier-transform infrared spectroscopy (FTIR, Spectrum 400 FT-IR/FT-NIR spectrometer, PerkinElmer).

Nanoparticle Preparation. The preparation procedure of stable and uniform FGC NPs was investigated using different DoF compounds in different pH (5 or 7) environments and changing the final concentration of NPs in the aqueous medium (0.25, 0.5, or 1.0 mg/mL). The optimal DoF, concentration, and pH for FGC NP preparation would then be obtained. The general procedure for NP preparation is described as follows: the purified FGC compound obtained by the G/F feeding molar ratios of 12:1, 6:1, or 4.5:1 was added to the mixture of acetate buffer pH 5 or phosphate buffer pH 7 and ethanol with a ratio of 1:1 (v/v). The concentration of FGC calculated in aqueous solution was varied in the range from 0.25 to 1 mg/mL to study the influence of the concentration on the resulting NP characteristics. The mixture was stirred vigorously until complete solubilization of FGC was achieved. Subsequently, ethanol was evaporated by rotary evaporator at 260 rpm, 40 °C, and 40 mbar. The NPs were spontaneously self-assembled in aqueous medium (the illustration of FGC NPs is shown in Figure 1A). The residue ethanol was then removed by membrane dialysis (molecular weight cut off, MWCO, 500 Da) at the same pH of the sample for 4 h. The particles were then kept at 4 °C for stabilization and characterized to obtain hydrodynamic diameter, PDI, and ζ -potential (Z-Sizer, Malvern). At least three independent experiments were conducted in triplicate, and the results are expressed as the mean \pm standard deviation (SD).

NP Characterization. The characterization (hydrodynamic size, PDI, and ζ -potential) of particles was studied by dynamic light scattering (DLS, Zetasizer Nano-ZS, Malvern Instruments, Worcester, U.K.) equipped with a 4 mW He-Ne laser employing a wavelength of 633 nm and backscattering angle of 173° at 25 °C. The reported size is the z-average hydrodynamic diameter (intensity based) of three measurements.

Elemental Analysis. The elemental percentages of nitrogen (%N), hydrogen (%H), and carbon (%C) in GC and purified FGC compounds, which could form stable and uniform NPs, were further determined using a Leco CHN-900 analyzer. The final DoF expressed as the percentage of farnesylated glucosamine units (DoF (%)) would be calculated according to eq 1

$$\text{DoF (\%)} = \frac{\%C - 6.82}{21.82 - 6.82} \times 100 \quad (1)$$

where %C/%N = 6.82 if there was no farnesyl moiety conjugated to the glucosamine units of GC, and %C/%N = 21.82 if there was one farnesyl moiety conjugated to each of the glucosamine units of GC.

Stability of FGC NPs at Different pH. The stability of different FGC NPs with targeted sizes of 200, 300, and 500 nm (obtained from the self-assembly of FGC-11%, 0.5 mg/mL; FGC-11%, 1 mg/mL; and FGC-16%, 1 mg/mL; respectively) prepared in acetate buffer pH 5 was investigated by either incubating particle suspensions in acetate buffer pH 2 or HBSS pH ~7.4 at room temperature at a concentration of 25 $\mu\text{g/mL}$. Samples were analyzed by DLS (for hydrodynamic size, PDI, and ζ -potential, Z-Sizer, Malvern) after predetermined incubation times (1, 3, and 24 h). The samples incubated in HBSS were further kept under storage conditions, 4 °C, and analyzed again after 10, 20, and 30 days. Three independent experiments were conducted in triplicate, and results are expressed as the mean \pm standard deviation (SD).

Cell Viability: MTT Assay. Cell viability after incubation of A549 cells with FGC NPs was assessed by MTT assay. On a 96-well plate, A549 cells were seeded at a density of 1×10^5 cells per well. Cell culture propagation and maintenance is reported in the Supporting Information.

The cells were grown for 3 days before the assay to allow for ~80% cell confluency. Cells were further incubated with different concentrations of drug-free FGC NPs (300 nm, obtained from the self-assembly of FGC-16% at pH 5 and 0.5 mg/mL) at concentrations ranging from 31.25 to 1250 $\mu\text{g/mL}$ dispersed in HBSS for 4 h at 37 °C and 5% CO₂. To minimize the use of pH 5 buffer from the NP suspension, NP solutions were first concentrated to a target concentration of 2500 $\mu\text{g/mL}$ using a concentrator operated at 10,000g at room temperature and 40 mbar for 1 h (Concentrator, Eppendorf, Germany). After the incubation time, cells were washed twice with PBS, and MTT (0.5 mg/mL in HBSS) was incubated for 4 h in the dark. The supernatant was further removed from the wells, and the formed formazan crystals were dissolved in DMSO. Finally, the absorbance was measured at 550 nm with a plate reader (Infinite M200Pro, Tecan, Germany). Cells incubated only with HBSS were used as a negative control (corresponding to 100% cell viability), and cells treated with 1% TritonTM X-100 in HBSS medium were used as positive control (designated as 0% cell viability). The percentage of viable cells was calculated in comparison to negative and positive controls.³¹ Three independent experiments were conducted at least in triplicate.

Loading of Model Compounds. Three model compounds, Nile red, CholEsteryl BODIPY, and fluorescent albumin, representing different molecular weights and hydrophobicities were used to investigate drug loading capacity of the newly prepared FGC NPs. The hydrophobic molecules, Nile red, and CholEsteryl BODIPY were expected to be localized in the interior core of the NPs, whereas the hydrophilic macromolecule, fluorescent albumin, would be loaded in the exterior shell of the NPs. Thus, different protocols were optimized for loading of model compounds to NPs as below:

i. Loading of Nile Red and CholEsteryl BODIPY. FGC (0.5 mg, DoF 11%) compound was solubilized in 2 mL of a solution of

ethanol:acetate buffer pH 5 (1:1 v/v). The predetermined amount of Nile red or CholEsteryl BODIPY (Table S2) was added to the prepared solution of FGC. The NPs were spontaneously formed when ethanol was removed during the rotary evaporating process. One milliliter of ethyl acetate was then added to the suspension of loaded NPs and stirred at 200 rpm to allow the free Nile red or CholEsteryl BODIPY to be solubilized in the organic phase. The organic phase was collected and diluted in ethanol for further determination of the unloaded amount, calculation of drug encapsulation efficacy (EE%), and drug loading capacity (LC%). The aqueous phase with the NPs was also collected, centrifuged, and washed in acetate buffer pH 5 twice to obtain the loaded NPs. NPs were then kept for 4 h at 4 °C to allow for system equilibration and characterization. At least three independent batches of all Nile red- or CholEsteryl BODIPY-loaded FGC NPs were prepared.

ii. Loading of Fluorescent Albumin. The optimal protocol to load the model protein fluorescent albumin on NPs is as follows: FGC-11% NPs were prepared in advance at 0.5 mg/mL concentration and then diluted in acetate buffer pH 5 to 0.25 mg/mL. Then, 1 mL of the prepared NP suspension was added dropwise to 1 mL of fluorescent albumin solution at a concentration of 25 $\mu\text{g/mL}$. The resulting mixture was then stirred at 200 rpm for 2 h at room temperature, allowing the absorption of fluorescent albumin onto the NP surface due to charge interaction. The protein-loaded NPs were then centrifuged for 30 min at 24,400g and washed twice in acetate buffer at pH 5. The supernatant was collected and used to analyze protein EE% and LC% of FGC NPs. The protein-loaded NPs were also characterized. At least three independent batches of fluorescent albumin loaded-NP samples were prepared.

Quantification of Model Compound Loading. The loaded quantity of model molecules was determined indirectly by measuring the unloaded molecules in the supernatant (loaded amount = initial amount - amount in the supernatant). Quantification was done by fluorescence intensity analysis (Infinite M200PRO, Tecan, Germany). Calibration curves were performed with different defined concentrations ranging from 0 to 10 $\mu\text{g/mL}$ for Nile Red in ethanol (Ex/Em = 540/600, $r^2 = 0.9839$) and for CholEsteryl BODIPY in ethanol (Ex/Em = 495/550, $r^2 = 0.9897$) and ranging from 0 to 31.25 $\mu\text{g/mL}$ for fluorescent albumin in acetate buffer at pH 5 (Ex/Em = 490/540, $r^2 = 0.9986$). All standards were measured five times, and all measurements were performed at room temperature.

The EE% and the drug LC% were calculated according to the equations

$$\text{EE\%} = \frac{\text{weight of encapsulated drug in NPs}}{\text{initial weight of used drug}} \times 100 \quad (2)$$

$$\text{LC\%} = \frac{\text{weight of drug in NPs}}{\text{weight of NPs}} \times 100 \quad (3)$$

where "weight of NPs" was calculated as (weight of NPs = weight of polymeric materials + weight of encapsulated drug in NPs).

Release Study. Release profiles of Nile red, CholEsteryl BODIPY, or fluorescent albumin from the model compound-loaded FGC NPs were obtained in PBS (pH 7.4) at 37 °C. Briefly, Nile red, CholEsteryl BODIPY, or fluorescent albumin-loaded FGC NPs were diluted in PBS to a final NP concentration of 10% (w/w) and placed on a shaker at 400 rpm at 37 °C. The concentration of released compound was analyzed by timely collecting samples from the supernatant over 24 h. The hydrophobic compounds Nile red and CholEsteryl BODIPY were extracted from the supernatant using ethyl acetate. The volume was kept constant by refilling with an identical volume of PBS. The cumulative released drug (%) over 24 h was determined. Three independent experiments were conducted in triplicate, and results are expressed as the mean \pm SD.

Surface Modification of FGC NPs. The FGC NPs (targeted size 200 nm, obtained from the self-assembly of FGC-11%, at pH 5, 0.5 mg/mL) were prepared and diluted in Milli-Q water. An amount of NBD-Cl (1% w/w) was presolubilized in ethanol and added dropwise to the NP solution. The mixture was then stirred at 200 rpm at room

temperature for 12 h. The NP suspension was then purified by membrane dialysis (MWCO 1000 Da) for 24 h. The NPs were then characterized and observed by fluorescent microscopy (Nikon Ti-U, Netherlands) to confirm the possibility of surface functionalization. The fluorescent-conjugated NP suspension was diluted in Milli-Q water to 50 $\mu\text{g}/\text{mL}$ concentration for observation.

Transmission Electron Microscopy (TEM). The morphology of FGC NPs, obtained from the self-assembly of FGC-16%, pH 5, 0.5 mg/mL concentration, was investigated by transmission electron microscopy (TEM, JEM 2011, JEOL). Samples for TEM were prepared by adding an appropriate amount of NP suspension on a copper grid (carbon films on 400 mesh copper grids, Plano GmbH, Germany). The grid was blotted after 10 min incubation, and samples were stained with 0.5% (w/w) of PTA solution to enhance the contrast for TEM visualization.

Confocal Laser Scanning Microscopy (CLSM). A drop of diluted fluorescent-loaded FGC NP suspension was deposited on a slide and observed using confocal laser scanning microscopy (CLSM, TCS SP 8, Leica, Mannheim, Germany) equipped with a 63 \times water immersion objective (HC APO CS2 63 \times /1.20). Image analysis was performed using LAS X software (Leica Application Suite X; Leica, Mannheim, Germany).

NP Tracking in Native Human Mucus. Human native tracheal mucus samples were obtained from the endotracheal tube of patients undergoing elective surgery after having obtained informed consent and in compliance with the protocol approved by the Ethics Commission of the "Ärztammer des Saarlandes" (file number 19/15), as previously described.^{35,49} For video microscopy, fluorescently labeled, Nile red-loaded FGC NPs with targeted sizes of 200 nm (obtained from the self-assembly of FGC-11%, pH 5, 0.25 mg/mL) and 300 nm (obtained from the self-assembly of FGC-16%, pH 5, 0.5 mg/mL) were prepared at a concentration of 0.01% (w/v) and named FGC 200 nm and FGC 300 nm, respectively. Commercially available polystyrene NPs (Fluospheres, Invitrogen) coated with a dense layer of polyethylene glycol (PEG) with an equivalent hydrodynamic diameter were used as muco-inert control NPs (Table S3).³⁴

A volume of 3 μL of each particle stock was mechanically dispersed with a pipet into $\sim 25 \mu\text{L}$ of undiluted native human tracheal mucus. The whole mixture was then transferred to a chamber (Gene Frame, Thermo Fisher Scientific), sealed with a coverslip, and placed in the microscope stage. Video sequences were captured at a frame rate of 50 fps with a microscope (Nikon TI Eclipse) equipped with a spinning confocal unit (CSU W1, Andor Technologies), an EMCCD camera (Hamamatsu), and a 60 \times Plan Apo oil immersion objective with a numerical aperture of 1.4. For improving the visualization of the particles and reducing the background noise, image preprocessing was performed adjusting the brightness and contrast of the images and applying FFT bandpass filters available at ImageJ (<https://imagej.nih.gov/ij/>). Further, X-Y coordinates for each particle at each frame were obtained using the ParticleTracker utility from the MOSAIC ToolSuite (an add-on of ImageJ).⁵⁰ The raw data of each particle trajectory was converted to time-averaged mean squared displacement (MSD or Δr^2) as a function of the time scale (τ) by means of a custom-developed Python script:

MSD values at each τ were computed according to

$$\Delta r(\tau)^2 = \{x(t + \tau) - x(t)\}^2 + \{y(t + \tau) - y(t)\}^2 \quad (4)$$

Individual MSD as a function of τ were plotted in log-log scales. Further, the slope of each individual MSD trajectory, α , was determined (τ between 0.02 and 1 s) as

$$\alpha = \frac{d \log \Delta r(\tau)^2}{d \log(\tau)} \quad (5)$$

where α describes the diffusive properties of the NPs: $\alpha = 0$ for purely elastic materials and $\alpha = 1$ for Newtonian fluids.⁵¹ The effective diffusion (D_{eff}) for each particle was computed from its MSD value

$$\Delta r(\tau)^2 = 4D\tau \quad (6)$$

For each type of NP, 12 video microscopy files from three independent native human mucus samples were analyzed.

3. RESULTS AND DISCUSSION

Synthesis of Farnesylated Glycol Chitosan (FGC). The new amphiphilic GC derivatives were synthesized by chemical modification of GC with farnesal (Figure 1A), a sesquiterpenyl derivative, using reductive amination reaction in the presence of NaCNBH_3 .⁴⁸ The DoF was varied by different initial feeding molar ratios of G/F 12:1, 6:1, and 4.5:1, respectively. The average isolated yield from the synthesis was as high as $80 \pm 10\%$. Interestingly, the resulting FGC compounds were soluble in the reacting mixture, which is clearly advantageous compared to the previously reported lack of solubility of squalenyl chitosan derivative.⁴⁸

FGC compounds were first characterized by ^1H NMR. The spectra of such conjugates were compared to the spectra of GC and farnesal to confirm the successful farnesylation. As shown in Figure 1B and Figure S2, the ^1H NMR spectrum of farnesal presents its characteristic peak at position "1", $\delta \sim 5.795$ ppm, which is next to the aldehyde functional group (expanded description in Figure S2). This peak, however, became absent in the spectra of FGC compounds (an expanded description is provided in Figure S3, the peak is pointed by a black arrow), proving the absence of unreacted farnesal in the final FGC compounds and thus indicating the successful purification. Furthermore, the characteristic peak of farnesal at position "2", $\delta 5.000$ – 5.200 ppm, became overlapped with the proton peaks in position "1" of glucosamine units (Figure 1B; expanded description in Figure S3, proton 1(D–F) and 2'(F)). In addition, the proton in position "3" resulting from the amine reductive linkage was clearly observed and overlapped with the proton peaks in position "2" of glucosamine units (Figure S3, proton 2(D–F) and 3'(F)) in comparison to the spectrum of GC (Figure 1B and Figure S1). The clear alkyl chain proton peaks of farnesal were also observed in the spectra of FGC compounds (Figures S2 and S3, respectively), which were absent in the spectrum of GC. All analyses mentioned above in ^1H NMR spectra prove the successful conjugation of farnesyl moieties to GC.

Additionally, the purified FGC compounds were also characterized by FTIR to confirm the conjugation of GC with farnesyl moieties (Figure 1C). The characteristic peaks at 2800 – 3000 cm^{-1} representing C–H stretching of farnesal (Figure 1C-c1) and the peaks at 1000 – 1100 cm^{-1} from the C–O–C vibration of the glucosamine units in GC (Figure 1C-c2) could be seen in the purified FGC compounds (Figure 1C-c3, -c4, and -c5). Furthermore, the absence of carbonyl (C=O) band at 1720 cm^{-1} in the spectra of FGC compounds indicated that the purified samples did not contain unreacted farnesal. Moreover, the intensity of the peak at 2800 – 3000 cm^{-1} is a qualitative indicator for the amount of farnesyl moieties and correlates fairly with the targeted G/F molar ratios, which shows more intensive peaks when raising the targeted degree of farnesylation by changing the G/F molar ratios from 12:1 to 4.5:1.

Optimizing the Preparation of Drug-Free Farnesylated Glycol Chitosan NPs. Like other reported amphiphilic polymers/polysaccharides, the assembly of the amphiphilic FGC in aqueous media would result in core-shell-structured particles.^{25,29,52} In such a system, the hydrophobic farnesyl moieties would be assembled in the core of the particles according to Abed et al.⁵³ and Wang et al.,²⁵ whereas the

hydrophilic and cationic GC moieties would play a role as the shell of the NPs (depicted in Figure 1A). The stability and characteristics of such NPs would be mainly dependent on the degree of farnesylation, the association of amine functional groups on GC moieties, as well as the concentration of the FGC compound dispersed in the NP preparing solution. As the resulting FGC compounds are amphiphilic macromolecules, the medium used to solubilize such compounds was a mixture of acetate buffer (pH 5) or phosphate buffer (pH 7) and ethanol with a 1:1 (v/v) ratio in which acetate buffer (pH 5) or phosphate buffer (pH 7) was aimed at solubilizing GC moieties and ethanol was employed for the solubilization of farnesyl moieties. The formation of NPs was based on spontaneous self-assembly of farnesyl moieties when ethanol was removed from the solution by rotary evaporation.⁵³ The optimal feeding G/F molar ratio and NP preparing conditions were investigated by changes in (i) FGC compounds obtained from different feeding G/F molar ratios (12:1, 6:1, and 4.5:1), which were further called FGC_12:1, FGC_6:1, and FGC_4.5:1, respectively, (ii) buffer pH values, and (iii) concentration of FGC calculated in aqueous medium. Interestingly, all FGC compounds could form self-assembled NPs at a low concentration of 0.25 mg/mL (Table S1). However, at a feeding G/F ratio of 12:1, the obtained FGC could not form uniform NPs in any case (PDI > 0.45 in most cases, Table S1) regardless of pH or concentration changes, which means that this particular DoF might not be sufficient to enhance strong enough hydrophobic assembly of farnesyl moieties, possibly in both inter- and intramolecular interactions.⁵⁴ Conversely, at G/F ratios of 6:1 and 4.5:1, uniform particulate systems were formed (Table S1).

The pH values of the aqueous phase, in turn, played an essential role in the NP preparation procedure. The suitable pH environment for stable and uniform particle formation (considering PDI < 0.3) is at pH 5 (Table S1). The phenomena could be explained by the pK_a value at pH 6.5 of chitosan derivatives;⁵⁵ at pH 5, the amine functional groups of GC moieties would be associated. As a result, the FGC compounds would be completely solubilized in the mixture of acetate buffer pH 5 and ethanol. The soluble amphiphilic FGC would then be self-assembled into NPs well upon evaporating ethanol under pressure. On the contrary, in phosphate buffer pH 7, the amine functional groups of GC moieties would not be fully associated, which would affect the solubility of FGC compounds before the assembly took place, leading to aggregating samples (Table S1). Despite the formation of NPs from G/F ratios of 6:1 and 4.5:1, at pH 7 and low concentration (FGC at 0.25 mg/mL), the PDIs of the obtained NPs were characterized by high values: 0.39 ± 0.03 and 0.79 ± 0.20 in the case of G/F ratios of 6:1 and 4.5:1, respectively. Thus, the FGC NPs could conclusively be better assembled at pH 5.

According to these results, the FGC_6:1 and FGC_4.5:1 were chosen for NP preparation at pH 5 for the rest of our study.

Elemental Analysis. As G/F ratios of 6:1 and 4.5:1 could be used to form NPs, the relative degree of farnesylation in both samples was further investigated by elemental analysis. Table 1 summarizes the elemental analysis of G/F ratios of 6:1 and 4.5:1 in comparison to GC. On the basis of eq 1, the DoF was calculated at 10.93 and 15.80% in the case of G/F ratios of 6:1 and 4.5:1, respectively. Although the DoFs for uniform NP preparation in the present study were higher compared to

Table 1. Elemental Analysis of Glycol Chitosan and Farnesylated Glycol Chitosan Derivatives and the Corresponding Degree of Farnesylation and Yield of Substitution

sample	%C	%H	%N	%C/%N	DoF	yield of substitution
GC	39.98	6.93	5.86	6.82	0	
FGC_6:1	51.18	8.72	6.05	8.46	10.93	~69%
FGC_4.5:1	54.70	8.69	5.95	9.19	15.80	~80%

~2.5% squalenylation of chitosan reported by Lepeltier et al.,⁴⁸ the good solubility of FGC compounds is a remarkable advantage in larger scale production. Furthermore, a DoF at ~10% is a reasonable degree of hydrophobic modification to maintain the naturally useful properties of chitosan derivatives, e.g., solubility, adhesiveness, biocompatibility, and biodegradability. Moreover, functionalizing these carriers would be possibly facile due to the abundant amount of accessible amine functional groups when the degree of hydrophobic substitution is low. The yields of substitution from each conjugation were also reported to be higher than 69%.

The FGC compounds used for NP formation are in the following named FGC-11% and FGC-16% for the compounds having a DoF of 10.93 and 15.80%, respectively, which should facilitate the reading.

Dependence of FGC NP Characteristics as a Function of DoF and Concentration. The NPs characteristics formed at pH 5 varied as a function of FGC concentration and DoF (Figure 2, Table S1). The hydrodynamic diameter of the NPs could be tuned in the range from ~200 to ~500 nm. At an equal concentration of FGC, a higher DoF would define a larger size due to the presence of a higher amount of farnesyl moieties in the core of the colloids.^{54,56,57} Similarly, particle size would also increase by increasing FGC concentration at a constant DoF. Although there were slight differences in size from different NP-preparing conditions, three targeted NP size groups of 200, 300, and 500 nm were defined. A uniform NP size with a reasonable PDI (<0.3) was recorded in all samples. The presence of the cationic hydrophilic GC polymer in the exterior of the assembly rendered all NPs positively charged with a ζ -potential >25 mV. Furthermore, the morphology of the NP representatives was spherical, as confirmed by TEM (Figure 3A).

Storage Stability of FGC NPs. The stabilities of the FGC NPs in three targeted size groups, 200, 300, and 500 nm, under storage conditions is reported in Figure S4. Despite some minor changes in NP characteristics, they were stable over 30 days without aggregation, which shows advantages over chitosan-based cationic polyplex systems as reported by Yasar, Ho et al.,³⁰ and other chitosan-based assembled NPs.^{29,41}

Stability of FGC NPs in Different Biological Relevant pH Environments. The prepared FGC NPs were aimed to be applied as drug delivery systems. Thus, the stability of such a system in different pH environments, from the acidic gastric pH (1–3) to the more common neutral pH (7.4), should be addressed. As the NPs formed by self-assembly of amphiphilic FGC molecules in aqueous medium, their stability would depend on both their surface properties and the hydrophobic interaction in their core. The surface properties are, in turn, influenced by responses of GC moieties to the surrounding environmental factors, e.g., ionic strength and pH values. It is

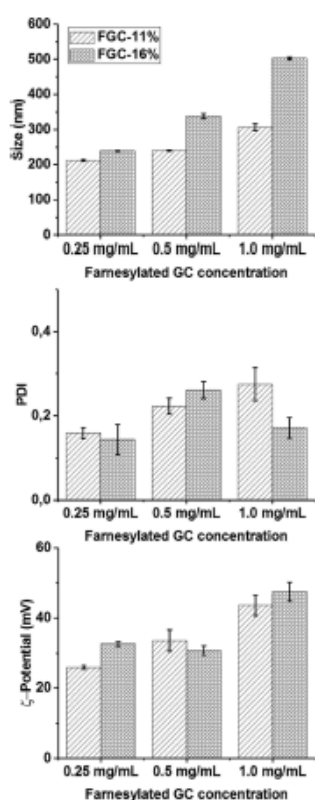


Figure 2. Properties of different NP batches depending on FGC concentration (mg/mL) calculated in an aqueous medium (acetate buffer pH 5) and DoF in FGC compounds. $n = 3$, mean \pm SD.

hypothesized that the self-assembled NPs would disassemble once the solubility of GC moieties would increase, particularly at lower pH at which GC would possibly become more associated in an aqueous medium. As a result, the self-assembly resulting from intra- and intermolecular interaction of farnesyl moieties could not be favorable over the strong electrostatic repulsions and enhanced water solubility of high density charged polymer molecules.^{53,54} Interestingly enough, however, the self-assembly of FGC NPs showed stable characteristics regarding hydrodynamic diameter, PDI, and ζ -potential even at a pH value of 2 for a 24 h incubation period (Figure 4), meaning that the hydrophobic interaction of farnesyl moieties could overcome the association of GC moieties at such low pH. In more detail, the particles with a targeted size of 200 nm showed a slight increase in size after incubation for 1 h in pH 2 buffer, which might be caused by the dramatic protonation on amine functional groups on GC moieties. However, there were slight decreases in particle size in all three targeted size groups after incubating the particles longer than 1 h in pH 2 buffer, which was interestingly proven for compression and densification in hydrophobic intraparticles. At that pH, the hydrodynamic diameter of chitosan-based NPs should be increased due to the swollen phenomena of chitosan

derivatives, but in this case, the increase in hydrophilicity of GC moieties would simultaneously enhance the amphiphilicity of FGC molecules, which might result in a more intensive interaction leading to denser packing of farnesyl moieties. Thus, slightly smaller size of the NPs was recorded at pH 2 after 3 and 24 h incubation in all cases. The PDI and ζ -potential of the NPs in all three targeted size groups were stable with just some minor changes.

When incubating the FGC NPs in HBSS, pH \sim 7.4, it is expected that the deprotonation of the GC amine groups occurs and that the hydrodynamic diameter decreases. Indeed, after 1 h of incubation, the mean NP size in the group with a targeted size of 200 nm decreased from 240.2 ± 1.5 to 175.8 ± 1.5 nm, whereas it decreased from 306 ± 8.8 to 226.5 ± 6.7 nm and 502.4 ± 4.2 to 329.1 ± 7.9 nm in the case of the groups with a targeted size of 300 and 500 nm, respectively. The disassociation of amine functional groups was confirmed by a remarkable reduction in ζ -potential from \sim 30–40 (mV) to \sim 10–20 (mV) in all studied samples and predetermined time points. Moreover, the stability of all samples at pH 7.4 could be demonstrated with reasonable PDI values (<0.3) (Figure 4) despite the aggregating behavior observed if NPs were prepared at neutral pH (Table S1). The stability of FGC NPs of different size ranges over a broad range of pH values clearly indicates flexibility in the potential pharmaceutical application of such a particulate system. This drug delivery platform could be considered for use in pulmonary delivery, where the local pH is nearly neutral,⁵⁸ for gastrointestinal or vaginal delivery,^{53,59,60} where a lower pH environment is encountered, as well as for other applications.

The use of chitosan derivatives and the assemblies thereof as drug delivery systems might be restricted by their tendency to precipitate at neutral pH (7–7.4). Furthermore, certain toxicity, resulting from the use of acidic pH conditions in which NPs show stability, could be expected if such an NP suspension would be applied in vivo. One of the solutions is to dilute the carrier systems into a physiological pH environment (7–7.4), which is however not favorable for chitosan-based nanocarriers due to its fast precipitation within hours or a few days.^{30,41} Although all FGC NP samples incubated in HBSS buffer for 24 h were confirmed to be stable, we further kept them at 4 °C and later characterized them to investigate the stability for a longer period of time, up to 30 days. As presented in Figure S5, despite some small recorded changes, the FGC NPs remained stable in HBSS buffer over 30 days of investigation. The good stability of the prepared carrier system might be explained not only by the good solubility of GC at neutral pH, which was highly maintained due to a relatively low hydrophobic modifying degree, but also by the spectacular self-assembly of sesquiterpenyl-derivative farnesyl moieties.

Cell Viability: MTT Assay. The biocompatibility of the FGC-based drug delivery platform was studied via MTT assay. We determined cell viability after incubating A549 cells with FGC NPs for 4 h. The FGC NPs showed cytotoxicity at relatively large NP concentration. At $750 \mu\text{g/mL}$, cell viability was lower than 50%. Nevertheless, FGC NPs appeared as a safe system for use at concentrations up to $250 \mu\text{g/mL}$ with cell viability over 75% (Figure 5).

Loading Capacity of FGC NPs and Release Study. The drug loading capacity of the newly prepared NPs was explored by loading different model compounds to the system. Nile red and CholEsteryl BODIPY were selected as model hydrophobic molecules with different molecular weights (318.36 and 786.98

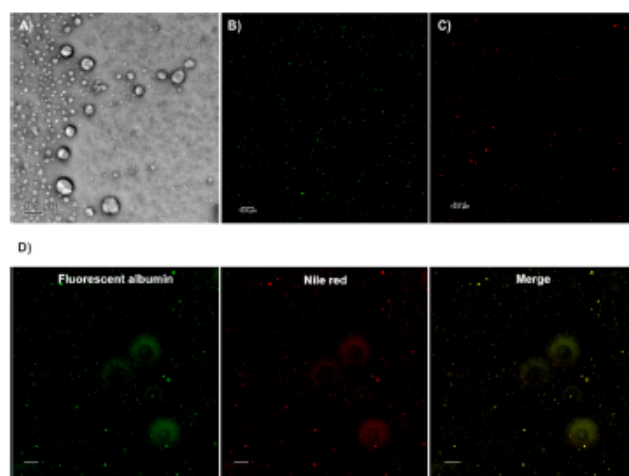


Figure 3. TEM image (A) of FGC NPs 300 nm (obtained from the self-assembly of FGC-11%, pH 5, 0.5 mg/mL), scale bar = 0.2 μm . (B–D) CLSM images of (B) CholEsteryl BODIPY-loaded FGC NPs, (C) Nile red-loaded FGC NPs, and (D) fluorescent albumin and Nile red coloaded-FGC NPs; scale bar = 10 μm (all loaded FGC NPs were obtained from the self-assembly of FGC-11%, pH 5, 0.5 mg/mL).

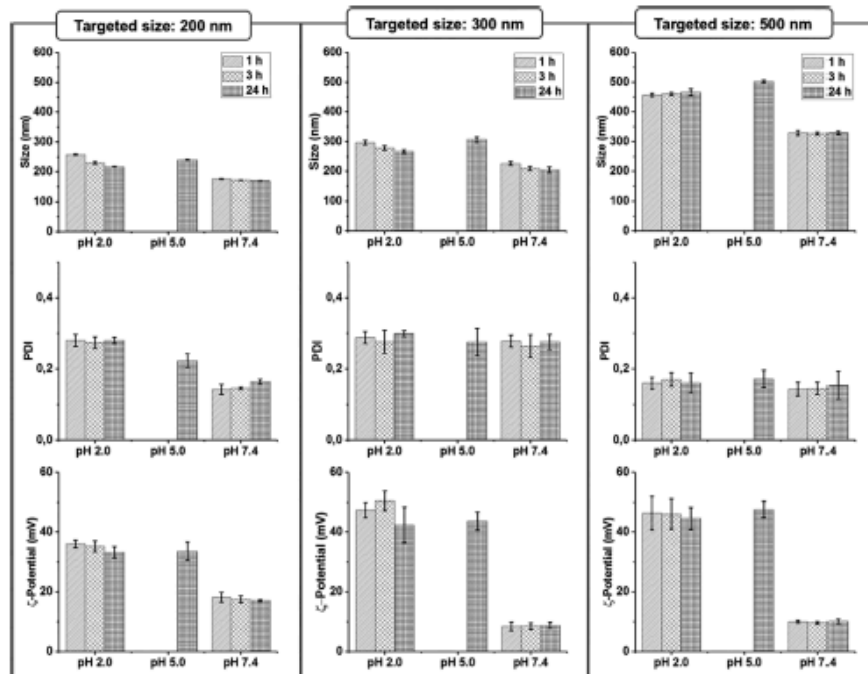


Figure 4. Characteristics of different targeted size (200, 300, and 500 nm obtained from the self-assembly of FGC-11%, 0.5 mg/mL; FGC-11%, 1 mg/mL; and FGC-16%, 1 mg/mL; respectively, at pH 5) FGC NPs after 1, 3, and 24 h incubation in pH conditions ranging from 2 to 7.4 at room temperature. The initial pH value of the samples was 5, which was used throughout the stability test. $n = 3$, mean \pm SD.

Da for Nile red and CholEsteryl BODIPY, respectively). The two compounds are not water-soluble; thus, they were expected to be localized in the core of the self-assembled

NPs during the assembly of farnesyl moieties upon removing ethanol from the solution. The NPs loaded with the fluorescent model compounds were readily detected using

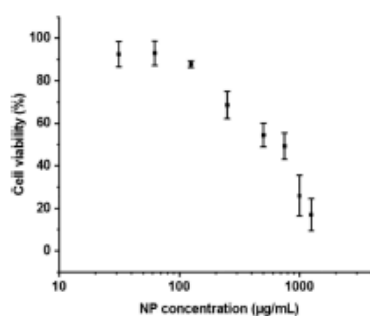


Figure 5. MTT assay: FGC NPs (300 nm, obtained from the self-assembly of FGC-16%, at pH 5, 0.5 mg/mL) were incubated with A549 for 4 h. All measurements were conducted in triplicate. $n = 3$, mean \pm SD.

CLSM (Figure 3B and C) which proves the localization of the hydrophobic model drugs in the lipid core of the FGC NPs, as both Nile red and CholEsteryl BODIPY analogues are known to become strongly fluorescent only in a lipophilic environment.⁶¹ The EE% and LC% of the NPs were investigated and optimized using various initial feeding amounts of Nile red or CholEsteryl BODIPY. The loading strategy results in good EE% with maximum mean values of $81.87 \pm 7.37\%$ and $85.21 \pm 5.55\%$ when loading Nile red or CholEsteryl BODIPY, respectively (Table 2 and Table S2). Despite a higher M_w , the highest LC% was $7.85 \pm 0.47\%$ in the case of loading CholEsteryl BODIPY, and the maximum loading capacity of Nile red was achieved at $5.35 \pm 0.41\%$. This tendency can be explained by the higher hydrophobicity of CholEsteryl BODIPY molecule ($\log P$ of 16.5 for CholEsteryl BODIPY, estimated by Chemdraw 17.0, PerkinElmer, USA; vs $\log P$ of 5 for Nile red).⁶² CholEsteryl BODIPY could thus be better encapsulated in the NP core, which might also serve to explain the slower release profile of CholEsteryl BODIPY compared to that of Nile red (Figure 6).

As the poorly water-soluble compounds were integrated with the farnesyl moieties, the particle size was slightly increased (Table S2). The characteristics of the loaded NPs otherwise remained stable, enabling further application in the study.

Fluorescent albumin was used as a model macromolecule to investigate the loading of hydrophilic drugs. The albumin loading was based on the electrostatic interaction between a cationic net charge of FGC NP surface and an anionic net charge of albumin.⁶³ The presence of the fluorescent albumin on the surface of NPs was confirmed by a marked decrease of the ζ -potential from 33.6 ± 3.0 (mV) of albumin-free NPs to 17.1 ± 0.3 (mV) of the loaded ones. The optimal fluorescent albumin-loaded NPs yielded an EE% of $85.21 \pm 13.31\%$ and an LC% of $4.08 \pm 0.61\%$ for the carrier system ranging

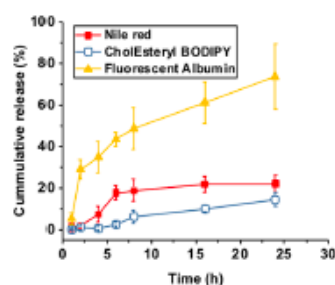


Figure 6. Cumulative release of Nile red, CholEsteryl BODIPY, and fluorescent albumin from FGC NPs. Experiments were performed in PBS at 37°C ; $n = 3$, mean \pm SD.

between 200 and 300 nm. The release of the hydrophilic protein was much faster compared to that of the hydrophobic model compound. The burst release of fluorescent albumin ($\sim 40\%$) was obtained after 4 h incubation, which kept increasing over 24 h (Figure 6).

The fluorescent albumin and Nile red-co-loaded FGC NPs were also obtained by further loading fluorescent albumin on the surface Nile red-loaded FGC NPs (LC% of $0.90 \pm 0.05\%$). The colocalization of the two fluorescent dyes in the FGC NPs was confirmed by CLSM images (Figure 3D).

The prepared FGC NPs could thus be considered a versatile platform for drug delivery.

FGC NP Surface Modification. Surface functionalization of the carrier systems would render them attractive for future *in vivo* application. Therefore, we performed a simple NP surface modifying step using a model fluorescent compound, NBD-Cl, which is known to be reactive toward primary amine (synthetic scheme is shown in Scheme S1). Interestingly, NBD-amines, the resulting conjugating products, are known to have strong fluorescent intensity, whereas the free NBD-Cl would not be sensitive enough.^{31,64} As a result, the NBD surface-modified FGC NPs would be observed by fluorescent microscopy (as shown in Scheme S1). Although the proposed model reaction was simple, our study shows that the FGC NPs are surface-modifiable while the stability of colloidal system could be still maintained for the aim of drug delivery. The more specific moieties selected for surface functionalization would be studied to aim for a particular application, which, however, falls beyond the scope of the present work.

FGC NP–Mucus Interactions. The epithelia of most noninvasive drug delivery routes, e.g., the whole gastrointestinal tract, vaginal tract, and airways, are covered with a protective mucus layer.³² Therefore, if FGC NPs are intended for mucosal drug delivery, they need to comply with the requirements of this barrier. The main organic component of mucus, mucin glycoproteins,⁶⁵ form a covalently linked, three-

Table 2. Summary of Characteristics of Model Molecule-Loaded FGC NPs and Representatives of Encapsulation Efficacy and Loading Capacity^a

loading compound	size (nm)	PDI	ζ -potential (mV)	EE (%)	LC (%)
Nile red	285.2 ± 5.5	0.32 ± 0.03	25.3 ± 2.0	56.55 ± 4.52	5.35 ± 0.41
CholEsteryl BODIPY	260.3 ± 4.0	0.28 ± 0.01	35.4 ± 1.8	85.21 ± 5.55	7.85 ± 0.47
fluorescent albumin	260.3 ± 4.0	0.27 ± 0.01	17.1 ± 0.3	85.21 ± 13.31	4.08 ± 0

^aAll measurements were conducted in triplicate; $n = 3$, mean \pm SD.

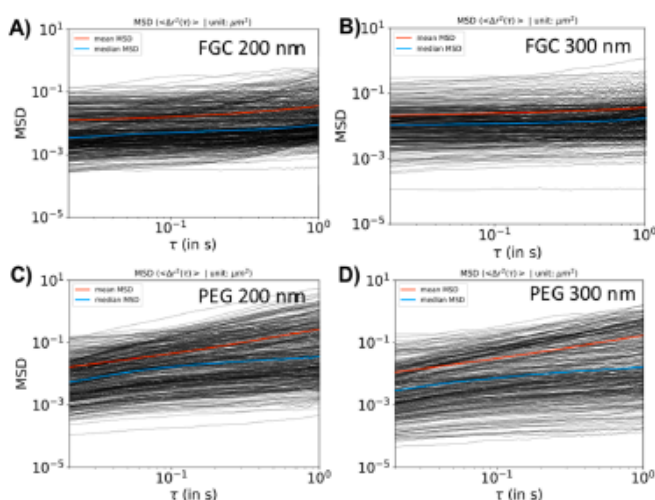


Figure 7. Mean squared displacement (MSD) of farnesylated glycol chitosan (FGC) particles: (A) FGC 200 and (B) FGC 300 nm and polyethylene glycol-coated polystyrene (PEG) particles (C) PEG 200 and (D) PEG 300 nm in undiluted human tracheal mucus. The mean and median of all individual particles are indicated by red and blue lines, respectively; $n = 12$, from three independent mucus samples.

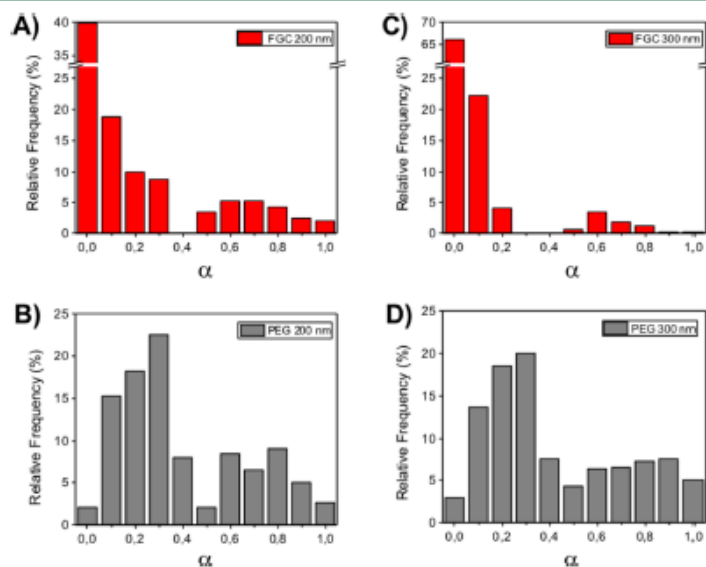


Figure 8. Histograms depicting the distribution of the slopes (α) of the MSDs (time scale τ interval 0.02–1 s) of farnesylated glycol chitosan (FGC) particles: (A) FGC 200 and (C) FGC 300 nm and polyethylene glycol-coated polystyrene (PEG) particles (B) PEG 200 and (D) PEG 300 nm. Shown are the relative frequencies of $n = 12$ experiments from 3 independent undiluted human tracheal mucus samples.

dimensional network of a strict pore size (<500 nm) with ubiquitous sites for hydrophobic interactions and net negative charge at neutral pH.³² Two main strategies are used to improve the therapeutic effect of drug delivery systems in mucosal drug delivery: muco-adhesion and muco-penetration. The former exploits the natural characteristics of mucus and intentionally seeks the interaction between drug delivery

systems and mucus components to prolong the retention time of drugs within mucosal tissues;⁶⁶ conversely, the latter aims at avoiding interactions with mucus components to cross the mucus layer and reach further cellular targets.⁶⁷ Chitosan derivatives are well-known muco-adhesive polymers;⁶⁸ however, one could speculate that their chemical modification could modify their muco-adhesive properties as well.⁶⁹ In

particular, glycol functionalization of chitosan could decrease the adhesiveness of the polymer to mucus.⁶⁹ Hence, we mechanically dispersed FGC NPs in human tracheal mucus and analyzed their behavior by means of particle tracking. Further, we compared the obtained results to those achieved with NPs coated with a dense layer of PEG, a surface modification that renders NPs muco-penetrating.^{54,70} During video microscopy, FGC NPs appeared aggregated and rather immobile. Irrespective of the size, the MSD plots of FGC NPs show a constant mean MSD as a function of τ , indicating that FGC NPs are strongly immobilized by the mucus gel (Figure 7A and B). PEGylated NPs, on the contrary, showed a mean increasing MSD as a function of τ indicative of increased diffusion compared to FGC NPs (Figure 7C and D).

Figure 8 depicts the distribution of the slopes (α) of all MSD curves for FGC and PEGylated NPs. We applied an arbitrary cutoff for the α value classifying particles with $\alpha > 0.5$ as diffusive and particles with $\alpha < 0.5$ as immobile.⁵¹ All plots show bimodal distributions, which can be explained by the inhomogeneous microstructure of mucus. In particular, the analysis of noninteracting PEG-coated particles indicates the existence of areas of different mucin cross-linking intensities with a significant fraction of the analyzed mucus area having a pore size < 200 nm.

According to the α value classification, 76 and 90% of the FGC NPs with sizes of 200 and 300 nm, respectively, were immobilized by human mucus, indicating a slight NP size dependency in terms of diffusion (Table 3). Such a rate of

Table 3. Slopes (α Value) of the Mean MSD Values, Water/Mucus Effective Diffusion (D_{eff}) Ratios, and Percentages of NPs in an Elastic Environment for Each Particle Type^a

particles	mean α value	$D_{\text{eff(water)}}/D_{\text{eff(mucus)}}$	% NP elastic
FGC 200 nm	0.29	356	76.2
FGC 300 nm	0.15	267	89.9
FGC 200 nm	0.48	47	63.0
FGC 300 nm	0.45	56	67.2

^a $n = 12$ experiments from three independent mucus samples; the theoretical diffusion of particles in water ($D_{\text{eff(water)}}$) was calculated with the Stokes–Einstein equation.

immobile particles was hypothesized due not only to the positive charge of the NPs but also to the hydrophobic character of the NP core, which may promote NP adsorption to nonglycosylated domains of mucin glycoproteins.^{34,51}

PEGylation improved the diffusion of particles through native mucus as shown by the higher effective diffusion in mucus of PEGylated NPs compared to FGC NPs (Table 3). Interestingly, PEG functionalization could eventually be implemented in FGC NPs by coupling PEG to the available surface amine functional groups, which will be explored in future studies for serving other specific applications.

4. CONCLUSIONS

We report a facile synthesis method to produce a new amphiphilic glycol chitosan derivative, FGC, which could spontaneously self-assemble into NPs in an aqueous medium. The changes of DoF as well as NP-forming conditions, including pH and NPs concentration, were applied to tune the FGC NPs characteristics. The FGC compounds with DoF of 11 and 16% were able to form stable and uniform FGC NPs with tunable hydrodynamic diameters in the range of 200–500

nm. This drug delivery platform can carry hydrophobic compounds in the lipophilic NP core as well as hydrophilic drugs on the NP shell, even allowing for surface modification of the NPs. We investigated the biocompatibility of FGC-based NPs with A549 cells, and we could demonstrate the stability of the NPs over a wide range of physiologically relevant pH values (range 2–7.4) as well as their suitability for long-term storage. Without further surface modification, the newly established, positively charged NPs had a strong interaction with mucus compared to that of PEGylated NPs. Thus, with the appropriate surface characteristics, FGC NPs could be nominated as versatile drug delivery systems in various mucosal pathways, e.g., pulmonary, oral, or vaginal delivery.

■ ASSOCIATED CONTENT

Supporting Information

The Supporting Information is available free of charge on the ACS Publications website at DOI: 10.1021/acs.biomac.8b00795.

Cell culture, PEGylated polystyrene nanoparticle preparation, ¹H NMR spectrum of glycol chitosan and degree of deacetylation analysis, ¹H NMR spectrum of famesal, representative ¹H NMR of FGC 4.5:1, summary of NP characteristics obtained from the assembly of different FGC compounds (FGC 12:1, FGC 6:1, and FGC 4.5:1) at different pH values (5 and 7) and different NP-targeted concentrations ranging from 0.25 to 1 mg/mL, summary of FGC NP characteristics in three targeted size groups (200, 300, and 500 nm) after 30 days of storage at 4 °C, summary of FGC NP characteristics in three targeted size groups (200, 300, and 500 nm) after 30 days after incubation in HBSS at room temperature for 24 h and further kept at 4 °C, surface modification of FGC NPs with a model compound, NBD-Cl, in aqueous solution and the fluorescent microscopy image of FGC NPs ~ 200 nm (dispersed in Milli-Q at 50 μ g/mL concentration), confirming successful fluorescent surface modification of FGC NPs, summary of characteristics of model molecule-loaded FGC NPs, encapsulation efficacy, and loading capacity, and summary of FGC and PEGylated PS NP characteristics, which were used for multiple particle tracking (PDF)

■ AUTHOR INFORMATION

Corresponding Author

*E-mail: Xabier.MurgiaEsteve@helmholtz-hzi.de.

ORCID

Brigitta Loretz: 0000-0003-0057-5181

Xabier Murgia: 0000-0002-9760-3240

Funding

This project has received funding from the European Union's Framework Programme for Research and Innovation Horizon 2020 (2014–2020) under the Marie Skłodowska-Curie Grant Agreement No. 642028

Notes

The authors declare no competing financial interest.

■ ACKNOWLEDGMENTS

The authors thank Petra König and Jana Westhues for support and handling of cell cultures.

■ ABBREVIATIONS

GC, glycol chitosan; FGC, farnesylated glycol chitosan; DoF, degree of farnesylation; NPs, nanoparticles; EE%, encapsulation efficacy; LC%, loading capacity; MSD, mean squared displacement; CLSM, confocal laser scanning microscopy; PS NPs, polystyrene nanoparticles; PEG, polyethylene glycol; FGC 200 nm, Nile red labeled-farnesylated glycol chitosan nanoparticles size 200 nm; FGC 300 nm, Nile red labeled-farnesylated glycol chitosan nanoparticles size 300 nm; PEG 200 nm, fluorescently labeled-PEGylated polystyrene nanoparticles 200 nm; PEG 300 nm, fluorescently labeled-PEGylated polystyrene nanoparticles 300 nm.

■ REFERENCES

- (1) Stella, V. J.; Nti-Addae, K. W. Prodrug Strategies to Overcome Poor Water Solubility. *Adv. Drug Delivery Rev.* 2007, 59 (7), 677–694.
- (2) Stegemann, S.; Leveillé, F.; Franchi, D.; de Jong, H.; Lindén, H. When Poor Solubility Becomes an Issue: From Early Stage to Proof of Concept. *Eur. J. Pharm. Sci.* 2007, 31 (5), 249–261.
- (3) Savjani, K. T.; Gajjar, A. K.; Savjani, J. K. Drug Solubility: Importance and Enhancement Techniques. *ISRN Pharm.* 2012, 2012, 1–10.
- (4) Almeida, A. J.; Souto, E. Solid Lipid Nanoparticles as a Drug Delivery System for Peptides and Proteins. *Adv. Drug Delivery Rev.* 2007, 59 (6), 478–490.
- (5) De Jong, W. H.; Borm, P. J. a. Drug Delivery and Nanoparticles: Applications and Hazards. *Int. J. Nanomed.* 2008, 3 (2), 133–149.
- (6) Markman, J. L.; Rekechenetskiy, A.; Holler, E.; Ljubimova, J. Y. Nanomedicine Therapeutic Approaches to Overcome Cancer Drug Resistance. *Adv. Drug Delivery Rev.* 2013, 65 (13–14), 1866–1879.
- (7) Zhu, X.; Radovic-Moreno, A. F.; Wu, J.; Langer, R.; Shi, J. Nanomedicine in the Management of Microbial Infection - Overview and Perspectives. *Nano Today* 2014, 9 (4), 479–498.
- (8) Pelaz, B.; Alexiou, C.; Alvarez-Puebla, R. A.; Alves, F.; Andrews, A. M.; Ashraf, S.; Balogh, L. P.; Ballerini, L.; Bestetti, A.; Brendel, C.; et al. Diverse Applications of Nanomedicine. *ACS Nano* 2017, 11 (3), 2313–2381.
- (9) Abed, N.; Couvreur, P. Nanocarriers for Antibiotics: A Promising Solution to Treat Intracellular Bacterial Infections. *Int. J. Antimicrob. Agents* 2014, 43 (6), 485–496.
- (10) Hu, C.-M. J.; Aryal, S.; Zhang, L. Nanoparticle-Assisted Combination Therapies for Effective Cancer Treatment. *Ther. Delivery* 2010, 1 (2), 323–334.
- (11) Cheng, Y.; Moshed, R. A.; Auffinger, B.; Tobias, A. L.; Lesniak, M. S. Multifunctional Nanoparticles for Brain Tumor Imaging and Therapy. *Adv. Drug Delivery Rev.* 2014, 66, 42–57.
- (12) Sau, S.; Alsaab, H. O.; Bhise, K.; Alzhrani, R.; Nabil, G.; Iyer, A. K. Multifunctional Nanoparticles for Cancer Immunotherapy: A Groundbreaking Approach for Reprogramming Malfunctioned Tumor Environment. *J. Controlled Release* 2018, 274, 24–34.
- (13) Torchilin, V. P. Multifunctional, Stimuli-Sensitive Nanoparticulate Systems for Drug Delivery. *Nat. Rev. Drug Discovery* 2014, 13, 813–827.
- (14) Gao, W.; Thamphiwatana, S.; Angsantikul, P.; Zhang, L. Nanoparticle Approaches against Bacterial Infections. *Wiley Interdiscip. Rev. Nanomed. Nanobiotechnol* 2014, 6 (6), 532–547.
- (15) Masood, F. Polymeric Nanoparticles for Targeted Drug Delivery System for Cancer Therapy. *Mater. Sci. Eng., C* 2016, 60, 569–578.
- (16) Perez, R. A.; Kim, H. W. Core-Shell Designed Scaffolds for Drug Delivery and Tissue Engineering. *Acta Biomater.* 2015, 21, 2–19.
- (17) Pathak, Y.; Thassu, D. *Drug Delivery Nanoparticles Formulation and Characterization*, 2009; Vol. 191.
- (18) Chatterjee, K.; Sarkar, S.; Jagajani Rao, K.; Paria, S. Core/Shell Nanoparticles in Biomedical Applications. *Adv. Colloid Interface Sci* 2014, 209, 8–39.
- (19) Wei, S.; Wang, Q.; Zhu, J.; Sun, L.; Lin, H.; Guo, Z. Multifunctional Composite Core-Shell Nanoparticles. *Nanoscale* 2011, 3 (11), 4474.
- (20) Liu, Q.; Boyd, B. J. Liposomes in Biosensors. *Analyst* 2013, 138 (2), 391–409.
- (21) Xing, P.; Zhao, Y. Multifunctional Nanoparticles Self-Assembled from Small Organic Building Blocks for Biomedicine. *Adv. Mater.* 2016, 28, 7304–7339.
- (22) Soppimath, K. S.; Tan, D. C. W.; Yang, Y. Y. PH-Triggered Thermally Responsive Polymer Core-Shell Nanoparticles for Drug Delivery. *Adv. Mater.* 2005, 17 (3), 318–323.
- (23) Lee, S. J.; Min, H. S.; Ku, S. H.; Son, S.; Kwon, I. C.; Kim, S. H.; Kim, K. Tumor-Targeting Glycol Chitosan Nanoparticles as a Platform Delivery Carrier in Cancer Diagnosis and Therapy. *Nanomaterials* 2014, 9 (11), 1697–1713.
- (24) Zhang, L.; Chan, J. M.; Gu, F. X.; Rhee, J. W.; Wang, A. Z.; Radovic-Moreno, A. F.; Alexis, F.; Langer, R.; Farokhzad, O. C. Self-Assembled Lipid-Polymer Hybrid Nanoparticles: A Robust Drug Delivery Platform. *ACS Nano* 2008, 2 (8), 1696–1702.
- (25) Wang, Y.; Gao, S.; Ye, W. H.; Yoon, H. S.; Yang, Y. Y. Co-Delivery of Drugs and DNA from Cationic Core-Shell Nanoparticles Self-Assembled from a Biodegradable Copolymer. *Nat. Mater.* 2006, 5 (10), 791–796.
- (26) Aspden, T. J.; Mason, J. D. T.; Jones, N. S.; Lowe, J.; Skaugrud, Ø.; Illum, L. Chitosan as a Nasal Delivery System: The Effect of Chitosan Solutions on in Vitro and in Vivo Mucociliary Transport Rates in Human Turbinates and Volunteers. *J. Pharm. Sci.* 1997, 86, 509–513.
- (27) Bernkop-Schnürch, A.; Dünhaupt, S. Chitosan-Based Drug Delivery Systems. *Eur. J. Pharm. Biopharm.* 2012, 81 (3), 463–469.
- (28) Dodane, V.; Vilivalam, V. D. Pharmaceutical Applications of Chitosan. *Pharm. Sci. Technol Today* 1998, 1 (6), 246–253.
- (29) Liu, Z.; Jiao, Y.; Wang, Y.; Zhou, C.; Zhang, Z. Polysaccharides-Based Nanoparticles as Drug Delivery Systems. *Adv. Drug Delivery Rev.* 2008, 60 (15), 1650–1662.
- (30) Yasar, H.; Ho, D. K.; De Rossi, C.; Hermann, J.; Gordon, S.; Loretz, B.; Lehr, C. M. Starch-Chitosan Polyplexes: A Versatile Carrier System for Anti-Infectives and Gene Delivery. *Polymers* 2018, 10 (3), 252.
- (31) Ho, D. K.; Costa, A.; De Rossi, C.; De Souza Carvalho-Wodarz, C.; Loretz, B.; Lehr, C. M. Polysaccharide Submicrocarrier for Improved Pulmonary Delivery of Poorly Soluble Anti-Infective Ciprofloxacin: Preparation, Characterization, and Influence of Size on Cellular Uptake. *Mol. Pharmaceutics* 2018, 15 (3), 1081–1096.
- (32) Murgia, X.; Loretz, B.; Hartwig, O.; Hittinger, M.; Lehr, C.-M. The Role of Mucus on Drug Transport and Its Potential to Affect Therapeutic Outcomes. *Adv. Drug Delivery Rev.* 2018, 124, 82–97.
- (33) Caramella, C. M.; Rossi, S.; Ferrari, F.; Bonferoni, M. C.; Sandri, G. Mucoadhesive and Thermogelling Systems for Vaginal Drug Delivery. *Adv. Drug Delivery Rev.* 2015, 92, 39–52.
- (34) Schuster, B. S.; Suk, J. S.; Woodworth, G. F.; Hanes, J. Nanoparticle Diffusion in Respiratory Mucus from Humans without Lung Disease. *Biomaterials* 2013, 34 (13), 3439–3446.
- (35) Murgia, X.; Yasar, H.; Carvalho-Wodarz, C.; Loretz, B.; Gordon, S.; Schwanzkopf, K.; Schaefer, U.; Lehr, C.-M. Modelling the Bronchial Barrier in Pulmonary Drug Delivery: A Human Bronchial Epithelial Cell Line Supplemented with Human Tracheal Mucus. *Eur. J. Pharm. Biopharm.* 2017, 118, 79–88.
- (36) de la Fuente, M.; Raviña, M.; Paolicelli, P.; Sanchez, A.; Seijo, B.; Alonso, M. J. Chitosan-Based Nanostructures: A Delivery Platform for Ocular Therapeutics. *Adv. Drug Delivery Rev.* 2010, 62 (1), 100–117.
- (37) Yoon, H. Y.; Son, S.; Lee, S. J.; You, D. G.; Yhee, J. Y.; Park, J. H.; Swierczewska, M.; Lee, S.; Kwon, I. C.; Kim, S. H.; Kim, K.; Pomper, M. G. Glycol Chitosan Nanoparticles as Specialized Cancer

- Therapeutic Vehicles: Sequential Delivery of Doxorubicin and Bcl-2 siRNA. *Sci. Rep.* 2015, 4, 1.
- (38) Kim, J. H.; Kim, Y. S.; Park, K.; Kang, E.; Lee, S.; Nam, H. Y.; Kim, K.; Park, J. H.; Chi, D. Y.; Park, R. W.; et al. Self-Assembled Glycol Chitosan Nanoparticles for the Sustained and Prolonged Delivery of Antiangiogenic Small Peptide Drugs in Cancer Therapy. *Biomaterials* 2008, 29 (12), 1920–1930.
- (39) Pereira, P.; Morgado, D.; Crepet, A.; David, L.; Gama, F. M. Glycol Chitosan-Based Nanogel as a Potential Targetable Carrier for siRNA. *Macromol. Biosci.* 2013, 13 (10), 1369–1378.
- (40) Kwon, S.; Park, J. H.; Chung, H.; Kwon, I. C.; Jeong, S. Y.; Kim, I. S. Physicochemical Characteristics of Self-Assembled Nanoparticles Based on Glycol Chitosan Bearing 5 β -Cholanolic Acid. *Langmuir* 2003, 19 (24), 10188–10193.
- (41) Kim, K.; Kwon, S.; Park, J. H.; Chung, H.; Jeong, S. Y.; Kwon, I. C.; Kim, I. S. Physicochemical Characterizations of Self-Assembled Nanoparticles of Glycol Chitosan-Deoxycholic Acid Conjugates. *Biomacromolecules* 2005, 6 (2), 1154–1158.
- (42) Kim, Y. H.; Gihm, S. H.; Park, C. R.; Lee, K. Y.; Kim, T. W.; Kwon, I. C.; Chung, H.; Jeong, S. Y. Structural Characteristics of Size-Controlled Self-Aggregates of Deoxycholic Acid-Modified Chitosan and Their Application as a DNA Delivery Carrier. *Bioconjugate Chem.* 2001, 12 (6), 932–938.
- (43) Yuan, W.; Zhao, Z.; Gu, S.; Ren, J. Synthesis, Characterization, and Properties of Amphiphilic Chitosan Copolymers with Mixed Side Chains by Click Chemistry. *J. Polym. Sci., Part A: Polym. Chem.* 2010, 48 (15), 3476–3486.
- (44) Yuan, W.; Li, X.; Gu, S.; Cao, A.; Ren, J. Amphiphilic Chitosan Graft Copolymer via Combination of ROP, ATRP and Click Chemistry: Synthesis, Self-Assembly, Thermosensitivity, Fluorescence, and Controlled Drug Release. *Polymer* 2011, 52 (3), 658–666.
- (45) Wang, J. J.; Zeng, Z. W.; Xiao, R. Z.; Xie, T.; Zhou, G. L.; Zhan, X. R.; Wang, S. L. Recent Advances of Chitosan Nanoparticles as Drug Carriers. *Int. J. Nanomed.* 2011, 6, 765–774.
- (46) Arias, J. L.; Reddy, L. H.; Othman, M.; Gillet, B.; Desmaële, D.; Zouhiri, F.; Dosio, F.; Gref, R.; Couvreur, P. Squalene Based Nanocomposites: A New Platform for the Design of Multifunctional Pharmaceutical Therapeutics. *ACS Nano* 2011, 5 (2), 1513–1521.
- (47) Reddy, L. H.; Couvreur, P. Squalene: A Natural Triterpene for Use in Disease Management and Therapy. *Adv. Drug Delivery Rev.* 2009, 61 (15), 1412–1426.
- (48) Lepeltier, E.; Loretz, B.; Desmaële, D.; Zapp, J.; Herrmann, J.; Couvreur, P.; Lehr, C. M. Squalenoylation of Chitosan: A Platform for Drug Delivery? *Biomacromolecules* 2015, 16 (9), 2930–2939.
- (49) Vukosavljević, B.; Murgia, X.; Schwarzkopf, K.; Schaefer, U. F.; Lehr, C.-M.; Windbergs, M. Tracing Molecular and Structural Changes upon Mucolysis with N-Acetyl Cysteine in Human Airway Mucus. *Int. J. Pharm.* 2017, 533 (2), 373–376.
- (50) Sbalzarini, I. F.; Koumoutsakos, P. Feature Point Tracking and Trajectory Analysis for Video Imaging in Cell Biology. *J. Struct. Biol.* 2005, 151 (2), 182–195.
- (51) Murgia, X.; Pawelczyk, P.; Schaefer, U. F.; Wagner, C.; Willenbacher, N.; Lehr, C.-M. Size-Limited Penetration of Nanoparticles into Porcine Respiratory Mucus after Aerosol Deposition. *Biomacromolecules* 2016, 17 (4), 1536–1542.
- (52) Rijcken, C. J. F.; Soga, O.; Hennink, W. E.; Nostrum, C. F. v. Triggered Destabilisation of Polymeric Micelles and Vesicles by Changing Polymers Polarity: An Attractive Tool for Drug Delivery. *J. Controlled Release* 2007, 120 (3), 131–148.
- (53) Abed, N.; Saïd-Hassane, F.; Zouhiri, F.; Mougin, J.; Nicolas, V.; Desmaële, D.; Gref, R.; Couvreur, P. An Efficient System for Intracellular Delivery of Beta-Lactam Antibiotics to Overcome Bacterial Resistance. *Sci. Rep.* 2015, 5, 1.
- (54) Philippova, O. E.; Korchagina, E. V. Chitosan and Its Hydrophobic Derivatives: Preparation and Aggregation in Dilute Aqueous Solutions. *Polym. Sci., Ser. A* 2012, 54 (7), 552–572.
- (55) Riva, R.; Ragelle, H.; Des Rieux, A.; Duhem, N.; Jérôme, C.; Pr at, V. Chitosan and Chitosan Derivatives in Drug Delivery and Tissue Engineering. *Adv. Polym. Sci.* 2011, 244, 19–44.
- (56) Akagi, T.; Baba, M.; Akashi, M. Preparation of Nanoparticles by the Self-Organization of Polymers Consisting of Hydrophobic and Hydrophilic Segments: Potential Applications. *Polymer* 2007, 48 (23), 6729–6747.
- (57) Zhang, C.; Ding, Y.; Ping, Q.; Yu, L. Novel Chitosan-Derived Nanomaterials and Their Micelle-Forming Properties. *J. Agric. Food Chem.* 2006, 54 (22), 8409–8416.
- (58) Mura, S.; Hillaireau, H.; Nicolas, J.; Kerdine-R omer, S.; Le Droumaguet, B.; Delom enie, C.; Nicolas, V.; Pallardy, M.; Tsapis, N.; Fattal, E. Biodegradable Nanoparticles Meet the Bronchial Airway Barrier: How Surface Properties Affect Their Interaction with Mucus and Epithelial Cells. *Biomacromolecules* 2011, 12 (11), 4136–4143.
- (59) Evans, D. F.; Pye, G.; Bramley, R.; Clark, A. G.; Dyson, T. J.; Hardcastle, J. D. Measurement of Gastrointestinal pH Profiles in Normal Ambulant Human Subjects. *Gut* 1988, 29 (8), 1035–1041.
- (60) Ensign, L. M.; Cone, R.; Hanes, J. Nanoparticle-Based Drug Delivery to the Vagina: A Review. *J. Controlled Release* 2014, 190, 500–514.
- (61) Greenspan, P.; Mayer, E. P.; Fowler, S. D. Nile Red: A Selective Fluorescent Stain for Intracellular Lipid Droplets. *J. Cell Biol.* 1985, 100 (3), 965–973.
- (62) Wang, J. D.; Douville, N. J.; Takayama, S.; Elsayed, M. Quantitative Analysis of Molecular Absorption into PDMS Microfluidic Channels. *Ann. Biomed. Eng.* 2012, 40 (9), 1862–1873.
- (63) Baler, K.; Martin, O. A.; Carignano, M. A.; Ameer, G. A.; Vila, J. A.; Szeifer, I. Electrostatic Unfolding and Interactions of Albumin Driven by pH Changes: A Molecular Dynamics Study. *J. Phys. Chem. B* 2014, 118 (4), 921–930.
- (64) Forbes, D. C.; Peppas, N. A. Polymeric Nanocarriers for siRNA Delivery to Murine Macrophages. *Macromol. Biosci* 2014, 14 (8), 1096–1105.
- (65) Thornton, D. J.; Sheehan, J. K. From Mucins to Mucus. *Proc. Am. Thorac. Soc.* 2004, 1 (1), 54–61.
- (66) Shaikh, R.; Raj Singh, T. R.; Garland, M. J.; Woolfson, A. D.; Donnelly, R. F. Mucoadhesive Drug Delivery Systems. *J. Pharm. BioAllied Sci.* 2011, 3 (1), 89–100.
- (67) Huckaby, J. T.; Lai, S. K. PEGylation for Enhancing Nanoparticle Diffusion in Mucus. *Adv. Drug Delivery Rev.* 2018, 124, 125–139.
- (68) Kootala, S.; Filho, L.; Srivastava, V.; Linderberg, V.; Moussa, A.; David, L.; Trombotto, S.; Crouzier, T. Reinforcing Mucus Barrier Properties with Low Molar Mass Chitosans. *Biomacromolecules* 2018, 19 (3), 872–882.
- (69) Trapani, A.; Palazzo, C.; Contino, M.; Perrone, M. G.; Cioffi, N.; Ditaranto, N.; Colabufo, N. A.; Conese, M.; Trapani, G.; Puglisi, G. Mucoadhesive Properties and Interaction with P-Glycoprotein (P-Gp) of Thiolate-d-Chitosans and -Glycol Chitosans and Corresponding Parent Polymers: A Comparative Study. *Biomacromolecules* 2014, 15 (3), 882–893.
- (70) Schneider, C. S.; Xu, Q.; Boylan, N. J.; Chisholm, J.; Tang, B. C.; Schuster, B. S.; Henning, A.; Ensign, L. M.; Lee, E.; Adstamgonkul, P. Nanoparticles That Do Not Adhere to Mucus Provide Uniform and Long-Lasting Drug Delivery to Airways Following Inhalation. *Sci. Adv.* 2017, 3 (4), e1601556.

6.4. PAPER 4: “Squalenyl Hydrogen Sulfate nanoparticles for simultaneous delivery of tobramycin and alkylquinolone quorum sensing inhibitor to combat *P. aeruginosa* biofilm infections”

The data presented in this chapter are subjects of a forthcoming manuscript, authored by Duy-Khiet Ho, Anastasia Andreas, Xabier Murgia, Antonio G. Hübner de Mello Martins, Chiara De Rossi, Marcus Koch, Jennifer Herrmann, Rolf Müller, Martin Empting, Rolf W. Hartmann, Didier Desmaele, Brigitta Loretz, Patrick Couvreur and Claus-Michael Lehr.

Squalenoylation is a unique technology allowing spontaneously self-assembly of drug bioconjugated with just one squalenyl moiety, which at the same time results in a significant high loading capacity, usually higher than 30%, mostly depending on the molecular weight of drug molecule (1). This innovative approach has been widely applied for anticancer drugs, e.g. gemcitabine and doxorubicin, as well as antibiotics, e.g. penicillin G, and shown considerable improvement in efficacy against cancer and intracellular infection (2,3). The technique is, however not successfully employed for other drug molecules having abundant amount and different functional groups, e.g. aminoglycosides antibiotics. Moreover, the overall concept of the squalenoylation is to synthesize the amphiphilic structure of the conjugated drugs which would further assemble into a particulate formulation. The solubility of the resulting compounds thus becomes a severe limitation, especially in common solvents, for the nano-precipitation procedure (4). Consequently, despite the usefulness of such innovative technology, their use has not yet been completely explored. To take advantages of the squalenoylation technology and to further exploit the drug loading capacity of systems based-squalenyl derivatives, I propose here a newly synthesized amphiphilic anionic lipid, squalenyl hydrogen sulfate, which could easily assemble into nano-sized particles in aqueous solution. The self-assembling property of the new compound is much stronger compared to the carboxylic squalenyl derivative due to the high polarity of the hydrogen sulfate functional group. The compound was moreover synthesized and isolated with a high yield, and the synthetic procedure is promising for a large scale production. The synthetic scheme and isolated yield of each step are shown in Figure 1A.

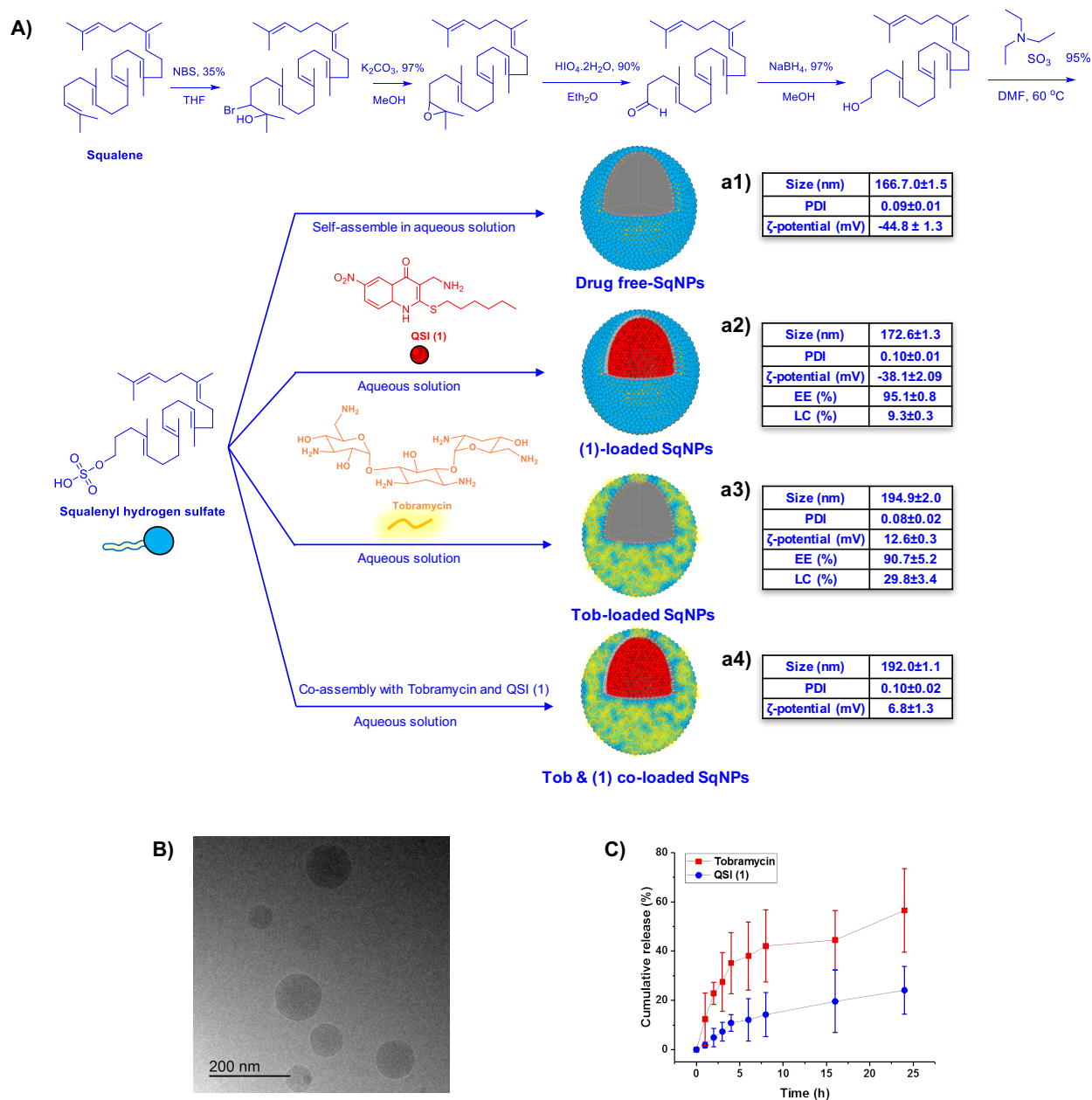


Figure 1. (A) Synthetic scheme of Squalenyl Hydrogen Sulfate (Sq) and the assemblies of Sq into drug-free SqNPs, QSI (1)-loaded SqNPs, Tob-loaded SqNPs and Tob & (1) co-loaded SqNPs; the attached table (a1-a4) indicate the NPs characteristics, encapsulation efficacy (EE%) and loading capacity (LC%). (B) Cryo-TEM image of Tob & (1) co-loaded SqNPs. (C) Cumulative release of Tob and QSI (1) in PBS, at 37 °C. All data are presented as mean \pm SD, at least three independent experiments performed in triplicate each.

The obtained drug-free self-assembled NPs were stable in storage conditions (4 °C) and in biologically relevant medium for more than a month (data not shown), and biocompatible on human cell line A549. The single drug-loaded SqNPs, and drugs co-loaded SqNPs were simply obtained by co-precipitation of the drug molecules and Sq in aqueous media. The procedures are depicted in Figure 1A. Impressively, the drug loading capacity of the system is remarkably higher than the conventional drug delivery systems reported in previous studies (5,6). Particularly, the loading capacity of Tob is at maximum 30%, and the highest loading capacity of QSI (1) is at nearly 10% which are notably higher than the 0.05% loading capacity reported by Nafee et. al. (7). The NPs characteristics are summarized in table (a1-a4) attached in Figure 1A. Morphology of such co-loaded SqNPs was observed by Cryo-TEM and presented in Figure 1B.

The release study of Tob and QSI (1) co-loaded SqNPs was performed in PBS at 37 °C, and the results are depicted in Figure 1C. It is undoubted that the hydrophobic QSI (1) shown a slower release profile as the molecules localized in the core side of NPs, while tobramycin was released faster when being decorated on the outer part of the systems. The release of tobramycin shown burst effect at around 30% which was recorded after 4h incubation. This result proves the strong electrostatic interaction between amine and hydrogen sulfate functional groups in tobramycin and Sq, which is an advantage over the liposomal tobramycin formulation. In addition, the system holds the potential of co-loading high amount of different active compounds, which is a remarkable improvement in comparison to existing nano-formulation systems.

Experts voice that the cell density-dependent cell-to-cell communication system used by PA strains which is referred to as quorum sensing system is for coordinating group behavior such as the production of virulence factors such as pyocyanin, elastase B and hydrogen cyanide (8,9). As a result, the biofilm formation is occurred to protect bacteria from environmental stresses and promoted the resistance development. Within the PA signal quorum sensing system, PqsR (pseudomonas quinolone signal R) is a vital DNA-binding receptor, which in particular means the system is specific to PA and a critical regulator that fine-tunes a set of genes encoding for virulence factors (10–13). Pyocyanin is, in part a generator of reactive oxygen species superoxide and hydrogen peroxide which benefit the bacterial colonization by damaging a variety of host cells and inhibiting the

dual-oxidase based antimicrobial system in the respiratory regions (14,15). Moreover, the pseudomonas quinolone signal also prompts PA to convert to a metabolically less active state in which bacteria are not sensitive to antibiotics. As pseudomonas quinolone signal shows a prominent role in PA biofilm formation, development and resistance, it is thus considered an attractive target for combatting bacterial resistance (16). A highly affine PqsR antagonist, QSI (1) (the structure is shown in Figure 1A), was discovered and synthesized for such purpose. This QSI was determined to strongly inhibit the virulence pyocyanin of PA wt, which as a consequence influences the formation of biofilm (17). The therapeutic effect of such potent compound is restricted by its poor water-solubility. Hence, a drug delivery system would be a solution to improve the availability of the QSI (1) in aqueous solution. Figure 2 compares the production of pyocyanin level (%) after incubating PA14 wt strain with either free QSI (1) or the QSI (1)-loaded SqNPs at different concentrations. As can be seen, the effectiveness in inhibiting pyocyanin production was improved more than three times by loading the compound to SqNPs. This proves the importance of drug availability enhancement in an aqueous-like environment.

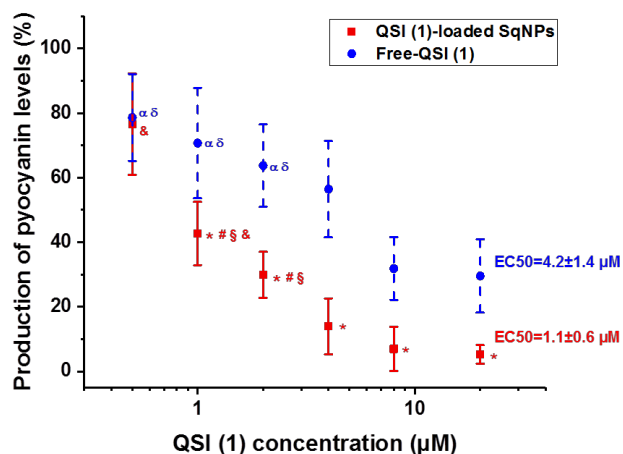


Figure 2. Pyocyanin assay performed on PA14 wt; starting OD600 (0.02), incubation time 16h. The EC50 values of each treatment was calculated by fitting sigmodal curve, OriginPro 2018 (OriginLab Corp., USA). Significant different shows at level * $p < 0.001$ compared with sample treated with 0.5 μM QSI (1), # $p < 0.001$ compared with sample treated with 20 μM ; § $p < 0.001$ compared with sample treated with 8 μM ; & $p < 0.001$ compared with sample treated with 4 μM . The production of pyocyanin level of PA14 wt, and PA14 wt incubated with drug-free SqNPs were also measured and served as controls. The drug-free SqNPs did not show any inhibition to pyocyanin production on PA14 wt at the tested concentrations. PA14 wt bacteria were grown in PPGAS (protease peptone glucose ammonium salt medium which is composed of (1 g/L NH_4Cl ,

1.5 g/L KCl, 19 g/L Tris-HCl, 10 g/L peptone, glucose 5 g/L and 0.1 g/L MgSO₄•7H₂O), the medium was adjusted to pH 7.4, and sterilized before use). All data are presented as mean ±SD, at least three independent experiments performed in triplicate each.

The mucus layer presents in the airway is always the first contact of bacteria once they start colonizing and infecting the host. The pulmonary mucosal barrier would of course be a protecting layer to prevent the first state in colonization of pathogens, clinical studies have however revealed that such barrier becomes a superior environment for bacterial resistance development, in particular PA associated infections in cystic fibrosis patients (18). Hence, I investigated the pyocyanin production level of PA14 wt strain in the presence of mucin, a main component of mucus, and native human tracheal mucus at different concentrations. The results are shown in Figure 3 (A-B). Interestingly, our study pointed out that at the highest tested concentrations of mucin and mucus, pyocyanin production in PA14 wt was inhibited which importantly proves the natural defending function of mucus layer which is in addition to the size- and charge-filtering and mechanisms. On the contrary, when decreasing the concentration of mucin and mucus which meaning increasing the ratio of bacteria availability to mucin and mucus weight, the pyocyanin production was not inhibited but even enhanced significantly, in particular when incubating PA14 wt with mucin 0.25% or mucus 0.05% concentration, the results are depicted in Figure 3 (A-B).

QSI is aimed to inhibit pyocyanin production level, which as a consequence prevents the biofilm formation and rescues the utilities of antibiotics in the treatment of infections. As described in Figure 10 of the “Introduction” section, QSI should be active at all stages of infection so that antibiotic therapeutic efficacy would be enhanced, and biofilm would possibly be eradicated completely. Although both free QSI (1) and QSI (1)-loaded SqNPs performed their pyocyanin inhibiting functions, the presence of mucus or mucin at which concentrations favor the production of pyocyanin would reduce and even inactivate the action of QSI in either form. The pyocyanin assay was carried out to check this hypothesis, all PA14 wt samples grown in either bacterial culture medium (PPGAS), 0.1% mucin in PPGAS, or 0.025% mucus in PPGAS were treated with either 2 μM QSI (1) as free form or loaded in SqNPs. In all these media, the PA14 wt bacteria were also grown without treatment and served as controls. The results are summarized and presented in

Figure 3C. Our hypothesis holds true in cases using free form QSI (1) for treatment, its inhibiting actions were decreased and even not functioned in present of 0.025% mucus and 0.1% mucin, respectively. On the contrary, QSI (1)-loaded SqNPs still shown the similar effects compared to ones observed in the assays performed in the absence of mucus or mucin. Furthermore, at a significantly lower concentration of mucus, the performance of free form QSI was not notably reduced. Thus, the remarkable reduction in therapeutic efficacy observed when applying QSI (1) in the presence of mucin would be explained by the limitation in solubility of the QSI (1) molecules. The argument is quite understandable due to the rather viscous solution resulting from dissolving mucin in PPGAS solution. Moreover, the glycoprotein mucin has heterogeneous properties and holds hydrophobic regions in its structure which would adsorb QSI (1) molecules upon contacting in aqueous solution thank to the hydrophobic interaction. Therefore, such QSI molecules are not well dispersed and available to inhibit the production of pyocyanin. On the other hand, the QSI-loaded SqNPs would have a better dispersion in the medium and show relatively consistent efficacy of inhibition.

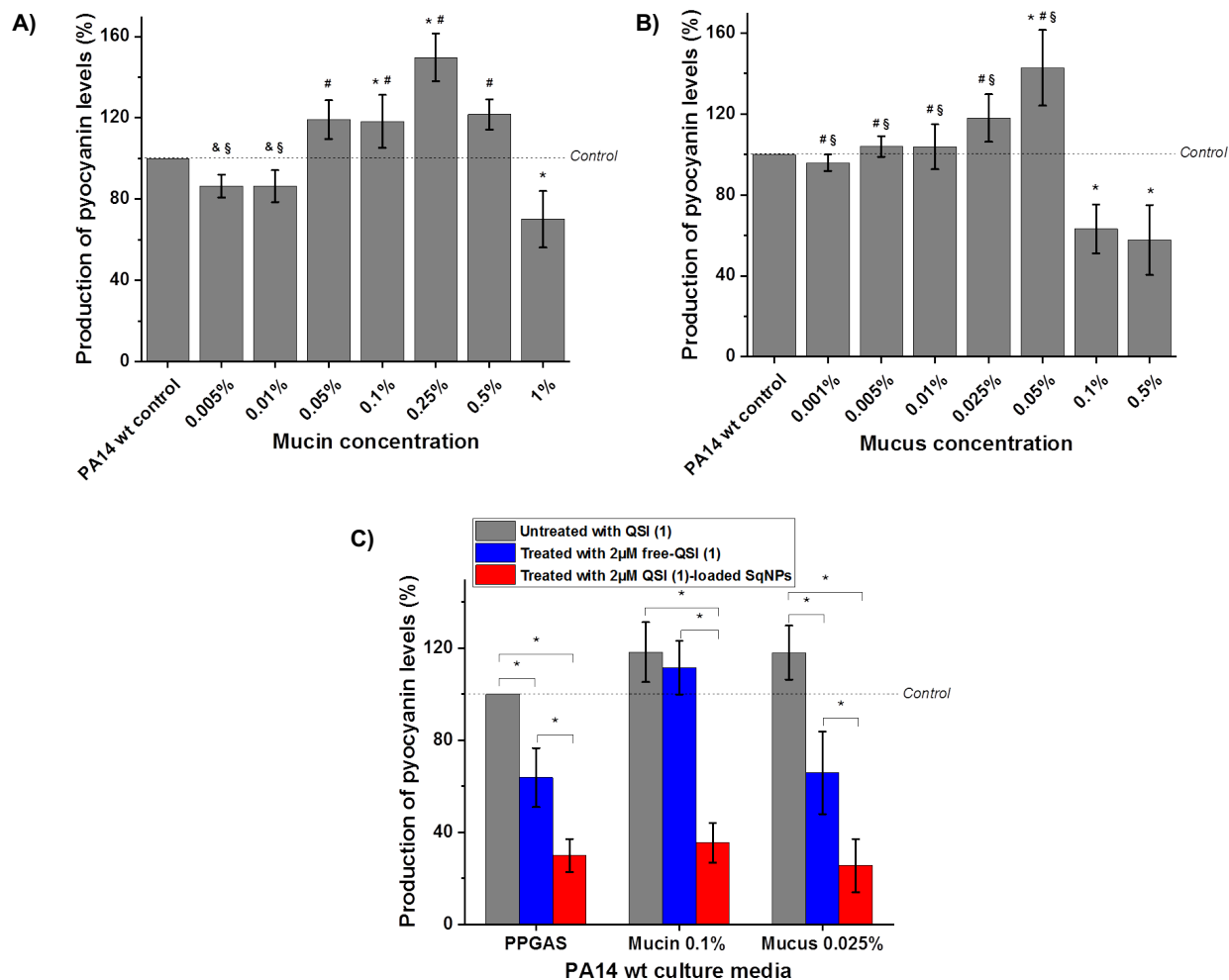


Figure 3. Pyocyanin assay

A) The production of pyocyanin levels in present of mucin compared to the control PQ14 wt grown in PPGAS culture medium. Significant level show at * $p < 0.001$ compared with controls; # $p < 0.001$ compared with samples incubated with mucin 1%; & $p < 0.001$ compared to samples incubated with mucin 0.25%; § $p < 0.001$ compared to samples incubated with mucin 0.1%. B) The production of pyocyanin levels in present of mucus compared to the control PQ14 wt grown in PPGAS culture medium. Significant level show at * $p < 0.001$ compared to controls; # $p < 0.001$ compared to samples incubated with mucus 0.5%; § $p < 0.001$ compared to samples incubated with mucus 0.1%. C) Comparison of pyocyanin production level in PA14 wt samples grown in either bacterial culture medium (PPGAS), 0.1% mucin in PPGAS, or 0.025% mucus in PPGAS were treated with either 2 μ M QSI (1) as free form or loaded in SqNPs. * $p < 0.001$. All data are presented as mean \pm SD, at least three independent experiments performed in triplicate each.

As shown in Figure 4A, once bacteria are protected in biofilm, the concentration of tobramycin needed to completely eradicate bacterial infection was 200 μ g/mL or higher which is remarkably higher than that needed to against planktonic PA14 wt. The fact of

higher Tobramycin dose needed to eliminate biofilm is known and was verified here. The need of a higher dose is a challenge in biofilm-associated infections, especially that could promote bacterial antibiotic resistance development. The tob-loaded SqNPs holding controlled release profile of tobramycin shows a slight improvement with an identified MBEC value at 200 $\mu\text{g}/\text{mL}$. The free-form mixture of tobramycin and QSI (1) in which QSI (1) concentration was kept constantly at 20 μM performed better in combatting PA14 wt biofilm compared to the aforementioned treatments. In addition to the decreasing of MBEC value of tobramycin down to 100 $\mu\text{g}/\text{mL}$, the overall bacteria availability in all tobramycin treating concentrations was reduced compared to those treated without QSI (1). The results show encouraging therapeutic effect of the antibiotic and QSI combination. One might hypothesize that QSI would inhibit the production of pyocyanin and prevent the further development of the already established biofilm, which thus causes a weaker biofilm structure and increase the sensitivity of bacteria to antibiotic. Moreover, the less formation of biofilm would further limit the transformation of bacteria to persister stage, which would restrict the resistance development. Having known that QSI (1)-loaded SqNPs would enhance the inhibiting functions of QSI (1), we further applied the tob & QSI (1)-co-loaded SqNPs in MBEC assay, in which QSI (1) concentration was also incubated continuously at 20 μM . The results are shown in Figure 4D. Interestingly, tobramycin needed for the complete biofilm eradication was significantly reduced and reached around 12.5 $\mu\text{g}/\text{mL}$ which is nearly 16-fold lower than that of free tobramycin. The interestingly remarkable enhancement would be the results of better bioavailability of QSI (1) through the biofilm due to the good dispersion and transportation of such hydrophobic drug loaded in SqNPs, which was further confirm by CLSM images shown in Figure 5. In summary, the results of the MBEC assay show that the novel drugs co-loaded SqNPs have a remarkable complementary therapeutic effect that benefit the biofilm eradicating properties and are superior to free tobramycin. The proposed platform and gained knowledge in this research would definitely devote to the further studies in combatting bacterial biofilm resistance development.

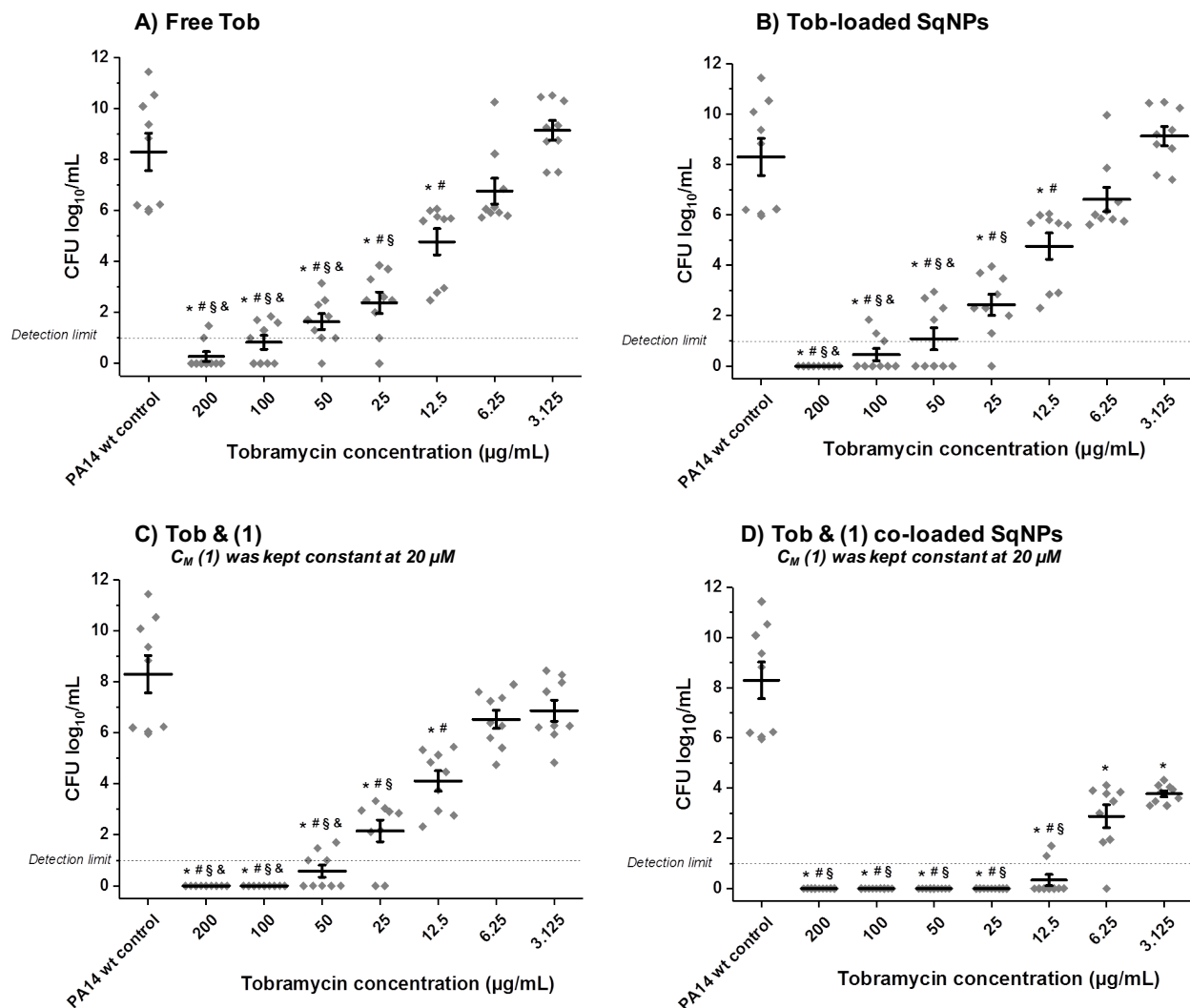


Figure 4. Minimum Biofilm Eradicating Concentration Assay.

PA14 wt biofilm grown in PPGAS for 24h (starting OD₆₀₀=3.0) were treated with A) Tobramycin (Tob); B) Tob-loaded SqNPs; C) both Tob and QSI (1) as free form; D) Tob and (1) co-loaded SqNPs. The concentration of QSI (1) was kept constant at 20 µM in all experiments. After 24h incubation, efficacy was assessed by determination of cfu/mL. Cfu/mL values are depicted logarithmically for n = 3 experiments with technical triplicates each. PA14 wt biofilm, and PA14 wt biofilm treated either with drug-free SqNPs, or with QSI (1), or QSI (1)-loaded SqNPs were served as controls. The dotted line indicates the detection limit. Significant different shown at level *p<0.001 compared to controls; #p<0.001 compared to samples treated with Tob 3.125 µg/mL; §p<0.001 compared to samples treated with Tob 6.25 µg/mL; and &p<0.001 compared to samples treated with Tob 12.5 µg/mL.

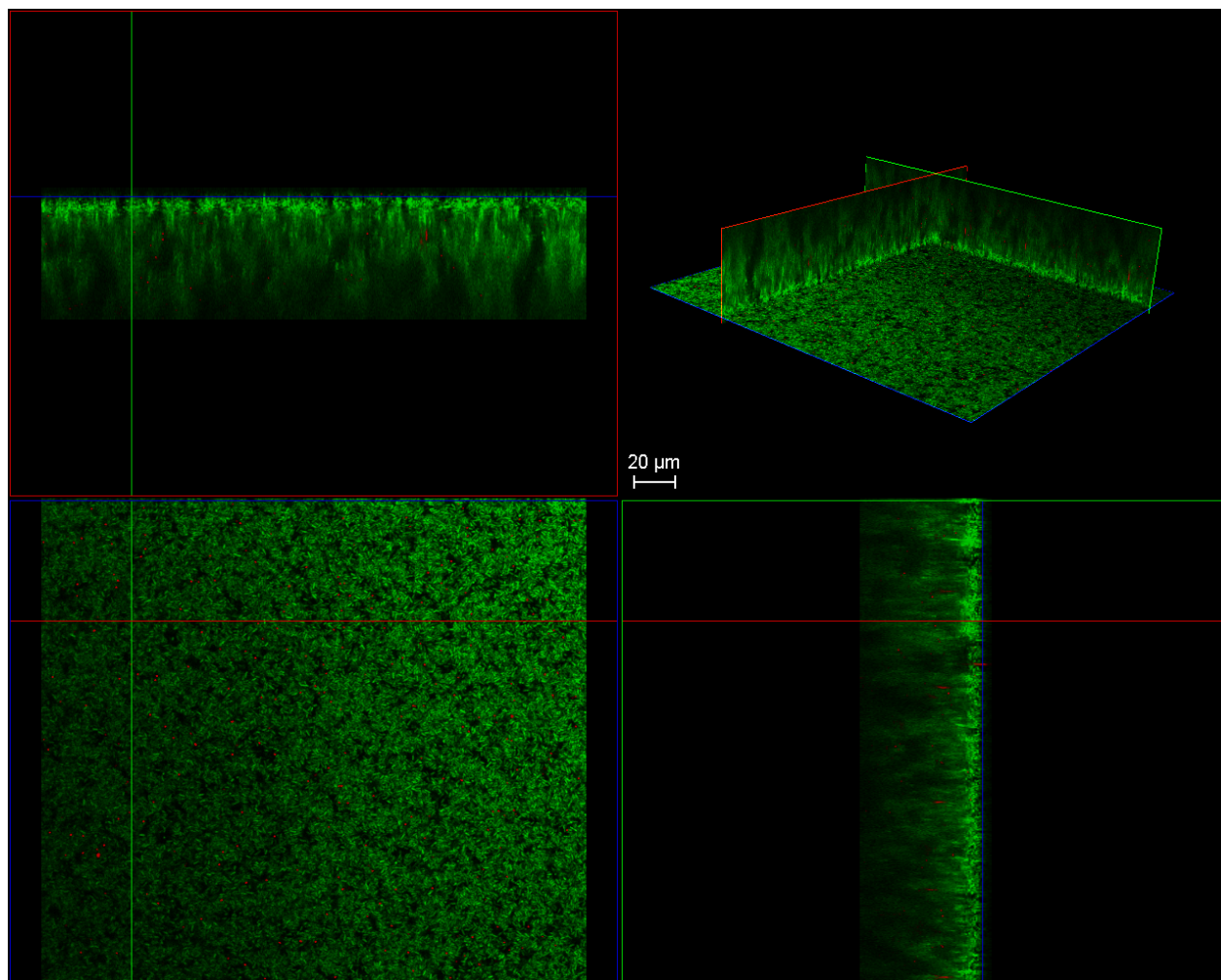


Figure 5. CLSM study of Tob & Nile-red-co-loaded SqNPs 190 nm (Tob concentration was 25 µg/mL which is below the MBEC value of Tob-loaded SqNPs) interaction and transport through PA GFP 24h-old biofilm (starting OD600=3.0) after 4h incubation (PA GFP: *Pseudomonas aeruginosa* green fluorescent protein in Green, Nile-red loaded SqNPs in red). The images show the bottom layer of the PA biofilm in which SqNPs are found proving for the penetration of such system through the biofilm.

References

1. Couvreur P, Stella B, Harivardhan Reddy L, Hillaireau H, Dubernet C, Desmaëie D, et al. Squalenoyl nanomedicines as potential therapeutics. *Nano Lett.* 2006;6(11):2544–2548.
2. Miramoth NS, Di Meo C, Zouhiri F, Saïd-Hassane F, Valetti S, Gorges R, et al. Self-assembled squalenoylated penicillin bioconjugates: An original approach for the treatment of intracellular infections. *ACS Nano.* 2012;6(5):3820–3831.
3. Réjiba S, Reddy LH, Bigand C, Parmentier C, Couvreur P, Hajri A. Squalenoyl

- gemcitabine nanomedicine overcomes the low efficacy of gemcitabine therapy in pancreatic cancer. *Nanomedicine Nanotechnology, Biol Med.* 2011;7(6):841–9.
4. Lepeltier E, Loretz B, Desmaële D, Zapp J, Herrmann J, Couvreur P, et al. Squalenylation of chitosan: A platform for drug delivery? *Biomacromolecules.* 2015;16(9):2930–9.
 5. Deacon J, Abdelghany SM, Quinn DJ, Schmid D, Megaw J, Donnelly RF, et al. Antimicrobial efficacy of tobramycin polymeric nanoparticles for *Pseudomonas aeruginosa* infections in cystic fibrosis: Formulation, characterisation and functionalisation with dornase alfa (DNase). *J Control Release.* 2015;198:55–61.
 6. Yasar H, Ho DK, De Rossi C, Herrmann J, Gordon S, Loretz B, et al. Starch-chitosan polyplexes: A versatile carrier system for anti-infectives and gene delivery. *Polymers (Basel).* 2018;10(3):252.
 7. Nafee N, Husari A, Maurer CK, Lu C, De Rossi C, Steinbach A, et al. Antibiotic-free nanotherapeutics: Ultra-small, mucus-penetrating solid lipid nanoparticles enhance the pulmonary delivery and anti-virulence efficacy of novel quorum sensing inhibitors. *J Control Release.* 2014;192:131–40.
 8. Cao H, Krishnan G, Goumnerov B, Tsongalis J, Tompkins R, Rahme LG. A quorum sensing-associated virulence gene of *Pseudomonas aeruginosa* encodes a LysR-like transcription regulator with a unique self-regulatory mechanism. *Proc Natl Acad Sci.* 2001;98:14613–8.
 9. Déziel E, Gopalan S, Tampakaki AP, Lépine F, Padfield KE, Saucier M, et al. The contribution of MvfR to *Pseudomonas aeruginosa* pathogenesis and quorum sensing circuitry regulation: Multiple quorum sensing-regulated genes are modulated without affecting lasRI, rhlRI or the production of N-acyl-L-homoserine lactones. *Mol Microbiol.* 2005;55:998–1014.
 10. Mulcahy LR, Burns JL, Lory S, Lewis K. Emergence of *Pseudomonas aeruginosa* strains producing high levels of persister cells in patients with cystic fibrosis. *J Bacteriol.* 2010;192(23):6191–9.
 11. Diggle SP, Matthijs S, Wright VJ, Fletcher MP, Chhabra SR, Lamont IL, et al. The *Pseudomonas aeruginosa* 4-Quinolone Signal Molecules HHQ and PQS Play Multifunctional Roles in Quorum Sensing and Iron Entrapment. *Chem Biol.* 2007;14(1):87–96.

12. Pesci EC, Milbank JBJ, Pearson JP, McKnight S, Kende AS, Greenberg EP, et al. Quinolone signaling in the cell-to-cell communication system of *Pseudomonas aeruginosa*. *Proc Natl Acad Sci*. 1999;96:11229–34.
13. Xiao G, Déziel E, He J, Lépine F, Lesic B, Castonguay MH, et al. MvfR, a key *Pseudomonas aeruginosa* pathogenicity LTTR-class regulatory protein, has dual ligands. *Mol Microbiol*. 2006;62:1689–99.
14. Hassan HM, Fridovich I. Mechanism of action of pyocyanine. *J Bacteriol*. 1980;141(1):156–63.
15. Denning GM, Wollenwebber LA, Railsback MA, Cox CD, Stoll LL, Britigan BE. *Pseudomonas* pyocyanin increases interleukin-8 expression by human airway epithelial cells. *Infect Immun*. 1998;66(12):5777–84.
16. Häussler S, Becker T. The *pseudomonas* quinolone signal (PQS) balances life and death in *Pseudomonas aeruginosa* populations. *PLoS Pathog*. 2008;4(9).
17. Kamal AAM, Petretera L, Eberhard J, Hartmann RW. Structure-functionality relationship and pharmacological profiles of: *Pseudomonas aeruginosa* alkylquinolone quorum sensing modulators. *Org Biomol Chem*. 2017;15(21):4620–30.
18. Anderson MJ, Parks PJ, Peterson ML. A mucosal model to study microbial biofilm development and anti-biofilm therapeutics. *J Microbiol Methods*. 2013;92(2):201–208.

6.5. PATENT APPLICATION: “Excipient-free nano-assemblies of aminoglycoside antibiotics and farnesyl quorum sensing inhibitors for combatting bacterial biofilm infections”

This chapter is the following filed patent application:

Duy-Khiet Ho, Brigitta Loretz, Claus-Michael Lehr; Aminoglycoside derivatives and nano-assemblies thereof, including those with quorum sensing inhibitory function.

European Patent Application, EP 17 179 011.6

International Patent Application, PCT/EP2018/065232

6.5.1. Proof of European Patent Application



European Patent Office
80293 MUNICH
GERMANY

Questions about this communication ?
Contact Customer Services at www.epo.org/contact



LORETZ, Brigitta
Schinkelstrasse 16
66123 Saarbrücken
ALLEMAGNE

Date	23.08.17
------	----------

Reference	Application No./Patent No. 17179011.6 - 1453
Applicant/Proprietor Heimholtz-Zentrum für Infektionsforschung GmbH	

Designation as inventor - communication under Rule 19(3) EPC

You have been designated as inventor in the above-mentioned European patent application. Below you will find the data contained in the designation of inventor and further data mentioned in Rule 143(1) EPC:

DATE OF FILING : 30.06.17
 PRIORITY : //
 TITLE : AMINOGLYCOSIDE DERIVATIVES AND NANO-ASSEMBLIES THEREOF, INCLUDING THOSE WITH QUORUM SENSING INHIBITORY FUNCTION
 DESIGNATED STATES : AL AT BE BG CH CY CZ DE DK EE ES FI FR GB GR HR HU IE IS IT LI LT LU LV MC MK MT NL NO PL PT RO RS SE SI SK SM TR

INVENTOR (PUBLISHED = 1, NOT PUBLISHED = 0):

1/HO, Duy-Khiet/274 Le Sao Street Phu Thanh Ward Tan Phu District/70000 Ho Chi Minh City/VN
 1/LORETZ, Brigitta/Schinkelstrasse 16/66123 Saarbrücken/DE
 1/LEHR, Claus-Michael/Franz-Schubert-Strasse 6/66125 Saarbrücken/DE

DECLARATION UNDER ARTICLE 81 EPC:

The applicant(s) has (have) acquired the right to the European patent as employer(s).

Receiving Section



6.5.2. Proof of International Patent Application

Unsere Akte: AN0005P-WO
Ihre Akte: 02-00351 Nano-Assembly of Aminoglycosides



Datenblatt

Anmelder	Helmholtz-Zentrum für Infektionsforschung GmbH Inhoffenstraße 7 38124 Braunschweig Deutschland
Schutzrechtsart	Internationale Patentanmeldung
Bestimmungsländer	Alle Länder und Organisationen des PCT
Titel	AMINOGLYCOSIDE DERIVATIVES AND NANO-ASSEMBLIES THEREOF, INCLUDING THOSE WITH QUORUM SENSING INHIBITORY FUNCTION
Priorität	17179011.6 EP vom 30. Juni 2017
Anmeldetag	8. Juni 2018
Anmeldenummer	PCT/EP2018/065232
Offenlegung	frühestens am 30. Dezember 2018
Schutzdauer	bis zum 8. Juni 2038
Erfinder	Dr. Brigitta Loretz Schinkelstrasse 16 66123 Saarbrücken Deutschland Nationalität: österreichisch;

13. Juni 2018

1/2

Unsere Akte: AN0005P-WO
Ihre Akte: 02-00351 Nano-Assembly of Aminoglycosides



Duy-Khiet HO

Secretary Office of Department of Drug Delivery
Department of Drug Delivery
Helmholtz Institute for Pharmaceutical Research
Saarland (HIPS)
Building E 8.1, Saarland Campus, Saarland
University
D-66123 Saarbrücken
Deutschland
Nationalität: vietnamesisch;

Prof. Claus-Michael Lehr

Franz-Schubert-Str. 6
66125 Saarbrücken
Deutschland
Nationalität: deutsch;

13. Juni 2018

2/2

6.5.3. Summary of the invention

In this section, the description of state-of-the-art and some results in the invention will be summarized and presented. The invention will be published online from January 2019.

Aminoglycosides is an important antibiotic family which is widely used in clinical to treat many infectious diseases, especially for many types of gram-negative bacteria and biofilm. Tobramycin, for instant, is widely used for several infectious diseases with different formulating strategies, e.g. i) TOBI® solution for inhalation (product of Novartis) is a tobramycin solution for inhalation for lung infection, particularly in cystic fibrosis patients. This product is recommended to use as 300mg tobramycin in 5 mL ampule for a single use for 28 days. ii) TOBI® PODHALER™ (product of Novartis) is tobramycin inhalation powder. This product is administered 28 mg capsules for inhalation twice-daily for 28 days (1–3). iii) Tobramycin Ophthalmic Solution, USP 0.3% (product of Bausch and Lomb) is tobramycin for ophthalmic infection (4). iv) and many other examples such as gentamicin and neomycin for infectious skin, amikacin for a wide range of multi-resistant bacteria.

Although there are tremendous development in therapeutic approach, particularly new drug class synthesis, as well as formulating and administering strategies, the clinical treatments using aminoglycosides remain failures because: (i) The drugs could only accomplish the termination of spreading bacteria, while biofilms and mucus-embedded biofilms could impossibly be eradicated completely; (ii) The high dose of aminoglycosides, e.g. in case of TOBI® solution for inhalation, which is required for the treatment of cystic fibrosis related infection, causes side effects on patients when the drug is burstly released; (iii) The naturally highly charged structure of aminoglycosides would cause strong interaction with biological barriers, e.g. biofilm or mucus, leading to a slow or incomplete penetration of drug to infected side. As a result, aminoglycosides dose could be below MIC value which is a main cause of bacterial resistance.

With mentioned reasons, the uses of aminoglycosides are necessary, but there are limitations that need to be solved. Although new analogs of aminoglycosides could be synthesized and introduced to expectedly improve antimicrobial properties, their highly

positive charged structure could potentially again be a problem causing resistance in bacteria due to its strong interaction with biological barriers, especially in complex infectious diseases. Hence, it is important to prepare new analogs of such antibiotic family, and to innovate a strategy to overcome biological barriers. Formulating and combining aminoglycosides with other active agents as the complementary treatment in the nano-sized carriers would be a good problem solving approach.

Nanotechnology in pharmaceutical applications has been evaluated as a high efficacy technique in the delivery of drugs, which aims to protect drugs from degradation and burst release, and to deliver a sustainable amount of drugs to targeting sites. Particularly considering novel strategies of drug delivery for infectious diseases treatment, nanotechnology is the most advantageous technique, which could locally delivery sufficient doses of anti-infective, allows a combination of more than one active agent in targeting site to maximize treatment efficiency, and avoids drugs side effects as well as bacterial resistance development. Although there are many intense studies on developing nanomedicines for severely infectious diseases, it is obvious that few nanomedicine products have reached to clinical stage and market. Those failures are because of: (i) The poor loading rate with respect to carrier materials; (ii) The burst release of encapsulated drugs right after administration; (iii) It is hard to choose the materials which are biodegradable, biocompatible, and easy for the design of carrier systems that could overcome biological barriers; (iv) Lack of multifunctional nano-carrier systems, or limitation in multi-loading carrier system regarding loading capacity, types of loading agents, loading efficiency and loading rate.

In this invention, we propose an innovative strategy which is 'excipient free nano-assembly of aminoglycosides and quorum sensing inhibitors' by farnesylation of aminoglycosides molecules. Farnesol is a natural and biocompatible lipid ($C_{15}H_{26}O$) belonging to the sesquiterpene alcohols, which is widely employed in many medical products. "Farnesylation" means the covalently chemical linkage, or electrostatic interaction of farnesyl derivatives and drug molecules via a "single step" preparation which is proposed in this innovation. Without the need of any other supporting materials, the innovated technique allows spontaneous formation of aminoglycosides nanoparticles based on self-assembly of farnesol derivatives. Moreover, farnesol and its derivatives

have known pharmacological effects (5,6) which are: i) anti-biofilm activity (7); ii) bacteria (e.g. *Pseudomonas aeruginosa*) and fungi quorum sensing inhibitory properties, as well as improving treatment efficiency when co-administrating with antibiotic (8–10); iii) antibacterial and antifungal (5,11,12); and iv) induction of apoptosis in cancer cells (13,14). Those properties of farnesol derivatives, particularly quorum sensing inhibitory properties, would be greatly employed in this innovation. Therefore, in this innovation, the 'excipient free nano-assembly of Aminoglycosides and quorum sensing inhibitors' by farnesylation is composed of antibiotic, aminoglycosides, and quorum sensing inhibitor derivatives, farnesol derivatives, which is considered 100% nano-assembly medicine for infectious diseases treatment.

Such remarkable self-assembly properties were demonstrated before for squalene ($C_{30}H_{50}$; Mw = 410 g/mol) the precursor of steroids. Squalenylation was shown to be a viable strategy for drug delivery (15). However, the Squalenylation technology has unsolved disadvantages compared to the innovative 'Aminoglycosides Nano-assembly' by farnesylation, which are: (i) Squalene derivatives do not have quorum sensing inhibitory properties; hence, it is just a novel carrier system, or pro-drug form. Meanwhile, in this innovation, the 'Aminoglycosides Nano-assembly' is considered as 100% therapeutic nano-medicine (the excipient free nano-assembly) as it is composed by antibiotic, aminoglycosides, and quorum sensing inhibitory derivatives, farnesol derivatives; (ii) Preparation of squalene derivatives is multi-step synthesizing procedure (generally more than 5 steps) and poor isolated yield, especially around 30% isolated yield for 1st step of synthesis procedure, which results in low overall isolated yield (16,17); (iii) Conjugation of squalene derivatives to highly charged compounds causes serious solubility problem of resulting products, which is a huge limitation for nano-carriers preparation and application as reported by Lepeltier et. al. (18); (iv) Farnesol derivative is a precursor of squalene, so squalene derivatives have almost double molecular weight and are harder available and producible. The drugs loading rate of nano-carriers based on squalene derivatives would be definitely lower compared to farnesol derivatives considering same drug molecules.

Besides, farnesol derivatives were previously used to modify with penicillin G (19,20); however, the aim of that research was completely different compared to the focus of this innovation, with reasons as following: (i) The research aimed to treat intracellular

infection, in eukaryotic cells, the non-biofilm infection. The function as quorum sensing inhibitor of farnesol derivatives was not employed and studied, and farnesol derivative in their research was just used as a carrier. While the aim of this innovation is 'Aminoglycosides Nano-assembly' for dual delivery of aminoglycosides and quorum sensing inhibitor, the farnesol derivatives, for biofilm treatment. (ii) In the proposed research by Abed et. al. (20) non-cleavable (ester bonds) and intracellular cleavable linkage (acylal linkage) of farnesol derivatives and drug molecules were used resulting in non-active properties of farnesol for intracellular infection. While in this innovation the linkage of farnesol derivatives and aminoglycosides is designed and synthesized to be cleaved due to pH gradient of biofilm (e.g. imine, enamine) as environmentally sensitive linkage (the linkage in this innovation is not designed to be cleaved intra- eukaryotic cells), or is statistic interaction. Hence, quorum sensing inhibitory function of farnesol derivatives would be maintained in targeting sites (e.g. biofilm). Besides, the conjugation of farnesol derivatives and penicillin G by Abed et. al. (20) required spacing molecules (for better conjugation and control environmental sensitivity of linkage), while in this invention aminoglycosides and quorum sensing inhibitors, farnesol derivatives, were directly conjugated by pH-sensitive linkage. As a result, cleaved products of modified compounds in such approach are not quorum sensing inhibitors due to the presence of spacing molecules, while in this invention the conjugation without spacing molecules of the excipient free nanomedicine will directly release farnesol derivatives, which are quorum sensing inhibitors, and aminoglycoside molecules. (iii) The use of farnesol derivatives in their research did not help to improve antimicrobial activity of penicillin G as mentioned in Table 2 in their publication, and even dramatically decrease antimicrobial activity of penicillin G, or non-active compound after conjugation (by showing the remarkable increase of minimum inhibitory concentration (MIC) at more than 3250 folds higher compared to free drug. Note: the result in MIC assay shows that one of the modified drugs with farnesol derivative does not have antimicrobial activity). While in this innovation, the active sites of aminoglycosides (amine functional groups) are maintained in targeting sites as selectively cleavable linkage and/or statistic interaction of quorum sensing inhibitors, farnesol derivatives, and aminoglycosides are prepared. Moreover, the dual-delivery of 100% therapeutic nanomedicine (the excipient free nano-assembly) shows great improvement in treatment efficiency as the function of two active agents, with

dramatically decreasing in MIC value. (iv) In their research, the β -Lactam antibiotic family was studied, which is used in completely different aim from aminoglycosides antibiotic family, the focus in this innovation; hence, they have different problems considering their applications and development. And in this innovation, problems of aminoglycosides are carefully addressed.

In addition, the introduction of lipophilic moieties into molecules of aminoglycosides; particularly modification of Tobramycin, or Kanamycin, were investigated in previous research proposed by Fosso et. al. (21) and Berkov-Zrihen et. al. (22). The aim in these researches was to use chemical modification to introduce lipophilic derivatives into aminoglycosides to make cationic amphiphiles which could promote better penetration of modified compound to bacteria cell walls, or vary the anti-microbial activity (which was studied by MIC assay). However, such modification in those studies could not bring great impact in infectious diseases treatment compared to the modification in this invention. The main disadvantages in those researches and the differences compared to this innovation are mentioned as below: (i) The lipophilic moieties which were used in those researches are linear hydrocarbon (from C4 to C15). Those hydrocarbon derivatives do not have self-assembly properties so that the formation into nano-sized carriers is not possible. While in this innovation the use of farnesol derivatives is for self-assembly of aminoglycosides into nano-sized carrier systems. (ii) The lipophilic moieties which were used in those researches do not have quorum sensing inhibitory properties. While the farnesol derivatives in our innovation are employed as quorum sensing inhibitors which are greatly employed for a formulation of 100% therapeutic nanomedicine (the excipient free nano-assembly). (iii) In those researches, lipophilic moieties were modified to aminoglycosides derivatives with stable linkage (non-cleavable linkage) toward aminoglycosides, which definitely changes properties of the active sites of aminoglycosides; therefore, the modified drugs could be considered as new compounds. Consequently, in most cases, the introduction of lipophilic moieties results in poor anti-microbial activities. While in this innovation, the introduction of farnesol derivative does not compromise anti-microbial properties of aminoglycosides, but dramatically increases the treatment efficiency due to dual action of two active agents in 100% therapeutic nanomedicine (the excipient free nano-assembly). (iv) The introduction of lipophilic

moieties was done by heavily employing chemical synthesis, which is multi-step synthetic procedure (generally more than 7 steps) with poor isolated yield, and non-scalable strategy. While in this innovation we have developed the 'single step' preparation of aminoglycosides nano-assembly which incorporates more than one active compound for better treatment efficiency, and is a scalable procedure with 100% conversion yield and 95% isolated yield.

Finally, the incorporating administration of an antibiotic (ciprofloxacin) and quorum sensing inhibitor (farnesol) by formulating them into liposome vehicle to treat biofilm infections results in greater treatment efficiency compared to single administration of each free drug proposed by Bandara et. al. (10). However, i) the novel carrier, liposome, used in their research has poor loading rate due to its natural characteristic of such carrier system and the use of abundant amount of lipids to formulate liposome which are dominant compared to amount of loading drugs; and ii) there is no direct connection (linkage) between antibiotic molecules and quorum sensing inhibitors in their research, they were just applied as free form in the formulation; hence, the release of drugs were not well controlled; iii) Moreover, ciprofloxacin could easily form crystal in an aqueous medium in short time at storage conditions, so the use of ciprofloxacin in aqueous phase of liposome is not a good approach. Hence, the differences between this innovation and the work by Bandara et. al. (10) are: (i) In this innovation, the 100% therapeutic nanomedicine (the excipient free nano-assembly) without any supporting materials has been innovated which is a huge advantage compared to liposome carrier; (ii) moreover, the cleavable linkage or statistic interaction of farnesol derivatives and aminoglycosides is able to form stable nano-assembly to avoid burst release, and manage to have the release of drugs in a controlled manner.

With all above mentioned reasons, this innovation proposes a completely different approach for nanomedicine formulation of aminoglycosides and farnesol derivatives.

The concept of self-assembly antibiotic aminoglycosides and quorum sensing inhibitory farnesol derivatives into a nanomedicine system is unique, and a completely different focus on nanomedicine development compared to previous studies.

In this innovation, such unique nano-assembly has created a 100% therapeutic nanomedicine (the excipient free nano-assembly), which means all components function as active agents in targeting sites (biofilm).

Nano-assembly of aminoglycosides is employed by farnesylation of aminoglycosides, in which sensitively covalent bonding (e.g. imine, enamine) is formed by conjugating equivalent molar ratio of farnesol derivative and amine functional groups of aminoglycosides' molecules, or statistic interaction of farnesol derivative and functional groups of aminoglycosides' molecules. This modification introduces the lipophilic moiety into drug molecules. Consequently, the farnesylation of aminoglycosides could spontaneously form nano-assembly. Burst release could be avoided, while sustained release could be achieved by a chemical linkage which is sensitive to surrounding environmental factors at infectious sites, especially to pH gradient in biofilm.

The main advantages of this innovative platform are as following: (i) A "single step" preparation facilitates the dramatic increase in drug loading of aminoglycosides (e.g. Tobramycin) up to 70%, and of both aminoglycosides and quorum sensing inhibitory farnesol derivatives up to 100%. Notably, the 'Aminoglycosides nano-assembly' in this innovation is 100% therapeutic nano-medicine (the excipient free nano-assembly). (ii) Farnesol derivatives are small molecules, and they enable the stable self-assembly complexes. Hence, the drug loading capacity is much higher compared to conventional encapsulation strategies and Squalenoylation approach. Moreover, aminoglycosides are generally highly charged molecules; hence, their conjugation with capably assembling molecules (e.g. squalene derivatives) would result in insoluble products in common solvents. However, in this innovation, the farnesylation of aminoglycosides does not cause such problem, and the nano-assembly could be effortlessly formed. Structure of tobramycin nano-assembly by farnesylation in nano-size and spherical shape has been convincingly proved by Cryo-TEM image shown in Figure 1.

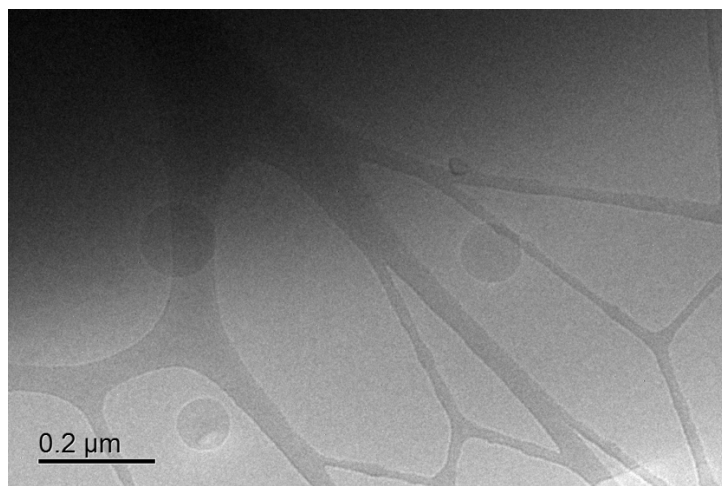


Figure 1. Cryo-TEM image of the farnesyl-conjugated tobramycin nano-assemblies.

(iii) “Dual functioned” nanomedicines due to the presence of farnesyl derivatives’ quorum sensing inhibiting activity increases anti-microbial activities of the nano-medicine ‘Aminoglycosides nano-assembly’. The quorum sensing inhibitory effects of farnesyl derivatives are summarized in Table 1. Notably, the farnesyl hydrogen sulfate derivative performed impressively improvement in inhibiting pyocyanin production of PA14 wt, which would be explained by the self-assembly of such derivative in comparison to non-water-soluble phase of farnesol or farnesal. The self-assemblies of farnesyl hydrogen sulfate are observed by Cryo-TEM, and a representative image is presented in Figure 2. (iv) The introduction of lipophilic moieties, Farnesol derivatives, can improve the penetration of aminoglycosides through bacteria cell walls. Moreover, the presence of lipophilic moieties by chemical linkage or statistic interaction strongly decreases charge of aminoglycosides molecules; as a result, the modified aminoglycosides in this innovation do not have strong interaction with biological barriers like mucus, biofilm, and penetrate faster through such barriers. The hypothesis is fully proved by the results obtained from MBEC assays shown in Figure 3. Moreover, the incorporation of either farnesal, farnesol or farnesyl hydrogen sulfate with tobramycin into the nano-assemblies enhances significantly the efficacy against PA14 wt biofilm. Although the pyocyanin inhibiting effects of both farnesol and farnesal could not be determined at the tested concentration, the complementary effects with antibiotics of these two natural-lipid-based quorum sensing inhibitors were clearly shown when being assembled into the nano-assemblies. (v) The formulation avoids burst

release of aminoglycosides by sensitive (e.g. pH) chemical linkages (e.g. imine, enamine) of farnesol derivatives and aminoglycosides, or statistic interaction of farnesol derivatives and aminoglycosides. (vi) The rich positively charged surface of aminoglycosides nano-assembly stabilizes really well such carrier system, and could also be used for further surface modification, while the hydrophobic core would be also further employed to load hydrophobic compounds, which altogether makes great innovation of multiple drugs delivery systems.

Table 1. Pyocyanin inhibiting efficacy on PA14 wt of farnesyl derivatives ^(a)

Farnesyl derivatives	Function in the innovative nanoassemblies	Stock solvent for solubilization	EC50 of pyocyanin inhibiting level (µg/mL)
Farnesal	Farnesylation of aminoglycosides based on pH sensitive chemical linkage, and function as a QSI	Ethanol	N/A ^(b)
Farnesol	Function as a QSI	Ethanol	N/A ^(b)
Farnesyl hydrogen sulfate	Farnesylation of aminoglycosides based on charge interaction, and function as a QSI	Ethanol	~10

^(a) The inhibition of pyocyanin level on PA14 wt strain after being treated with either farnesal, farnesol or farnesyl hydrogen sulfate was measured compared to untreated PA14 wt control. All PA14 wt bacteria samples were grown in PPGAS. At least three independent experiments performed in triplicate each.

^(b) N/A: not available. The EC50 values of farnesal and farnesol were not determined. The inhibitory level of both compounds was lower than 50% at the highest tested concentration of 30 µg/mL.

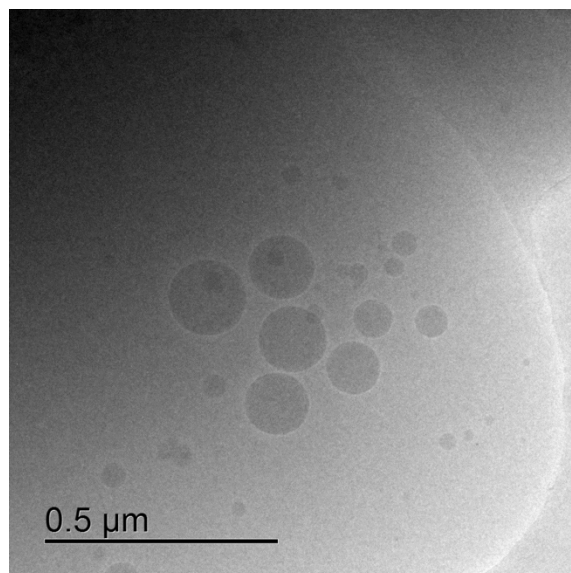


Figure 2. Cryo-TEM image of farnesyl hydrogen sulfate nanoassemblies in aqueous solution

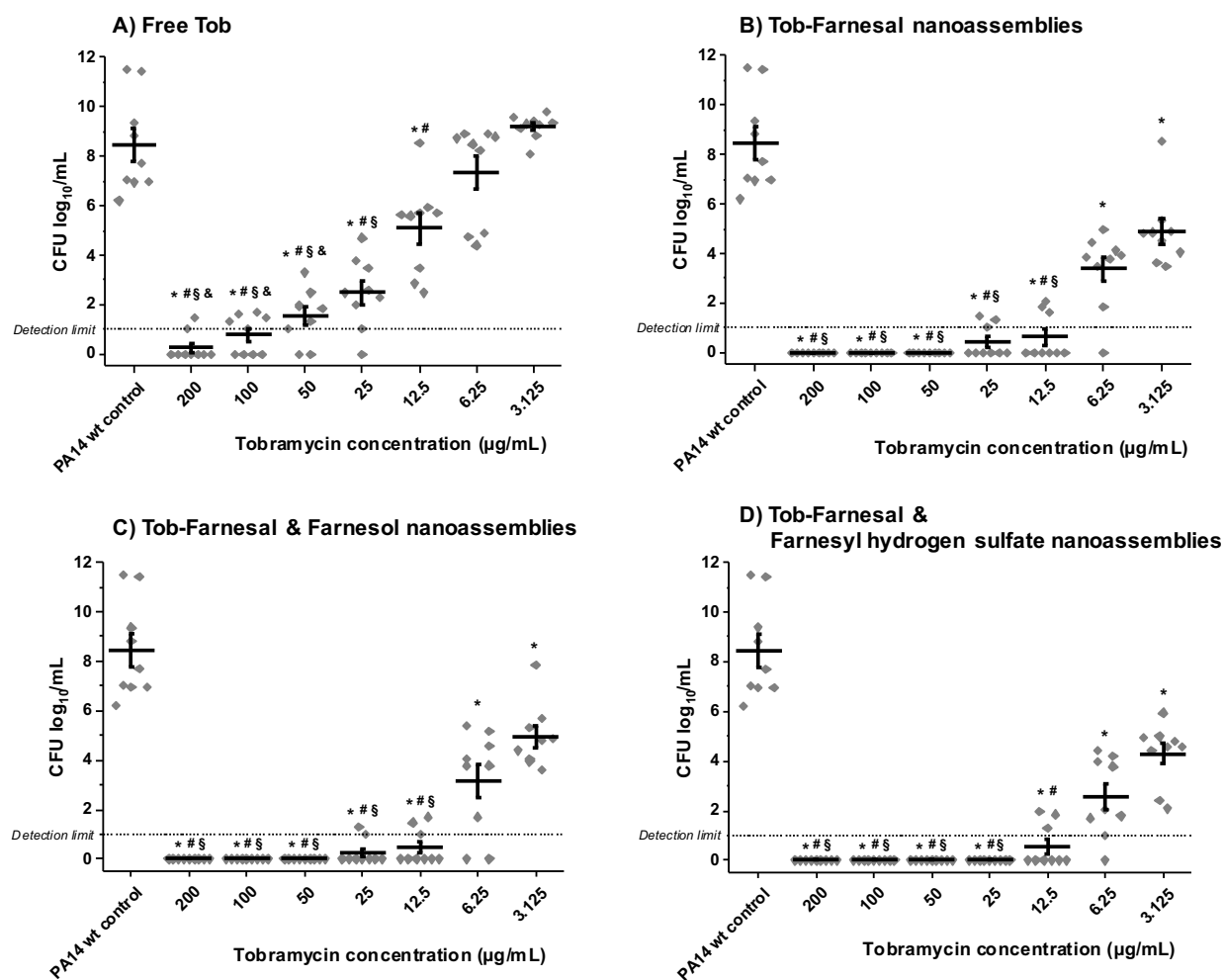


Figure 3. Minimum Biofilm Eradicating Concentration Assay.

PA14 wt biofilm grown in PPGAS for 24h (starting OD₆₀₀=3.0) were treated with A) Tobramycin (Tob); B) Tob-Farnesal nanoassemblies; C) Tob-Farnesal & Farnesol nanoassemblies; D) Tob-Farnesal and Farnesyl hydrogen sulfate nanoassemblies. The total concentration of farnesyl QSI was kept constant at 100 µg/mL in all experiments treated with QSI. After 24h incubation, efficacy was assessed by determination of cfu/mL. Cfu/mL values are depicted logarithmically for n = 3 experiments with technical triplicates each. PA14 wt biofilm samples served as controls. The dotted line indicates the detection limit. Significant different shown at level *p<0.001 compared to controls; #p<0.001 compared to samples treated with Tob 3.125 µg/mL; §p<0.001 compared to samples treated with Tob 6.25 µg/mL; and &p<0.001 compared to samples treated with Tob 12.5 µg/mL.

References

1. Cheng JY, Zhang T, Ruangwattanapaisarn N. HHS Public Access. 2016;42(2):407–20.
2. Elborn JS, Vataire AL, Fukushima A, Aballea S, Khemiri A, Moore C, et al. Comparison of Inhaled Antibiotics for the Treatment of Chronic *Pseudomonas aeruginosa* Lung Infection in Patients With Cystic Fibrosis: Systematic Literature Review and Network Meta-analysis. *Clin Ther.* 2016;38(10):2204–26.
3. Newhouse MT, Hirst PH, Duddu SP, Walter YH, Tarara TE, Clark AR, et al. Inhalation of a dry powder tobramycin pulmosphere formulation in healthy volunteers. *Chest.* 2003;124(1):360–6.
4. Torkildsen GL, Cockrum P, Meier E, Hammonds WM, Silverstein B, Silverstein S. Evaluation of clinical efficacy and safety of tobramycin/dexamethasone ophthalmic suspension 0.3%/0.05% compared to azithromycin ophthalmic solution 1% in the treatment of moderate to severe acute blepharitis/blepharoconjunctivitis. *Curr Med Res Opin.* 2011;27(1):171–8.
5. Bonikowski R, Witakowska P, Sienkiewicz MS, Zakłos-Szyda M. Selected compounds structurally related to acyclic sesquiterpenoids and their antibacterial and cytotoxic activity. *Molecules.* 2015;20(6):11272–96.
6. Holstein SA, Hohl RJ. Isoprenoids: Remarkable diversity of form and function. *Lipids.* 2004;39(4):293–309.

7. Cugini C, Calfee MW, Farrow JM, Morales DK, Pesci EC, Hogan DA. Farnesol, a common sesquiterpene, inhibits PQS production in *Pseudomonas aeruginosa*. *Mol Microbiol.* 2007;65(4):896–906.
8. Nickerson KW, Atkin AL, Hornby JM. Quorum sensing in dimorphic fungi: Farnesol and beyond. *Appl Environ Microbiol.* 2006;72(6):3805–3813.
9. Kaur S, Saad O, Xu K. Water soluble farnesol analogs and their use. Patent WO/2014/101051. 2009.
10. Bandara HMHN, Herpin MJ, Kolacny D, Harb A, Romanovicz D, Smyth HDC. Incorporation of Farnesol Significantly Increases the Efficacy of Liposomal Ciprofloxacin against *Pseudomonas aeruginosa* Biofilms in Vitro. *Mol Pharm.* 2016;13(8):2760–70.
11. Dinamarco TM, Goldman MHS, Goldman GH. Farnesol-induced cell death in the filamentous fungus *Aspergillus nidulans*. *Biochem Soc Trans.* 2011;39(5):1544–8.
12. Liu P, Luo L, Guo J, Liu H, Wang B, Deng B, et al. Farnesol induces apoptosis and oxidative stress in the fungal pathogen *Penicillium expansum*. *Mycologia.* 2010;102(2):311–8.
13. Kuete V, Efferth T. Molecular determinants of cancer cell sensitivity and resistance towards the sesquiterpene farnesol. *Pharmazie.* 2013;68(7):608–15.
14. Joo JH, Jetten AM. Molecular mechanisms involved in farnesol-induced apoptosis. *Cancer Lett.* 2010;287(2):123–35.
15. Couvreur P, Stella B, Harivardhan Reddy L, Hillaireau H, Dubernet C, Desmaëie D, et al. Squalenoyl nanomedicines as potential therapeutics. *Nano Lett.* 2006;6(11):2544–2548.
16. Couvreur P. Squalenoylation: A novel technology for anticancer and antibiotic drugs with enhanced activity. *Nanosci Nanotechnol Evol or Revolution?* 2016;253–72.
17. Ceruti M, Balliano G, Viola F, Cattel L, Gerst N, Schuber F. Synthesis and biological activity of azasqualenes, bis-azasqualenes and derivatives. *Eur J Med Chem.* 1987;22(3):199–208.
18. Lepeltier E, Loretz B, Desmaële D, Zapp J, Herrmann J, Couvreur P, et al. Squalenoylation of chitosan: A platform for drug delivery? *Biomacromolecules.* 2015;16(9):2930–9.

19. Miramoth NS, Di Meo C, Zouhiri F, Saïd-Hassane F, Valetti S, Gorges R, et al. Self-assembled squalenoylated penicillin bioconjugates: An original approach for the treatment of intracellular infections. *ACS Nano*. 2012;6(5):3820–3831.
20. Abed N, Saïd-Hassane F, Zouhiri F, Mougín J, Nicolas V, Desmaële D, et al. An efficient system for intracellular delivery of beta-lactam antibiotics to overcome bacterial resistance. *Sci Rep*. 2015;5.
21. Fosso MY, Shrestha SK, Green KD, Garneau-Tsodikova S. Synthesis and Bioactivities of Kanamycin B-Derived Cationic Amphiphiles. *J Med Chem*. 2015;58(23):9124–9132.
22. Berkov-Zrihen Y, Herzog IM, Feldman M, Fridman M. Site-selective displacement of tobramycin hydroxyls for preparation of antimicrobial cationic amphiphiles. *Org Lett*. 2013;15(24):6144–6147

7. LIST OF PATENTS, PUBLICATIONS, ORAL AND POSTER PRESENTATIONS

Patent application

1. 'Aminoglycoside derivatives and nano-assemblies thereof, including those with Quorum Sensing inhibitory function'
Inventors: Duy-Khiet Ho, Brigitta Loretz, Claus-Michael Lehr
European Patent Application, **EP 17 179 011.6**
International Patent Application, **PCT/EP2018/065232**

Articles published in international peer-reviewed journals

1. **Duy-Khiet Ho**, Ana Costa, Chiara De Rossi, Cristiane de Souza Carvalho-Wodarz, Brigitta Loretz and Claus-Michael Lehr. 'Polysaccharide Submicrocarrier for Improved Pulmonary Delivery of Poorly Soluble Anti-infective Ciprofloxacin: Preparation, Characterization, and Influence of Size on Cellular Uptake'. *Mol. Pharm.*, 2018, 15 (3), 1081–1096.
2. **Duy-Khiet Ho***, Hanzey Yasar*, Chiara De Rossi, Jennifer Herrman, Sarah Gordon, Brigitta Loretz and Claus-Michael Lehr. 'Starch-Chitosan Polyplexes: A Versatile Carrier System for Anti-Infectives and Gene Delivery'. *Polymers*, 2018, 10 (3), 252. ((*)) These authors contribute equally)
3. **Duy-Khiet Ho**, Sarah Frisch, Alexander Biehl, Emmanuel Terriac, Chiara De Rossi, Konrad Schwarzkopf, Franziska Lautenschlaeger, Brigitta Loretz, Xabier Murgia and Claus-Michael Lehr. 'Farnesylated Glycol Chitosan as a Platform for Drug Delivery: Synthesis, Characterization and Investigation of Mucus-Particle Interactions'. *Biomacromolecules*, 2018, 19 (8), 3489-3501.

Manuscripts under preparation

4. **Duy-Khiet Ho**, Anastasia Andreas, Xabier Murgia, Antonio G. Hübner de Mello Martins, Chiara De Rossi, Marcus Koch, Jennifer Herrmann, Rolf Müller, Martin Empting, Rolf W. Hartmann, Didier Desmaele, Brigitta Loretz, Patrick Couvreur and

Claus-Michael Lehr. 'Quorum Sensing Inhibitor and Aminoglycoside Antibiotic Dual-Loaded Nano-assemblies as Complementary Therapy Against *Pseudomonas aeruginosa* Biofilm Infection'.

5. **Duy-Khiet Ho**, Chiara de Rossi, Brigitta Loretz and Claus-Michael Lehr. 'Farnesylated Aminoglycosides: An Original Excipient-Free Dual-functional Nano-assemblies for Combating *Pseudomonas aeruginosa* biofilm infection'.
6. **Duy-Khiet Ho**, Rebekka Christmann, Sarah Frisch, Chiara De Rossi, Marcus Koch, Xabier Murgia, Brigitta Loretz, Patrick Couvreur, Didier Desmaele and Claus-Micheal Lehr. 'Self-assemblies of Squalenyl Derivatives: Platforms for Versatile Drug Delivery Systems'.

Presentations at international conferences

Oral Presentations

1. **Duy-Khiet Ho**, Didier Desmaele, Xabier Murgia, Antonio G. Hübner de Mello Martins, Chiara De Rossi, Marcus Koch, Martin Empting, Rolf W. Hartmann, Brigitta Loretz, Patrick Couvreur and Claus-Micheal Lehr. 'Quorum Sensing Inhibitor and Aminoglycoside Antibiotic Dual-Loaded Nano-assemblies as Complementary Therapy Against *Pseudomonas aeruginosa* Infection'. 12th International Conference and Workshop on Biological Barriers. August 27-29, **2018**, Saarbrücken, Germany.
2. **Duy-Khiet Ho**, Didier Desmaele, Antonio G. Hübner de Mello Martins, Chiara De Rossi, Marcus Koch, Martin Empting, Rolf W. Hartmann, Brigitta Loretz, Patrick Couvreur and Claus-Micheal Lehr. 'Squalenyl Hydrogen Sulfate Nanocarrier for Dual-Delivery of Anti-infective Quorum Sensing Inhibitor and Aminoglycoside Antibiotic Tobramycin'. XII Spanish-Portuguese Conference on Controlled Drug Delivery. January 14-16, **2018**, Coimbra, Portugal.
3. **Duy-Khiet Ho**, Ana Margarida Martins Maia da Costa, Chiara De Rossi, Cristiane de Souza Carvalho-Wodarz, Brigitta Loretz and Claus-Michael Lehr. 'Polysaccharide Sub-Microcarrier for Anti-infectives Delivery'. 13th Zsigmondy colloquium, April 5-7, **2017**, Saarbrücken, Germany.

Poster Presentations

1. Alexander Biehl, **Duy Khiet Ho**, Sarah Frisch, Brigitta Loretz, Konrad Schwarzkopf, Xabier Murgia, Claus-Michael Lehr. 'Investigating nanoparticle-based drug delivery systems and mucus interaction with Profor MPTA (Protocol for Multiple Particle Tracking Analysis)'. 12th International Conference and Workshop on Biological Barriers. August 27-29, **2018**, Saarbrücken, Germany.
2. **Duy-Khiet Ho**, Didier Desmaele, Xabier Murgia, Antonio G. Hübner de Mello Martins, Chiara De Rossi, Marcus Koch, Martin Empting, Rolf W. Hartmann, Brigitta Loretz, Patrick Couvreur and Claus-Micheal Lehr. 'Increasing *Pseudomonas aeruginosa* Biofilm Eradicating Efficacy by Dual-Delivery of a Novel Alkylquinolone Quorum Sensing Inhibitor and Tobramycin using Squalenyl Hydrogen Sulfate Nanocarrier'. 45th Annual Meeting & Exposition of the Controlled Release Society, July 21-24, **2018**, New York, USA.
3. Sarah Frisch, **Duy-Khiet Ho**, Alexander Biehl, Chiara De Rossi, Brigitta Loretz, Xabier Murgia and Claus-Michael Lehr. 'Nanoparticle Tracking Analysis (NTA): a Facile Method for Addressing Nanoparticles and Mucin Glycoproteins Interaction'. 12th International Conference and Workshop on Biological Barriers. August 27-29, **2018**, Saarbrücken, Germany.
4. **Duy-Khiet Ho**, Didier Desmaele, Xabier Murgia, Antonio G. Hübner de Mello Martins, Chiara De Rossi, Marcus Koch, Martin Empting, Rolf W. Hartmann, Brigitta Loretz, Patrick Couvreur and Claus-Micheal Lehr. 'Squalenyl Hydrogen Sulfate-based Dual-Delivery Platform for Complementary Therapy of a Novel Alkylquinolone Quorum Sensing Inhibitor and Tobramycin Against *Pseudomonas aeruginosa* Biofilm'. 8th HIPS Symposium on Pharmaceutical Sciences Devoted to Infection Research, June 14, **2018**, Saarbrücken, Germany
5. Alexander Biehl, **Duy-Khiet Ho**, Sarah Frisch, Brigitta Loretz, Konrad Schwarzkopf, Emmanuel Terriac, Xabier Murgia, Claus-Michael Lehr. 'Applying multiple particle tracking to pharmaceutical research: a computational toolbox to address the transport and diffusion of nanoparticles through mucus'. 11th World Meeting on Pharmaceutics, Biopharmaceutics and Pharmaceutical Technology. March 19-22, **2018**, Granada, Spain.

6. Sarah Frisch, **Duy-Khiet Ho**, Alexander Biehl, Chiara De Rossi, Brigitta Loretz, Xabier Murgia and Claus-Michael Lehr. 'Investigating the Interaction between Nanoparticles and Mucin Glycoproteins by Nanoparticle Tracking Analysis'. 22nd annual meeting German Controlled Release Society Local Chapter. March 01-02, **2018**, Halle, Germany.
7. Alexander Biehl, **Duy Khiet Ho**, Sarah Frisch, Brigitta Loretz, Konrad Schwarzkopf, Claus-Michael Lehr, Xabier Murgia. 'Profor MPTA - Protocol for Multiple Particle Tracking Analysis: A toolbox to address the behaviour of nanoparticle-based drug delivery systems in mucus. 22nd annual meeting German Controlled Release Society Local Chapter. March 01-02, **2018**, Halle, Germany.
8. Brigitta Loretz, **Duy-Khiet Ho**, Sarah Barthold, Sara Menina, Sarah Gordon, Claus-Michael Lehr. 'Carrier technologies for local delivery of anti-infectives'. 11th World Meeting on Pharmaceutics, Biopharmaceutics and Pharmaceutical Technology. March 19-22, **2018**, Granada, Spain.
9. Sarah Frisch, **Duy-Khiet Ho**, Alexander Biehl, Chiara De Rossi, Brigitta Loretz, Xabier Murgia, Claus-Michael Lehr. 'Interaction Between Nanoparticles with Different Surface Functionalization and Mucin Glycoproteins'. Doctoral Conference in Saarland University. November 15, **2017**, Saarbrücken, Germany.
10. Alexander Biehl, **Duy-Khiet Ho**, Sarah Frisch, Chiara De Rossi, Brigitta Loretz, Xabier Murgia, Claus-Michael Lehr. 'Profor MPT – Development of a toolbox for Multiple Particle Tracking (MPT) video evaluation'. Doctoral Conference in Saarland University. November 15, **2017**, Saarbrücken, Germany.
11. **Duy-Khiet Ho**, Hanzey Yasar*, Ana Margarida Martins Maia da Costa*, Chiara De Rossi, Jennifer Herrmann, Cristiane de Souza Carvalho-Wodarz, Brigitta Loretz and Claus-Michael Lehr. 'Polysaccharides based Versatile Nano-carriers for Pulmonary Anti-infective Delivery'. 44th Annual Meeting & Exposition of the Controlled Release Society, July 16-19, **2017**, Boston, USA. ((*)) Authors contribute equally)
12. **Ho, Duy-Khiet**; Costa, Ana; De Rossi, Chiara; Carvalho-Wodarz, Cristiane de Souza; Loretz, Brigitta and Lehr, Claus-Michael. 'Pulmonary Targeted Anti-infectives Delivery System of Chitosan-Cyclodextrin Based sub-MicroCarrier'. 7th

- HIPS Symposium on Pharmaceutical Sciences Devoted to Infection Research, June 29, **2017**, Saarbrücken, Germany.
13. **Ho, Duy-Khiet**; Costa, Ana; DeRossi, Chiara; Carvalho-Wodarz, Cristiane de Souza; Loretz, Brigitta and Lehr, Claus-Michael. 'Versatile Polysaccharide sub-Micro Coacervate for Antibiotics Delivery'. 21st Annual Meeting of The Controlled Release Society Germany Local Chapter, March 2-3, **2017**, Marburg, Germany
 14. Xabi Murgia, **Duy-Khiet Ho**, Brigitta Loretz, Ulrich Friedrich Schaefer, and Claus-Michael Lehr. 'Addressing the size-dependent mobility of nanoparticles through human tracheal mucus'. 21st Annual Meeting of The Controlled Release Society Germany Local Chapter, March 2-3, **2017**, Marburg, Germany
 15. **Duy-Khiet Ho***, Hanzey Yasar*, Chiara De Rossi, Sarah Gordon, Brigitta Loretz and Claus-Michael Lehr. 'Starch-Chitosan polyplexes as a versatile drug delivery platform with tunable release characteristics'. 6th HIPS Symposium, Recent Developments in Infection Research, June 29, **2016**, Saarbrücken, Germany ((* Co-first authors)
 16. Xabier Murgia, **Duy-Khiet Ho**, Brigitta Loretz, Konrad Schwarzkopf, Ulrich Friedrich Schaefer, and Claus-Michael Lehr. 'Nanoparticle transport through human undiluted tracheal mucus'. CLINAM European Foundation for Clinical Nanomedicine, June 26-29, **2016**, Basel, Switzerland.
 17. Hanzey Yasar, **Khiet Ho-Duy**, Chiara De Rossi, Sarah Gordon, Brigitta Loretz and Claus-Michael Lehr. 'Starch-Chitosan polyplexes as a novel, versatile drug carrier system for transfollicular vaccination'. GPEN2016, November 9-12, **2016**, University of Kansas, USA.

8. ACKNOWLEDGEMENTS

I am deeply thankful to all supervisors, colleagues and friends who were involved in the process of my PhD study and made this thesis successful in less than three year.

Firstly, I would like to express my sincere gratitude to Prof. Dr. Claus-Michael Lehr, my doctor-father, for giving me this great opportunity working as a PhD student and an Early European Researcher in his team, which is a great platform for my future career development. I would especially like to thank for his trust, his optimistic encouragement and support during my study.

Moreover, I would like to thank to Prof. Claus-Michael Lehr together with Dr. Brigitta Loretz and Dr. Xabier Murgia for providing me an enthusiastic supervision not only in doing good scientific research but also for being a good scientist.

I would sincerely like to thank to Dr. Brigitta Loretz for her contribution to the success of this thesis. I am deeply appreciated her hard-work, encouraging, patience and many more positive factors that tremendously supported me finishing the PhD study.

A lot of special thanks to Dr. Chiara de Rossi for her dedicated works and contribution to the success of this thesis.

Three years in Germany becomes even more meaningful with my two big brothers Dr. Branko Vukosavljevic, and Dr. Xabier Murgia.

I would also like to thank to Prof. Dr. Patrick Couvreur and Dr. Didier Desmaele for hosting and supervising me during my secondment in CNRS, Paris, France.

I would also like to thank to all my co-authors in all of my publications, patents, oral and poster presentations. My warm and sincere gratitude also goes to all colleagues in Drug Delivery Department, Helmholtz Institute for Pharmaceutical Research Saarland, for discussing scientific works, and having a good time with me.

As a Marie Skłodowska-Curie Actions PhD fellow, I am really proud for being trained within and deeply thankful for the financial support from the ITN (Initial Training Networks), NABBA project (Design and Development of advanced **NA**nomedicines to overcome **B**iological **BA**rriers and to treat severe diseases) for the last three years.

Finally, I would like to thank to all my family members and my friends. It has been long time for me living abroad and following my dreams, and I still keep moving on with a warm and proud heart, because I know your encouraging, believe, support, and love are always with me.

Curriculum Vitae

Personal information

Full Name
E-mail
Nationality
Date of birth

Duy-Khiet Ho
DuyKhiet.Ho@helmholtz-hzi.de
Vietnamese
30.11.1988

Current position

Oct. 2015 – Present

EU Researcher, Marie Sklodowska-Curie Fellow
Helmholtz Centre for Infection Research (HZI)
Helmholtz Institute for Pharmaceutical Research Saarland (HIPS)
Drug Delivery Department (DDEL), Germany

Work experience

Apr. 2016 – Oct. 2016

Visiting Researcher within the framework of the Marie Sklodowska-Curie project

Centre National de la Recherche Scientifique (CNRS), Institut Galien Paris-Sud, France.

Supervisors: Prof. Dr. Patrick Couvreur, Dr. Didier Desmaele.

Mar. 2015 – Aug. 2015

Research Associate

Research Institute of Advanced Materials, Seoul National University, South Korea

Feb. 2012 – Dec. 2012

Research Associate

The National Key Laboratory of Polymer – Composite Materials, Ho Chi Minh City, Viet Nam

Education

Oct. 2015 – Present

Helmholtz Institute for Pharmaceutical Research Saarland, Saarland University, Germany

PhD student in Department of Pharmacy

Supervisors: Prof. Dr. Claus-Michael Lehr, Dr. Brigitta Loretz

Mar. 2013 – Feb. 2015

Seoul National University, South Korea

Master of Science in Materials Science and Engineering, College of Engineering.

Supervisor: Prof. Dr. Cheol-Hee Ahn

Sep. 2006 – Jan. 2011

Viet Nam National University, Ho Chi Minh City University of Technology, Viet Nam

Bachelor of Engineering in Polymeric Materials Technology

Scholarships and Awards

Oct. 2015 – present

Marie Sklodowska Curie PhD Fellowship in Helmholtz Institute for Pharmaceutical Research Saarland (HIPS), Helmholtz Centre for Infection Research (HZI)

July 2018

DAAD-funded project “GradUS Global” in Saarland University for excellent doctoral researcher abroad

August 2017

Best pitch (in a team) for project “VagiTen” in Technical University of Denmark

July 2017

DAAD-funded project “GradUS Global” in Saarland University for excellent doctoral researcher abroad

Mar. 2013 – Mar. 2015

Seoul National University Global Scholarship 1 for postgraduate study in Seoul National University, South Korea

Mar. 2014 – Mar. 2015

ASAN Foundation Scholarship for excellent student in Seoul National University, Korea

2006

Vietnamese National Award for Excellent Student in Chemistry